POLITECNICO DI MILANO
DEPARTMENT OF MECHANICAL ENGINEERING
DOCTORAL PROGRAM IN MECHANICAL ENGINEERING

TYRE-SOIL INTERACTION FOR OFF-ROAD VEHICLE APPLICATIONS

Doctoral Dissertation of:
Ramadhani Omari Kivugo

Supervisor:
Prof. Francesco Braghin

Tutor:
Prof. Masimiliano Gobbi

The Chair of the Doctoral Program:
Prof. Bianca Maria Colosimo

2014 – 30

Preface

The work described in this thesis was carried out at Polytechnic University of Milan in Mechanical Engineering Department between November 2014 and October 2017.

I would like to express my special appreciation and thanks to my supervisor Professor Francesco Braghin. He has given me a tremendous advisor and thanks for his expert advice and encouragement throughout this difficult research work. I also give thanks to my tutor Professor Massimiliano Gobbi for his expert support for my research. I thank Professor Alessandro Tasora for his technical support in this research work.

I would like also to greatly appreciate Fondazione Politecnico di Milano for funding my studies through a collaboration project of 'Capacity Building in Tanzania' between Politecnico di Milano and Dar es Salaam Institute of Technology. Greatly thanks to Professor Emanuela Colombo for her extraordinary effort and making this collaboration successful.

I also thanks the Principal of Dar es Salaam Institute of Technology, Professor Preksedis M. Ndomba for his support and encouragement during my PhD studies. Also my great thanks to stuffs of Mechanical Department, Politecnico di Milano for their brilliant support, suggestions and encouragement during this research period.

I would like also to thank all my good friends at Politecnico di Milano, Dr. Michele Vignati, Dr. Davide Ivone and Dr. Muhammad Izadi, here few mentioned whose friendship and support throughout this project were invaluable.

A very special thanks to my family for their emotional, moral support and all of the sacrifices they have made on my behalf to make this work succeed. At the end I would like to express appreciation and thanks to my beloved wife Saphia who was always supportive and incentive during my PhD period.

This dissertation is the result of my own work and the support of Chrono::Engine Software developer. No part of the work has already been, or is currently being, submitted for any degree or diploma. This work includes 5 chapters.

Ramadhani O. Kivugo, June 2017

Abstract

AGRICULTURAL AND OTHER OFF-ROAD tyres primarily have to satisfy differents operational requirements, such as better traction performance, limit slip sinkage, limit soil compaction and support weight of the machine. These requirements strongly depends on the soil characteristics and tyre tread design.

Little attention has been devoted to discrete element method (DEM) model that can be used to predict the traction performance as a function of tyre tread design with respect to to soil characteristics considering the effects of discontinuous behaviour of terrain during interaction. An early attempt to predict the tyre-soil interaction has been done by modelling terrain as a collection of deformable layer springs and tyre as deformable ring with tread geometry. Moreover, recently attempts in numerical and discrete element models have been studied and developed, these models can predict traction performance, stresses and sinkage of wheel, but have the weakness of predicting the effects of build-up and cleaning which rise due to discreteness deformation of terrain during interaction.

Given the fact that, deformation of terrain is discontinuous in nature during interaction which rise to bulldozing effects, build-up and cleaning phenomenon and these mostly affects performance of wheel and off-road vehicles, then modelling terrain as assemblage of rigid colliding bodies must be studied and developed to predict those effects with respect to soil rheology. In this work a multi-body dynamic software chrono::engine based on discrete elements method for non-smooth contact detection and computational and Bekker-Wong semi-empirical methodology has been used to model tyre-soil interaction to study the effects of terrain deformation with respect to wheel performance during interaction. This has been achieved by using C++ multi-body library in the software for modelling single tyre-soil interaction simulation model.

Simulations of tyre-soil interaction has been carried out with this model to study the influence of soil particles characteristics such as particle size, friction, cohesion force, mass/size distribution, shape and tyre tread design parameters such as lugs angle, type, height and spacing on interaction parameters such as wheel slip, traction, slip sinkage, slip velocity and forward velocity. Also, sensitivity and performance analysis has been carried out with the model considering terrain properties.

Finally, semi-empirical soft terrain model has been developed in this model. This terrain model is an alternative to granular terrain, in which soil properties depends on Bekker-Wong parameters. The model improves computational time and sinkage estimation accuracy and simulation time as in granular terrain. These two terrain models used in this simulation model gives reliable results of interaction parameters and contact pressure during interaction. The model has been validated with experimental and numerical data available in literature and guarantees an error less that 10% for traction force with respective slip.

Summary

STUDY of the interaction between tire and ground has been a challenging problem in vehicle dynamics, terramechanics, agriculture, exploration, exploitation, cross-country transportation, and civil engineering research. Off-road applications are critical in many fields such as ones mentioned above and the complexity of the tire-terrain interaction due to different terrain properties, behaviours and response to wheel loading, deeply affects off-road vehicle performances [12, 20, 29, 32, 71, 87, 88, 90, 107, 109]. This is because the interaction between both deformable, rigid tyres and deformable terrain are very complex and include manifold effects such as sinkage, multi-pass, slip sinkage, build-up and cleaning [29, 71].

In order to study these effects correctly and accurately appropriate model that can realistically estimates both continuous and discontinuous of the terrain deformation should be developed, that can be used to study and estimate properly the behaviour, response and effects of these challenging problem both in research and advisory purposes for a given mission and environment [71, 107]. The performance of the off-road vehicles to a greater extent depends on the manner in which the vehicle interacts with the given terrain, therefore understanding of the mechanics of vehicle-terrain interaction is of importance to the proper selection of the vehicle configuration and design parameters to meet specific operation requirements. In terramechanics the issue is to establish a quantitative relationship between the performance and design of an off-road vehicle for a given operating environment of unpaved terrain [71, 90, 107].

Recently, researchers in this field shows growing interest on this problem, in particularly to the problem of predicting the effects of slip sinkage, build-up and cleaning during wheel-terrain interaction especially for deformable terrain. In these studies, tyre and terrain deformation has been accounted using different approaches like Finite Element Method (FEM) and Discrete Element Method (DEM) with promising results. But still, the effects due to discontinuous deformation of the terrain such as build-up and cleaning could not be correctly reproduced [113]. This is due to the facts that, the soil was schematised as the continuous surface that making it impossible to reproduce the terrain particles that build up in front of the tire and the soil particles adhering to the tread pattern which to the greater extent affects the performance of the tire [20, 71, 113].

Since one of the key purposes for estimating terrain behaviour was to enable the engineers and researchers in this field to estimates performance of the off-road vehicles in a systematic and convenient manner using mathematical function that relates the vehicle performance and terrain response parameters, it is difficult to predict tire and vehicle performance on the soil due to the complexity behaviour of the interaction between deformable tire and road [109]. To be able to numerically reproduce these phenomena, Chrono::Engine software has been used for modelling both the discontinuous deformability of terrain and the granulometry of the ground due to its capacity of representing the terrain as the collection of the colliding rigid bodies [71].

Little attention has been devoted to Discrete Element Method (DEM) model that can be used to predict the traction performance as a function of tyre tread design with respect to soil characteristics taking into account the effects of discontinuous behaviour of terrain. An early attempt to predict the tyre-soil interaction has been done by modelling the terrain as a collection of the deformable layer of springs and the tyre as deformable ring with tread geometry.

Moreover, recently attempts in numerical and discrete element models have been studied and developed, these models are capable of predicting the traction performance, stresses and sinkage of the wheel [69] [70], but has the weakness of predicting the effect of build-up and cleaning [71] which rise due to discontinuous behaviour of the terrain.

Given the fact that, the deformation of terrain is discontinuous in nature during interaction which rise to the effect of build-up and cleaning phenomenon which affect performance of the wheel and off-road vehicles as well, then modelling terrain as assemblage of rigid colliding bodies has to be studied and developed to predict such effects [71].

In this work Multi-Body Dynamics software Chrono::Engine based on Discrete Element Method methodology has been used to model the tyre-soil interaction to study the effects of terrain discontinuous deformation to the wheel performance during interaction. This has been achieved by using a C++ multi-body library in Chrono::engine and discontinuous discreteness of terrain has been accounted for. The simulation of tyre-soil interaction has been carried out with this model, to study the influence soil particles characteristics and tyre tread design to wheel performance, sensitivity of the pattern to traction force and sinkage of the wheel as well, the effects of build-up and cleaning to the wheel performance in terms of traction force and slip, slip velocity and slip sinkage.

An alternative to granular terrain, a soft deformable terrain has been developed in the model. Soil model is a modified improved model from original semi-empirical soft soil contact model (SCM) developed in DLR Institute of Robotics and Mechatronics, Germany [46]. In chrono soft soil model, soil surface grid has been extended to include other form of grids such as triangular grid for fast and accuracy solver computational. The contact body in chrono engine is the rigid wheel in which mass and inertia has been taken into account in the multi-body dynamics computation of contact dynamics. Contact dynamics computational initialised by grid nodes sinkage and employed Bekker empirical formula that relates sinkage and soil parameters to realise contact pressure, and from contact force resistive torque was computed from multi-body dynamics solver in chrono taking into account interaction motion resistance. Traction force was computed from resistive driving torque developed by the soil longitudinal motion resistance

due to deformation and sinkage.

Fine tuning of the model has been carried out in order to properly reproduce the deformability of terrain, and validation of the model has been carried out through comparison of the results with experimental data from the existing literature.

The model realistically simulate the dynamic behaviour of off-road traction wheels in terms of traction, slip, slip sinkage, forward velocity, acceleration, slip velocity and contact pressure while taking into account bulldozing effects such as build-up and cleaning, soil compaction and motion resistance with respect to soil particle properties.

Finally, the model also was used for improvement and optimisation of the tread pattern design in terms of maximum traction and reasonable slip sinkage at selected wheel slip,these has been achieved through sensitivity and optimisation analysis carried out in this work.

This thesis will be structured from chapter 1 to chapter 5 as hereby follows;

· In chapter 1; Introduction; where scientific and industrial relevancy of the thesis has been introduced. Also expected results of the model has also been demonstrated in this chapter

· In chapter 2; State of the art; review of the previously reseach in this field has been careful reviewed in this chapter. The main objective of the thesis has been derived in this chapter. Tire-soil interaction analysis, field and experimental tests as per state of the art has been carried out.

· In chapter 3; Tire-soil interaction model; methodological and strategical approach, terramechanics theories on modelling, chrono modelling and simulation model has been detailed in this chapter. Also simulation results for granular and soft deformable terrains, has been analysed and explained. Finally validation of the model from available experimental and model data has been carried out in this chapter

· In chapter 4; Sensitivity analysis; of the tread pattern design has been performed for both granular and soft soil terrains, results and analysis of interaction parameters been presented based on traction tyres (combined lugs tyres) and appropriate conclusions has been drawn.

· In chapter 5; Optimisation analysis; of the selected tyre and pattern parameters with respect to soil properties has been carried out. Results and analysis of traction force, slip sinkage, slip velocity, forward velocity and contact pressure analysed and conclusions has been drawn.

· In chapter 6; Conclusions of this thesis based on the results analysis were drawn in this chapter.

Nomenclature

τ	shear stress at the tire-soil contact
σ	normal stress at tire-soil contact
k'_c	cohesion dependent parameter
k'_ϕ	internal shearing dependent parameter
y	slip sinkage of the wheel
ϕ	angle of internal shearing resistance of terrain material
j	shear displacement
K	shear displacement modulus
W	wheel load
δ	angle of the resultant pressure at the contact
p	normal pressure at the contact
s_d	dynamic wheel slip
s	wheel slip ratio
R	radius of the wheel
ω	angular speed of the wheel
θ	angular position of stress at the conact point
θ_b	contact entry angle
θ_e	contact exit angle
a	contact entry point
b	contact exit point
k_1	soil parameter befre maximum sinkage
k_2	soil parameter after maximum sinkage
DEM	discrete element method
FEM	finite element method
q	position of the contact between particles
$\dot{q}$	differential algebraic equation of the contact
v	velocity of dynamic contact
L	linear transformation of dynamic ocntact equation
f	contact inertia force

g_q^T	constraint force
t	time of contact occurrence
t_0	time of initiation of contact
MBD	multi body dynamics
F_n	normal contact force
F_t	tangential contact force
u_n	normal contact overlap
u_t	tangential contact overlap
u	local contact displacement
R_i	radius of curvature of contact in i particle
R_j	radius of curvature of contact in j particle
m_i	mass of particle i
m_j	mass of particle j
m	effective mass of contact
R	effective radius of contact curvature
c	soil particle cohesion force
V_j	wheel slip velocity
V_z	wheel linear velocity
λ	terrain rebound-ness factor
a_0, a_1	interaction dependent parameters
F_T	wheel traction force
T_w	wheel driving torque
DP	drawbar pull
σ_{n_1}	normal stress from the entry to the maximum point
σ_{n_2}	normal stress from the maximum to the exit point
n	sinkage modulus
$comb$	combined lugs
str	straight lugs
$nonDir$	non directional lugs
v_n	contact normal relative velocity vector
v_t	contact tangential relative velocity vector
k_n	contact normal stiffness
k_t	contact tangential stiffness
γ_t	contact damping coefficient
DVI	differential variational inequality
$DAEs$	differential algebraic equations
$\dot{y}_P$	sliding speed of the contact yield surface
c^i	yield surface cohesion stabilization term
d	distance between cone and ball in Minkowski yield surface
h	lugs center length
θ_l	angle between lugs
D_0	wheel outside diameter
l_w	lugs width
l_s	lugs spacing
l_h	lugs height
n_l	lugs number

γ_s	terrain weight density
γ_b	terrain bulky density
p_{size}	particle size
p_n	number of particles
p_f	particle friction coefficient
p_c	particle cohesion force
p_{shape}	particle shape
ρ_p	particle density
w	wheel width
k	Janosi deformation parameter
c_A	node contact area
A	wheel contact area
y_i	node sinkage
v_i	contact velocity
n_i	node contact surface normal vector
t_i	node contact surface tangential vector
$n_{contact}$	number of node contact
w_i	width of node
w_{total}	total contact patch width
z	soil sinkage
R_c	wheel motion resistance
η	tractive efficiency

List of Figures

List of Tables

Contents

CHAPTER 1

Introduction

1.1 Scientific and Industrial Relevance of the Topic

Off-road operation of the vehicle is a field of interest in agriculture, construction, exploration, mining, military applications, cross-country transportation [36, 37, 84, 90, 106, 107]. The performance of an off-road vehicle to the greater extent depends on the manner in which the vehicle interacts with the given terrain [36]. On other hand the mobility of vehicle and its dynamical characteristics are determined by the tire-soil interaction during operations [33, 80–82, 84, 90]. Considering the number of tractors and soil-cultivating implements used in agriculture, earthmoving machines used in construction industry, highway trucks used in the off-road transportation industry, combat and logistic vehicles used in military, one can with no doubt appreciate the interaction applications in the field of interest [109].

Consequently, systematic studies of the principles underlying the mechanics of tire-terrain interaction is of importance in the proper selection of the vehicle configuration, design parameters and tire tread pattern design/size to meet the operation requirements [6, 17, 19, 33, 36, 71, 88, 106, 107]. In broad sense, terramechanics is the systematic study of the overall performance of the machine in relation to its operating environment/terrain, which provide guiding principles for the rational development, design and evaluation of off-road vehicles and terrain working machinery. Recently, the growing concern over the energy conservation and environmental preservation has further stimulated the development of off-road operations studies [106, 107].

Furthermore, in addition to being a good engineering design of the vehicle, an off-road vehicle is now expected to attain high level of energy efficiency and not to cause severe damage to the operating environment, such as excessive soil compaction in agriculture. Increasing activities in the exploration and exploitation of the natural resources in the new frontiers, and the growing demand for greater mobility over a wide range

of terrains in all conditions, such as USA, European Union, Russia, China, Japan India and other nations in the exploration of the Moon, Mars have also given much stimulated attention to the advancements in interaction studies for off-road operations [106, 107].

Despite the fact that, pneumatic tires have decades of replaced rigid wheels in most off-road wheeled vehicles, the mechanics of interaction for the rigid wheels still of interest, as rigid wheels are still in use under certain circumstances such as exploration robot and extremely high temperature condition or chemical environment, also pneumatic tires can behave like rigid wheel in soft terrain [106].

Wheel slip and sinkage has been shown to be a prime key variable in estimating and predicting wheel-terrain interaction phenomenon [11, 16, 33, 51, 80, 82]. During tire-terrain interaction, deformation occurring on the terrain along the direction normal to the contact surface is the one known as wheel sinkage [16]. During this deformation, total sinkage of the wheel consist of two parts, which are sinkage due to static axle load and one due to slip of the wheel under traction [16, 80, 106, 107]. Little attention has been devoted to the study of dynamic effects occurring at wheel-terrain interface such as slip ratio and slip sinkage [82]. These effects compromise the traction performance and may results in the traverse failure of the wheeled vehicle in deformable terrain [33, 80].

Proper techniques of estimating slip ratio, slip-sinkage and associated slip-velocity may leads to the improvement of off-road vehicle mobility performance [33, 51, 80, 82]. When wheel interacts with ground on running gear, it applies the normal load to the terrain surface which results in sinkage and motion resistance [11, 16, 106, 107]. The torque applied to the wheel initiates shearing of the terrain layer which in turn results thrust and associated slip of the wheel [16, 106, 107].

1.2 Expected Results and its Application

The simulation results will be studied and analysed based on the literature and experimental data available for the interaction studies and analysis methods. Simulation study results and the experimental data available will lead to the conclusions of developed model to be drawn accordingly. The expected results of the present study will be useful for both off-road vehicles, tire industry, exploration robot planing, design and locomotion performance evaluation as well for environmental policies that aim at preserving the productivity of ground/land (that is severely affected by soil compaction e.g. in agriculture activities).

Once all these steps are fulfilled, the model will be a useful tool in different applications of the tire-soil interaction:

1. Tool for accurately predict soil compaction and deformation of the unpaved roads/ground due to vehicle traffic and wheel load/design.

2. Tool for study of soil interaction behaviour and characteristics under different wheel operating conditions such as load, sizes, lugs design, speed with respect to soil rheology.

3. Tool for analyse influence of tire tread design on interaction performance of wheels in deformable terrain.

4. Tool to estimate slip ratio, traction force, slip and static sinkage, slip velocity, drawbar pull and tractive efficiency of wheel with respect to tread pattern design, size and soil rheology.

5. Tool for tread pattern sensitivity and optimisation analysis for off-road vehicle tires in the given operating and terrain conditions.

CHAPTER 2

State of the art

Off-road vehicles should satisfy many different requirements, achieving a good tractive pull, guaranteeing a safe and comfort level for the operator and avoiding large soil compaction, which leads to difficulties for the plants root growth [20, 32, 71, 109]. Furthermore, those achievements should be satisfied working over different soils in which its properties can be significantly vary according to the terrain composition, air humidity and temperature conditions [32, 90].

A lot of the researchers in this field put much effort in the study of the wheel-soil interaction which shows the importance of the interaction problems in many fields applications [32]. Recently years, off-road vehicles' speed has increased, involving an increase in comfort problems related to dynamic behaviour, vehicle and tire performances, complexity of the interaction problems between the tire and road and drivers vibration exposure [20, 89].

An accurate tire-soil interaction model will lead to proper and accurate study of the effects of the discontinuous deformability of the terrain such as build-up, cleaning with respect to terrain conditions, how they affects mobility, traction performance of vehicle, tire performance as well as the soil compaction [6, 20, 108, 109, 113] and since tire-soil contact area is a function of the terrain and tire deformability [85] which is factor for soil vertical stress under the contact patch. Large variation of the soils behaviour impose several difficulties and complexities for accurately predictive studies of the interaction especially for both deformability of tire and road soil [29, 50, 60].

Since decades, many research works in the studies of tire-soil interaction was based on the numerical and experimental approaches which are too expensive and time consuming, in which some of the studies or methods did not give accurate prediction of the behaviours for deformable roads/ground or snow due to the weakness of their approaches and some assumptions [29], but some of the studies they employ the finite

element method (FEM), discrete element method (DEM), and few focus their studies in DEM method based on particle approach, just to the study of shear effect on subsoils for deformable road [71]. From the work in [71], was based on planar and particle modelling of deformable tire on deformable road for tread pattern design optimization problem. The planar model of the tire-soil interaction presented were considered the forces and displacements in vertical and longitudinal directions only, this approach neglects the lateral forces and displacements. The planar model is designed to perform simulation of the tire moving in the longitudinal direction, and paying attention to the particular stationary conditions [71].

The soil is modelled as a layer of springs, which pressure on the tire is proportional to the compression caused by the sinkage due to the tire. The tire is modelled considering both the tread pattern geometry, tire dimensions and structure properties such as lugs height, lugs orientation, lugs number, tire radius, width, modes shapes, frequency and damping and the carcass flexibility. The first approximation of the model, tire deformation was neglected, since the soil one is markedly large. However, the flexibility have been added, because of its great influence on the vibration transmission and interaction surface deformation [83].

These are the characteristics which have strong impact to the achievements of the off-road vehicle requirements [20, 20, 71]. The simulation carried out in planar model for the tire-soil interaction was aimed to study the influence of tire and soil parameters on traction force, driver comfort, soil sinkage and compaction, also the model was interacted with multi-body model of the whole tractor for the study of the influence of tire on tractor dynamics, and left behind the effects of build up and cleaning which has impact on traction efficient and soil compaction [20, 71].

The planar model did not give results on compaction and deformation of the subsoils, because modelling the soil as a continuous surface it is not possible to take into account the factors affects the tire performances like slip-sinkage, build up and cleaning. These effects was addressed as the weak part of the model. In order to face some of these effects the soil was modelled as the particles set, representing different dimension and properties and moving relative to one another.

Author commented on her study that, the advantage of the formulation provided by Chrono::Engine library, can be applied to large amount of multi-body problems and improved subsoil simulation, although a more efficient solver is required to simulate a large amount of colliding bodies. This gives out one of the factors for choosing the particle approach capacity provided by Chrono::Engine open source software.

B. J. Chan and C. Sandu (2007) they developed a methodology to represent 3-D wheel-soil interaction model based semi-empirical approach taking into account the plasticity theory and equilibrium analysis. The model was aimed for use in off-road vehicle dynamic simulations and control development purposes by employing the soil bearing capacity theory. The method of the work combined the advantage of the plastic theory for calculating the stresses with empirical data. The model lack the transient effects, tire dynamic lag, and combined traction/cornering and braking/cornering effects of the flexible tires. The formulation also lack the unilateral contact condition to facilitate off-road vehicle dynamic simulations [12].

C. Senatore and C. Sandu (2011), presented semi-empirical off-road tire model based on the effort of several researchers which brought together into a single model

able to investigates the effect of torque distribution on the tractive efficiency of the off-road vehicles. In order to realistically evaluate the tractive efficiency of a full size vehicle it is necessary to properly model separately the dynamics of the tire and vehicle body. They modelled the tire first by evaluating the stress distribution on the contact patch assuming that the tire is on the steady state condition based on the work by Wong and Reece [88, 88].

They evaluated the normal stress based on Reece pressure-sinkage equation, while the shear stress was evaluated based on the Hanamoto and Janosi empirical expression. In their work the slip-sinkage of the wheel was improved by linearly relating the sinkage exponent with the slip ratio of the wheel to realistically improve the evaluation of the normal stress using pressure-sinkage equation in multi-pass condition. The work also implemented the cohesion and cohesion dependent parameter to depend on the number of pass for multi-pass effect evaluation [87, 88].

Thomas Keller and M. Lamande in their work (2005, 2010) respectively presented the study of the prediction of the contact area and the distribution of the vertical stress below the tire, and they mentioned that contact area and distribution of the vertical stress at the contact to be the upper boundary condition for the soil compaction models and therefore it is important to have proper and accurate prediction of the stresses at the contact patch [41, 43].

He also use wheel load, tire inflation pressure, recommended tire inflation pressure, tire width and tire diameter as the critical input parameters of the model. It described the influence of the wheel load and tire inflation pressure on contact pressure distribution to provides significantly improved input data for the soil compaction models and increase the accuracy of predictions of soil stress and compaction. This describes the influence of the wheel load and tire inflation pressure on contact pressure distribution to provides significantly improved input data for the soil compaction models and increase the accuracy of predictions of soil stress and compaction [41, 43].

Furthermore, by considering elastic response of the geomaterials a new non-linear elastic law was suggested by C.H.Liu and J.Y.Wong(1996, 1999), C.H.Liu, J.Y.Wong and H.A.Mang(2000) for the study of large strain finite element analysis of sand applied to numerical simulation of the tire-sand interaction basically for prediction of the traction performance of the tire on dry sand. They considered the area of large strains for the implicit return mapping algorithm, and the algorithms were applied to the modified critical state model in conjunction with elastic law suggested and implemented to the general purpose finite element software MARC for numerical simulation of the tire-sand interaction [55, 56].

They evaluated the capability of the proposed numerical method by comparing the predicted traction performance from the simulation results with the set of experimental data which were available, and the consideration of the large strains yield more accurate numerical results. Predicted results of the drawbar performance, stress distribution and measured value were closely agreed which shown the applicability of the model [56].

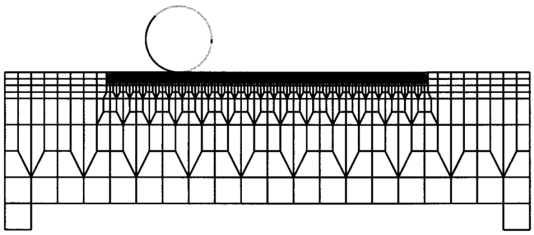

Figure 2.1: *Finite Element Mesh for simulation of wheel-sand interaction [56].*

A two-dimensional model for soil stress and compaction due to agriculture field traffic analysis was presented by T. Keller, P. Defossez, P. Weisskopf, J. Arvidsson and G. Richard (2007) on their study on soil stress and compaction due to agriculture traffic. The model was based on the analytical equations for stress propagation in soil for predicting contact area and stress distributions, and the mechanical properties of the soil in their study was estimated by pedo-transfer functions [42].

The model is flexible in terms of model inputs and outputs for different conditions of the interaction conditions. The model provide satisfactory prediction of the stress propagation and the bulk density changes by calculating the stress state, change in volume and the displacements in soil. They also claims that the degradation of the soil is one of the major environmental problems, and soil compaction is the most factor for soil physical degradation. The soil compaction models are important tools for controlling soil compaction due to agriculture field traffic. The weakness of the analytical approach mentioned in their study was to consider only one homogeneous layer for stress propagation, which may results in less accuracy prediction for strong heterogeneous soil conditions [42].

Based on the multiple source of uncertainties of the interaction of tire and soft terrain, statistical approach for better characterization of these uncertainties was done by developed stochastic model of tire-soil interaction by Jonah H. Lee (2015), by considering both longitudinal and lateral slips which occur simultaneously with longitudinal motion. The methods used to validate the model was the developed Gaussian metamodel process and the calibration of the model parameter using the approach of maximum likelihood with the new test data by using two types of models, which were deterministic vehicle-terrain and statistical models. Also in this study it considered the rigid tire in a combined slip phenomenon which is more challenging problem for the study than considering only longitudinal slip [50].

In the work presented by C. Zhao and M. Zang (2014) and H. Nakashima and A. Oida (2004) respectively, they combine the capabilities of both the Finite Element(FEM) and Discrete Element(DEM) Methods to obtain the accurate contact analysis on implementation of the simple algorithms. Despite the fact that the FEM and DEM been used by many researchers in this interaction problem and showing better results as explained by researchers implemented the methods, it has been noted that FEM has the weakness in the contact point of tire lag tip which behaves as singular stress point, and also the DEM method has weakness on the computational time at the contact check and the incremental time step although it has the capability of handling the microscopic deformation accurately [67, 113].

They implemented the algorithm to the simple tire sinkage problem and the soil

region below the tire shows some gaps which implies that there is the deformation of the soil, this prove that the algorithm works in solving this simple sinkage problem. Although the algorithm work on the sample problem, it shows that there is insufficient damping effect as indicated to the original vibratory calculation results. For this reason further development of the program should be added in order to solve this sinkage problem qualitatively and quantitatively [67].

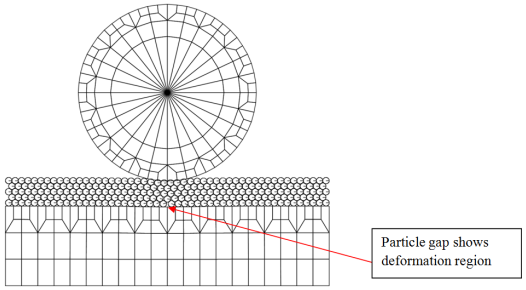

Figure 2.2: *Initial Mesh Configuration [67].*

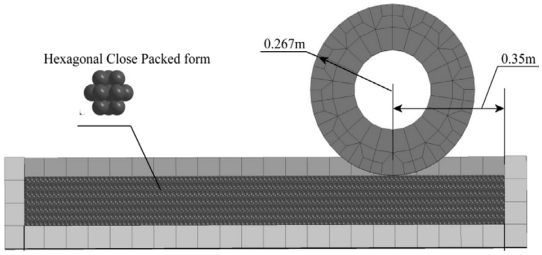

Figure 2.3: *Configuration of 3D Numerical Model [113].*

Also there has to be some method to fix the problem of spring constant adjustment in order to avoid severe overlap at the boundary in the contact region of the FE-DE model/method presented which is one of the weakness of the formulation of the method [67]. Nakashima extends his model to include a more practical tire-soil interaction system which can be capable of addressing not only sinkage but also travel effect of a driven tire [69]. Considering the results of the previously work by Nakashima, he also applied his model to tractive performance analysis of real two vehicle tires with two different tread patterns [70] to analyse its effect on tractive effort, motion resistance and drawbar pull.

The accuracy and reliability on Finite Element Method (FEM) has been addressed on the work done by C. W. Fervers (2004), N. Moslem and G. Hossein (2014). Fervers further developed the 2D-FEM model of an air-filled tire in special view of the carcass as the basic component that transmit the axial load from the rim to the ground and challenging part of the tire and not the tire global reaction mathematical descriptions [21, 65].

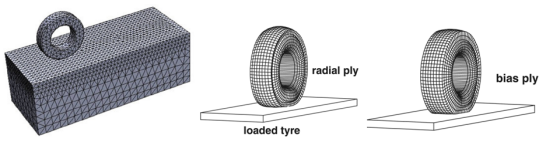

Figure 2.4: *Mesh Generated and simple 3D tire model [21, 65].*

Beside the fact that, 3-D models were used for modelling and simulation of the interaction problem, Fervers also mentioned in his work that, the importance of reducing the computational effort of the computer by transferring 3-D model into 2-D model for the simulation. In the context of transferring the 3-D to 2-D models for reduction of the computational effort, he elaborates the weakness of the 2-D models in their groups of categories classical spring-damper, built by the tire-ring and parametric models as mentioned. The first group been capable of rigid road simulation only, the second group been capable for simulation of deformable road but with limits to an air-filled tire situation of low pressure and high deformation. Third group of his category have the capability of real time conditions simulation but require testing of each tire under various conditions which may lead to extremely high test cost and time to achieve the data to represent the tire [21, 65].

He also extends the capability of his 2-D model on uneven roads just by simulating the model on step curb stone, the results of the simulation shows the promising consistence to the experimental data and this proves the validation of the model capability to uneven roads [21]

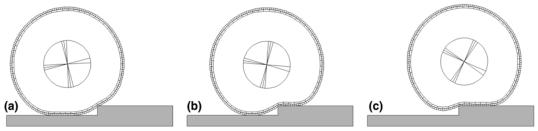

Figure 2.5: *Simulation of uneven road in 2-D model [21].*

Also, he extended the simulation by accounting the propulsion torque of the elevation of the wheel, simulation results gives out a good correlation to the test results which also proves that the maximum torque for deformable air-filled tire on stepped road is less as compared to rigid tire. Both simulation results of the model in deformable road and rigid road shows the correlation of the test data and simulation results which proves the ability of the 2-D model developed, further effort should be kept in developing the model which will account the dynamic properties of the soils by implementing the non-constant soil elasticity [21, 65].

N. Moslem and G. Hossein (2014)in their work on numerical simulation of tire/soil interaction using a verified 3D finite element model, they tried to contradict the weakness of the 2D model as the work of FERVERS and instead they put their effort on 3D model to by considering the capability of the computers nowdays. They obtained the data from the experimental setup on their work, they model the tire on SolidWorks software to acquire the structure components of the tire. They consider the energy stored in the tire rubber as strain energy by the Mooney-Rivlin equation, the mesh of the model was 8-nodes linear hexagonal element [65].

They employed the phenomenon of the yield criterion for the deformation of the soil for the analysis of plastic behaviour of the soil, and they use Drucker-Prager model for stress and strain calculations of the soil in their work. The simulation was conducted and the results were analysed, the results shows that they correlates with the empirical data available on their study which proves that the model gives out the positive results of the prediction of the behaviours of the tire/terrain interaction in relation to the inflation pressure [65].

In their work the soil model was considered as two regions and the boundaries of the soil are far enough to avoid virtual deformation on the deformation field, the thin layer in contact with the tire and the thick bottom layer [65].

In the work presented by K. Xia and Y. Yan (2012), instead of using rigid wheel in finite element model they model the wheel as rubber in almost incompressible finite strain hyperelasticit rubber materials. They model the tire as bias type and embedded still rebars within the structure and combine to ground model for accurately prediction of compaction, pavement response and pavement damage in dynamic response of the ground to moving vehicle [109].

The model was able to accommodates different tire conditions in tire/ground interactions which proves the applicability of the model developed. The model helps in decision making on off-road vehicle design, pavement structure design and control ground overlay deformation in applications to terramechanics, transportation and pavement engineering [109].

Authors in different studies mentioned that ground response is direct related to the tire structure, inflation pressure, soil properties, tire/ground interface properties and vehicle load, and the tire structure and inflation pressure been the main two driven factors for the influence of contact area and pressure at tire/terrain interface for a particular load [14, 87, 104, 107].

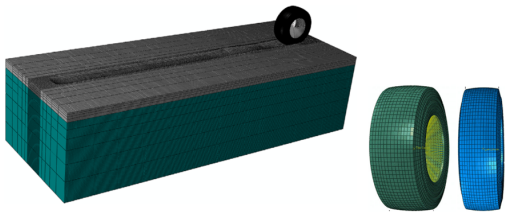

Figure 2.6: *FEM interaction and tire models [109].*

In the work of S. Hutangkabodee (2006), he uses composite Simpson's Rule to approximate the integrals of original interaction model to increase the speed of identification, since the identification algorithms does not need to re-execute numerical integration for each computation cycle. He also use Newton's Raphson method to modify non-linearity of the wheel-terrain interaction for high accuracy and rapid convergence identification of the soil unknown parameters.

The soil parameters of interest in his work was cohesion, angle of internal resistance, shear deformation and pressure-sinkage coefficient of the terrain. He noted also the Newton's Raphoson method can be used to measure noise and initial conditions of the interaction. He uses the identified unknown soil parameters to predict wheel drive torque and drawbar pull for traversing unknown terrain [32].

On the work of L.E. Ray (2008), uses proprioceptive sensors to estimate physical and empirical terrain parameters for a given terrain model based on Bayesian approach using rigid-wheel terrain model developed by Bekker. The methodology used does not need to assume the underlying semi-empirical or physical-based vehicle-terrain model.Net traction forces and resistive torque against slip generated at the contact was estimated first, resistance and thrust of terrain to the wheel was estimated based on the first estimation values of the terrain parameters taking into account the assumption of the robot dynamics and stress distribution on the contact between terrain and wheel.

The trafficability of the terrain was inferred based on the estimated parameters. The methodology considered mathematical uniqueness for sufficient unique mapping of the terrain parameters and the vehicle dynamical forces generated during interaction. Finally she uses the Bayesian multiple-model to encounter the weakness of the uniqueness mapping of the first estimates approach [79].

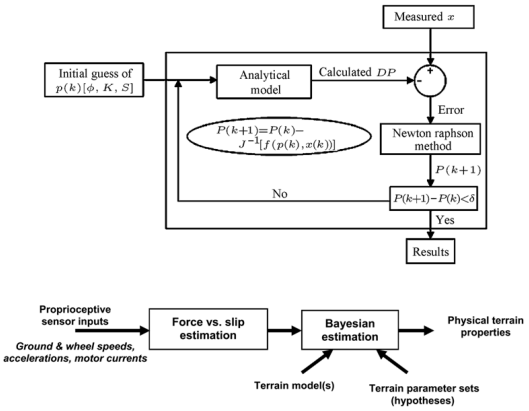

Figure 2.7: *Newton Raphson's Method and Bayesian hypothesis approach [79].*

Also the empirical method primarily developed by the US Army Waterways Experiment Station(WES) to asses vehicle mobility on a go/not go basis, and it was based on the measured index as cone index and mobility index and the soil strength parameters which were obtained experimentally. The traction performance were predicted using computational calculation, while the motion resistance calculated by integrating the horizontal component of the soil pressure in the contact path and the overall traction was calculated from the relationship between shear stress and slip displacement of the soil [20, 87].

Krenn and Hirzinger (2009) modelled simulation tool called Soil Contact Model (SCM). The soil model is a collection of quadrilateral grids in which realisation of contact and computation of force, pressure and torques starts by computation of soil sinkage. Sinkage was realised by analysing displacement of each grid nodes of the soil surface with respective vertical height employed in so called Digital Elevation Model(DEM) with regular space. Area of the contact was computed as the integral sum of the grid areas.

The contact body such as wheel was modelled ordinary polygonal mesh by defining its outer surface by faces and vertices. Using Bekker's semi-empirical formula that relates sinkage, cohesion modulus, internal friction modulus, sinkage exponent and contact width employed in the solver then the contact pressure was realised. The soil

properties depends on Bekker soil parameters and they did not explicitly defined the soil bulk density because it is implicitly included in Bekker soil parameters [45,46,83].

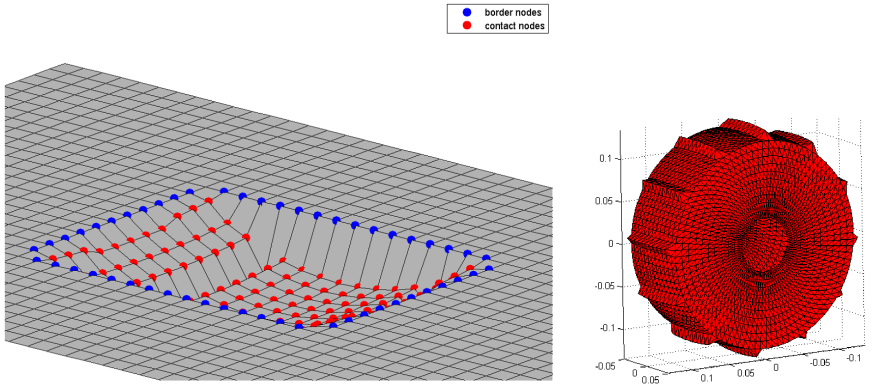

(a) *SCM soil with integrated footprint* **(b)** *SCM polygonal contact body*

Figure 2.8: *SCM soil model and contact body [46]*

The model has been validated with experimental bevameter and ExoMars rover results and the results has good agreements with experimental results and this shows high capability of the model in contact dynamics simulation. Although the model represented well the effects like bulldozing, multi-pass, lateral ruts guidance, but the soil grids are limited to quadrilateral grids only and contact body parameters such as mass and inertia does not included in the SCM parameters.

Krenn, Hirzinger and Gibbesch (2008) they used PCM (polygonal contact model) and SCM (soft contact model) models in multi-body simulation tool to simulates rover in hard obstacles and soft terrain environment. Simulation model was developed on the effort of chassis design and dimensioning phase of planetary rovers based on the analysis of actuator power to be installed in rover drivers. In multi-pass configuration simulation results shown that follower wheel experiences lower motion resistance than leading wheel due to soil compaction. These results shows applicability of model to rover wheel drive design and multi-pass effects analysis [44].

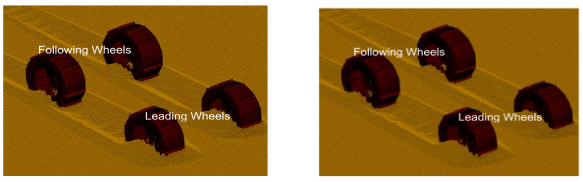

(a) *rover on rocky terrain* **(b)** *wheel configuration for multi-pass analysis*

Figure 2.9: *rover on rocky and soft terrains [44]*

Gallina A (2015) uses SCM (soft contact model) model developed at DLR [46] to study effects of soil parameters uncertainty to prediction of interaction based on probabilistic and non-probabilistic rover position estimates. He carries out experimental tests and numerical simulation of rover for the study. Experimental test was to measure a range of variations of soil properties and rover reference path which has to be compared

to simulation results to analyse effects of uncertainty to soil parameters in interaction prediction.

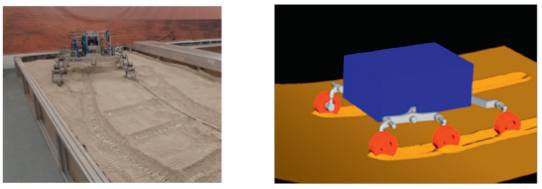

(a) *rover experimental model* **(b)** *rover simulation model*

Figure 2.10: *Simulation and experimental rovers [24]*

Based on the results of three analysing methods, the study shows large uncertainty in rover position due to uncertainty to soil properties. For this results, uncertainty to interaction simulation has to be taken into consideration for better prediction results and proper decision making during interaction for deformable terrain. In particular interval and fuzzy analyses has to be utilised in uncertainty studies due to their promising results shown in his study [24].

In his proceeding work (2016) Gallina A, uses his techniques to treat uncertainty of soil parameters to reduce its effects in interaction for accuracy rover position prediction. He also proposed Bayesian approach based on his analysis for off-line soil parameters estimation for use in on-board measured data for post processing [25].

Gibbesch A (2010), developed a multi-body simulation tools to simulate dynamical performance of rovers typically in rough and sloped terrains based on effort for design optimisation and configuration evaluation. He uses polygonal contact model (PCM) for hard soil and soft contact model (SCM) for soft soil terrains [31,46]. In his results analysis the tools shows good correlation and they can be used for planning, performance prediction, stability analysis and design support of complete mechanical system bases on actuator trade of power-train design [26].

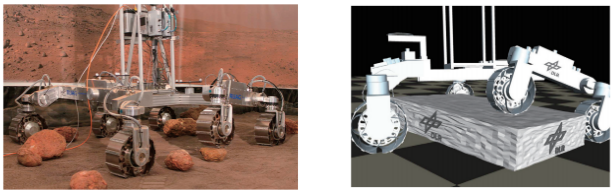

(a) *ExoMars laboratory rover* **(b)** *ExoMars simulation rover*

Figure 2.11: *Rover's simulation and laboratory environments [26]*

Lichtenheldt R (2013) he modelled soil interaction model for planetary locomotion simulations. As the shear strength of granular matter strongly depends on interparticle friction and rotation, the model extended DEM approach to account the effects of particles shapes, geometry in rotational, relocation and resulting plastic deformation. Shape of particles in his formulation was based on the spherical for contact detection and additional two dimension rectangular shape for rotational resistive around particles local

axis. This approach leads less inter-particle contacts as well computational effort improvement as compared to clumped spherical or single polygonal shaped particles [54].

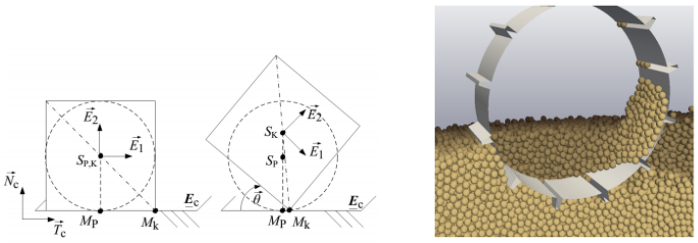

(a) *Mapping spherical grains rolling resistance*

(b) *Simulation wheel on granular terrain*

Figure 2.12: *Spherical grains mapping and simulation wheel on granular terrain [54]*

Since formulation is direction dependent elongation of the particles, it was capable to reproduce anisotropic rolling behaviour. In order to cover arbitrarily shaped particles, he introduced particle dimension aspect ration angle and rotational plane was defined for each axis of rotation. The model was capable to simulates the effect of grousers, formation of bumps from displaced soil and soil flow into the open geometry of the wheel on locomotion performance of rover wheel [54].

2.1 Tire-soil interaction

The interactions of tire and deformable soil have been studied since 1960s and the successful models have also been developed [37, 71, 87]. The first proposed and developed model was based on Bekker and Coulomb equations. The equations were mainly to calculate the normal pressure and shear stress in the soil beneath the tire-soil contact respectively [37, 71, 87].

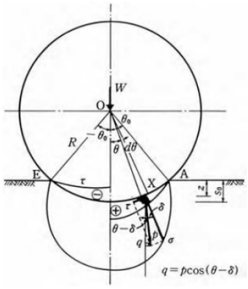

Figure 2.13: *stress distribution at the contact patch, wheel at rest [71].*

The Bekker equation allows computing of the normal pressure σ as a function of sinkage z as shown in the equation below.

$$\sigma = (\frac{k_c}{b} + k_\phi) \tag{2.1}$$

Where b is the tire width and the parameters k_c,k_ϕ and n are associated to the soil properties and can be determined by using a dynamic plate loading tests.

Also the shear stress can be calculated by using the Coulomb equation which later modified according to Janosi and Hanamoto work to take into account the shear displacement of the soil as shown in the equation below [38, 71].

$$\tau = [k_{cohesion} + sin(\phi)\tau].(1 - e^{\frac{j}{k}}) \tag{2.2}$$

Where k, j are the soil shear deformation and displacement parameters, while $k_{cohesion}$ and ϕ are the cohesion and internal shear resistance angle of the soil respectively.

Taking into consideration the case of wheel at driving state, the distribution of slippage can be represented as in figure 2.14 below, although the amount of slippage beneath the wheel is symmetrical, the non-symmetry stress distribution must be accounted and applying the same procedure for analysis as the wheel at rest state.

For the case of wheel at rest state, due to the axle load W the soil develops reaction force at the contact, which is the product of the symmetrical distribution of the normal stress σ and shear stress τ. In order to create zero torque at rest state of the wheel due to shear resistance, the sign of the shear stress between two sides of the symmetrical distribution should be reversed in the left side.

The resultant pressure p due to normal and shear stresses at an arbitrary point X of the contact surface, which inclined at an angle δ, the inclination of resultant pressure can be calculated using the formula 2.3.

$$\delta = arctan(\frac{\tau}{\sigma}) \tag{2.3}$$

In order to take into account the modulus of stress at the arbitrary point X it is necessary to estimate the sinkage z and slippage j_θ at that point. The amount of wheel sinkage can be calculated taking the angle of half the symmetrical distribution of the stress, in which is θ_0 as shown in figure 2.13 above. Therefore, sinkage of the wheel can be calculated from the equation 2.4, while the slip displacement can be calculated using the equation 2.5 given below.

$$z = [cos(\theta) - cos(\theta_0)] \tag{2.4}$$

$$j_0 = R[\theta_0 - sin(\theta)]\frac{\theta_0 - \theta}{\theta_0} \tag{2.5}$$

Where θ_0, θ and R are the half an angle subtended by the contact, angle subtended by the contact point X and the radius of the wheel respectively.

The vertical component of the resulting stress $q(\theta)$ can be calculated from Bekker 2.1 above, and the resulting stress $p(\theta)$ can be calculated using 2.6 below.

$$p(\theta) = \frac{q(\theta)}{cos(\theta - \delta)} \tag{2.6}$$

By substituting the values of vertical component reaction $q(\theta)$ in expressed from Bekker equation above, the equation 2.7 that relates resulting stress and sinkage of the wheel is obtained as shown below.

$$p(\theta) = (\frac{k_c}{b} + k_\phi)\frac{z^n}{cos(\theta - \delta)} \tag{2.7}$$

The equations can be used to calculate the stress at the interface between the tire and soil as a function of the sinkage, meanwhile, it is necessary to state some hypothesis of the shape of the patch or by considering the equilibrium of each tire points.

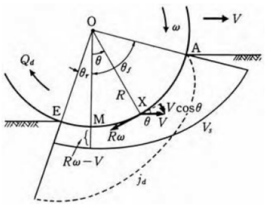

Figure 2.14: *Slippage distribution under the rigid wheel at driving state [71].*

There is a slippage between the tire and the soil at an arbitrary point X of the contact and amount of slippage j_d which results from the integration of slip velocity V_s can be expressed by the equation below.

$$j_d = R\int_0^t \omega[1-(1-s_d)cos(\theta)]dt \tag{2.8}$$

$$= R\int_\theta^{\theta_f} \omega[1-(1-s_d)cos(\theta)]d\theta$$

$$= R\omega[\theta_f - \theta - (1-s_d)(sin(\theta_f) - sin(\theta)]$$

$$V_s = R\omega - Vcos(\theta) \tag{2.9}$$

$$s_d = 1 - \frac{V}{R\omega} \tag{2.10}$$

$$V_s = R\omega[1-(1-s_d)cos(\theta)] \tag{2.11}$$

Where ω and V are the angular velocity and forward speed of the wheel respectively, and θ is the central angle of the contact point X.

Taking the integration of slip velocity given in equation 2.9 above, from the beginning of the contact to the instant time t which can be solved as a function of the central angle θ of the contact patch it is possible to calculate the amount of slippage as from previously equation 2.8 and its distribution is as shown in figure 2.14.

The sinkage required to account for the vertical component of the resultant stress $p(\theta)$, can be calculated as the length of the vertical component of the trajectory of a point on the peripherical surface of the wheel during the contact with the soil. The trajectory of this peripherical surface is as shown in the figure 2.15 below at driving state of the wheel.

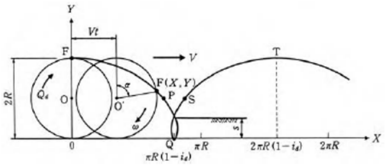

Figure 2.15: *The trajectory point F on the peripherical surface of the wheel at driving state [71].*

The length of the trajectory shown in figure above of the rolling locus of a point on the peripherical surface of the wheel can be calculated using the equation 2.12, where the trajectory is integrated from the beginning of the contact at point a to point b.

$$l(\theta) = \int_a^b \sqrt{1 - (\frac{dY}{dX})^2} dX \tag{2.12}$$

The coordinates of a point on the peripherical surface of the wheel are the coordinates of a point on a trochoid curve, and their values are expressed as in equations below which makes possible to express the derivative as shown below.

$$X = \frac{V\alpha}{\omega} + Rsin(\alpha) = R[\alpha(1 - s_d) + sin(\alpha)] \tag{2.13}$$

$$Y = R[1 + cos(\alpha)] \tag{2.14}$$

$$\frac{dY}{dX} = -\frac{sin(\alpha)}{1 - s_d + cos(\alpha)} \tag{2.15}$$

After changing the integration domain from the abscissa of the trajectory X to the rotation angle α of the wheel, the travelled length of the trajectory can be calculated from the equations below.

$$l(\theta) = \int_{\alpha_f}^{\alpha} \sqrt{1 + [-\frac{sin(\alpha)}{1 - s_d + cos(\alpha)}]^2}.R[1 - s_d + cos(\alpha)]d\alpha \tag{2.16}$$

The vertical component can be evaluated as in previous equations before and after the maximum sinkage point.

For

$$\theta_max \leq \theta \leq \theta_f q(\theta) = k_1 \zeta [d(\theta)]_1^n$$

$$-\theta_r \leq \theta \leq \theta_m axq(\theta) = k_1 \zeta [d(\theta)]_1^n + k_2 \zeta [d(theta_m ax) - d(\theta)]_2^n$$

The coefficients k_1 and k_2 are the soil behaviour parameters before and after reaching the maximum sinkage, and can be calculated from the equations 2.172.18.

$$k_1 = (\frac{k_{c,1}}{b} + k_{\theta,1}) \tag{2.17}$$

$$k_2 = (\frac{k_{c,2}}{b} + k_{\theta,2}) \tag{2.18}$$

Where $k_(c, 1)$, $k_(, 1)$, $k_(c, 2)$ and $k_(, 2)$ are Bekker equation coefficients and can be obtained from a dynamic plate loading test, as well the coefficient ζ.

Therefore, the resulting stress $p(\theta)$ can now be calculated from the following equations.

$$p(\theta) = \frac{q(\theta)}{cos(\zeta + \theta - \delta)} \tag{2.19}$$

$$\zeta = arctan(\frac{T_d}{W}) \tag{2.20}$$

Where δ, θ, and ζ are the angle between shear and normal stresses, the centre angle, and the angle between the longitudinal force and the normal load W respectively.

The early equations by Bekker and Coulomb equations were subsequently modified by other researchers to account for other factors in order to improve the estimation of the terrain and interaction parameters. The details of the modifications of the equations and how they are used to improve parameters and behaviour estimation are detailed in chapter 3 of this work.

According to classical terramechanics theories, three states of the tire-soil interaction has to be considered in the analysis and prediction of the parameters and behaviour of interest. These states are wheel in braking, driving and rest respectively. In this work the focus is on the rest state for static sinkage evaluation and driving state of the wheel since the engine mode in chrono::engine model gives constant angular speed to the wheel from its initial static sinkage and registers the output resisting torque due to interaction motion resistance.

2.2 Field and Laboratory Experimental Tests

Besides the facts that, many research works have been carried out which tries to model the interaction of the tire and soil in both analytical and numerical approaches, different experimental tests have been carried out and reported in this field of research, in particular focusing the stresses distribution at the contact patch, which have strong influence in the soil compaction, traction, sinkage and vibration transmission [71].

In the work carried out by G. Botta (2008, 2012), to analyse the influence of the soil state in the interaction of the tyre and soil by testing three different interaction conditions in the soil states: direct sowing, seedbed and ploughing soil conditions. The analysis and comparison between these three conditions carried out proves that the residual bulk density of the top soil and tyre sinkage affects largely the loose soil, which leads to high motion resistance and soil compaction [7, 8].

Different experimental test was focused on the measured bulk density of the soil and cone index, after the tyre passed on the soil, this bulk density has strong impact to the roots growth of the plants. The effects of the compaction on the sub-soil and top-soil are different and compared at different factors, when the ground pressure increases it affects mostly the top soil by increasing the bulky density, while in the sub-soil the compaction is mostly affected by the wheel dynamical loads, although this result was partially opposed by the work of Arvidsson and Keller by their finding that, neither of both tyre inflation pressure and wheel load are the functions of the top and sub-soil stresses respectively [4, 105].

Although a low inflation pressure reduce the tyre life span, decreasing the inflation pressure reduces the effects on soil physical properties which proves that the ground pressure caused by tire print and wheel load is quiet affected by inflation pressure [4,9]. Lowering inflation pressure and increasing the tyre size, reduces the magnitude of the soil bulky density and cone index values, which proves that the sub-soil compaction does not depends on the vehicle ground pressure, instead influences the top-soil compaction levels [71].

This has been also agreed by the work of Smerda and Cupera (2010), on their study of the influence of the tyre inflation pressure on the drawbar pull, providing that the reduction of the rolling resistance and physical degradation of the loose soil will be influenced by increasing the contact area between the tyre and the ground [93].

Soil displacement occurring due to wheel passages on loose soil plays an important role in interaction problem to analyse effects of soil destruction resulted from tyre-soil interaction [71]. The displacement of the loose soil was also addressed by the work of T. R. Way (2005),by observing that the loose soil compressed in vertical and longitudinal directions and elongates in lateral direction, this is not accounted in the soil bulky density changes information and therefore, soil bulky density information only may not be enough to express the strain beneath the tyre [103].

Furthermore, the distribution shape of the normal and shear stresses of the tyre contact patch largely depends on the tyre configuration parameters (size, wheel load, stiffness and slip), soil conditions and operational conditions of the ground vehicle. The distribution of the normal stress is not uniform with high inflation pressure tyres since the maximum soil stress occurs in front of the contact patch near the center line of the wheel, where as with low inflation pressure tyres, the distribution of the stress is uniform in the contact patch [71].

The effects of the plastic flow on soft soil like clay under the tyre occurs when there are the rapid increase of shear and normal stresses and diminishes immediately after reaching the maximum value, which is different in the hard clay soil where the soil stress distribution is uniform as in loam sand [74].

Vibration transmission is one of the aspect of the interaction problem, this is because the vibration transited from the soil to the driver seat must be minimum or to the tolerable value of the human being for the comfort driving effects to the vehicle operator. Some of the study carried out at different inflation pressure of the tyre to study the influence of the tyre to the vibration transmission on the road and loam sandy, shows that the vibration transmitted is largely influenced by the lugs and tyre eccentricity since they are main excitation factors of the vibration [73]. The eccentricity of the tyre strongly affects the wheel load variations at the first harmonics of the excitation frequency, decrease in tyre inflation pressure and the increase of the forward speed of the off-road vehicle. The effects is more largely when the vehicle moves on the soft loam sandy than in hard sandy [71,73]

Based on the careful review of the state-of-art, it has been noted that there is a growing research interest in realistically and accurately estimating both terrain and interaction parameters and behaviour of tire-soil interaction using simulation tools. In fact, the rising capacity of the computer has led to more complex approaches both in the Finite Element Method (FEM) and in the Discrete Element Method (DEM) thus allowing to simulate tire-soil interaction at a scale that was previously considered less possible or

almost impossible [21, 65, 67, 113]. Still a general model which account for both continuous and discontinuous deformability of terrain and discreteness representation of the terrain is missing or less utilised [12, 21, 29, 65, 109, 113].

Despite the fact that, there are useful results and understandings of underlying phenomena of tire-terrain interaction, there should be further improvements to accurately address discontinuous deformability of the terrain which rise the phenomena such as build up, slip sinkage, cleaning and bulldozing effects on deformable terrain for off-road applications [65, 71]. Therefore, an appropriate approach to tire-soil interaction problem modelling that accounts for these phenomena is still searched for. A discrete (particle based) rather than a continuous approach seems more promising due to the discontinuity of the phenomena to be investigated and for this became the push factor to the main objective of this research work. The comprehensive increase of the knowledge and skills of the tire-soil interaction problem in order to state and develop the appropriate tool or model for the accurate, proper and realistically modelling of the interaction, was concretized by the experimental tests and analysis review from different research works presented in this section.

2.3 Innovative Features with respect to state-of-the-art

Estimation of static sinkage, slip sinkage, slip ratio and slip velocity are of prime importance in the prediction and evaluation of the running wheel and vehicle performance in deformable terrain [11, 64, 80]. Estimation of the above interaction parameters are based on the terrain response to the applied load of the wheel and applied tractive effort, while estimation of the static and slip sinkage of the wheel gives pressure-sinkage relationship, while estimation of the slip ratio, slip velocity gives the shear stress-shear displacement relationship which are both of prime importance to the evaluation and prediction of traction performance for off-road vehicles [16, 64, 106].

Furthermore, the terrain response in repetitive loading (multi-pass effect) should be correctly estimated to realistically predict off-road vehicle performance and soil compaction or soil failure, which is based on the correct estimation of wheel static sinkage, slip sinkage, slip ratio and slip velocity under different soil characteristics and tire design parameters [106]. Proper prediction of the interaction parameters are valuable indicators of the terrain soil composition [51, 80, 82], not only in better planning and design of the off-road vehicles but also useful for control scheme strategies and algorithms planning for autonomous wheeled robot for safely terrain traverse ability and reduction of odometric errors in exploration mission [11, 34, 80, 106, 107].

Moreover, terrain identification algorithms and mobility analysis can be inferred by the absolute sinkage estimation [11, 80]. Application of the above methods in practical is very complex and mostly suites for accurate dynamical model and feature identification for tracking algorithms [11]. Being the facts that terrain is not a continuous plain surface and deforms in discreteness during interaction, then particle approach model is more attractive and focus on more accurate prediction of interaction behaviour for deformable terrains [3, 62, 99], chrono model to be developed reflect to real terrain since terrain is assemblage of frictional colliding rigid bodies (like sand particles) [2, 62, 78, 99] and deformation of particles reflect also to discreteness.

Little research has addressed the problem of slip ratio, static and slip sinkage mea-

surement or estimation in this research field [82]. In previous studies, estimation of sinkage is based on the method of measuring change in an articulated suspension configuration for odometer reading improvement and determining the sinkage of wheels relative to one another [11]. Other researcher described an online visual sinkage estimation algorithm that relied on the analysis of grey scale intensity along the wheel rim by differentiating the wheel and terrain colours, the method is simple and efficient but very sensitive to light intensity variations [11, 51, 80, 82]. The method presented in the work [80, 82] based on detection and estimating the ill-effects of wheel-terrain interaction which considers only the longitudinal dynamics of the wheel and neglect the effect of lateral dynamics effects like surcharge due to bulldozing effect [80].

The mechanics of interaction between wheel and terrain has been studied since decades in terramechanics field of research, and there have been a lot of researches devoted to the wheel-terrain interaction [37]. The difficulty faced in navigating mobile robots and other off-road vehicles with complex drive dynamics, high deform-ability and slip sinkage over challenging terrains that covered by a mix of rock exposures and high deformable soils has highlighted the importance of developing accurate simulation tools for use in a predictive mobility, discreteness of terrain, interaction parameter estimation, modelling and design of both the vehicle and its elements such as tyres that contributes in the interaction [35]. Discrete Element Method (DEM) approach is relatively useful for an analysis of flexible wheel on deformable terrain and resulted to better estimation of interaction and terrain parameters, but left behind the effects of discontinuous deformation of terrain such as, build-up, cleaning and bulldozing effects.

Although DEM approach requires high computational effort to handle the collision of large number of elements in wheel-terrain interaction [37, 107] but also shows a promising soil interaction and terrain parameters estimation, chrono model employs DEM methodology in contact and collision detection while dynamics of wheel and vehicle are handled in rigid objects, this ensures improvements in computational effort and simulation time [2, 62, 99]. Chrono model handles particles in different shapes, such as spheres, squares, tetrahedral and convex hulls, this also improves interlocking mechanism and rotational behaviour of terrain particles [62, 99], since soil shear strength strongly influenced by inter-particle friction and rotation [54]. Also this model employs mass/size distribution probability of particles, this ensures improvements of particles packing and gives a good compromise of terrain void ratios, bulky density and strength [49, 100].

Modified version of original semi-empirical soft contact model (SCM) [46] has been integrated in the interaction model. This version extended to take into account different mesh such triangular, height-map and regular tiled mesh for computational effort and simulation time improvements. Mesh automatic refinement resolution can be selected according to user requirements, low mesh refinement values ensures accuracy but for the sake of computational time. The model developed in [46] only the dimension of the contact body was taken into account and left behind its mass and inertia, while in chrono model contact object is the rigid wheel in which its mass and inertia has been accounted for in multi-body dynamics.

CHAPTER 3

Tire-terrain interaction model

3.1 Methodological and Strategical Approach

With respect to available FEM/DEM codes, Chrono::Engine allows to consider both continuous and discrete bodies at the same time. Thus, in one single simulation environment, both the longitudinal and lateral deformability of terrain and the discreteness of soil can be accounted for. However, the interaction between these two worlds has to be validated and eventually improved. Thus, while developing the model also specific code properties will have to be critically analysed, fine tuned and eventually improved, thanks to the fact that Chrono::Engine is that it is an open software.

In chrono engine model the contact dynamics employed DEM contact methodology for aasemblage of non-smooth colliding bodies. DEM method was initially developed in early work which aimed for the study of rock mechanics and extended in the proceedings to other fields of engineering such as vehicle-terrain interaction [107].

Basic different of ordinary DEM method and chrono:engine models are their representation of the soil/terrain, where by DEM method represents soil as assemblage of number of discrete elements, while in chrono::engine model represents terrain as assemblage of colliding bodies/particles be it sphere, square or convex hulls. Although chrono::engine employed typical DEM methodology for contact force realisation, but also it adds cohesion, compliance and plasticity in contacting particles by extending original Derivative Variational Inequalities (DVI) formulation method and introducing non-linear stiffness of contact to handle high contact tangential stiffness for simplification of DEM integration [97]. Short-range interactions of particles models as one employed by Johnson-Kendall-Roberts (JKR) and Derjaguin-Muller-Toporov (DMT) are modelled as non-linear forces acting between particles. This leads to the ability of the model to handle two major difficulties for cohesive contact which are high tangential stiffness and dissipative nature. High tangential stiffness leads to stiff yet smooth

contact which can be solved with ODEs and implicit integration while the second difficulty fits to DVI context [97].

When irreversible breaking of contact bond happen between contacting particles, contact force between them may depend on loading trend, and original DVI contact model is modified to handle material flow which leads to plasticization. Cohesion force can withstand tension up to limit value and beyond that plastic flow will exist and leads to simple plasticization in this phenomenon is versatile when compliance is added to the contact. Hardening and softening of contact plasticity is characterised in the a general DVI model by introducing tangential effects of contact such as friction [97]. For these reasons made chrono::engine to be more powerful to handle non-smooth contact as compared to ordinary DEM methodology by modification on original DVI to account contact cohesion, plasticity and compliance and this leads to account behaviours of terrain such as plastic or elastic medium [107]. Detailed normal and tangential forces realisation in chrono model has been explained in section **??**.

Once the model has been set-up and the influence of the various code features assessed, tested and validated, experimental tests with dynamometric hubs will be carried out. Besides measuring the forces at the hub, also high speed cameras will be used to assess build up phenomena and laser scanners to have a quantitative measure of the footprint left on the soil. Results from the simulations and the experiments will be compared and analysed for validation purposes. Finally, to assess the validity of the developed model, critical testing conditions will be searched for and tests will be carried out (e.g. slip-sinkage conditions).

3.2 Terramechanics theories of Terrain Modelling

3.2.1 Terrain as an Elastic and Plastic Medium

Understanding of terrain behaviour under vehicular load is of important to the study of terramechnics. In the past some researchers in this field modelled the terrain as an elastic medium/rigid, perfectly plastic. Modelling the terrain as rigid, perfectly plastic material together with the theory of plastic equilibrium has the application on estimation of the maximum traction, prediction of the forces developed by the lugs of the tire, but still can be applied to the prediction of the terrain soil deformation [106, 107].

Despite, the fact that modelling the terrain as an elastic medium together with the theory of elasticity have been providing the critical basis for the study of soil compaction, but still its application is limited to dense terrain with limited level of vehicular load.The theory of plastic equilibrium can only be applied to the estimation of the maximum vehicular load that can be supported by the terrain without causing failure to it, but cannot be applied to predict the sinkage of the vehicle due to its normal load or the slip of the wheel due to terrain shearing caused by its running gear [106, 107].

Concept of critical state of the soil mechanics have been applied to model the terrain to overcome the limitation of plastic equilibrium theory and it has the capability to predict both stress and strain in the terrain under vehicular load. Given the fact that the terrain material in the field may sometimes behave like non homogeneous, the application of the critical state of the soil mechanics to the tire-soil interaction are sometimes still limited to the non homogeneous situations. Performance of off-road vehicles defined in terms of its motion resistance, tractive effort, drawbar pull, tractive efficiency

is determined by normal and shear stresses beneath the tire soil-interaction [106, 107].

Under certain circumstances, the behaviour of dense terrain such as compact sand may be compared with that of an ideal elasto-plastic medium in terms of stress-strain relationship, that has basically two major parts; elastic behaviour and plastic behaviour. Elastic behaviour is when the vehicular load does not exceed a certain level limit and the corresponding stress is lower than the upper limit and plastic behaviour is when the vehicular load exceed the level limit and the corresponding stress exceed the elastic limit [106, 107].

This idealization of the terrain as elastic medium together with classical theory of elasticity has lead to the prediction of the stress distribution at the contact patch and the assessment of vehicular traffic on soil compaction or terrain failure. Stress distribution in a semi-infinite elastic medium subjected to loading on its surface and for homogeneous and isotropic elastic medium may be predicted.

Under this concept of stress distribution, the stresses in the medium under applied load does not depend on the modulus of elasticity of the material, but only a function of applied load and distance from point of applied load. The Boussineq equation [107] can only be used to predict stresses which are not too close to the point of applied load location because the material in the vicinity of the applied load does not exhibit elastic behaviour [106, 107].

Recently advancement of computer technologies and computational techniques has lead to the successful modelling the terrain as an assemblage of finite elements using Finite Element Method (FEM). The methods has the capability to greater detail to examine certain aspects of physical nature of tire-terrain interactions. However, the development of a robust method for determine the values of the parameters of the finite element model to properly represent the terrain properties remain to be resolved. Furthermore, the finite element method is developed in the sense that the terrain is continuum and it has inherent limitations in simulating large, discontinuous terrain deformation that usually occurs during tire-soil interaction [106, 107].

To overcome the limitation of finite element method in order to study the interaction between a tire and granular terrain, such as sand, Discrete Element Method (DEM) has been introduced with unique features. The development of a reliable method for determining the value of model parameters to realistically represent terrain properties in the field still remain to be resolved. Addition to that, still improvements in computing techniques are needed for full-scale simulation of the vehicle-terrain interaction, which would require millions of discrete elements to represent terrain and high computational time even in super computers [106, 107].

3.2.2 Characteristics of terrain in vehicle loading

A vehicle through its elements applies normal load to the terrain under the applied tractive force of the running gear which results to sinkage, and this in turn causes motion resistance of the wheel. For the case of multi-axle vehicles the terrain is subjected to repetitive loading of the consecutive wheels. In order to predict and estimate the pressure distribution under the contact-patch and the tractive performance of the off-road vehicles, the response of the terrain due to vehicular and repetitive loading must be estimated or measured [106, 107].

Under the classical terramechanics theories, one of the fundamental task in charac-

terisation of the terrain behaviour or response to the loading is by establishing the functional relationships such as stress-strain, pressure-sinkage, shear stress-shear displacement relationships. Since the structure and behaviour of the real terrain varies greatly under various conditions, the characterisation of the terrain response was only based in practical or experimental results and curve fitting to obtain terrain response in question, and the model for estimating the terrain response was less developed [106, 107].

Since one of the key purposes for estimating terrain behaviour was to enable the engineers and researchers in this field to estimates performance of the off-road vehicles in a systematic and convenient manner using mathematical function that relates the vehicle performance and terrain response parameters, the selection of particular function, methods and model to characterise terrain behaviour should be based not only in accuracy of represents terrain response but also its convenient to be integrated in the chosen frame work for predicting the vehicle performance [107].

3.3 Modelling of Tire-Terrain Interaction

Objective

The main objective of this work is to develop a model for the interaction of tire with deformable soil for off-road vehicle applications. The model should be able to give proper and realistically predictions and estimation of interaction and terrain parameters, as well as a thorough understanding of presently un-tackled effects on wheel and vehicle performances such as static sinkage, slip sinkage, build-up and cleaning. Such a model could be of great use in agriculture, cross-country transportation, exploration, construction and off-road vehicle dynamics applications.

Therefore, the specific objectives are:

1. Development of a simulation model that accounts for both the deformability of terrain in longitudinal and lateral as well as the fracture mechanics of soil.

2. Statistical validation of the developed model through comparison with the literature and experimental data.

3. Identification of limit conditions for the model to assess its validity.

4. Identification of design criteria for tires to reduce unwanted phenomena such as sinkage and soil compaction through sensitivity and optimisation analysis.

Modelling of wheel-terrain interaction has been studied since decades in this field of terramechanics. Since then it has been categorised to have two main objectives of the study; one is to establish a functional relationships between the vehicle and vehicle element performance with respect to its design parameters and terrain characteristics; two is to establish procedure to estimates and predict the changes in terrain condition due to passage of off-road vehicles or soil working machinery [107]. These two objectives of the study are of greater interest to the designers, off-road vehicle users, agriculture engineers and construction engineers in the field of agriculture, construction, exploration, cross-country transportation, military applications and exploitation engineering.

In this research work the focus is devoted to establishing the wheel-terrain model for off-road applications as the prime for estimating and predicting both off-road vehicles and tyre performances with respect to design parameters and terrain conditions and soil rheology. In a given terrain, the performance of off-road vehicle to a greater extent depends on the manner in which the vehicle interacts with that terrain. When the vehicle

interacts with the terrain, the results of the interaction parameters between the vehicle element so called wheel and terrain, the normal and shear stresses are developed on the contact patch. Different studies and models developed to study the interaction between the wheel and terrain, it has been shown and proven that this interaction is very complex phenomenon taking into account the dynamics and kinematics of terrain particles behaviour during interaction, which also change with different factors such as environment condition, terrain condition, wheel design and operational parameters [106, 107].

Since the performance of off-road vehicles defined by its motion resistance, tractive effort, drawbar pull, tractive efficiency is determined by the wheel-terrain interface parameters, the fundamental issue in terramechanics is the formulation of mathematical, experimental and even simulation models to predict and estimating interaction parameters based on the knowledge of terrain behaviour, design and operational parameters during interaction. Identifying the design parameters of the tyre that influence wheel-terrain interaction parameters are of greater importance in formulating both mathematical and simulation models for off-road vehicle element study applications. For instance tyre diameter, section width, section height, lugs angle, lugs spacing, lugs height, lugs number are considered to have a varying degrees of influence on the tyre-terrain interaction [106, 107].

A variety of approach methods to study off-road vehicle mobility and performance through wheel-terrain interaction has been developed over the years since then. They range from entirely empirical to highly analytical approach. Selection of the approach methods are greater influenced by factors such as; intended purposes, environmental, economic, and operational constraints. According to classical terramechanics, comparison and evaluation of these approach methods should be made in the context of their intended purposes and constraining factors [106, 107].

Since one of the key purposes for estimating terrain behaviour was to enable the engineers and researchers in this field to estimates performance of the off-road vehicles in a systematic and convenient manner using mathematical function that relates the vehicle performance and terrain response parameters, the selection of particular function, methods and model to characterise terrain behaviour should be based not only in accuracy of representing terrain response but also its convenient for it to be integrated in the chosen frame work for predicting the vehicle performance [106, 107].

Based on careful review of the state-of-art in this field of terramechanics and the application of these approach methods, this research work is devoted to computational approach method based on Discrete Element Method (DEM-C) and Discrete Element Method (DEM-P) methods adopted in an open source powerful multi-physics simulation software so called Chrono::Engine [22, 23, 61, 98].

Despite the fact that, it is intensive computational and require high computational capability computers, but also the rapid progress in advancement of computer technology recently invented in parallel computing technology and availability of computer commercial codes, makes this approach to be implemented in the modelling and analysis of the wheel-terrain interaction [98, 107]. This approach method has the potential of providing a tool with which aspects of mechanics of wheel-terrain interaction can be examined in details such as evaluation on relative basis the design and performance of tyres and soil mechanics of simple form engaging in the contact patch [107].

This approach method in chrono::engine has the capability of simulating both con-

tinuous and discontinuous deformation of the terrain which often occurs in off-road operations and give rise to the effects such as build-up and cleaning during wheel-soil interaction, and also overcome the limitation of the finite element method (FEM). Figure 3.1 below graphically explains the differences between FEM/DEM and Chrono::Engine approaches for tire-soil interaction. The red highlighted boxes are main key interaction performance effects which has to be addressed by proposed chrono::engine model, these are the major weaknesses for current tire-soil interaction simulation models.

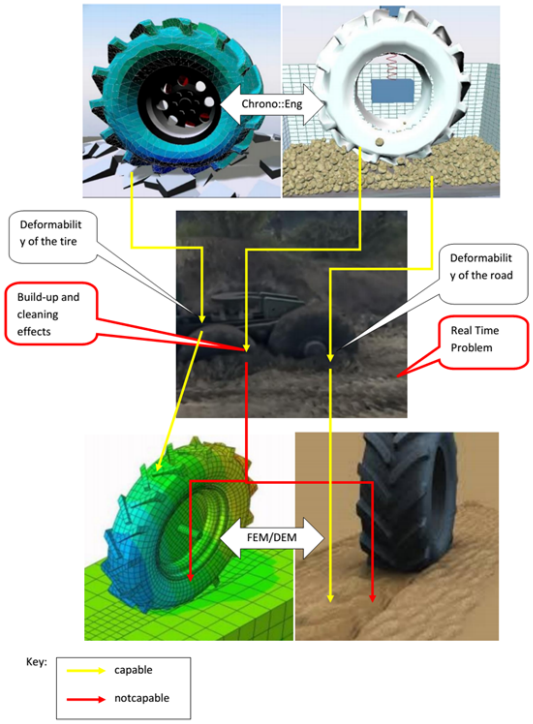

Figure 3.1: *fem/dem and chrono::engine tire-soil model.*

3.3.1 Chrono::Engine Terrain Modelling

Granular terrain

Contact and collision behaviour (DEM-C/DEM-P)

An understanding of terrain behaviour under wheel interaction load is of greater importance to the study and modelling of wheel-terrain interaction. As stipulated previously, this work is based on the approach method of modelling the terrain as both continuous and discontinuous through particle creation/assemblage adopted in chrono::engine. The method simply adopted the methodology of DEM-P and DEM-C to estimate and calculates the contact force between particle to particle and between wheel to particles [22, 23, 61, 98].

The basic concept approach method in chrono tire-soil interaction modelling; is that the terrain is modelled as the assemblage of the rigid colliding particles, here the shape of particles is spherical with specified collision shapes, surface quality and particle parameters such as density, size. By this idealization it is made possible to analyse the characteristics and behaviour of wheel-soil interaction by examining the mechanics of

interaction both between the wheel and adjacent particles and between colliding particles. Particles in contact with the wheel surface receives contact force from the wheel and transmit this load to adjacent colliding particles, and due to presence of the colliding surface property (friction) the contact forces (normal, tangential) between colliding particles are realised. The magnitude of the contact tangential force is realised from the deformation (relative displacement) of contacting particles with friction surface (specific friction coefficient) [98].

The particle approach method in its basic form assumes that the contact points has contact forces in both normal and tangential directions, characterised by the friction coefficient and contact load of the interaction. Between the wheel and contacted elements on the wheel surface it is assumed that the friction exist in tangential direction to the wheel circumference characterised by the same coefficient of friction [107]. The adhesion of the particles in contact is taken into consideration by adding the impulse force between the contact in each time intervals (step time) of simulation. Chrono calculates collision/contact behaviour by penalty (DEM-P) and complementarity methodology (DEM-C) conditions by considering small interpenetration of the contact points and enforcing non-penetration of the particles that come in mutual contact respectively. These methods ensure high accuracy of the contact force estimation in chrono::engine modelling [98].

To determine occurrence of the contact between the wheel surface and adjacent particles or between particles, their geometrical relationships are examined and if the distance between the wheel surface and the centre of an adjacent particle is less than the radius of the particle, this means that the contact has been established. On the other hand, if the distance between the centres of two particles is less than the sum of the radii of these two particles, means that the contact occurred. The position of each particle is determined step by step at specified step time and position and contact forces on each particle determine the motion of the particle [98].

Average incremental displacements are taken during each time step with respect to previous step in order to enhance the stability of the contact solution. By repeating the above procedures for all particles involved and over the duration specified during simulation, the interaction forces on the wheel-soil interface is determined and the movements of the soil particles in the wheel-soil interaction can be identified. Usually the solution process is initiated by wheel-soil system weight, angular motion (engine mode) and specified friction coefficient and cohesion force.

Normal and Tangential Contact forces

The dynamics of terrain composed of rigid particles is characterized by a system of Differential Algebraic Equations (DAEs) [98] as shown in the equations below.

$$\dot{q} = L(q)v \tag{3.1}$$

$$M(q)\dot{v} = f(t,q,v) - g_q^T(q,t)\hat{\lambda} + \sum_{i \in A(q,\delta)} \underbrace{\hat{\gamma}_{i,n} D_{i,n} + \hat{\gamma}_{i,u} D_{i,u} + \hat{\gamma}_{i,w} D_{i,w}} \tag{3.2}$$

$$0 = g(q,t) \tag{3.3}$$

$$i \in A(q(t)) : \begin{cases} 0 \leq \phi_i(q) \perp \hat{\gamma}_{i,n} \geq 0 \\ \hat{\gamma}_{i,u}, \hat{\gamma}_{i,w} = \sqrt{\frac{argmin}{\tilde{\gamma}_{i,u}^2 + \tilde{\gamma}_{i,w}^2}} \leq \mu_i \hat{\gamma}_{i,n} \quad v^T(\hat{\gamma}_{i,u} D_{i,u} + \hat{\gamma}_{i,w} D_{i,w}) \end{cases} \tag{3.4}$$

The differential equation 3.1 relates the time derivative of the generalized position q and velocity v through a linear transformation defined by $L(q)$. In order to balance forces,the equation 3.2 ties the inertia force to the applied and constraints forces which defined by $f(t, q, v)$ and $-g_q^T(q, t)\lambda$ respectively. The later are imposed by bilateral constraints that restrict the relative motion of the interacting rigid particles such as spheres in the soil-bin-wheel system. These bilateral constraints, which lead to, can be augmented by unilateral constraints associated with contact phenomena. To that extent, the concept of equations of motion is extended to employ differential inclusions [98]. The inclusion states that the frictional contact force lies somewhere inside the friction cone, with a value yet to be determined and controlled by the stick/slip state of the interaction between particle to particle and wheel to particle. In MBD the differential inclusion can be posed as a differential variational inequality problem, which brings along the last term of equation 3.2 and equation 3.4 [98].

In the case of interaction a set of contact complimentarity conditions are defined by unilateral constraints $0 \leq \phi_i(q) \perp \hat{\gamma}_{i,n} \geq 0$ for a simple potential contact i in that active set $i \in A(q(t))$, either the gap ϕ_i between two contact geometries is zero and consequently the normal contact force given by term $\hat{\gamma}_{i,n}$ is greater than zero or vice versa. The last equation poses an optimization problem whose first order Karush-Kuhn-Tucker optimality conditions are equivalent to the Coulomb dry friction model [95]. The frictional contact force associated with contact i leads to a set of generalized forces, shown last term of equation 3.2 and equation 3.4 [2,10,28,39,94,98], which are obtained using the projectors $D_{(i,n)}$, $D_{(i,u)}$ and $D_{(i,\omega)}$ [3,98].

The modelling methodology outlined above has been used in Chrono to analyze the dynamics of large multi-body systems and granular material in a so called Discrete Element Method (DEM) framework. Since the methodology uses complementarity (C) conditions to enforce non-penetration of the discrete elements that come in mutual contact, this method is called DEM-C. This differentiates it from DEM-P, a penalty (P) based methodology that is also implemented in Chrono and which accounts for the partial deformation of the bodies in mutual contact [98].

When using the DEM-P approach, or soft-body approach, Chrono regards the contacting bodies are 'soft' in the sense that they are allowed to 'overlap' before a corrective contact force is applied at the point of contact. Once such an overlap δ_n is detected, by any one of a number of contact algorithms, contact force vectors F_n and F_t, which are normal and tangential to the contact plane at the point of contact respectively are calculated using various constitutive laws based on the local body deformation at the point of contact [47,48,59]. In the contact-normal direction, n, this local body deformation is defined as the penetration (overlap) of the two quasi-rigid bodies, $u_n = \delta_n n$. In the contact tangential direction, the deformation is defined as a vector u_t that tracks the total tangential displacement of the initial contact points on the two quasi-rigid bodies, projected onto the current contact plane. DEM-P contact constitutive law, a slightly modified form of which is used in Chrono, is the following viscoelastic model based on either Hookean or Hertzian contact theory;

$$F_n = f(\bar{R}, \delta_n)(k_n u_n - \gamma_n \bar{m} v_n) \tag{3.5}$$

$$F_t = f(\bar{R}, \delta_n)(-k_t u_t - \gamma_t \bar{m} v_t) \tag{3.6}$$

The overlap of or local contact displacement of interacting bodies can be exressed by the equation 3.7, meaning while the effective mass of the contacting bodies and the effective radius of curvature of the contact can be expressed by equations 3.8 3.9 respectively.

$$u = u_n + u_t \tag{3.7}$$

$$\bar{m} = \frac{m_i m_j}{m_i + m_j} \tag{3.8}$$

$$\bar{R} = \frac{R_i R_j}{R_i + R_j} \tag{3.9}$$

For Hookean contact, the term $f(\bar{R}, \delta_n) = 1$ in equation 3.5, while for Hertzian contact the term $f(\bar{R}, \delta_n)$ can be treated as $f(\bar{R}, \delta_n) = \bar{R}\delta_n$ [59, 92, 98, 112]. The normal and tangential stiffness and damping coefficients k_n, k_t, and γ_t are obtained, through various constitutive laws derived from contact mechanics, such as physically measurable properties for the materials of the contacting bodies, such as Young's modulus, Poisson's ratio, and the coefficient of restitution.

The component of the contact displacement vector u in the contact-normal direction, $u_n = \delta_n n$, is obtained directly from the contact detection algorithm, which provides the magnitude of the 'inter-penetration' δ_n between the bodies. The tangential contact displacement vector u_t is formulated as;

$$u_t = \int_{t_0}^{t} v_t dt - (n \int_{t_0}^{t} v_t dt) n \tag{3.10}$$

where t is the current time and t_0 is the time at the initiation of contact [27, 98]. For the true tangential contact displacement history model, the vector u_t must be stored and updated at each simulation step time for each contact point on a given pair of contacting particles from the time that contact is initiated until that contact is broken.

To enforce the Coulomb friction law, if $|F_t| > \mu |F_n|$ at any given time step, then before the contributions of the contact forces are added to the resultant force and torque on the body, (stored) value of $|u_t|$ is scaled so that $|F_t| = \mu |F_n|$, where μ is the Coulomb (static and sliding) friction coefficient. Once the contact forces F_n and F_t are computed for each contact and their contributions are summed to obtain a resultant force and torque on each body in the system, the time evolution of each body in the system is obtained by integrating the Newton-Euler equations of motion, subject to the Courant-Friedrichs-Lewy (CFL) stability condition, which limits the integration time step-size to $h < h_{crit} \sim \sqrt{m_{min}/k_{max}}$ [76, 98]. For multi-body dynamics with or without frictional contact modelled using a penalty approach, Chrono implements DAE solutions [30, 72, 98]. For handling frictional contact within the differential variational inequality framework, Chrono implements the Nesterov algorithm [61, 98]. Many

bodies dynamics like tyre-terrain interaction involving thousands or even million contacts. In the case of many contacts bodies dynamics, DEM methods like that utilised by chrono::engine methodology which regularised on frictional contacts require small integration time steps with efficiency differential variational inequality (DVI) scheme as compared to FEM methodology [97].

In this case the model introduces the compliance and damping matrices associated in each contact in the simulation to handle plastic and elastic behaviour of terrain. By defining the yield surface for plastic flow in the contacts it is possible to account the cohesion phenomenon in which plasticization feature is added in the model [97].

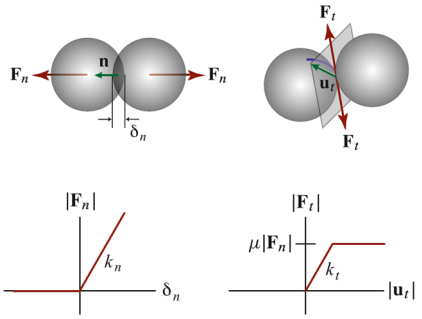

Figure 3.2: *Chrono Rigid Body Contact Penalty Methodology Model [98].*

Compliance

The Hertz-Mindlin linear damping spring which uses two Kelvin-Voigt spring dashpot systems in normal and tangential directions is employed in the model. The types of constitutive laws were posed by restricting the contact flow to the normal component of the contact force $\hat{\gamma}_n$ and the contact distance y_n which satisfies that $y_n \mapsto \hat{\gamma}_n$ figure 3.3. Figure 3.3 a shows that the DVI is a set-valued function where $y_n = 0, \hat{\gamma}_n \in \mathbb{R}^+$. And no penetration is allowed which is equivalent to the complimentarity constraint that satisfies the Signirini contact condition $y_n \geq 0, \langle y_n, \hat{\gamma}_n \rangle = 0$.

While figure 3.3 b describe a typical DEM contact which allowes the penetration depending on a finite stiffness of the contact. When introducing a non-linear stiffness such as figure 3.3 c, DEM code is much less complicated in the simulation when the tangent stiffness is lower, however the higher the tangent stiffness the more the difficult DEM integration. The chrono model employs the DVI method that has both the advantages of DVI and DEM method by extending the original DVI formulation to account for contact compliance while allowing the case of infinite stiffness as the case of figure 3.3 a.

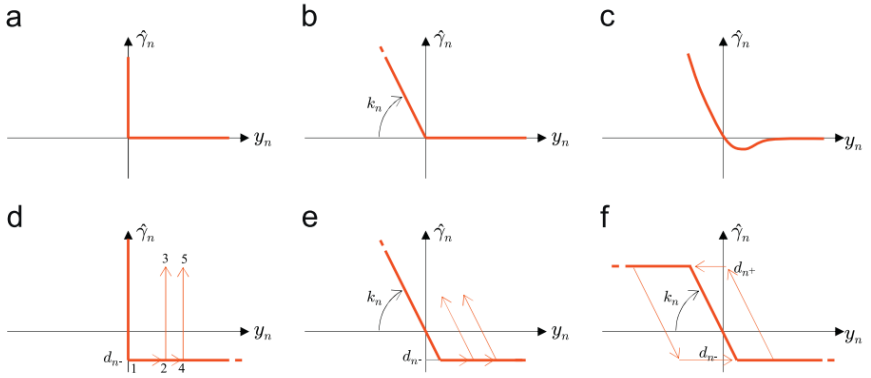

Figure 3.3: *Constitutive relations for contact normal reaction [97].*

Cohesion

Basically, in chrono model the cohesion of the particles is modelled by considering different physical mechanics such as liquid bridges between particles and chemical bonds. This complex physical phenomenon is significantly affect the behaviour of the particles in the terrain model.

In general this short-range interactions are handled as non-linear forces acting between two particles with a negative part in the fourth quadrant of contact flow figure 3.3 c. When the contact has high tangent stiffness or exhibit a dissipative nature, stiff yet smooth contact problem is solved with ODEs and implicit integration which fits in the DVI context.

Plasticity

When the contact exhibit a dissipative nature, the contact force depends on the load history of the contact which is taken in account by the classical mechanism of material flow in continua and micro/mesoscopic phenomenon that cannot be described by linear/non-linear elasticity alone. The contact model is modified to handle plasticization figure 3.3 d, in which when a pulling action is applied to the contact, the contact withstand a cohesion up to 1, after the displacement limit d_n, the plastic flow with constant cohesion will follow and when pushing action happen to the contact the force will go from 2 to 3, following further cycles of points 4 and 5. This plasticization is more versatile when a non-zero compliance is used as in figure 3.3 e.

Also a compression plasticization limit which described in figure 3.3 f can be used. Hardening and softening plasticity is characterised by the tangential effect of contact friction described previously which accommodated in the general DVI setting. These features added to chrono capability ensures that the behaviour of terrain in elastic and plastic medium is handled in the model proposed in this work. Other DVI schemes including the yield surface modelling in chrono contact model are detailed [97].

Yield surfaces

Different shapes of the yield surface along with stiffnes and damping are considered to approximate the physical properties of the contact such as cohesion. However, the simple shapes are considered to reduce the number of dependent parameters which

defined the yield shape for simplicity. The shapes features Coulomb, Mohr-Coulomb, Minkowski and capping for contact friction and cohesion properties [97].

The case depicted in figure 3.4 features Lorentz second order cone of the yield surface.

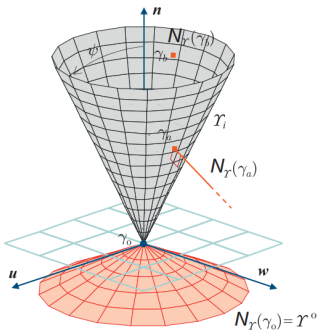

Figure 3.4: *Yield surface for Coulomb friction with associative flow [97].*

In this case , the tangential component of the contact force is forced to be contained in the circle with radius of magnitude of multiple of normal force and the coefficient μ where $\sqrt{(\gamma_u^i)^2 + (\gamma_w^i)^2} \leq \mu\gamma_n^i$. The angle of the cone defined by ϕ is given by the $\phi_c = arctan(\mu)$.

This consideration corresponds to Amotos-Coulomb friction for dry contact except, that sliding motion $\dot{y}_P$ of the yield surface is on the surface of the polar cone Υ^{i0} rather that been horizontal, which cause a dilatancy effect. However, the effect is reduced by stabilization of the cohesion term c^i assuming the stabilization makes the dilatancy to have small finite limit that takes zero values for small sliding speeds defined by h and μ for $h \downarrow 0$ or $\mu \downarrow 0$. Morover, by leaving the sliding motion $\dot{y}_P^{i,l}$ for all timesteps of the simulations, the stabilization term wii take this form; $c^i = (1/h)(y^{i,l})$ [97].

The simplest case is the one depicted in figure 3.5 which defines a cohesion set-valued contact law by introducing a single parameter c in the contact.

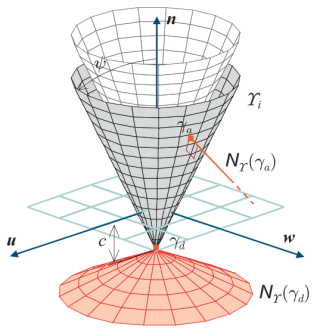

Figure 3.5: *Yield surface for friction and cohesion, inspired by Mohr-Coulomb [97].*

Since the result is still a cone, but has been translated in the vertical axis which makes the contact to withstand a normal pulling impulse to the limit of c, and above that limit, the cohsion contact will drift apart without breaking.

In the case shown in figure 3.6, which shows another alternative of the yield surface whereby the surface is rounded, and this feature a cone in figure 3.5.

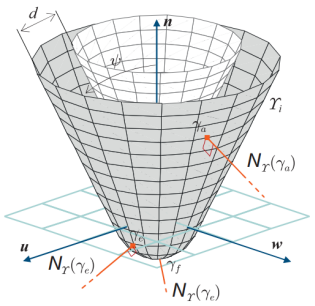

Figure 3.6: *Yield surface as a Minkowski sum of a cone and a ball [97].*

The sliding surface is Minkowski sum of an Amontons-Coulomb friction cone and a simple parameter d is introduced to define the cohesion of the contact. However, the more configurable surface that allowing anisothropy could be featured by introducing an ellipsoid defined by three parameters instead of sphere, but this will make the model to more calibration to be more difficult and also impacts the memory footprint for very large simulations [97].

The last case figure 3.7, shows the addition of parameter r and a simple modification of the approach in figure 3.6, which leads to yield capping.

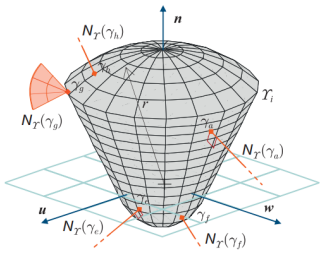

Figure 3.7: *Yield surface with capping for plasticization in compression(crunching) [97].*

Since the yield surface i bounded in the pushing direction, then the contact can withstand plasticization in the compression phase. Finally, taking into consideration of the large simulation that features large numbre of interactions such as tyre-terrain interaction model, the simple yield surface figure 3.43.5 and 3.6 are prefered to the cost of computational effort of the simulations [97].

Particle Size Fractions Distribution

According to soil science, mechanical analysis is the common process for determining the particle size distribution, which comprises with two steps known as dispersion and fractionation [100]. Dispersion involves removal of cementing material (compounds or substances which bind the particles together) to break secondary particles into primary particles or soil separates while fractionation is one which physically separates particles into different size ranges [49].

The common methods of fractionation are sedimentation and sieving, and the choice of an appropriate method depends on the particle size, objectives, and the facilities

available [49]. The later and simple method of sieving is the one adopted in this model by introducing the continuum particle distribution probability method.

Particle Shape and Geometry

Soil particles' shapes often depends on the size, parent material, and degree of weathering and varies widely. Coarse or large particles (e.g. sand and silt fractions) are often angular or zigzag in shape. Angularity reflects degree of weathering, highly angular particles, are less weathered and become rounded with progressive weathering by the grinding action of water and wind [49].

In contrast, clay particles are of plate or tubular shape. Particle shape is determined by micrographs, and may be expressed using two indices measure of roundness and sphericity. Roundness is a measure of the sharpness of the corner, while sphericity is a measure of how closely the particle approaches a sphere. The geometry of particles been it a spherical, cubical or plate-shaped gives important property know as specific surface area which varies with particle size [49, 100].

Packing Arrangement of Particles

Since soil is a heterogenous mixture of solid particles of different sizes and shapes. It is a dynamic mixture, under continuous change due to natural (e.g. climate, biota, gravity) and anthropogenic factors (e.g. ploughing, vehicular traffic). The packing arrangement of soil solids influences soil bulk density, pore size distribution and pore continuity, retention and movement of fluids, and substances contained in them (total porosity may not be affected by the packing arrangement) [49, 100].

These properties are extremely relevant to agricultural, industrial, urban, and other land uses. Understanding the impact of packing arrangements is, therefore, important to developing and identifying systems of soil manipulation to achieve the desired configuration [49, 100]. In this work the particle arrangement is mostly important for the strength, bulk density, stiffness the terrain. In chrono model different arrangements are obtained with the introducing the distribution probability in the particle generator class.

Porosity in particle arrangement

This is one of the particle arrangement configuration property of soil particles, where by the particles are packed either cubic, rhombohedra, orthorhombic and composite configuration. The packing of these arrangement may be either open or close form depending on the engineering application of the soil. Cubic form is the most open form of packing, with the maximum possible porosity around 48% figure 3.8. The porosity can be computed from simple geometric relationships including the volume of spheres [49, 100].

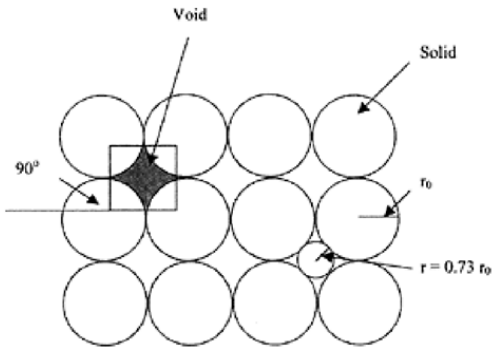

Figure 3.8: *Cubic form arrangement of particles [49]*

Orthorhombic configuration is the geometric form involves 3 axes perpendicular to one another figure 3.9 while rhombohedra configuration is a six-sided prism, whose faces form parallelograms figure 3.10 [49].

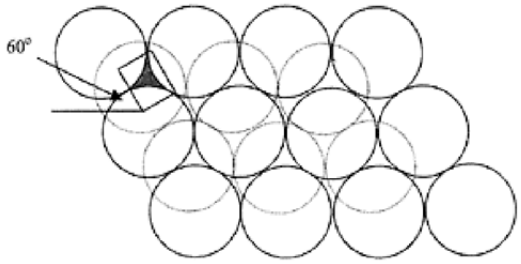

Figure 3.9: *Cubic form arrangement of particles [49]*

Composite configuration is the one formed by uniform spheres that can be arranged into composite packing involving cubic and rhombohedral configuration. This situation may happen if soil aggregates or secondary particles were spheres of uniform size. In such a scenario, total porosity of uniform spherical particles within the aggregates in a rhombohedra configuration will be simply the sum of porosity of each configuration [49].

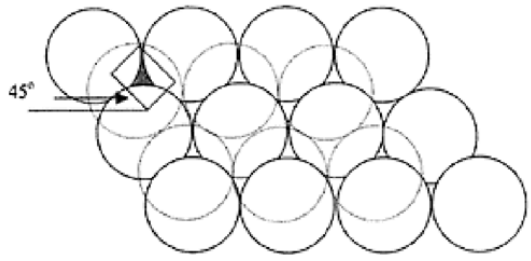

Figure 3.10: *Cubic form arrangement of particles [49]*

Open or closed packing form

The packing of soil particles is influenced by particle shape and size distribution. The open (low bulk density) figure 3.11 left or close (high bulk density) figure 3.11 right packing may be required for some engineering and agriculture applications(e.g. dam construction, road construction, embankment, foundation, etc.), a high density is required [49] while in agriculture tillage and plough soil low bulk density is required by plant route to grow and enough porous for soil aggregates retention.

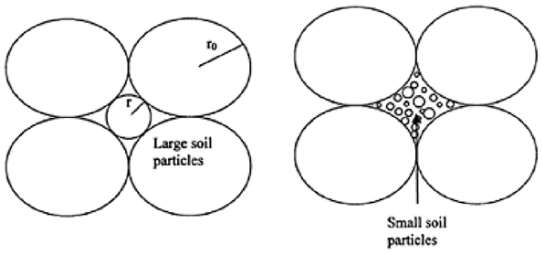

Figure 3.11: *Open and close packing of the particles [49]*

In close packing, the smaller particles are packed within the pore space of larger particles. The close packing is achieved by arranging the small grain sizes to fill voids created by large particles. Achieving a high density based on close packing necessitates having a material containing a diverse range of particle sizes. The other end of the scale involving open packing is based on a material containing particles of a uniform size. Thus, maximum porosity is achieved with open packing and the least with close packing [49]. The packing in chrono model can be achieved by introducing the pre-compaction mechanism at different weight.

Packing arrangement of soil material is of relevance to soil compaction and surface seal formation in agricultural soils. It is also of interest to civil engineers concerned with stable foundations. The 'well-graded' soil consists mostly of sand and gravel but also contains a small amount of silt and clay to facilitate close packing. 'Poorly-graded' soils are those with uniform size fraction, e.g., fine or coarse sand only with little material of other size fractions. Such materials are difficult to manipulate into close packing arrangements, or do not compact into a dense mass, and are 'poorly graded' soils. Clay soils, with high swell shrink capacity and ability to absorb a large volume of water, are also poor-grade material for construction purposes [49].

Knowledge of soil solids is important to sustainable use of soil resources for different soil functions and land uses. Soil solids have an important effect on agricultural and industrial/engineering land uses, and environments. Agriculturally, soil solids are important to soil tillage and trafficability, plant available soil water, leaching losses of fertilizers and chemicals, formation of soil structure, swell-shrink properties, and physical condition of the soil or soil tilth. In terms of engineering and industrial uses, soil solids are important to foundation strength and stability, water sorption properties, and transmission of fluids in relation to waste disposal. Environmental applications of soil solids are those related to water and air qualities, buffering capacity, and ability to filter contaminants [49].

The arrangement and placement of soil particles determines the response of soil to exogenous stresses such as tillage, traffic, and raindrop impact. This arrangement of

soil particles is called 'soil structure'. The arrangement is dynamic, complex, and is not very well understood. Yet, soil structure remains to be the most complex, the least understood, and among the most important soil physical properties [49].

One of the reasons for the complexity of soil structure is the range of scales it expresses. Another cause of complexity is the dynamic nature of soil structure. Structural attributes vary in time and space, and the attributes observed at any given time reflect the net effect of numerous interacting factors which may change at any moment [49]. Since in chrono model the particle generator, generates particles in the bin according to the continuum distribution introduced figure 3.12, the appropriate arrangement of particles as per soil science is guaranteed. Also introducing the pre-compaction of the terrain with different weight of the mechanism will ensure to get close or open packing.

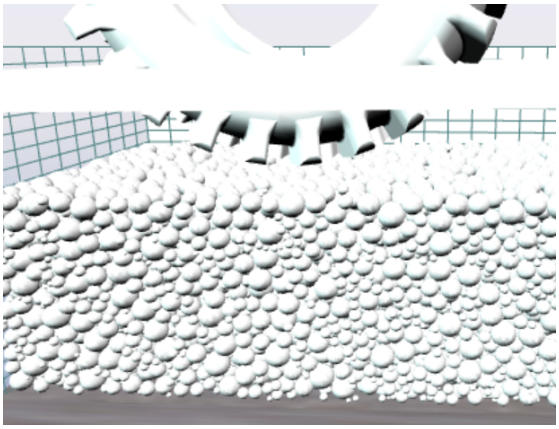

Figure 3.12: *Chrono model particles packing*

With engineering perspective, soil structure is the 'strength and stability of aggregates and voids in terms of their compressibility, bearing capacity, and permeability.' Another related term used in engineering is sensitivity, which is the ratio of strength of an undisturbed soil to that of a soil completely remoulded at constant volume. Sensitivity refers to the loss in strength of a soil when its original structure is destroyed by remoulding. Several terms are used to express easily identifiable structural units including structural form, fabric, aggregate, ped, granule, crumb, tilth, are used by different disciplines of soil science [49].

Soft deformable terrain

Contact detection and force computation

Normal contact stress or pressure p related to sinkage z takes into account Bekker-Wong pressure sinkage relationship as in equation 3.11.

$$p = \left(\frac{k_c}{b} + k_\phi\right) z^n \tag{3.11}$$

$$t = t_{max}(1 - e^{-j/k}) \tag{3.12}$$

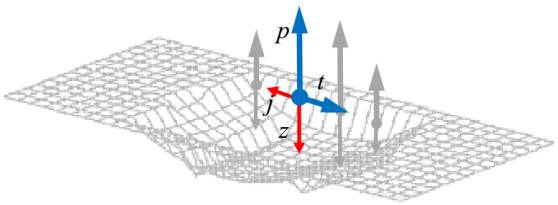

Figure 3.13: *soil model sinkage, pressure and tangential stress*

Tangential stress t (figure 3.13) is given by Janosi-Hanamoto relationship equation 3.12 and the maximum tangential stress is given by typical Mohr-Coulomb friction as in equation 3.13 respectively.

$$t_{max} = c + ptan(\phi) \tag{3.13}$$

Contact force is computed to each grid node associated in the contact print taking into account grid nodes area, and total contact force is numerically integral of the discrete node forces over the entire contact area.

$$F_n = A\left[\left(\frac{k_c}{b} + k_\phi\right) z^n\right] \tag{3.14}$$

The discrete approximation of the contact area was computed by considering number of nodes associated contact with respective node coordinates which is given by;

$$A = \left(\sum_{i=1}^{n_{contact}} c_A, contact, i + \sum_{j=1}^{n_{contour}} c_A, contour, j\right) dA \tag{3.15}$$

Node contact pressure was computed in the solver by considering node pressure correction factor γ_i which takes care of the pressure drops from the central region to border of the contact patch. this correction factor depends on node centrality inside the contact patch and balancing of internal soil friction and cohesion [45, 46].

$$p_i = \gamma_i \left(\left(\frac{k_c}{b} + k_\phi\right) z_i^n\right) \tag{3.16}$$

This consideration of pressure correction factor leads to the phenomenon of contact pressure distribution, which changes from central to the border of the contact patch and distribution shapes depends on the dominant soil parameters between internal friction or cohesion inside Bekker empirical formula [45, 46].

$$w_i = \sum_{j=1, j\neq i}^{n_{contact}} \frac{1}{fcn(|r_j - r_i|, c, \phi)} \tag{3.17}$$

$$w_{total} = \sum_{i=1}^{n_{total}} w_i \tag{3.18}$$

Discrete node local contact force, for each associated node in the contact patch was computed in the solver by implementing Mohr-Coulomb failure criterion and Coulomb friction between sliding surfaces taking into account components of shear stress. This

force is given by equation3.19 while total contact force taken as integral sum of discrete node forces is given by equation 3.20.

$$F_i = \begin{pmatrix} c \\ c \\ 0 \end{pmatrix} + p_i \begin{pmatrix} \tan\phi & 0 & 0 \\ 0 & \tan\phi & 0 \\ 0 & 0 & 1 \end{pmatrix} n_i + \mu p_i t_i \tag{3.19}$$

$$F_{n_{total}} = \sum_{i=1}^{n_{contact}} F_i \tag{3.20}$$

Soil plastic deformation or simply soil volume deformation is governed by the efficient manipulation technique implemented in the model in which it takes account node specific soil volume displaced depends on local sinkage of respective node. By taking into account each nodes associated to the contact and its respective sinkage the displacement of the area cluster of the contact was realised. The displacement law implemented depends on the local normal contact velocity at the contact grid node,by assuming that only this normal components of contact velocity is relevant to soil displacement [45, 46].

3.3.2 Tire-Terrain Interaction

Pressure-sinkage equation

Pressure-sinkage relationship is mostly depends on the tire parameters, structure and conditions of the terrain. Despite the fact that, pressure-sinkage is the major method for estimating both normal and shear stress developed at the interface of the interaction along the contact patch, but it's also very important in the selection of the framework for predicting the performance of the off-road vehicles. This is governed by the pressure-sinkage equation originally developed by Bekker and later modified by Reece [87,106].

$$p = (ck'_c + b\gamma_s k'_\phi)\left(\frac{y}{b}\right)^n \tag{3.21}$$

where p is the pressure, y is the sinkage, c is the cohesion of the soil, k'_c, k'_ϕ, γ_s and n are soil parameters related to the cohesion, angle of shearing material, weight density and sinkage exponent respectively, b is the smaller dimension of the contact patch (that is the width of the rectangular contact area). From the experimental penetration results shows that the parameters k'_c and k'_ϕ depends on the type characteristics of the soil whereby the parameters are negligible for dry cohesionless (sand) and frictionless (clay) respectively [106]. Reece modified the Bekker equation and introduce the ratio $\frac{y}{b}$ in order to make the soil parameters to be dimensionless and to account for different plate shapes in single equation, the trend of the relationship is defined by the exponent n of the equation [87, 106].

Despite the fact that in field of terramechanics, it is widely accepted to use Reece-Bekker equation in the calculation of the normal stress distribution along the contact patch of tire-terrain interaction, some limitations of the formulation must be well understood before applying this formulation. These limitations include (1) the constants are obtained for the plate sinking perpendicular to the terrain surface; the pressure acts along upwards direction, but for sinking wheel the stress calculated at any sinkage is

considered to act along the radial direction of the wheel and not along the upward direction. (2) The tire contact patch is considered as the penetrometer plate and the terrain to be homogeneous, the rotating wheel not only exerts a vertical load but also applies shear during penetration [71, 74, 87, 106].

In order to express the radial stress on the wheel contact patch as a function of the angular location θ (figure 3.15 right), sinkage relation should be expressed as a function of angular position of the wheel-terrain contact patch [32].

Shear Stress

A vehicle through its elements applies normal load to the terrain under the applied tractive force of the running gear which results to sinkage, and this in turn causes motion resistance of the wheel. For the case of multi-axle vehicles the terrain is subjected to repetitive loading of the consecutive wheels. In order to predict and estimate the pressure distribution under the contact-patch and the tractive performance of off-road vehicles, the response of the terrain due to vehicular and repetitive loading must be estimated or measured [106, 107].

Due to the applied torque to the wheel which is in contact with deformable terrain, shearing action is initiated on the tire-terrain interface and wheel sinkage increases from static sinkage due to so called slip sinkage [16]. In order to predict the wheel thrust and the associated slip, the shear stress-shear displacement relationship of the terrain is required [106]. Evaluation of the shear displacement developed along the contact patch of the tyre-terrain interaction, leads to the evaluation of the traction and slip of the rigid wheel [19, 106].

From the classical terramechanics theories, one of the fundamental task in characterisation of the terrain behaviour or response to the loading is by establishing the functional relationships such as stress-strain, pressure-sinkage, shear stress-shear displacement relationships. Since the structure and behaviour of the real terrain varies greatly under various conditions, the characterisation of the terrain response was only based in practical or experimental results and curve fitting to obtain terrain response in question, and the model for estimating the terrain response was less or not yet developed [106, 107].

The shear stress initially increases rapidly with an increase of shear displacement, and then approaches a constant value with further increase in shear displacement. This relationship of shear stress shear displacement is described by the exponential function proposed by Janosi and Hanamoto [106] and is widely used in the field of the off-road operations research and the limiting shear stress is obtained from the normal shear relationship by Mohr-Coulomb equation [37, 71, 87, 106].

$$\tau(\theta) = \tau_{max}(1 - e^{\frac{-j}{k}})$$

$$= (c + \sigma_n(\theta)tan\phi)(1 - e^{-\frac{j}{k}}) \tag{3.22}$$

τ_{max} is the limiting shear stress, j is the shear displacement of the terrain, c is the cohesion of the soil material and ϕ is the angle of the internal resistance of the soil, and k is the shear deformation parameter of the soil material in which it is usually estimated experimentally.

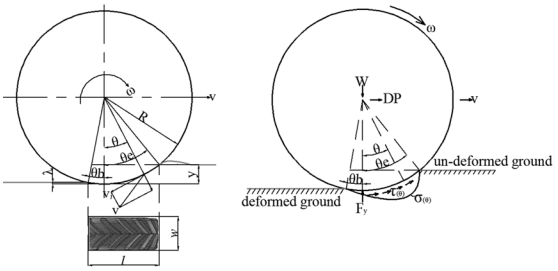

Figure 3.14: *Tire contact footprint dimension, shear and normal stress distribution.*

Pressure distribution at the contact patch which follow Wong (see figure 3.15(right)) [87] is governed by the pressure- sinkage relationship which is the exponential function of the wheel sinkage and pressure-sinkage coefficients as proposed by Reece [106] as explained previously equation 3.21.

The shear displacement j is calculated from the integration of the shear velocity of the terrain in contact with the wheel assuming that the velocity of the terrain particles at the interface matches the tire velocity [87] as explained below.

Slip Velocity and Shear Displacement

For the rigid wheel slip velocity V_j of a point on the wheel in the contact patch relative to the terrain is the tangential component of the absolute velocity at the same point(see figure 3.14 (left)) and its magnitude is defined by the angle θ as given to equation 3.23, Note that these analysis also applies to lugged wheels, since lugs can be modelled by increasing the effective radius of the wheel for which in this study is the outer radius of the wheel [33].

$$V_j = R\omega[1 - (1 - s)cos\theta] \tag{3.23}$$

Where R, s and ω are effective radius, slip ratio and angular speed of the wheel respectively, θ is the angular position describing the wheel element at the contact patch starting counter-clockwise from the centre of the wheel (see 3.14(left)).This relation shows that the slip velocity varies with the angle θ and the slip ratio of the wheel [19]. Thanks to chrono::engine model which estimate the slip ratio, wheel linear velocity values and register it in text file for further analysis.

Linear velocity and angular speed estimated from chrono::engine model leads to the estimation of the slip velocity based on the same principle for the deformable wheel, but for this case the terrain is the one deformed under wheel pressure and slip of the wheel lugs which cause the wheel to sink in the terrain. This was achieved after introducing a terrain deformation factor to forward velocity from the formula given by [77], the factor introduced relates sinkage, wheel radius and entry angle. Slip velocity was estimated from the relation given in equation 3.24.

$$V_j = R\omega - V_z\left(1 - \frac{y}{R}\right) \tag{3.24}$$

Where ω, V_z , y and R are the angular velocity, forward velocity of the centre of the wheel relative to the terrain, slip sinkage and radius of the wheel respectively. In

chrono::engine model absolute forward velocity V_z is estimated by integrating the position of the wheel centre of mass with respect to each simulation step time.

The integral of the equation 3.23 above from the entry to exit angles, gives the shear displacement along the wheel-terrain interface as given equation 3.25.

$$j(\theta) = \int_{\theta_b}^{\theta_e} R(\theta)[1 - (1 - s)cos(\theta)]d\theta$$

$$j = R[(\theta_e - \theta_b) - (1 - s)(sin\theta_e - sin\theta_b)] \tag{3.25}$$

Where the θ_e and θ_b are the entry and exit angles describing the element of the wheel contact which come into contact and leave contact with the terrain respectively, which are calculated based on the estimated slip, slip sinkage of the wheel and the soil rebound-ness parameters as explained below.

The entry and exit angles of the wheel contact patch can be calculated as:

$$\theta_e = cos^{-1}\left(1 - \frac{y}{R}\right) \tag{3.26}$$

$$\theta_b = cos^{-1}\left(1 - \frac{\lambda y}{R}\right) \tag{3.27}$$

where λ indicates the terrain rebound-ness due to soil elasticity, and y, R are sinkage and radius of the wheel respectively.

The slip ratio of the wheel is defined as the function of the longitudinal velocity of the wheel and the circumferential velocity of the wheel as;

$$s = \frac{R\omega - V_z}{R\omega}(drivingstate) \tag{3.28}$$

Where V_z is the absolute velocity of the wheel, R and ω are effective radius and angular speed of the wheel respectively. The values of the slip ratio are calculated direct by Chrono::Engine model during simulations.

Tractive Force and Driving Torque

Substituting the value of the shear displacement into the equation 3.22 leads to equation 3.29,

$$\tau(\theta) = (c + \sigma_n(\theta)tan\phi)\left(1 - e^{-(\frac{R}{k})(\theta_e - \theta_b) - (1-s)(sin\theta_e - sin\theta_b)}\right) \tag{3.29}$$

The angle θ describe the point of maximum normal stress at contact surface and was calculated as in equation 3.30

$$\theta = (a_0 + a_1 s)\theta_e \tag{3.30}$$

where s the slip ratio of the wheel in the longitudinal direction of the motion and the values of the parameter a_0 and a_1 depends on the interaction of the wheel and terrain. The values of the parameter a_0 and a_1 are $a_0 \approx 0.4$ and $0 \leq a_1 \leq 0.3$, in which this guarantee that θ increases with slip resulting into better prediction of the slip-sinkage behaviour [37, 87].

Integrating the horizontal component of the tangential stress (equation 3.29) over the entire contact area of the tire-terrain gives the total traction effort F_T.

$$F_T = Rb \int_{\theta_b}^{\theta_e} \tau(\theta) cos(\theta) d\theta \tag{3.31}$$

Therefore, the driving torque T_w on the wheel is given by equation that relates the shear stress at the contact area which is simply the product of the tractive effort given in equation 3.31 and the effective radius of the wheel.

$$T_w = R^2 b \int_{\theta_b}^{\theta_e} \tau(\theta) cos(\theta) d\theta \tag{3.32}$$

The equation above has two important unknowns for the stress distribution along the contact area: that is the angles of the entry θ_b and exit angle θ_e. The exit angle is smaller than the entry angle because the tire is sinking into the ground and in facts it compacts the soil while passing onto it. For the rigid wheel the exit angle is assumed to be constant and small in magnitude, this is because the tire is assumed to leaves the terrain flat as it compacting, so the angle cannot be large indeed, and it is governed by the slip phenomenon that displace the soil layer under the rotating tire and the plastic response of the terrain [17, 87].

The exit angle is very important for the determination of the tractive effort performance since it determines the size of the contact patch. The entry and exit angles of the wheel contact patch can be calculated as in equations 3.26 and 3.27 above [36, 37, 87].

From the experiments and theory of plastic equilibrium it has been shown that, even though the sinkage increases monotonically from the entry and reaching maximum at the bottom of the wheel, the pressure distribution does not follow this trend of the sinkage, instead the maximum pressure occurs somewhere between the entry point and exit point and it is a function of the slip ratio [87, 106] (see 3.15(right)). When the tire is passing to the deformable road, the section between the entry and discharge points in the contact patch rotates counter-clockwise and this phenomenon determine the amount of slip sinkage and it's a function of the slip, vertical load and contact patch area/size [87].

Since for non-cohesive sand particles wheel shows high static sinkage of approximately more than $11cm$, the smallest dimension of the projected contact patch for non cohesive particles is taken to be the width of the wheel b, which assessed at static sinkage of the wheel.

Given that at static sinkage, the entry and exit angles are assumed to be equal, and can be calculated from the static sinkage of the wheel, the effective radius of the wheel, in which for this work is always the same as the radius of the wheel since the tire is considered to be rigid as explained previously.

Normal and tangential stress distribution

In order to express the radial stress on the wheel contact patch as a function of the angular location θ, the sinkage relation is expressed as a function of θ as given in equation below [32].

$$y(\theta) = R(cos\theta - cos\theta_e) \tag{3.33}$$

where θ is the central angle describing the angular position of the tire element starting counter-clockwise from the bottom of the tire, θ_e is the entry angle at which the terrain enters in contact with the tire, and R is the effective radius of the tire in which for this case the effective radius is always equal to the radius of the tire since the tire is considered to be rigid.

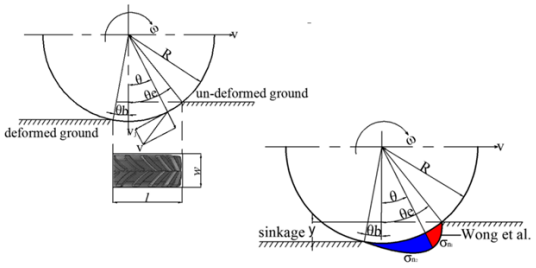

Figure 3.15: *Tire footprint dimension, stress zones between maximum point*

A tire operating on the deformable soil can be approximated as rigid if the contact patch does not deform the carcass of the tire and the effective radius is constant. The pressure distribution along the contact patch starts from zero at the entry angle and gradually increases to the maximum value which is reached at the point where the highest sinkage occurs; in which for the rigid wheel is located at the bottom of the wheel [29, 87].

The normal stress can be calculated from the equation 3.21 above by substituting the value of the sinkage as obtained from the relationship of the sinkage and radius of the tire equation 3.33. In this study we follow the stress distribution produced in the experiments and theory specifically the one adopted by Wong. From the entry point to the location of the maximum normal stress described by angle $\theta_e - \theta$ (see figure 3.15 (right)), the stress can be calculated using equation (2.16),

$$\sigma_{n_1}(\theta) = (ck'_c + b\lambda_s k'_\phi)\left(\frac{R}{b}\right)^n (cos(\theta) - cos(\theta_e)^n \tag{3.34}$$

Meaning while the normal stress that goes from the maximum normal stress to the exit point described by the angle θ_b will be calculated using equation 3.35,

$$\sigma_{n_2}(\theta_b) = (ck'_c + b\lambda_s k'_\phi)\left(\frac{R}{b}\right)^n \left(cos(\theta_e - \left(\frac{\theta - \theta_b}{\theta - \theta_e}\right)(\theta_e - \theta) - cos(\theta_e)\right)^n \tag{3.35}$$

The angle that describe the point of the maximum normal stress is the linear function of the slip ratio and the entry angle for correct estimates of the sinkage as proposed [87], this follows after the correction of estimates of that angle which based on the Mohr-Coulomb failure criterion and the theory of plastic equilibrium [13, 106, 107].

Vertical Balancing of Wheel Load

The vertical component of the shear stress on the contact area supports part of the vertical load of the wheel, this effect was neglected in the simplified version of the

analysis but it has to be considered for the accurate analysis of the tire soil interaction [37, 106, 107].The drawbar pull is calculated from the vertical forces balancing phenomenon, to ensures that the vertical forces at the contact patch balances the vertical load of the wheel. This is possible by knowing first the normal and tangential stress distribution at the contact patch between the tire and the soil [87]. Vertical load balance is governed by the equation 3.36 bellow.

$$W = Rb\left[\int_{\theta}^{\theta_e} \sigma(\theta)cos(\theta)d\theta + \int_{\theta}^{\theta_e} \tau(\theta)sin(\theta)d\theta\right] \tag{3.36}$$

W is the weight of the wheel, θ is the effective angle that the part of maximum stress makes with the vertical axis of the wheel. The drawbar pull can be calculated from the integration of the normal and shear stress along the longitudinal direction in the contact patch.

$$DP = Rb\left[\int_{\theta}^{\theta_e} \tau(\theta)cos(\theta)d\theta - \int_{\theta}^{\theta_e} \sigma(\theta)sin(\theta)d\theta\right] \tag{3.37}$$

From equation 3.37, it can be deduced that the first term of the integral is the total traction that can be supplied by the contact tangential stress and second term is the total motion resistance which is the work done by the vertical component of normal stress to make a rut of depth equal to sinkage. This expression gives the correct estimation of the drawbar pull since it include the soil internal compaction resistance, which also leads to a better estimates of the driving torque of the wheel [74, 87, 106].

Wheel motion resistance

When wheel interacts with terrain, there is a counter reaction to wheel motion developed due to soil deformation resistance and sinkage of the wheel. Early method to predict motion resistance of rigid wheel was introduced by Bekker and later modified by Wong which was based on prediction of pressure beneath the contact patch and wheel sinkage during interaction.

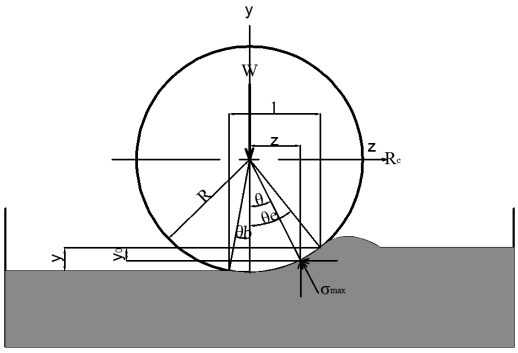

Figure 3.16: *wheel-soil interaction for motion resistance prediction*

Using Bekker's motion resistance prediction method and taking into account assumption that purely radial stress distribution at the contact patch [106], then equilib-

rium equations of rigid wheel that relates weight and motion resistance (figure 3.16) can be written as;

$$R_c = b \int_{\theta_b}^{\theta_e} R\sigma_{max} \sin\theta d\theta \tag{3.38}$$

$$W = b \int_{\theta_b}^{\theta_e} R\sigma_{max} \cos\theta d\theta \tag{3.39}$$

Using Bekker's pressure-sinkage equation 3.40 motion resistance can be written as

$$\sigma = (k_c/b + k_\phi) y^n \tag{3.40}$$

$$R_c = b \int_{\theta_b}^{\theta_e} (k_c/b + k_\phi) y^n dy = b \left[\left(\frac{k_c}{b} + k_\phi \right) \frac{y^{n+1}}{n+1} \right] \tag{3.41}$$

Motion resistance estimated by equation 3.41, with the assumption that for rigid wheel motion resistance is the work done to make a rut of depth equal to sinkage, total motion resistance is also referred as a compaction resistance of terrain during interaction. Estimation of motion resistance has to be expressed in terms of wheel parameters and soil properties [106]. From geometry of figure 3.16, longitudinal contact length z at point of maximum stress can related to maximum sinkage y, sinkage at that point y_0 and wheel diameter as;

$$z^2 = [2R - (y - y_0)](y - y_0) = 2R(y - y_0) \text{ for small sinkage} \tag{3.42}$$

$$2dz = -2Rdy_0 \tag{3.43}$$

$$W = b(k_c/b + k_\phi) \frac{\sqrt{2R}}{b^n} \int_0^y \frac{y_0^n}{2\sqrt{y - y_0}} dy_0 \tag{3.44}$$

Let $y - y_0 = t^2$, then $dy_0 = -2tdt$

$$W = b(k_c/b + k_\phi) \frac{\sqrt{2R}}{b^n} \int_0^{\sqrt{y}} (y - t^2)^n dt \tag{3.45}$$

Series expansion of $(y - t^2)^n$ gives, $(y^n - ny^{n-1}t^2 + n(n-1)y^n - 2t^4/2 - n(n-1)(n-2)y^n - 3t^6/6 + ...)$ and taking first two terms of the series,

$$W = b(k_c/b + k_\phi) \frac{\sqrt{2Ry}}{3} y^n (3 - n) \tag{3.46}$$

$$y^{\frac{2n+1}{2}} = \frac{3W}{b(k_c/b + k_\phi)\sqrt{2R}(3 - n)} \tag{3.47}$$

$$y = \left[\frac{3W}{b(k_c/b + k_\phi)\sqrt{2R}(3 - n)} \right]^{\frac{2}{2n+1}} \tag{3.48}$$

Substituting value of sinkage y into equation 3.41 and rearranging , motion resistance can be expressed in terms of wheel weight, radius, width and soil parameters as;

$$R_c = \frac{1}{(n+1)(3-n)^{\frac{2n+2}{2n+1}} b^{\frac{1}{2n+1}} (k_c/b + k_\phi)^{\frac{1}{2n+1}}} \cdot \left(\frac{3W}{\sqrt{2R}}\right)^{\frac{2n+2}{2n+1}} \tag{3.49}$$

Therefore, drawbar pull DP given in equation 3.37 can be simply expressed by subtracting total motion resistance R_c from total traction F_T as given in equation 3.50.

$$DP = F_T - R_c \tag{3.50}$$

3.4 Simulation Model

The model presented in this work considers only rigid wheels. Study of the rigid wheel is still relevant as some vehicles are equipped with rigid wheel as the case of the robot for extra terrestrial exploration where rubber compound cannot be used because in the severe environmental condition(extremely high temperatures, unfavourable chemical composition) [87, 106] but also flexible wheels behaves like rigid at high inflation pressure on high deformable terrains. The tires are modelled in SOLIDWORK CAD as the agriculture vehicle tire. The material of the tyre was chosen to be natural rubber in CAD (SolidWork) modelling with respective masses and inertia.

The tire model was then exported to CHRONO::Engine as (wavefront object .obj) file, thanks to chrono::engine as a free available C++ general purpose available software made up of collection of loosely coupled components that facilitate different aspect of multi-physics modelling, simulation and visualisation [62, 98], an optional module for third-part model import capability which enable the tyre model to be imported to chrono::engine for the soil-bin test mechanism [62, 99]. The soil-bin-wheel test mechanism was modelled whereby the soil bin was made as a collection of four walls and ground positioned accordingly, the front wall to the user was made to be transparent to facilitate the visibility of the interaction during simulation (see figure 3.17).

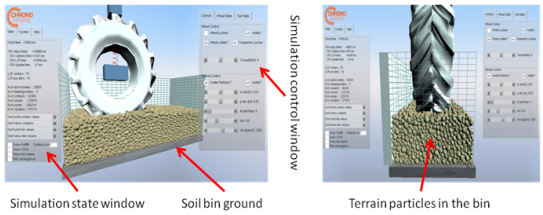

Figure 3.17: *Tire-terrain model in chrono::engine.*

Rigid block (truss) was added to account as a spindle, mass of the spindle to account for the hub, rim and axle masses, this block is attached to the centre of the wheel axis with revolute joint and made to be movable with the wheel by assigning the same linear velocity as that of the wheel at that point. Furthermore, another block is added to the system (suspended mass) which acts as vehicle weight and is supported with the spring to the spindle. The parameters of the spring, blocks (e.g, masses, spring constants)

are made to be global parameters for easy change at different simulation requirements, all blocks are made to move with the same velocity as the wheel. The motion of the wheel and masses was achieved by the additional of the engine to the system which gives wheel angular speed for simulation.

The wheel was given angular speed after release time and before come in contacts with the particles which is the same as the wheel simulation angular speed. Wheel comes in contact with the particles in bin after release time, in which particles are generated with the distribution size/mass based on the continuum distribution which account for the largest and smallest diameters of the particles at respective distribution probabilities. Some graphical user interface (GUI) and control sliders was added for turning during simulation.

Thanks to collision detection feature in chrono::engine for handling the large number of colliding bodies and triangle mesh capability which assign collision detection of particles in the terrain with high precision iteration solver of contact and simulation [98, 99]. Since the items in chrono::engine are organised in classes and name spaces, this ensures fast execution of the simulation program even in complex situation like collision between particles in terrain and particles-wheel in interaction and also for complex project which accounts for thousand of code line [62].

To account for issues of dependency and memory footprint the chrono::engine follows the modular approach by splitting the libraries modules that can be dynamically loaded only if necessary [62]. Moreover, in the case of providing compact algebra for managing the quaternion, static and moving coordinate system for the case of free particle and moving wheel, the operator overloading feature has been used with the adoption of modern programming techniques such as shared pointers [99].

Chrono::Engine has the capability to handle simulation of the non-smooth collision of rigid bodies through differential inclusion approach which calculates the contact forces by penalising the small interpenetration (DEM-P) of colliding rigid bodies and complimentarity condition (DEM-C) that enforce non-penetration of discrete elements that come in mutual contact [22, 47, 59, 72, 98], this also ensures the correct estimation and calculation of the friction and collision forces in contacts of particles and wheel during interaction [61, 62, 99]. Thanks to physical system object which handles the list of rigid bodies (truss, wheel, soil bin and vehicle body) and their constrains which can also be used to add forces, position, velocity, acceleration and auxiliary references to rigid bodies and specific constrains for the drivers (Engine::Mode) in test mechanism [98, 99].

To use soft deformable soil, the class to call up the soil type was modelled in the same soil bin with plane length and width equal to soil bin dimension (figure 3.18). This call up function forces particle generator to be off when using soft deformable soil. Semi-empirical soil added to the model assumes a continuous deformable plane represented by mesh and deformation of mesh is along vertical direction upward/-downward(see figure 3.13). Initial un-deformed mesh was created by a triangular mesh, and this model is a modified powerful version of original Soil Contact Model (SCM) [45, 46, 83]. Each grid node of the soil is associated with Bekker's soil dynamics parameters in which contact dynamics computation is achieved by applying Bekker's terramechanics theory during interaction.

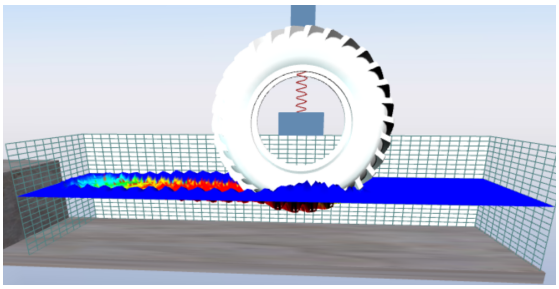

Figure 3.18: *chrono soft deformable terrain model*

In chrono model the contact body is multi body dynamic rigid wheel that comes into contact with the terrain. Width, radius, mass and inertia of the wheel are all taken into consideration for contact dynamics computation. In original soil contact model the contact body is defined only by its faces and vertices, while mass and inertia are not taken into consideration [46] and this modification in chrono to account mass and inertia in contact dynamics makes difference between chrono soft soil model and original version of soft soil contact model.

Since the model draws on semi-empirical Bekker-Wong theory then properties of terrain depends on Bekker-Wong parameters such as cohesion c, cohesion dependent parameter k_c, internal deformation friction angle ϕ, internal friction angle dependent parameter k_ϕ and sinkage exponent n. Tangential stress of the soil contact depends on Janosi-Hanamoto shear deformation relationship. Mesh of this model can be automatically refined and parameter of mesh triangles for refinement can be setted according to user requirement. The mesh is not limited to only quadrilateral grids and this also gives another difference to original soft contact model (SCM) developed previously. Build-up material and slope of rut is related to internal friction of material and amount of material displacement rate at the contact can be presented by percentage up to 100%.

Contact can be detected by comparing minimum vertices with respect to soil grid with the vertical coordinates of the corresponding soil grid nodes. Footprint is defined by the intersection volume of wheel and soil due to upward and downward deformation of soil grids [45, 46, 83]. Once the contact has been detected, sinkage of each node of footprint can be calculated and this sinkage is related to normal pressure according to Bekker empirical relationship given in equation 2.1 and the solver computes the contact pressure as explained in sub-section 3.3.1. Friction forces between wheel and soil surfaces can be calculated using typical Mohr-Coulomb friction relationship given in equation 3.13 whereby the internal friction angle is related to internal friction coefficient of material which also gives the measure of rut slope and build-up materials. Relationship of internal friction angle and internal friction coefficient are applied to each surface grids. Total volume of soil displaced at the contact is equal to the total volume of the footprint that has been created by the contact wheel and sinkage of wheel is given by total soil height reduction at each corresponding grid nodes respectively.

3.5 Simulation Results

Multi-threaded solver	
time step$[s]$	0.005
velocity iteration$[m/s]$	70
position iteration$[m]$	15
warm start[]	0
refinement resolution[]	0.04
number of erosion per t[]	5

Table 3.1: *model simulation parameters*

3.5.1 Granular terrain

The capability of Chrono::Engine model for estimating the contacts, traction force as well as the static-sinkage, slip ratio, slip velocity and slip-sinkage as a function of soil characteristics and tyre tread design has been achieved. The achievement was reached by simulations with the model considering soil particle rheology, tyre tread design and simulation parameters. The results shows that the model realistically predicts correctly the frictional contacts, longitudinal traction forces and at the same time provides the correct estimates of the slip ratio, slip velocity, static sinkage and slip-sinkage behaviours.

The static sinkage was estimated based on the variation of the centre of the wheel just after interacting with the terrain from released initial position. The resulting resistance of the soil to the wheel longitudinal motion was recorded as the output resistive torque of the wheel. Furthermore, the wheel was given a constant initial angular speed in different simulation sets, and the slip of the wheel was estimated by the ratio of the difference of wheel circumferential velocity and linear velocity to the linear velocity at the centre of the wheel, slip velocity was estimated by the difference between the absolute wheel circumferential velocity to the linear velocity of the wheel centre, while slip sinkage was estimated based on the variation of centre of the wheel vertically with respect to ground during simulation.

Simulations are carried out by considering grains size, shape, friction, number of grains in the bin, cohesion force, lugs number, lugs height, lugs type, lugs angle, wheel angular speed and wheel load to analyse its effects on wheel slip, slip sinkage, slip velocity and traction force. The results of variation of interaction parameters with respect to simulation time are detailed in sub-sections 3.5.1, 3.5.1 and 3.5.1.

effect of grains properties on interaction parameters

grains size(mean diameter)

With regards to particles size, figure 3.19 it was noted that traction force 3.19a, slip 3.19b, slip velocity 3.19c and slip sinkage 3.19d of the wheel are sensitive to particle size. Wheel traction force, slip, slip velocity and sinkage decreases with increase of particle size, larger particles have more deformation resistance as compared to smaller particles which leads to low sinkage as well longitudinal motion resistnace.

Also, particles size has effects to terrain bulky density and weight density due to increase and decrease of terrain weight and void ratio caused by particles packing and

relocation in the terrain which will cause contact pressure variations, this results is comparable with [58, 69].

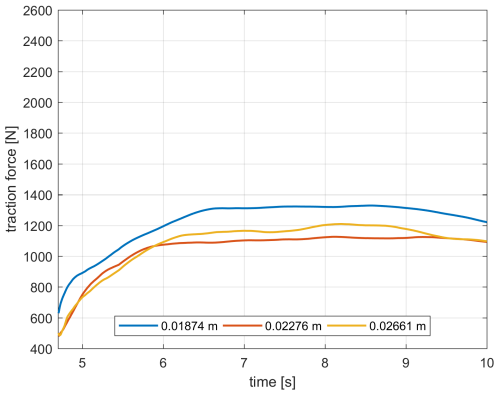

(a) *wheel traction as a function of time*

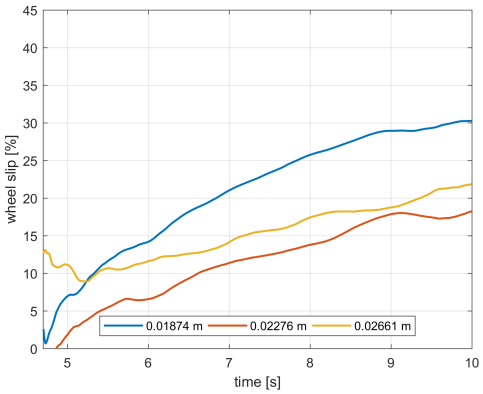

(b) *wheel slip as a function of time*

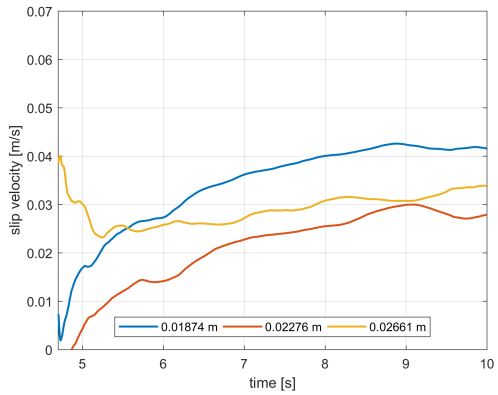

(c) *wheel slip velocity as a function of time*

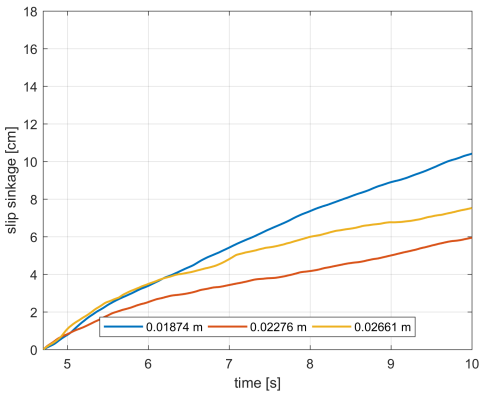

(d) *wheel slip sinkage as a function of time*

Figure 3.19: *effects of grain size in interaction parameters*

grain shape

From the simulation results in figure 3.20, it can be noted that particle shape affects interaction parameters. Traction force is lower with squares and mixed particles figure 3.20a as compared to sphere particles, this is because of high motion resistance due to high slip sinkage with sphere particles as compared to square and mixed particles figure 3.20d.

Wheel slip is decreases with square and mixed particles figure 3.20b as compared to sphere particles. This is because of high deformation resistance of the particles due to high resistance to rolling, interlocking and positioning of square and mixed particles during interaction. Although slip velocity is high at begining of interaction with mixed particles figure 3.20c but it decreases when wheel attaining its steady state, this is cause with high slip cause by particles packing which has more voids and reduce terrain weight density.

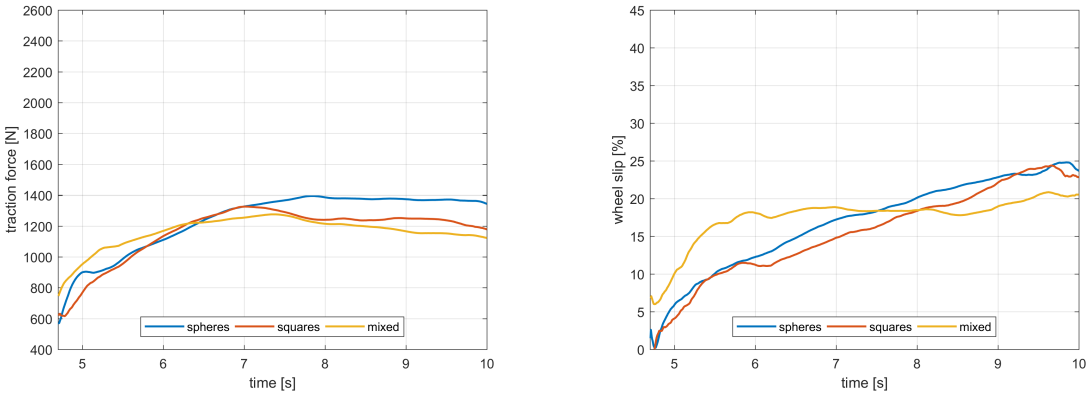

(a) *wheel traction as a function of time*

(b) *wheel slip as a function of time*

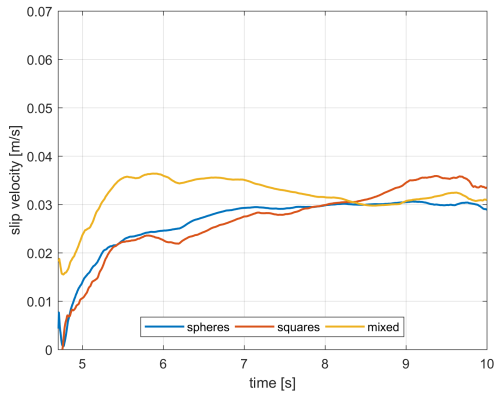

(c) *wheel slip velocity as a function of time*

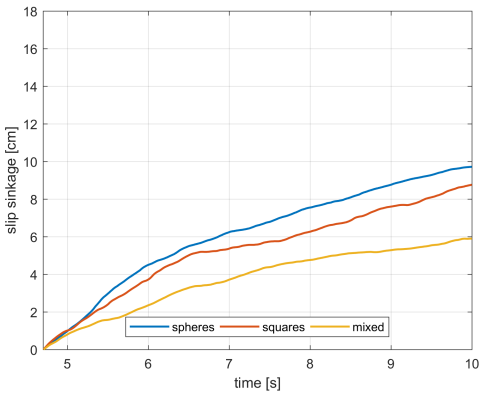

(d) *wheel slip sinkage as a function of time*

Figure 3.20: *effects of grain shape in interaction parameters*

particle friction

Simulations results in figure 3.21 it was noted that, deformation resistance increases with increase of friction between particles. Wheel slip, slip velocity and slip sinkage decreases with increase of friction figure 3.20b, 3.20c and 3.20d, this is because of high lateral deforamation resistance of particles due to high lateral friction force between particles [108].

The effect of friction is significant for slip, slip velocity and slip sinkage, for traction force the effect is small since increase of slip sinkage due to decrease of friction at the same time decreases motion resistance due to low deformation resistance with less friction. Also instead increasing friction force or deformation resistance of the particles increases traction per contact as well traction of the wheel with respect to terrain, this can be noted as an increase of terrain compaction resistance [69].

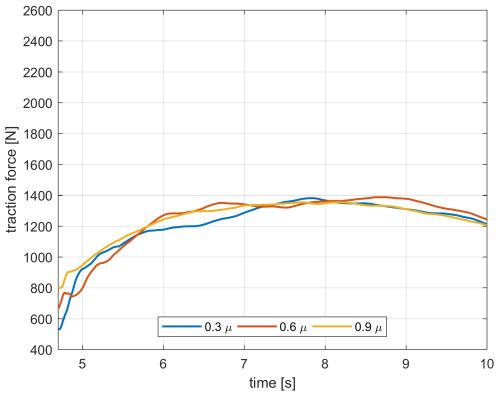

(a) *wheel traction as a function of time*

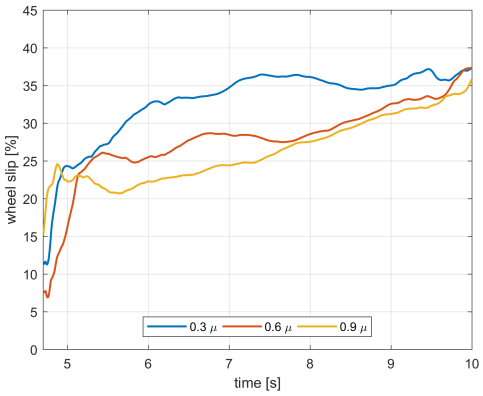

(b) *wheel slip as a function of time*

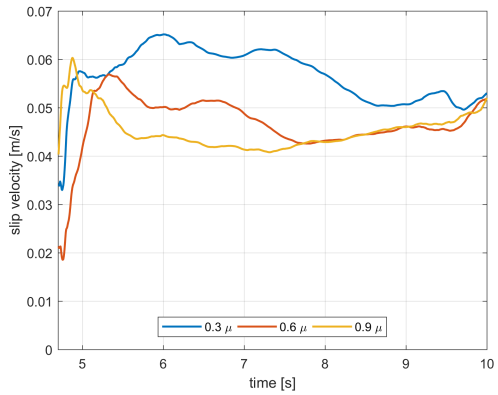

(c) *wheel slip velocity as a function of time*

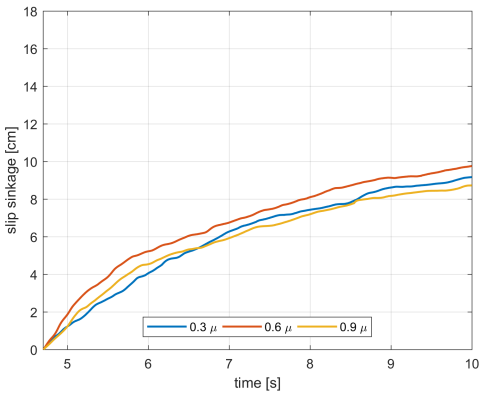

(d) *wheel slip sinkage as a function of time*

Figure 3.21: *effects of grains contact friction in interaction parameters*

number of particles

Simulations results obtained with different number of grains in the bin 3.22 , it was noted that traction force 3.22a is sensitive to grains number, it increases with increase of particle number. This is because of increase of terrain weight density with more particles in the bin which increases stiffness of terrain [69]. Also from the results shows that slip velocity figure 3.22c is sensitive to grains number at initial interaction and steady state more particles has high slip velocity, this is because of high slip. Slip sinkage has significant effect figure 3.22d , which shows high sinkage with 12000 particles as compared to other numbers.

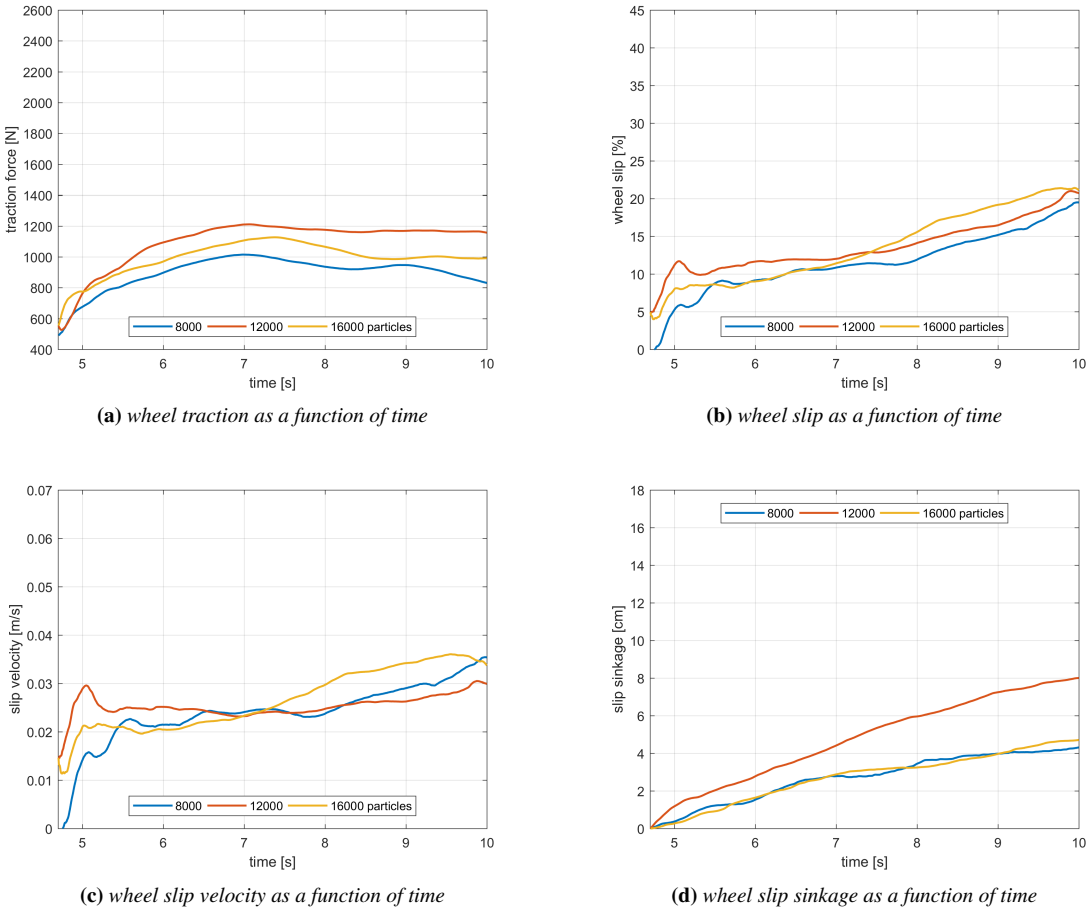

(a) *wheel traction as a function of time*

(b) *wheel slip as a function of time*

(c) *wheel slip velocity as a function of time*

(d) *wheel slip sinkage as a function of time*

Figure 3.22: *effects of number of grains in interaction parameters*

cohesion force

Simulation results in figure 3.23, it was noted that, cohesion force has significant effects on traction force at initial interaction up to when it attains maximum value and at steady state. Traction force decreases with increase of cohesion force due to decrease of slip sinkage figure 3.23a. Wheel slip decreases with increase of particles cohesion figure 3.23b due to increase of deformation resistance with cohesive particles.

Slip velocity decreases with increase of particles cohesion due to decrease of wheel slip and sinkage with more cohesive particles figure 3.23c and 3.23d. Cohesive terrain behave like elastic/plastic medium during deformation [106, 107] this can be noted at start of interaction where by effects of wheel inertia and load on deformation is high. Also it can be noted that even small cohesion force has large effects on slip and slip velocity as compared to non-cohesive particles.

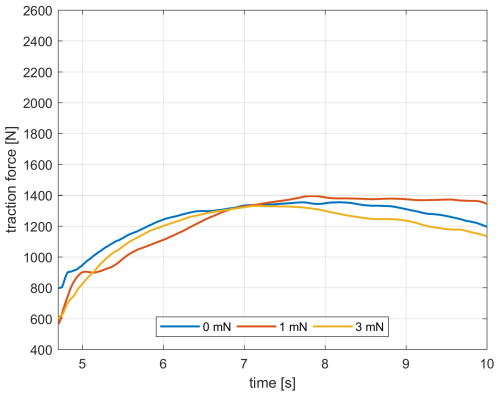

(a) *wheel traction as a function of time*

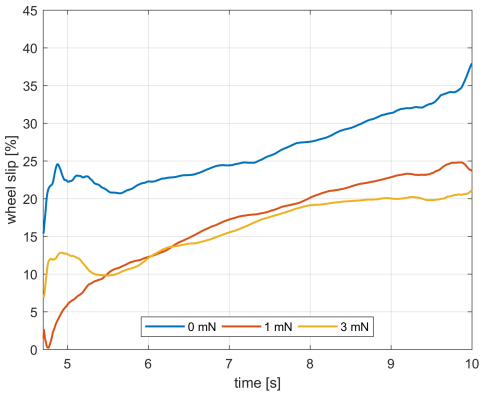

(b) *wheel slip as a function of time*

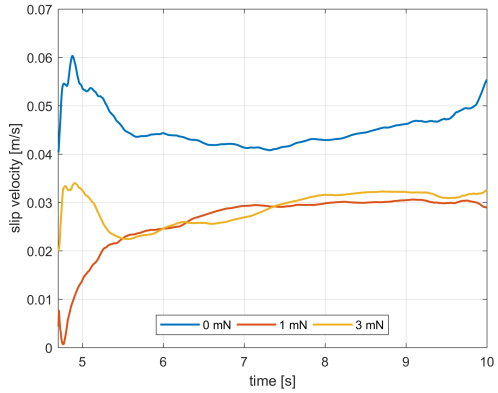

(c) *wheel slip velocity as a function of time*

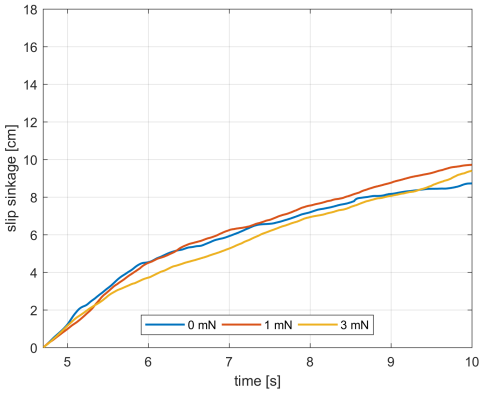

(d) *wheel slip sinkage as a function of time*

Figure 3.23: *effects of cohesion force in interaction parameters*

effect of tire tread design on interaction parameters

lugs number

From the simulation results in figure 3.24a, it was noted that there is a decrease of wheel traction with more lugs, this is because of decrease of slip sinkage. Wheel slip, sinkage and slip velocity decreases with more lugs, this is because reducing lug space and increases number of lugs that are in contact with the terrain which cause increase of deformation rut [40]. Increasing number of wheel lugs is beneficial to develop continuous shearing between the wheel lugs and the soil so as to improve traction efficient and drawbar pull [18]. Slip sinkage increases with decrease of lugs number, this is because of increase of lugs spacing figure 3.24d which cause large time span between smooth surface of wheel and lugs in the soil during interaction and results in increase of wheel slip and sinkage. This results correlates with [18].

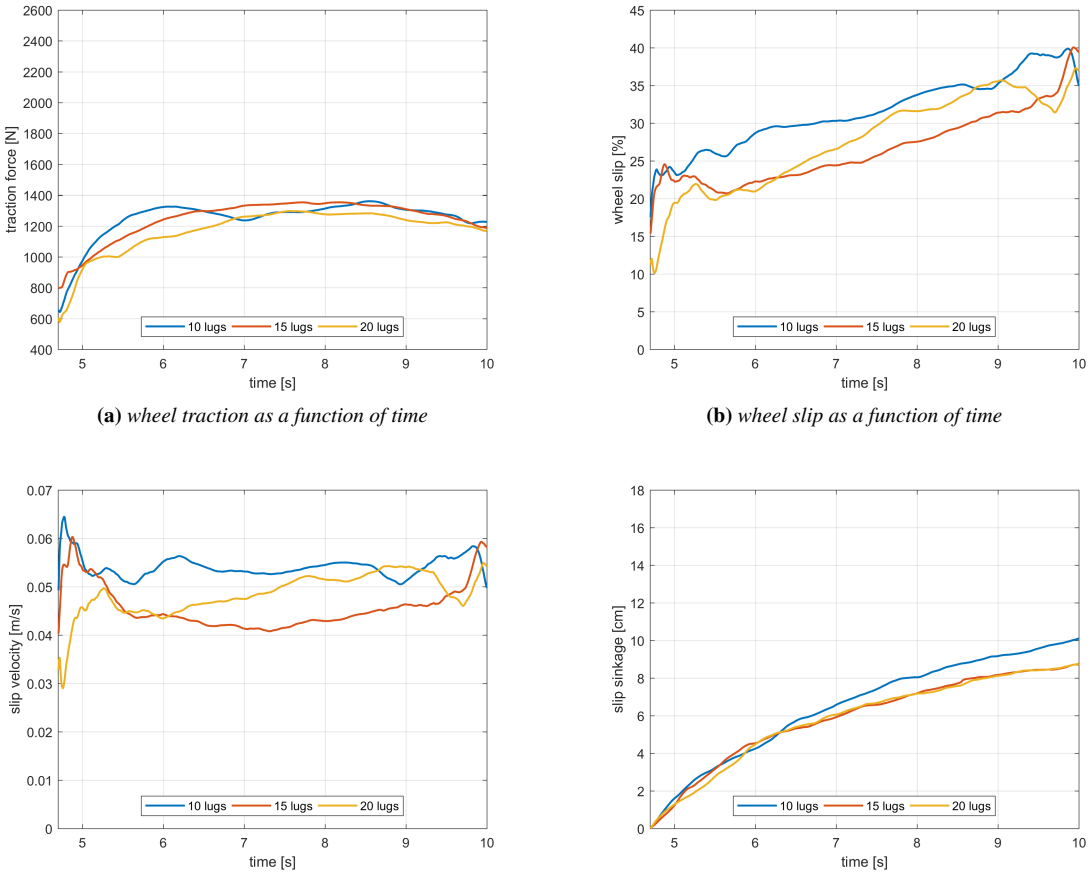

(a) *wheel traction as a function of time*

(b) *wheel slip as a function of time*

(c) *wheel slip velocity as a function of time*

(d) *wheel slip sinkage as a function of time*

Figure 3.24: *effects of lugs spacing in interaction parameters*

lugs height

From the simulation with $20mm$, $40mm$ and $60mm$ lugs height, results shown in figure 3.25, it was noted that both traction and slip sinkage of the wheel increases with increase of lugs height figure 3.25a3.25d, this is due to high digging of soil with high lugs than with low lugs [18] and high void ratio with high lugs which cause high traction. If wheel lugs are low, the slip of the soil mainly occurs at the surface between wheel surface and soil, but it will occur between the steady soil and movable soil adhering to the wheel if the lugs are high enough to form steady shearing loop [17]. Also the results shows that both slip and slip velocity figure 3.25b3.25c decreases with increase of lugs height, this is because of the effect of shearing radius due to mechanics relationship of the slip ratio for lugged tires with different lugs height [19].

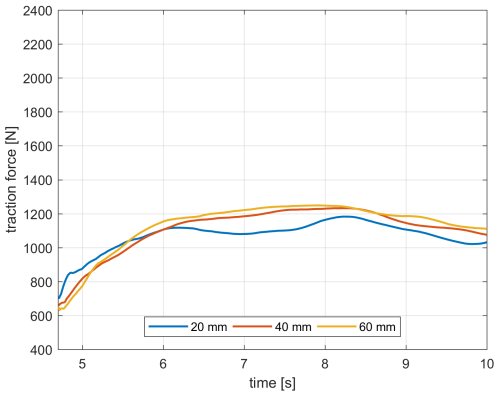

(a) *wheel traction as a function of time*

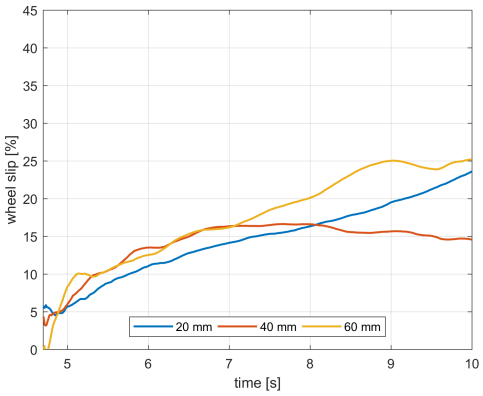

(b) *wheel slip as a function of time*

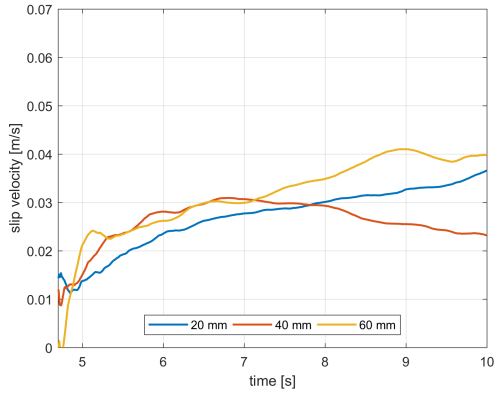

(c) *wheel slip velocity as a function of time*

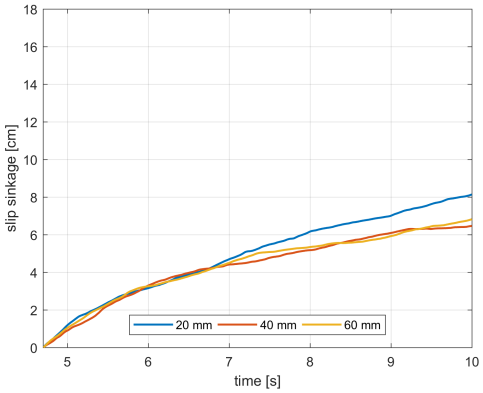

(d) *wheel slip sinkage as a function of time*

Figure 3.25: *effects of lugs height in interaction parameters*

lugs type

From the simulation results obtained with three lug types, straight, combined and non-DIR figure 3.26, it was noted that straight and Non-DIR lugs has traction force as compared to combined figure 3.26a. With regards to slip, slip velocity and slip sinkage combined lugs has low values as compared to straight and non-DIR lugs figure 3.26b3.26c3.26d, this is because combined lugs has high resistance to the soil flow during interaction which leads decrease of sinkage, slip and slip velocity. This is to say that combined lugs takes advantage of straight and Non-DIR lugs and gives better performance [71].

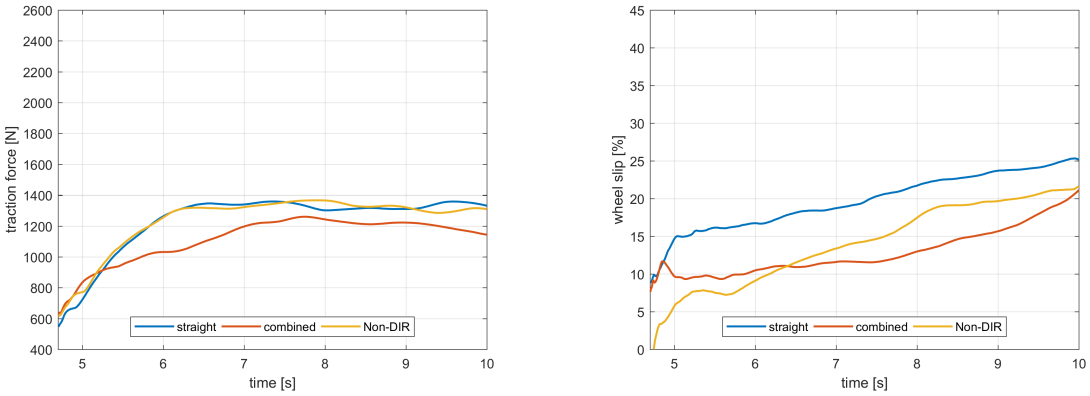

(a) *wheel traction as a function of time*

(b) *wheel slip as a function of time*

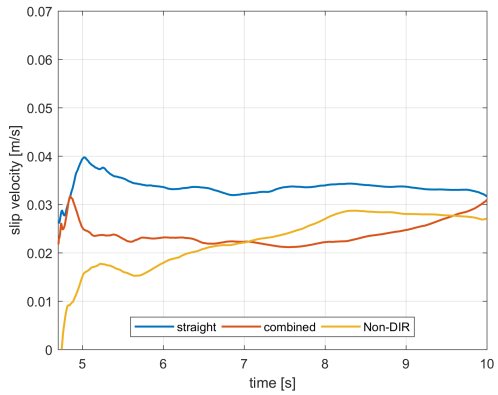

(c) *wheel slip velocity as a function of time*

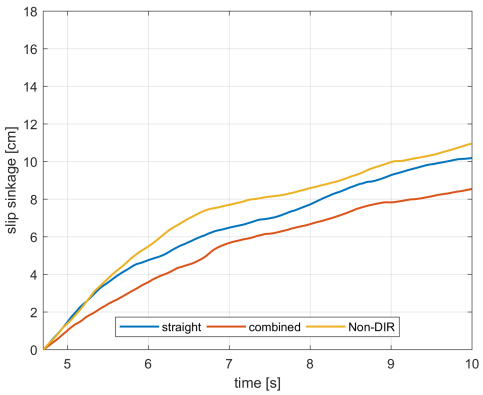

(d) *wheel slip sinkage as a function of time*

Figure 3.26: *effects of lugs types in interaction parameters*

lugs inclination angle

From the simulation results obtained with $25°$, $35°$ and $45°$ lugs inclination angles, it was noted that wheel slip and slip velocity increases with increase of lugs angle 3.27b and 3.27c, this is because of high lateral resistance to soil particle flow with small angle as compared to larger. Although small angle has low slip and slip velocity but $45°$ lugs angle has high traction force 3.27a as compared to $25°$ lugs angle, this is because of decrease of slip sinkage which results to low motion resistance [18].

Furthermore, with regards to slip sinkage of the wheel, the difference is small especially at steady state 3.27d, this is because at steady state influence of lugs angle is small due to continuous shearing of soil with sufficient number of the wheel lugs [18].

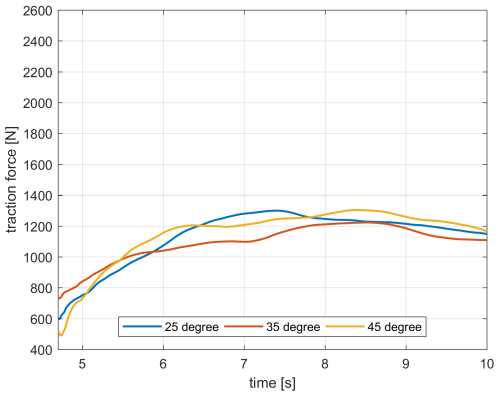

(a) *wheel traction as a function of time*

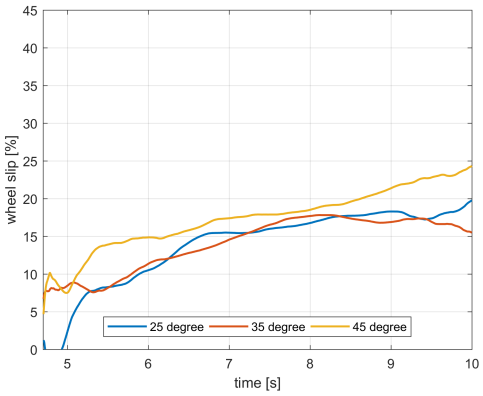

(b) *wheel slip as a function of time*

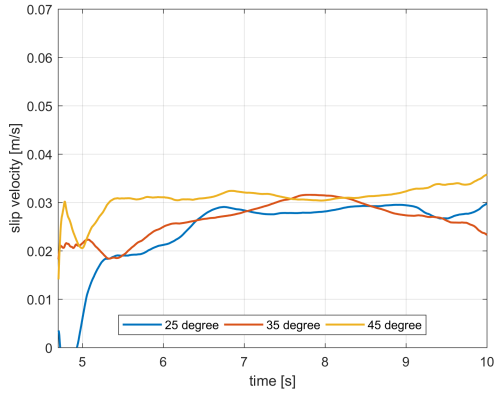

(c) *wheel slip velocity as a function of time*

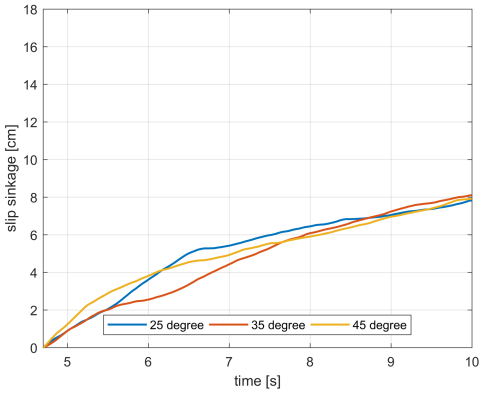

(d) *wheel slip sinkage as a function of time*

Figure 3.27: *effects of lugs inclination angle in interaction parameters*

effect of wheel speed and weight on interaction parameters

wheel angular speed

Wheel angular speed has effects on traction, slip, slip sinkage and slip velocity of the wheel figure 3.28. Traction force increases with increase of wheel speed figure 3.28a, this is because of increase of deformation resistance due to influence of wheel speed on shear and penetration deformation rate as well as inertia effects which also increase with wheel speed. Although traction increases with wheel speed, but more increase cause traction force to decrease more especially at steady state, this is bacause of wheel inertia overcome motion resistance and cause resistive torque to decrease.

Wheel slip sinkage decreases with increase of wheel speed 3.28d, this also is because of decrease of shear deformation with increase of wheel speed. This shows that there is an optimal wheel speed and slip which can be controlled to make the wheel comes not to sink more or stuck [75, 91] during interaction. However, there is an increase of slip and slip velocity with increase of wheel speed figures 3.28b , 3.28c, this is due to influence of angular speed on wheel slip and slip velocity [91].

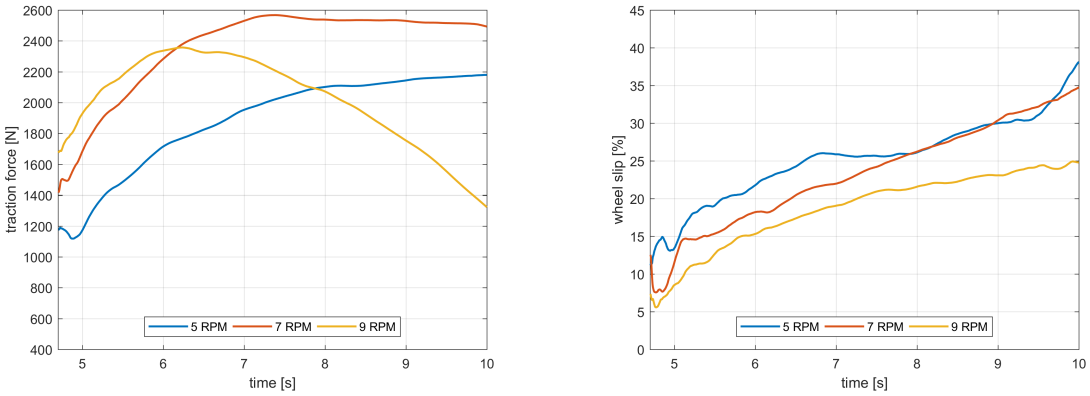

(a) *wheel traction as a function of time*

(b) *wheel slip as a function of time*

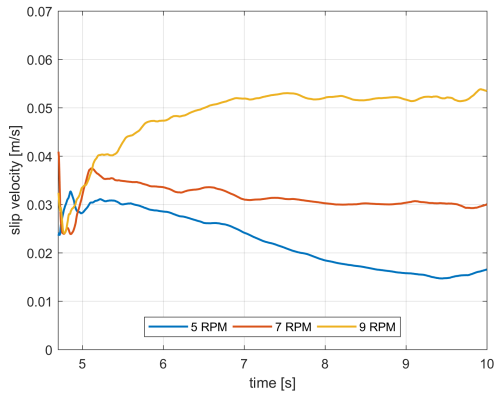

(c) *wheel slip velocity as a function of time*

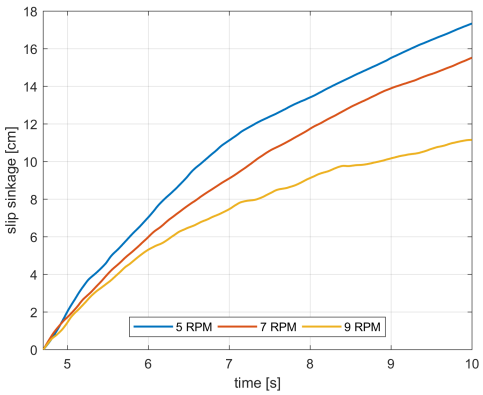

(d) *wheel slip sinkage as a function of time*

Figure 3.28: *effects of wheel angular speed in interaction parameters*

wheel weight

From the simulation results obtained with $5kN$ $7kN$ and $9kN$ wheel load, it was noted that wheel traction force increases with increase of wheel weight figure 3.29a, this is because of increase of terrain compaction resistance with increase wheel load [5,18,53] as a result cause high motion resistance . Also slip sinkage increases with wheel load figure 3.29d, this is because, wheel load increases deformation of the terrain and cause more soil particles to be raked out under the wheel [40,74] and also cuase high lateral flow of particles due to deformation.

Also wheel slip increases with wheel load and the effect is significant at steady state figure 3.29b, at which slip sinkage of the wheel increase monotonically and this signify that the effect of the soil deformation due to wheel load cannot be neglected [18,58]. Wheel slip velocity increases with increase of speed, this is due to influence of wheel slip on slip velocity which increases with load figure 3.29c.

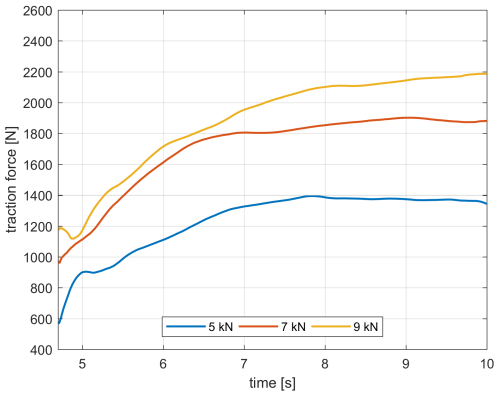

(a) *wheel traction as a function of time*

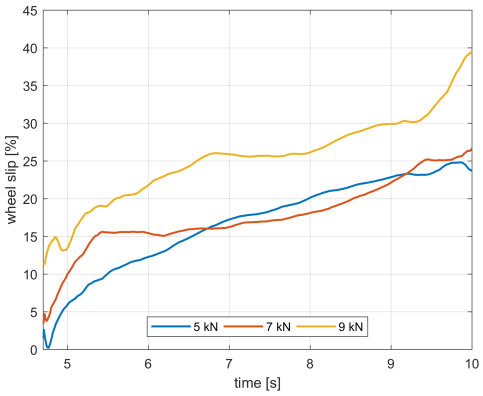

(b) *wheel slip as a function of time*

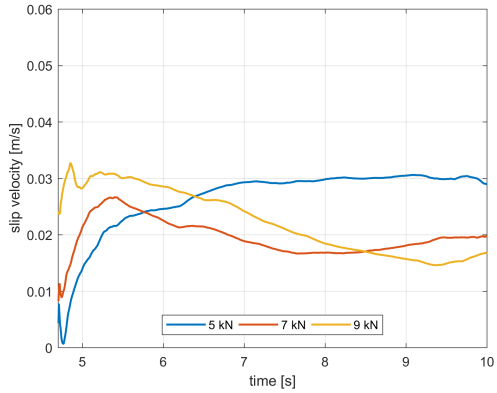

(c) *wheel slip velocity as a function of time*

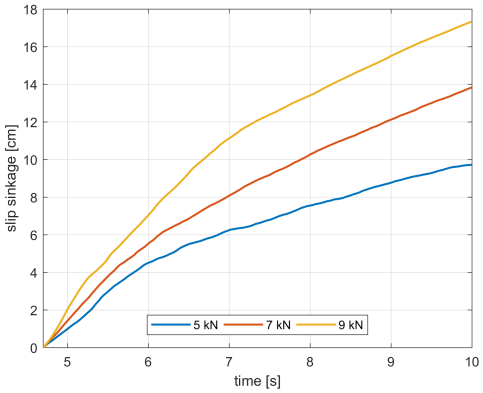

(d) *wheel slip sinkage as a function of time*

Figure 3.29: *effects of wheel weight in interaction parameters*

Pre-compaction of terrain

A compactor was added to the model in order to analysis effects of terrain pre-compaction in interaction parameters. The compactor is a rigid concrete and compaction was based on weight and released height, taking the same release height and changing compactor weight, pre-compaction of terrain at different compaction weight was achieved.

traction force

	compaction weight $[Kg]$				
slip$[\%]$	0	400	1200	5000	
5	3045	2814	2704	2546	traction
25	3716	3651	3575	3449	force$[N]$

Table 3.2: *traction as function of slip at various compaction weight*

slip sinkage

	compaction weight $[Kg]$				
slip$[\%]$	0	400	1200	5000	
5	4.12	3.40	2.96	2.10	slip
25	8.66	7.82	7.40	6.93	sinkage$[cm]$

Table 3.3: *slip sinkage as function of slip at various compaction weight*

slip velocity

	compaction weight $[Kg]$				
slip$[\%]$	0	400	1200	5000	
5	0.018	0.015	0.014	0.013	slip
25	0.049	0.042	0.040	0.038	velocity$[m/s]$

Table 3.4: *slip velocity as function of slip at various compaction weight*

forward velocity

	compaction weight $[Kg]$				
slip$[\%]$	0	400	1200	5000	
5	0.28	0.30	0.33	0.35	forward
25	0.12	0.14	0.15	0.17	velocity$[m/s]$

Table 3.5: *forward velocity as function of slip at various compaction weight*

From the simulation results analysis figure 3.30a, it was noted that traction force decreases with increase of compaction weight, both at 5% and 25% wheel slip. This was due to increase of compaction resistance of the terrain with increase of compaction weight, which cause decrease of motion resistance as well as traction.

Taking into account slip sinkage of the wheel, results in figure 3.30b, it was inferred that slip sinkage decreases with increase of compaction weight, this also was cause by increase of compaction resistance of the terrain with increase of compaction weight.

Pre-compaction of terrain has effects on slip velocity, as it was noted that slip velocity decreases with increase of compaction weight figure 3.30c, this was also due to increase of deformation resistance of the terrain due to increase of pre-compaction weight which reduce slip sinkage and slip velocity.

Forward velocity of the wheel increases with increase of pre-compaction weight, this was noted in results figure 3.30d, increase of pre-compaction increases compaction resistance of terrain which decrease slip sinakge as a results increase forward velocity which is the function of slip velocity and slip sinkage.

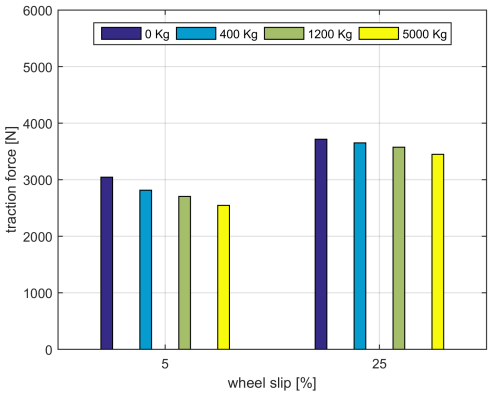

(a) *traction force as a function of wheel slip at various pre-compaction weight*

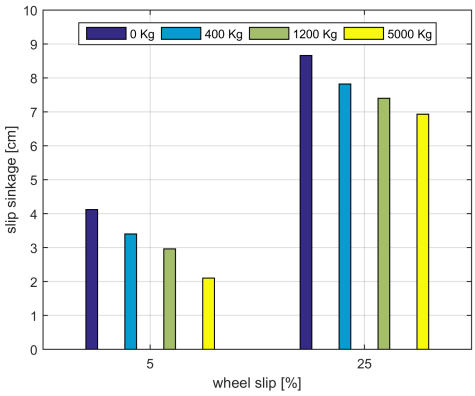

(b) *slip sinkage as a function of wheel slip at various pre-compaction weight*

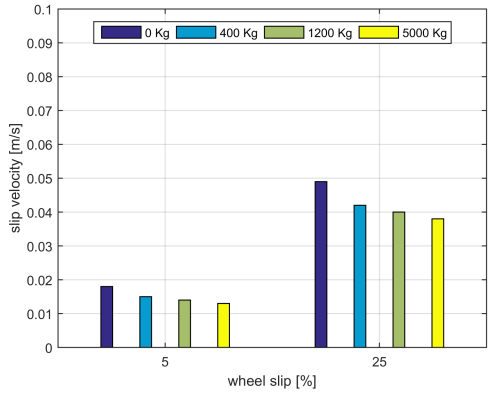

(c) *slip velocity as a function of wheel slip at various pre-compaction weight*

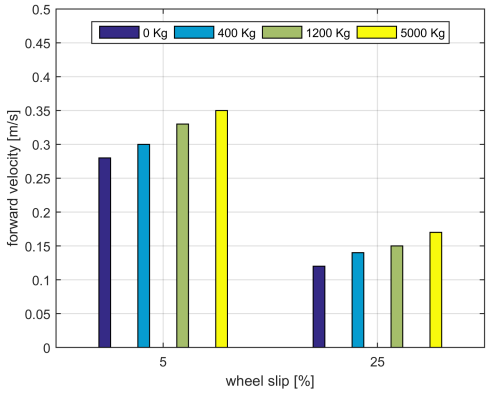

(d) *forward velocity as a function of wheel slip at various pre-compaction weight*

Figure 3.30: *interaction parameters at different pre-compaction weight*

3.5.2 Soft deformable terrain

traction force

Simulations were carried out by allowing a wheel to interacts with terrain adopted from [106] with parameters tabulated in table 3.6. Simulation results of traction force at respective wheel slip are tabulated in tables below for all terrains.

terrain	n	$k_c[kN/m^{n+1}]$	$k_\phi[kN/m^{n+2}]$	$c[kPa]$	$\phi[^\circ]$
dry sand (LLL)	1.1	0.99	1528.43	1.04	28
sand loam	0.9	52.53	1127.97	4.83	20
LETE sand	0.79	102	5301	1.3	31.1
grenville loam	1.01	0.06	5880	3.1	29.8
lean clay(WES)	0.2	16.43	1724.69	68.95	20

Table 3.6: *terrain parameters [106]*

	terrain					
slip [%]	dry sand (LLL)	sand loam	LETE sand	grenville loam	lean clay(WES)	
5	6838	7038	7568	7712	4351	
10	7865	8021	8336	8373	5518	
15	9488	8795	8663	8829	6106	traction
20	10390	9465	9429	9551	6971	force $[N]$
25	11030	10140	10080	11220	7191	
30	11580	11310	11330	12140	7776	

Table 3.7: *traction force at respective wheel slip*

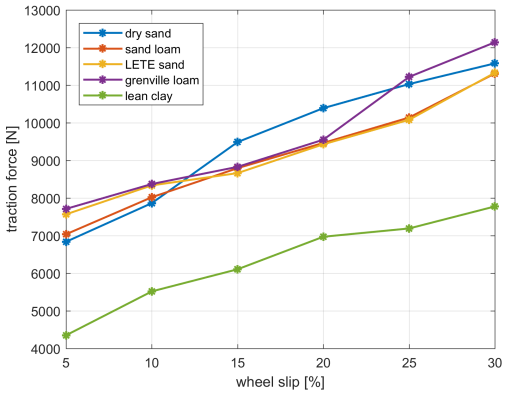

Figure 3.31: *traction force as a function of wheel slip*

From the simulation results in figure 3.31, it has been observed that increase of wheel slip increases traction force. Also it was possible to infer that traction force is a function of terrain properties, this was caused by difference in soil strength which represented by Wong's parameters such as angle of internal shearing resistance, sinkage exponent, cohesion, internal shear modulus parameter and cohesion modulus parameter which indicated in table 3.6.

For lean clay sand it was oberved that it supplies less traction force as compared to dry sand, sand loam, LETE sand and grenvile sand, this is because this type of soil it has very low sinkage exponent and angle of internal shearing, which leads to low motion resistance as well as traction force at respective slip. For dry sand, sand loam, LETE sand and grenvile sand, it was observed that the difference in traction force is small, this was because of small difference in angle of internal shearing and sinkage exponent. Although sand loam has high cohesion and cohesion dependent parameter as compared to dry sand, LETE sand and grenville loam, but these parameters has less impact to soil strength in this model as compared to angle of internal friction, internal friction dependent parameter and sinkage exponent.

Influence of wheel design on interaction parameters

The model developed in this chapter was used to analyse the effects of wheel parameters to traction force, sinkage, contact pressure. Traction force was evaluated at 10% and 20% wheel slip, while sinkage and pressure shown by colour bar was evaluated at 20% wheel slip for three wheels with different parameters. Pattern configurations of wheels

in this section are the same, instead lugs number, wheel diameter and width are different as shown in table 3.8. Variation of lugs number was done in order to maintain equal lug spacing for changing diameter of the wheel.

wheel	$\delta[^\circ]$	$l_h[mm]$	$h[mm]$	$D_0[mm]$	$n_l[]$	$w[mm]$
1	45	60	120	1220	18	479
2	45	60	120	1420	20	530
3	45	60	120	1620	23	611

Table 3.8: *wheel parameters*

wheel	slip 10%	slip 20%	
1	7472	8152	traction
2	7651	9158	force
3	7694	9169	$[N]$

Table 3.9: *traction force as a function of wheel slip*

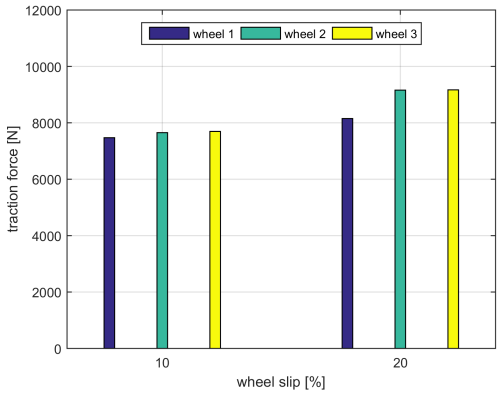

Figure 3.32: *traction force as a function of wheel slip*

From the simulation results in figure 3.32, it was noted that traction force results for all wheel is almost the same at 10% wheel slip, but when slip increases traction force increases significantly with wheel diameter, this was noted at 20% wheel slip. Taking into account sinkage in figure 3.33a, 3.34a and 3.35a, it was noted that changing colour intensity from blue to red increases with decrease of wheel diameter. This indicates that sinkage increases with decreases of wheel diameter. With regards to contact pressure figures 3.33b, 3.34b and 3.35b, it was noted that changing colour intensity from blue to red increases with decrease of wheel diameter which means that pressure at the contact decreases with increase of wheel diameter.

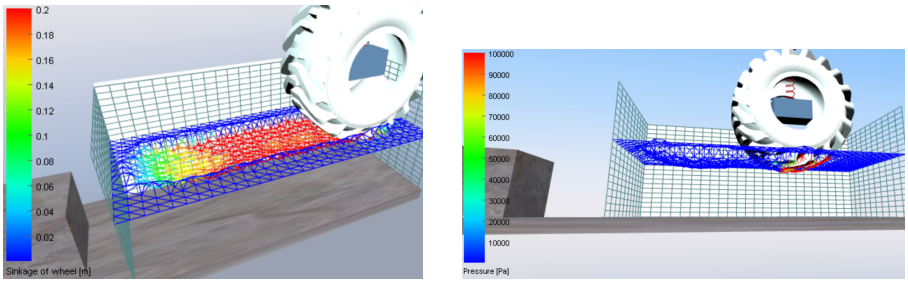

(a) *sinkage for wheel* 1 *at* 20% *slip* **(b)** *contact pressure for wheel* 1 *at* 20% *slip*

Figure 3.33: *slip sinkage and contact pressure at* 20% *wheel slip for wheel* 1

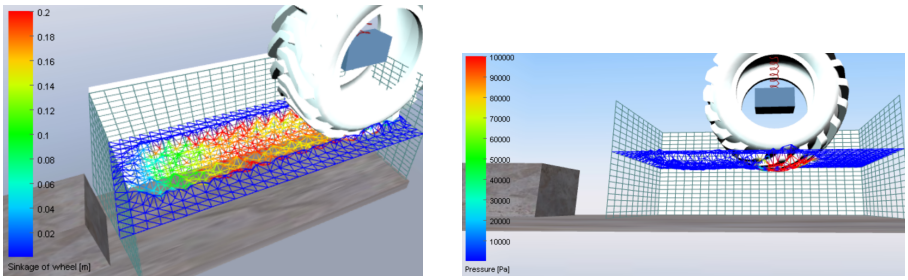

(a) *sinkage for wheel* 2 *at* 20% *slip* **(b)** *contact pressure for wheel* 2 *at* 20% *slip*

Figure 3.34: *slip sinkage and contact pressure at* 20% *wheel slip for wheel* 2

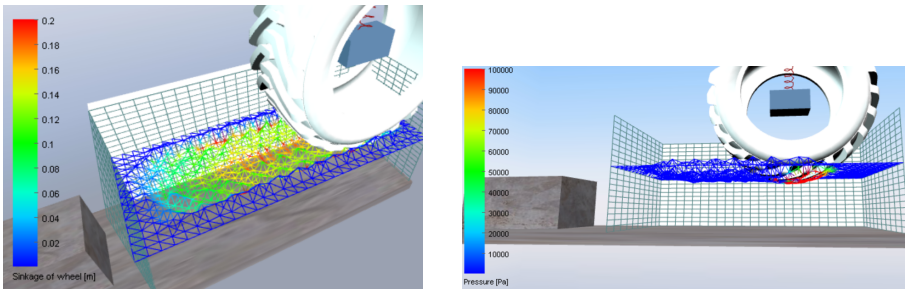

(a) *sinkage for wheel* 3 *at* 20% *slip* **(b)** *contact pressure for wheel* 3 *at* 20% *slip*

Figure 3.35: *slip sinkage and contact pressure at* 20% *wheel slip for wheel* 3

Also it was noted that higher pressures occurs in between point of maximum sinkage and entry point and not at the point of maximum sinkage, this results correlates with [106] stress distribution at the contact.

From the results analysis above, it was concluded that, although small change of wheel parameters such as diameter and width gives small change in traction force especially at low wheel slip, but gives high effects on sinkage and contact pressure and this effects increases with wheel slip. Therefore, even small change of wheel parameters has to be taken into consideration when analysing wheel performance and soil destruction since it affects wheel sinkage which is the measure of wheel performance and contact pressure which is the measures of soil failure in terms of maximum stresses respectively.

3.5.3 Conclusions

The capability of chrono::engine was utilised in this modelling of tyre-soil interaction. The rigid wheels with different lugs type and design were used in the simulation with respect to terrain particles characteristics. The simulation results shows that interaction parameters such as slip ratio, slip sinkage, static sinkage, slip velocity and traction force are the function of lugs type, lugs height, lugs inclination angle, lugs number, wheel load, wheel speed and soil particles characteristics.

The model gives out the interaction parameters with respect to soil characteristics such as traction, slip ratio, slip velocity, static sinkage and slip sinkage, and from these it was concluded that soil characteristics wheel parameters and tyre lugs design has to be taken into consideration for the interaction problem. The performance of the rigid wheel on deformable terrain gives out the promising results in which the effects of discontinuous deformation of the terrain such as build-up and cleaning by considering the longitudinal and lateral deformation of the terrain can be observed.

Also from the analysis results in section 4.3,it was inferred that pre-compaction of terrain has some effects on interaction parameters. Pre-compaction of terrain increases deformation resistance, this is because compacting soil particles increases bulky density as well as compaction resistance. This reduce sinkage of the wheel due to slip which results to lower motion resistance as well traction force. Since interaction parameters such as traction force, slip sinkage, slip velocity and forward velocity are functions of soil compaction resistance, then effect of pre-compaction weight of terrain has to be taken into account for wheel performance analysis during interaction for the case of positive impact to the ground as in construction.

From the fact that, the simulation results of the model shows the sensitivity of the tyre pattern design and the soil characteristics on interaction parameters, therefore the model can be useful tool for sensitivity analysis and optimisation analysis of tyre tread pattern design with respect to soil characteristics.

3.6 Model Validation

3.6.1 Granular terrain

The model has been validated by comparison with the results of an experimental tests done by NSDL single wheel traction research vehicle, which has been taken from [104] without modification. Since the experimental tests performed with flexible tyres and the model in chrono::engine considers only rigid tyres then, some assumptions has to be considered; first the tyres used in the experimental test has high inflation pressure enough to make the change in radius due to tyre deflection is small to be compared with rigid one in highly deformable terrain.

Simulations for model validation were carried out by considering a class of particles distribution according to figure 3.36, with smaller and larger diameters of $5mm$ and $50mm$ respectively. Diameters range was chosen in order to limit number of colliding bodies in the bin for reasonable simulation computational effort as well sufficient depth of the terrain. Particles densities, diameter are shown in table 3.10 with corresponding mass percentages.

Simulation for model validation was carried out with spheres only in the soil bin.

The appropriate simulation parameters such as number of particles, density and size (see table 3.10), were set to estimate the traction at different wheel load and particle properties, and the results are shown in table 3.11 with corresponding errors.

number[-]	mass percentage[%]	density[kg/m^3]	mean diameter[m]
18000	0.8	1270	0.02276
18000	0.8	1380	0.02276
18000	0.8	1750	0.02276

Table 3.10: *soil particles granulometry used in the chrono::engine simulations*

From the simulation results with given wheel load it was inferred that the traction force increases with increase of wheel load figures 3.37a, 3.37b, 3.37c, and reaches a constant value with the simulation time. This is because increase of wheel load increases compaction resistance as well as motion resistance. Also it can be noted that traction of the wheel increases with increase of slip figure 3.37d.

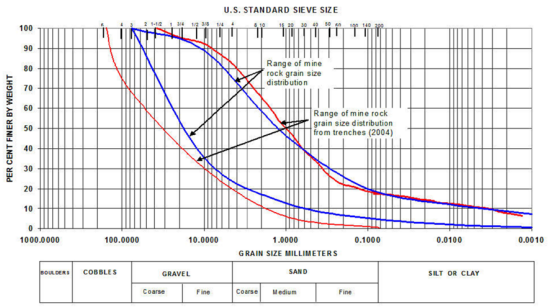

Figure 3.36: *soil sample granulometry according to sieve standard [63].*

traction force

wheel load[kN]	experimental traction force [kN]	simulation traction force [kN]	error[%]
13.2	4.7	4.4	6.4
19.8	7.1	7.0	1.4
25.3	8.9	8.5	4.5

Table 3.11: *comparison of experimental results [104] and chrono::engine model results*

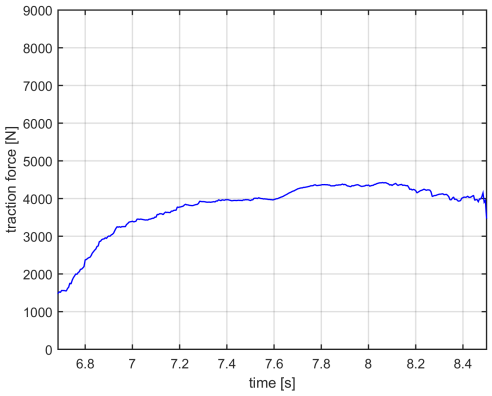

(a) *wheel traction as a function of time at 13.2 kN*

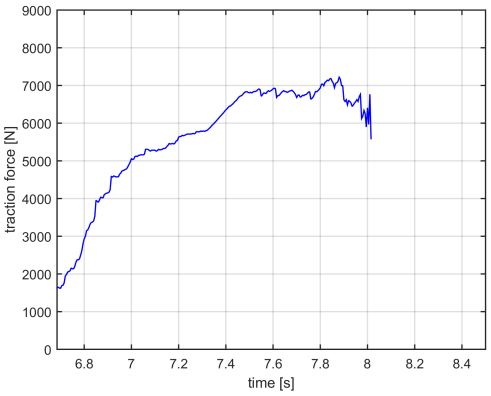

(b) *wheel traction as a function of time at 19.8 kN*

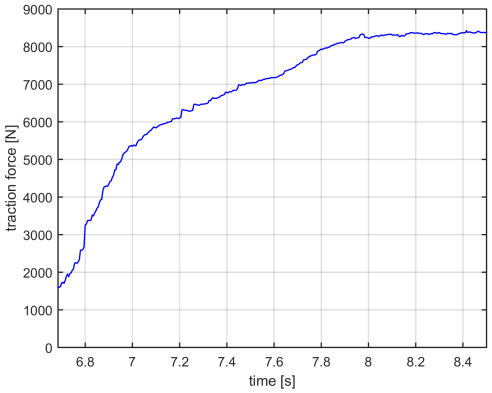

(c) *wheel traction as a function of time at 25.3 kN*

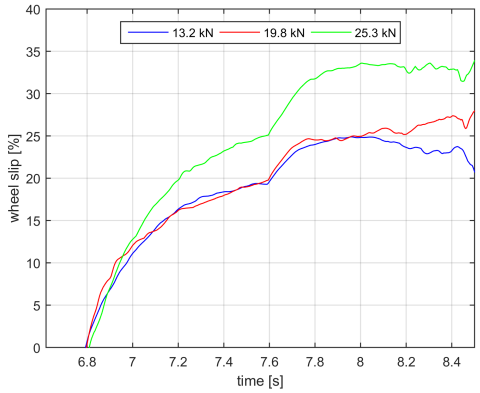

(d) *wheel slip as a function of time*

Figure 3.37: *model validation simulation results for traction force*

3.6.2 Soft deformable terrain

Semi-empirical model developed in this work was validated with experimental and numerical traction force results from the work of [71]. Model traction force results with corresponding errors for both experimental and numerical results are graphically presented in figure 3.38 and tabulated in table 3.12 below.

traction force

slip $[\%]$	model $[N]$	experimental $[N]$	error $[\%]$	numerical $[N]$	error $[\%]$
5	6750	6273	7.6	6730	0.3
10	7943	7892	0.6	7730	2.8
15	8354	8152	2.5	8190	2.0
20	8807	8922	1.3	8650	1.8
25	9459	8996	5.1	9243	2.3
30	9694	9226	5.0	10099	4.0

Table 3.12: *model traction force with corresponding errors from [71] results*

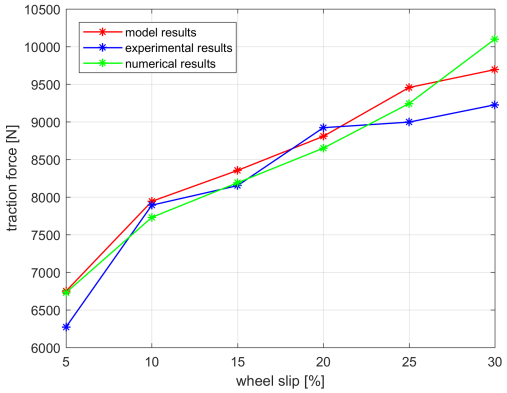

Figure 3.38: *traction force as a function of wheel slip*

From model validation results analysis, it was observed that the model guarantees traction force with an error below 8% as compared to experimental results from [71], while considering results of numerical model from the work of [71], semi-empirical model guarantees traction force results with 4% error.

3.6.3 Conclusions

The traction force increases with increase of wheel load, and it is possible to observe that the results of the model have good correlation with experimental results as seen from table 3.11, which guarantees an error less than 6.5%. The simulations of the model was carried out with sphere particles only which lucky interlocking mechanism, this may result into high sinkage and motion resistance, but it is possible to observe that the estimation error of the traction force is less than 6.5% which is reasonable estimation error.

This was achieved by setting appropriate particles density and tangential deformation resistance force which comes from friction force of the particles due to contact normal force and friction coefficient, this guaranteeing a minimum error in traction force estimation. Although terrain made by assemblage of sphere particles only, the particles lucky interlocking mechanism, it can be used to estimate interaction parameters such as traction force, slip, slip sinkage, slip velocity and forward velocity, and these cab be achieved by setting appropriate particle density, cohesion, friction coefficient, size, terrain layer size and wheel angular speed with given tread pattern design.

Also soft deformable terrain realistically expresses deformability of the terrain taking into account the effcts of lateral and longitudinal displacement of soil material under tyre-soil contact to wheel performance. Model also expresses wheel performance in terms of traction force, sinkage and contact pressure as a function of soil parameters, wheel slip and wheel parameters. Effects of the pattern configuration to the traction force, sinkage and contact pressure has been accounted by the model through sensitivity analysis performed.

From the validation analysis the model shows a good agreements with experimental ana numerical results of traction force as respective wheel slip with an acceptable error of less than 7%.

CHAPTER 4

Tread Pattern Sensitivity Analysis

Flexibility of chrono::engine tyre-soil interaction model developed in this work made easy to take into account different tread patterns and soil properties, hence sensitivity analysis during wheel-terrain interaction were performed and detailed in this chapter.The analysis of traction force and slip sinkage at selected wheel slip were done.

Traction force and slip sinkage are the major wheel performance parameters in deformable terrain as seen in chapter 3 section 3.5 and this made to be the reason to choose these interaction parameters for sensitivity analysis. The soil particles parameters to be considered in the analysis are those mentioned in chapter 3 such as type of particles and cohesion force.

In particular the tread pattern to be taken into consideration in this chapter are typical tread pattern for traction tyres [71] commonly known as combined lugs as in figure 4.1. The simulation will be carried out by varying the lugs centre length, angle, height and soil properties such as cohesion and particle types. Since the variation of parameters accounts for many simulation variables, the simulations and analysis of the pattern sensitivity will be divided into sections for simplicity. These sections were accounted by the lugs angle, lugs centre length, lugs height to find the optimal pattern configuration in terms of high traction force and low slip sinkage at selected wheel slip 10% and 25% for non-cohesive and cohesive particles.

Although, the common wheel slip for agriculture machines without and with attachments such as plough, planter or harrow during operation is in the range of 5% to 25% [71], besides the slip values for was selected because for highly deformable terrain like non cohesive dry sand particles, the model did not guarantee high accuracy at low slip values before steady state during simulation time. Besides, the reference parameters was $(80mm, 45^{\circ})$ lugs length, angle respectively adopted from [71], while the height reference of $60mm$ was taken from the previous simulation in chapter 3.

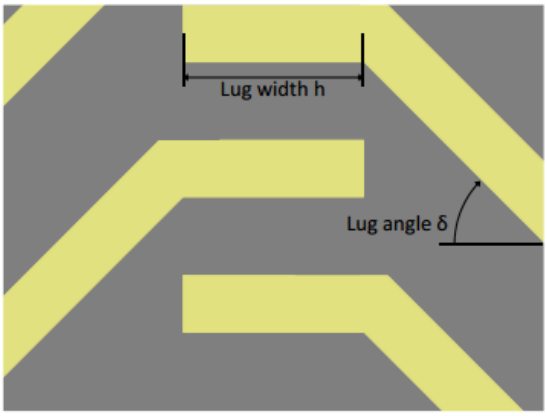

Figure 4.1: *Combined lugs-pattern parameters [71].*

The length h, angle δ and l_h height of the lugs were varied in order to find the optimal configuration with respect to soil characteristics. The reference parameters of length, height and angle were $80mm$, $60mm$ and $45°$ and the variation of lugs parameters tabulated in the table 4.1, will be accounted in the simulations.

$h[mm]$	60	80	100	120
$\delta[°]$	25	35	45	55
$l_h[mm]$	20	40	60	80

Table 4.1: *lugs parameters variations in sensitivity analysis*

4.1 Granular terrain

Simulations are carried out by interacting terrain made of different particle shapes such as sphere, square, convex hulls and mixing of particles with wheels having different lugs parameters such as lugs angle, lugs center length and lugs height as indicated in table 4.1. This is to analyse effects of particles shapes and properties on sensitivity of lugs design in terms of traction force and slip sinkage during interaction. Two terrains cohesive and non-cohesive are considered in each sections with respective particles shapes.

Particle mass distributions are kept constant in each sections simulation. Since particles shapes makes difference in parking and arrangements of particles and affects terrain depth for the same number of particles in the soil bin, number of particles was varied to maintain same terrain depth between different particle shapes as stated in the respective sections. Simulation parameters such as time step, wheel speed, wheel load, particles size, friction coefficient, cohesion force are kept constant for non-cohesive and cohesive terrains.

4.1.1 Terrain with spheres particles

Non Cohesive particles

The simulation results for traction and slip sinkage for selected slip of the wheel were tabulated in tables 4.2 to 4.7 respectively. The lugs angle, centre length and height are

marked at x-axis, while traction force, slip sinkage, forward velecity and slip velocity are marked at y-axis, and the bars refers to 10, 15, 20 and 25 lugs numbers respectively.

Traction Force

	slip 10%				slip 25%				
	lugs number				lugs number				
$\delta[^\circ]$	10	15	20	25	10	15	20	25	
25	832	1116	1116	1030	1594	1714	1806	1841	
35	494	918	1018	1153	1135	1467	1797	1753	traction force
45	891	1016	1147	1133	1412	1567	1855	1793	$[N]$
55	650	701	801	874	1400	1223	1430	1491	

Table 4.2: *traction force as a function of lugs angle*

	slip 10%				slip 25%				
	lugs number				lugs number				
$h[mm]$	10	15	20	25	10	15	20	25	
60	1244	941	750	922	1610	1457	1292	1703	
80	991	1016	1147	1133	1412	1567	1855	1793	traction force
100	1204	1272	948	848	1532	1853	1752	1532	$[N]$
120	1255	923	661	932	1504	1421	1458	1581	

Table 4.3: *traction force as a function of lugs centre length*

	slip 10%				slip 25%				
	lugs number				lugs number				
$l_h[mm]$	10	15	20	25	10	15	20	25	
20	592	731	855	985	1205	1302	1363	1533	
40	1034	869	687	827	1674	1526	1612	1730	traction force
60	991	1016	1147	1133	1612	1667	1855	1793	$[N]$
80	918	1098	918	1098	1537	1788	1856	1922	

Table 4.4: *traction force as a function of lugs height*

Figures from 4.2a to 4.2f shows influence of lugs parameters on the traction force while figures 4.3a to 4.3f shows the influence of lugs parameters on slip sinkage of the wheel.

Taking into account influence of lugs angle on traction force, it was noted that generally traction force increases with increase of slip figure 4.2. Traction force increase with lugs number up to optimal number, this is because more lugs increases lugs that interacts with the soil at contact and this leads to increase of traction force. Also lugs number changes lugs spacing and this changes amount of soil between lugs which affects deformation area of soil in between lugs. 20 lugs inclined at 45°, figures 4.2a and 4.2b gives high traction force both at low slip 10% and high slip 25% respectively, while 10 lugs inclined at 35° gives lowest traction force at respective slip. Large lugs angle such as 55° has low traction force, this is because increase of lugs angle increases lateral component force and this reduce longitudinal traction force.

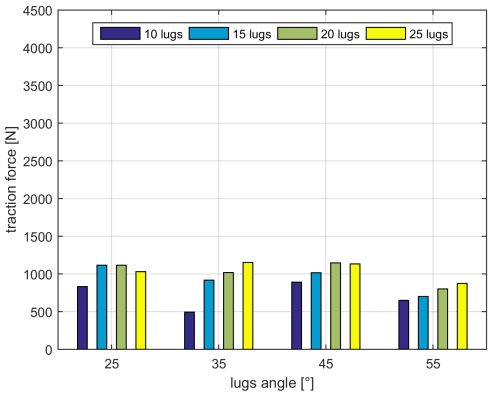

(a) *traction as a function of lugs angle at 10% slip*

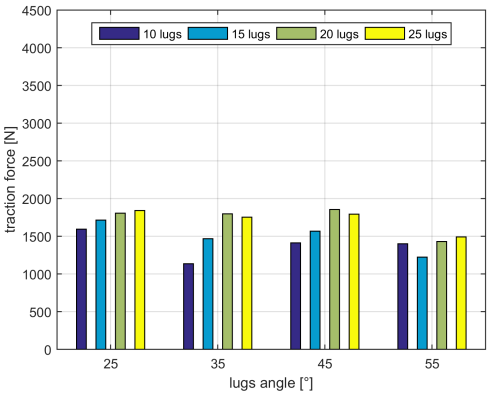

(b) *traction as a function of lugs angle at 25% slip*

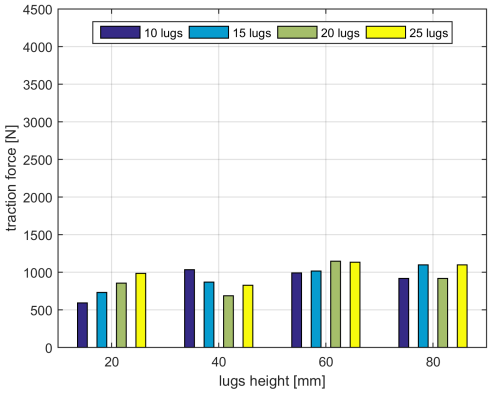

(c) *traction as a function of height at 10% slip*

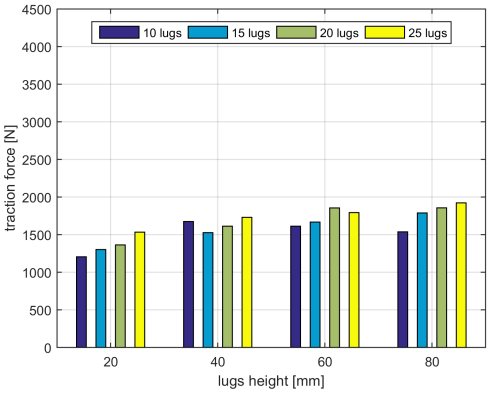

(d) *traction as a function of lugs height at 25% slip*

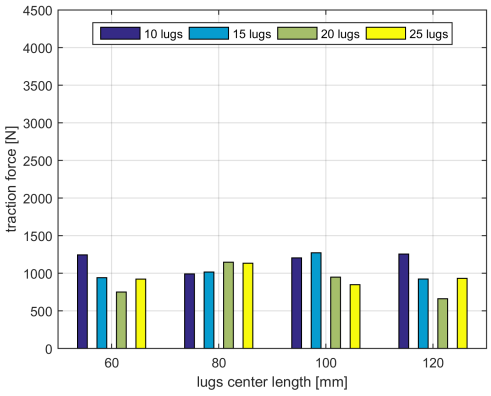

(e) *traction as a function of center length at 10% slip*

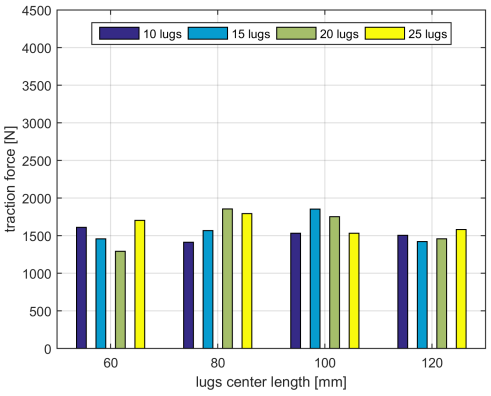

(f) *traction as a function of center length at 25% slip*

Figure 4.2: *traction force as a function of lugs angle, height and center length*

Also it was noted that 20 lugs with $60mm$ height gives high traction and 10 lugs with $20mm$ height gives lower traction at 10% slip 4.2c, while at 25% slip values, 25 lugs with $80mm$ height gives high traction force and 10 lugs with $20mm$ height gives lower traction figure 4.2d. From figure 4.2e, 15 lugs with center length of $100mm$ gives high traction and 20 lugs with $120mm$ center length gives lower traction at 10% wheel

slip, while at slip of 25% wheel slip, 20 lugs with center lengths of $80mm$ and $60mm$ figure 4.2f gives high and lower traction force respectively.

Slip sinkage

	slip 10%				slip 25%				
	lugs number				lugs number				
$\delta[^\circ]$	10	15	20	25	10	15	20	25	
25	2.02	2.27	1.84	0.92	4.30	4.85	3.98	3.23	
35	0.90	2.00	1.65	1.93	2.57	3.75	5.14	3.44	slip sinkage
45	2.36	2.59	2.59	2.17	3.80	4.55	5.58	4.24	$[cm]$
55	0.90	0.53	0.80	0.70	2.18	1.79	2.47	2.47	

Table 4.5: *slip sinkage a function of lugs angle*

	slip 10%				slip 25%				
	lugs number				lugs number				
$h[mm]$	10	15	20	25	10	15	20	25	
60	1.39	0.95	0.90	1.14	2.29	1.85	1.08	2.69	
80	2.36	2.59	2.59	2.17	3.80	3.80	4.58	4.24	slip sinkage
100	1.32	0.98	0.90	0.88	2.64	3.19	2.93	4.06	$[cm]$
120	2.03	1.78	1.06	0.96	3.91	2.83	3.14	1.65	

Table 4.6: *slip sinkage as a function of lugs centre length*

	slip 10%				slip 25%				
	lugs number				lugs number				
$l_h[mm]$	10	15	20	25	10	15	20	25	
20	0.48	1.16	0.48	1.86	2.18	3.27	1.74	3.67	
40	2.61	2.03	2.03	2.61	4.14	4.14	5.12	5.12	slip sinkage
60	2.36	2.59	2.59	2.17	3.80	3.80	4.58	4.24	$[cm]$
80	0.56	1.11	0.56	0.56	2.05	3.24	3.24	4.17	

Table 4.7: *slip sinkage a function of lugs height*

Considering lugs angle influence on slip sinkage of the wheel, it was noted that 15 and 20 lugs at an angle of 55° and 45° gives low and high slip sinkage at 10% wheel slip, figure 4.3a, while at high slip 25%, 15 and 20 lugs at an angle of 55° and 45° gives low and higher slip sinkage respectively figure 4.3b. Lugs height has influence on slip sinkage as it was noted that 20 and 10 lugs with height of $20mm$ and $40mm$ has low and higher slip sinkage at low slip of 10% figure 4.3c, while at high slip of 25% 20 lugs with height of $20mm$ and $40mm$ gives low and higher slip sinkage figure 4.3d respectively. Influence of lugs center length was noted in figure 4.3e and 4.3f, 25 and 20 lugs with center length of $100mm$ and $80mm$ gives low and higher slip sinkage both at 10% and 25% wheel slip.

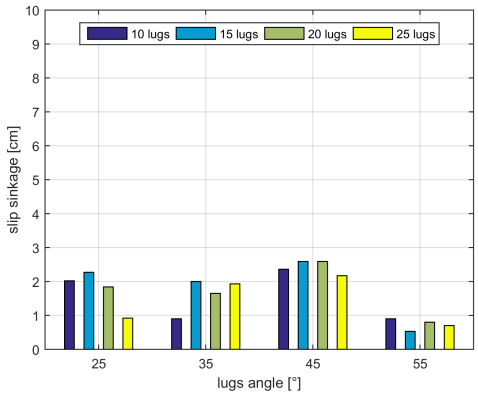

(a) *sinkage as a function of lugs angle at 10% slip*

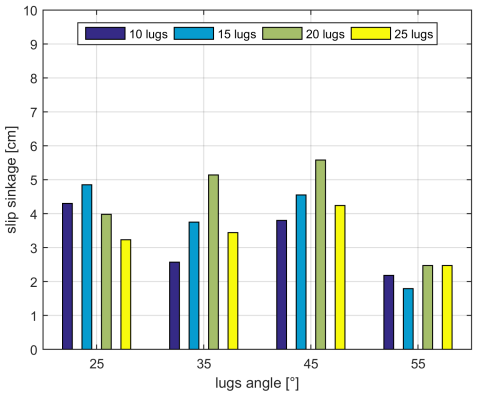

(b) *sinkage as a function of lugs angle at 25% slip*

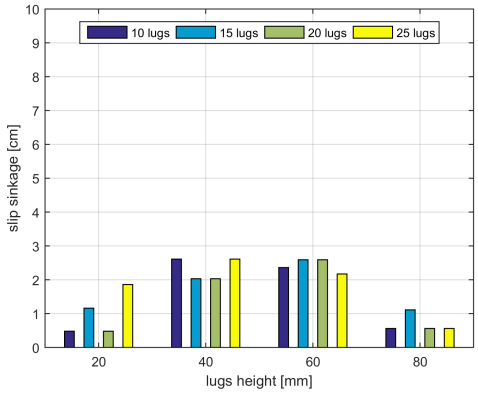

(c) *sinkage as a function of height at 10% slip*

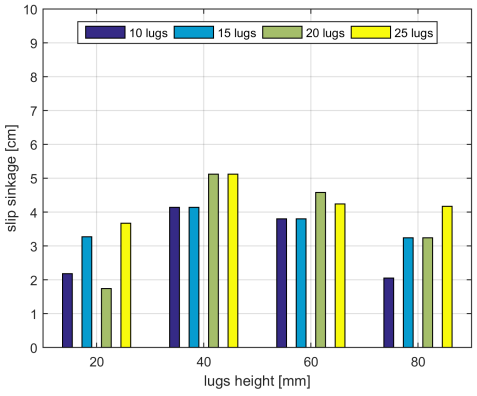

(d) *sinkage as a function of lugs height at 25% slip*

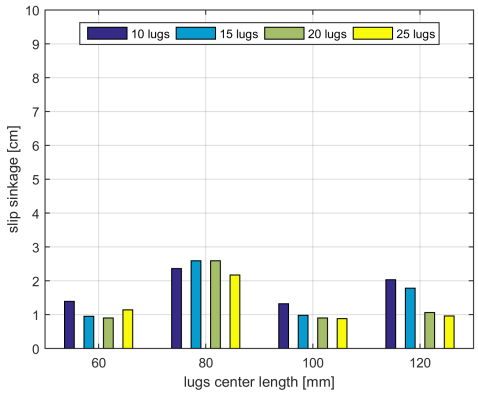

(e) *sinkage as a function of center length at 10% slip*

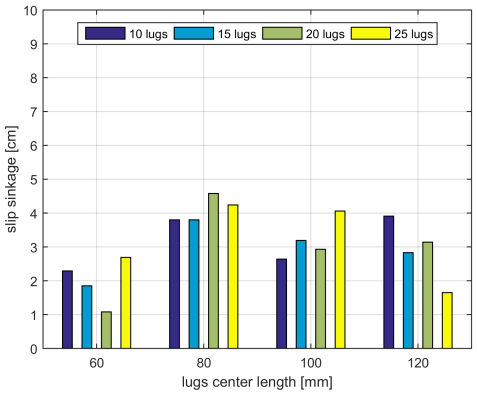

(f) *sinkage as a function of center length at 25% slip*

Figure 4.3: *slip sinkage as a function of lugs angle, height and center length*

Cohesive particles

Simulations in this section are carried out by varying the lugs parameters as explained in 4.1.1 above, instead the cohesive force is added to the particles in order to analyse its effect on pattern sensitivity. Simulation parameters such as wheel weight, speed, friction coefficient, time step and number of particles in the bin are same as in 4.1.1.

The values of the traction force and slip sinkage are taken at selected slip values as in section 4.1.1, and tabulated in tables 4.8 to 4.13.

Traction Force

	slip 10%				slip 25%				
	lugs number				lugs number				
$\delta[°]$	10	15	20	25	10	15	20	25	
25	2776	2762	2865	2815	3327	3327	3366	3327	
35	2464	2499	2603	2642	3276	3297	3256	3297	traction force
45	2591	2637	2703	2725	3115	3438	3325	3279	$[N]$
55	2585	2628	2628	2506	3375	3375	3117	3291	

Table 4.8: *traction force as a function of lugs angle*

	slip 10%				slip 25%				
	lugs number				lugs number				
$h[mm]$	10	15	20	25	10	15	20	25	
60	2397	2484	2621	2591	3115	3335	3257	3220	
80	2591	2637	2703	2725	3348	3438	3325	3279	traction force
100	2669	2550	2638	2499	3349	3340	3238	3230	$[N]$
120	2673	2721	2844	2599	3256	3386	3429	3220	

Table 4.9: *traction force as a function of lugs centre length*

	slip 10%				slip 25%				
	lugs number				lugs number				
$l_h[mm]$	10	15	20	25	10	15	20	25	
20	2077	2100	2125	2186	2817	3013	2994	2929	
40	2367	2408	2338	2338	3115	3272	3189	3228	traction force
60	2591	2637	2703	2725	3196	3438	3325	3279	$[N]$
80	2642	2823	2806	2846	3428	3437	3418	3371	

Table 4.10: *traction force as a function of lugs height*

Figures from 4.4a to 4.4f shows the influence of lugs inclination angle, centre length and height on wheel traction force while figures 4.5a to 4.5f shows influence of lugs inclination angle, centre length and height on wheel slip sinkage at selected slip values of 10% and 25% respectively.

Taking into account lugs angle figure 4.4a and 4.4d,it was noted that 20 and 10 lugs , inclined at $25°$ and $35°$ has high and lower traction both at 10% while at 25% slip 15 and 10 lugs inclined at $45°$ gives high and lower traction force respectively. Traction force increases with lugs height figures 4.4c and 4.4d, also it was noted that 25 and 10 lugs with $80mm$ and $20mm$ height has high and lower traction force at 10% wheel slip, while at 25% slip, 15 and 10 lugs with $60mm$ and $20mm$ has hight and lower traction force respectively. Traction force increases with increase of lugs center length, 10 and 20 lugs with center length of $120mm$ and $60mm$ figures 4.4e and 4.4f has high and lower traction force both at 10% and 25% wheel slip respectively.

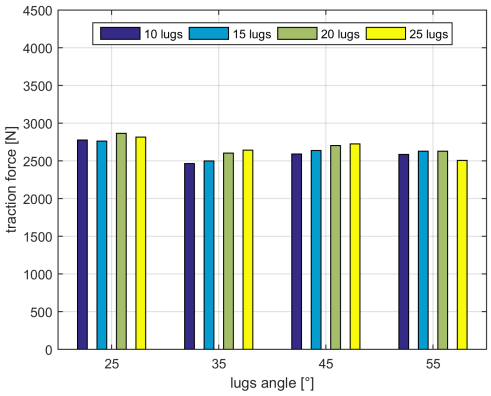

(a) *traction as a function of lugs angle at 10% slip*

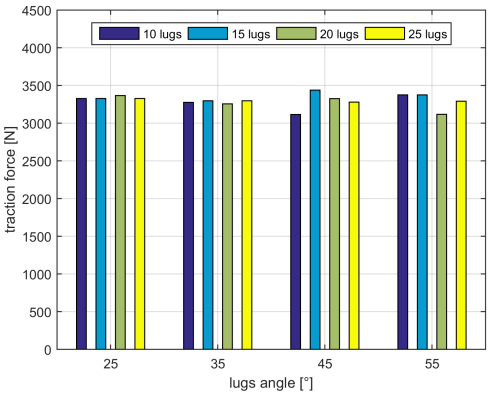

(b) *traction as a function of lugs angle at 25% slip*

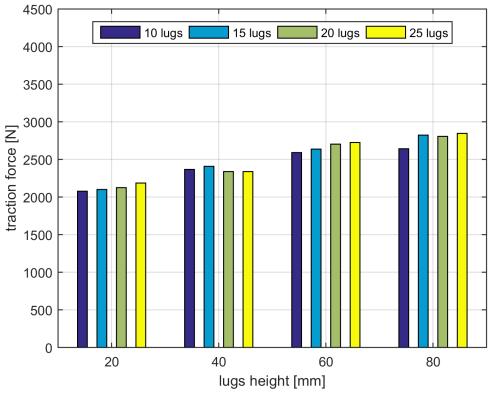

(c) *traction as a function of height at 10% slip*

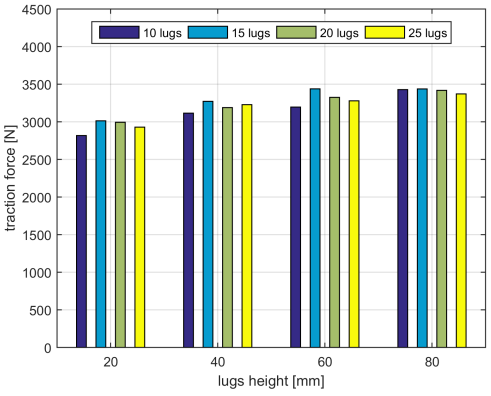

(d) *traction as a function of lugs height at 25% slip*

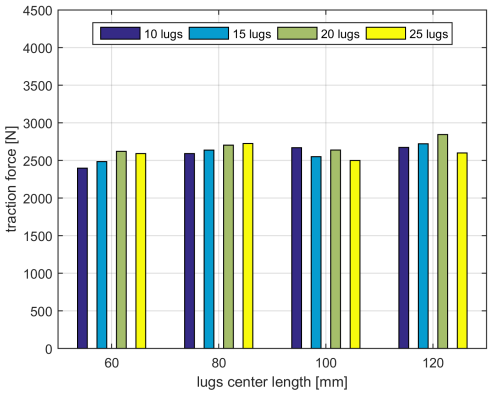

(e) *traction as a function of center length at 10% slip*

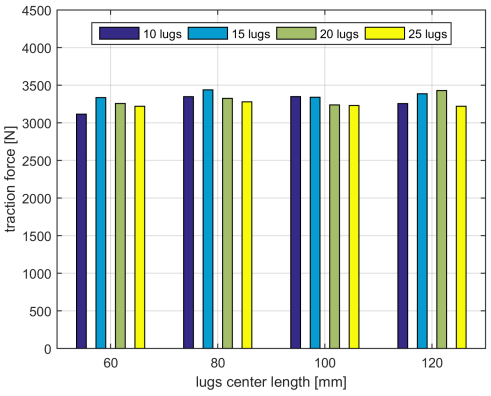

(f) *traction as a function of center length at 25% slip*

Figure 4.4: *traction force as a function of lugs angle, height and center length*

Slip Sinkage

	slip 10%				slip 25%				
	lugs number				lugs number				
$\delta[^\circ]$	10	15	20	25	10	15	20	25	
25	1.93	1.57	2.22	1.72	5.94	5.94	6.63	5.23	
35	1.07	1.36	1.84	1.20	4.44	5.44	6.30	5.92	slip sinkage
45	1.53	1.57	1.98	1.98	5.04	5.84	6.36	5.36	$[cm]$
55	1.01	1.01	1.26	0.88	5.13	5.13	4.59	4.12	

Table 4.11: *slip sinkage a function of lugs angle*

	slip 10%				slip 25%				
	lugs number				lugs number				
$h[mm]$	10	15	20	25	10	15	20	25	
60	1.02	1.25	1.50	1.01	5.04	5.27	5.61	5.03	
80	1.53	1.57	1.98	1.98	5.39	5.84	6.36	5.36	slip sinkage
100	1.54	1.33	1.47	1.69	5.73	6.06	5.63	5.33	$[cm]$
120	1.65	1.75	2.03	1.03	5.81	5.43	5.13	4.08	

Table 4.12: *slip sinkage as a function of lugs centre length*

	slip 10%				slip 25%				
	lugs number				lugs number				
$l_h[mm]$	10	15	20	25	10	15	20	25	
20	0.80	0.90	1.20	1.75	2.34	3.87	4.67	3.83	
40	1.05	1.32	0.94	0.73	4.49	4.49	5.75	5.10	slip sinkage
60	1.53	1.57	1.98	1.98	5.04	5.84	6.36	5.36	$[cm]$
80	1.94	2.06	1.94	2.49	7.08	7.56	6.74	5.71	

Table 4.13: *slip sinkage as a function of lugs height*

Considering effects of lugs parameters on slip sinkage of the wheel, taking into account lugs angle, wheel sinkage decreases with increase o f lugs angle, 20 and 25 lugs inclined at 25° and 55° figure 4.5a has higher and lower slip sinkage at 10% while at high wheel slip 25% figure 4.5b, 20 and 25 lugs with 25° and 55° has higher ans lower sinkage respectively.

With regards to lugs height wheel slip sinkage increases with increase of lugs height, taking into account sinkage at 10% wheel slip figure 4.5c it was noted that 25 and 15 lugs with $40mm$ and $80mm$ height gives low and high slip sinkage, while at 25% wheel slip figure 4.5d, 10 and 15 lugs with $20mm$ and $80mm$ height gives low and high slip sinkage respectively. Slip sinkage increases with increase of lugs center length especially for few lugs, and when lugs number increases slip sinkage increases until it reaches maximum with $100mm$ lugs center length, then it decreases with increase of center length figures 4.5e and 4.5f. It was noted that 10 and 20 lugs with $60mm$ and $120mm$ center length figure 4.5e gives low and high slip sinkage at 10% wheel slip, while at 20% slip figure 4.5f 25 lugs with $120mm$ center length gives low sinkage and 20 lugs with $80mm$ center length gives high sinkage.

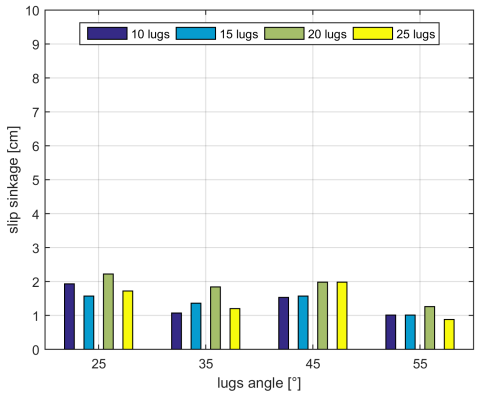

(a) *sinkage as a function of lugs angle at 10% slip*

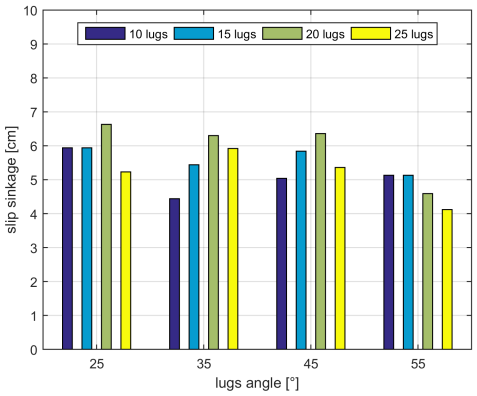

(b) *sinkage as a function of lugs angle at 25% slip*

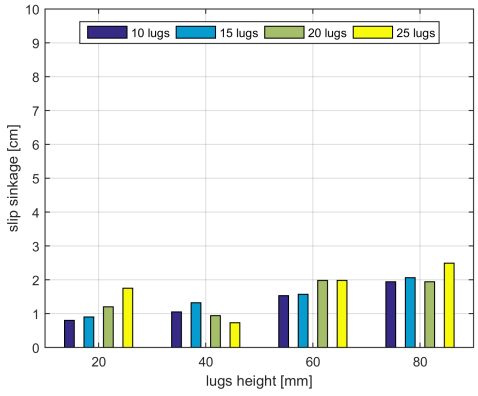

(c) *sinkage as a function of height at 10% slip*

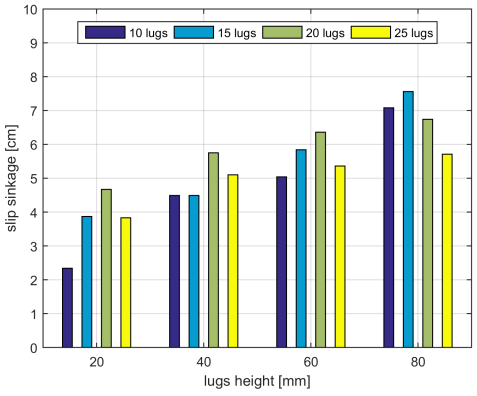

(d) *sinkage as a function of lugs height at 25% slip*

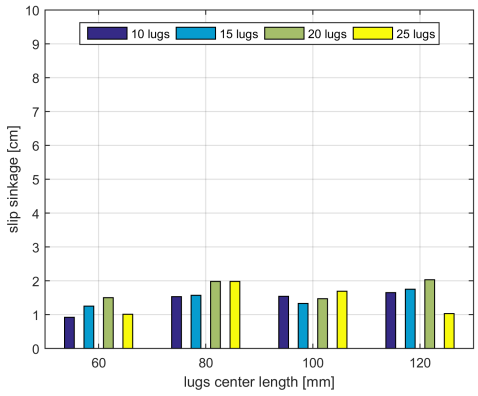

(e) *sinkage as a function of center length at 10% slip*

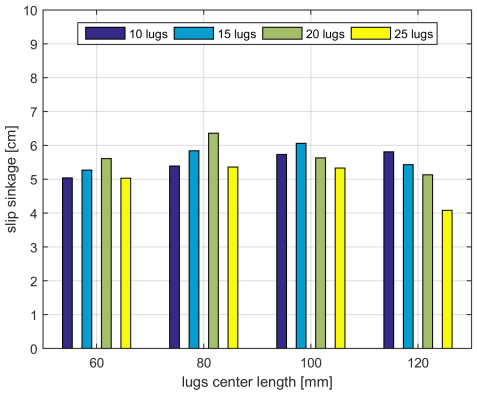

(f) *sinkage as a function of center length at 25% slip*

Figure 4.5: *slip sinkage as a function of lugs angle, height and center length*

4.1.2 Terrain with square particles

In this section simulations were carried out by considering terrain with square shaped particles. Size and mass distribution of the particles were same as in section 4.1.1. Simulation parameters such as friction coefficient, cohesion force, wheel speed, wheel

weight, particle density, step time, velocity and position iteration was also same as in previous section to analyse effects of particle type on sensitivity of the tread pattern performance. In order to make terrain depth to be approximately equal as with sphere particles due to arrangement and packing of particles, number of particles were reduced to 12000. Simulation results for non cohesive particles are analysed in subsection 4.1.2 while for cohesive particles in subsection 4.1.2 respectively.

Non Cohesive particles

Results of traction forces, slip sinkage, forward velocity and slip velocity were tabulated in tables 4.14 to 4.19. Effect of the lugs angle, lugs center length, lugs height, lugs number to traction forces and slip sinkage are shown in figures 4.6 and 4.7

Traction Force

	slip 10%				slip 25%				
	lugs number				lugs number				
$\delta[^\circ]$	10	15	20	25	10	15	20	25	
25	1509	1672	1552	1716	2455	2564	2348	2515	
35	1629	1674	1603	1409	2407	2465	2491	2580	traction force
45	1384	1384	1647	1733	2357	2527	2573	2559	$[N]$
55	1415	1463	1561	1373	2313	2317	2550	2482	

Table 4.14: *traction force as a function of lugs angle*

	slip 10%				slip 25%				
	lugs number				lugs number				
$h[mm]$	10	15	20	25	10	15	20	25	
60	1394	1661	1694	1589	2344	2385	2493	2537	
80	1384	1384	1647	1733	2357	2527	2573	2559	traction force
100	1538	1683	1678	1558	2461	2469	2560	2531	$[N]$
120	1510	1684	1709	1469	2294	2561	2629	2604	

Table 4.15: *traction force as a function of lugs centre length*

	slip 10%				slip 25%				
	lugs number				lugs number				
$l_h[mm]$	10	15	20	25	10	15	20	25	
20	1341	1341	1421	1344	2311	2391	2395	2370	
40	1395	1427	1592	1691	2315	2434	2534	2552	traction force
60	1384	1384	1647	1733	2357	2527	2573	2559	$[N]$
80	1792	1959	1672	1583	2517	2617	2770	2574	

Table 4.16: *traction force as a function of lugs height*

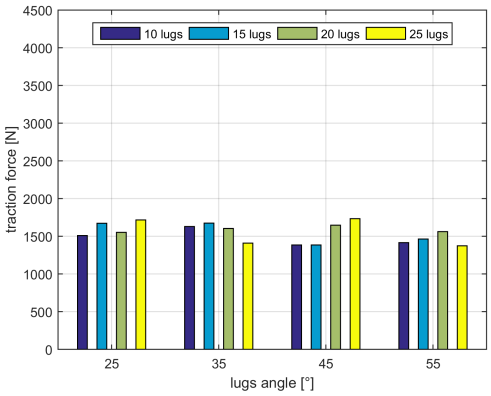

(a) *traction as a function of lugs angle at 10% slip*

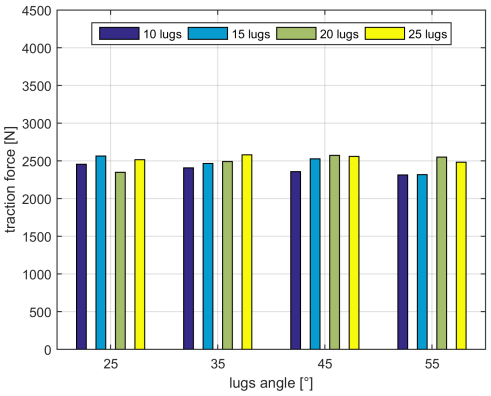

(b) *traction as a function of lugs angle at 25% slip*

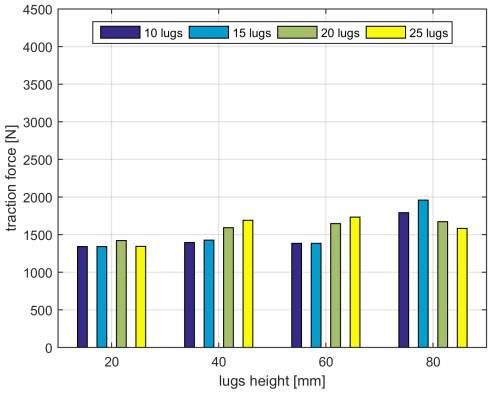

(c) *traction as a function of height at 10% slip*

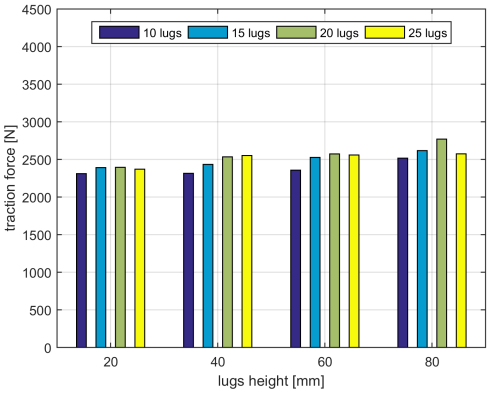

(d) *traction as a function of lugs height at 25% slip*

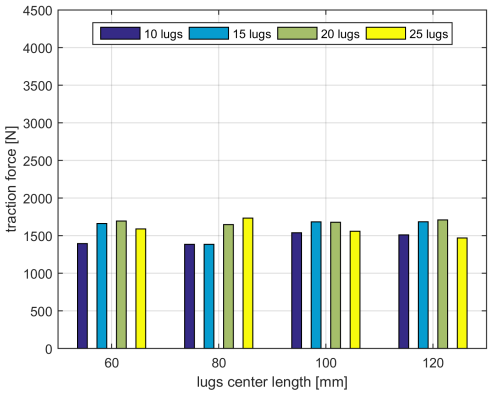

(e) *traction as a function of center length at 10% slip*

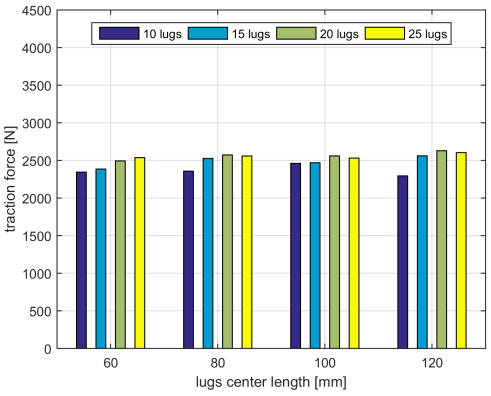

(f) *traction as a function of center length at 25% slip*

Figure 4.6: *traction force as a function of lugs angle, height and center length*

It was noted that traction force decreases with increase of lugs angle and taking into account traction force at 10% slip results in figure 4.6a, 25 and 10 lugs inclined at an angle of $45°$ has high and low traction force while at high slip 25% figure 4.6b, 25 and 15 lugs at $35°$ and $55°$ gives high and low traction force respectively. Also at low wheel slip, traction force increases with increase of lugs number especially for lugs

with $25°$, $45°$ and $55°$ while for lugs with $35°$ traction force decreases with increase of lugs number. At high wheel slip, traction force increases with increase of lugs number. With regards to lugs height traction force increases with increase of lugs height and number, but at 10% wheel slip lugs with $80mm$ height traction force decreases with increase of lugs number. 15 lugs with height of $80mm$ and $60mm$ gives high and low traction force at 10% figure 4.6c and at 25% wheel slip figure 4.6d wheel slip 20 and 10 lugs with $80mm$ and $20mm$ gives high and low traction force respectively. Considering lugs center length, it was noted that traction force increases with increase of lugs center length although at low slip the difference is very small. Also traction increases with increase of lugs number up to 20 lugs then decreases for 25 lugs at 10% wheel slip, while at 25% wheel slip, traction force increases with increase of lugs center length and number. 25 and 15 lugs with center length of $80mm$ has high and low traction at 10% wheel slip figure 4.6e, while at 25% wheel slip, figure 4.6f 20 and 10 lugs with $120mm$ center length has high and low traction force respectively.

Slip Sinkage

	slip 10%				slip 25%				
	lugs number				lugs number				
$\delta[°]$	10	15	20	25	10	15	20	25	
25	2.94	2.84	2.28	2.08	6.40	6.88	5.71	5.15	
35	1.61	2.19	2.28	2.77	4.75	5.40	6.34	6.64	slip sinkage
45	1.45	1.97	2.11	1.68	4.56	5.53	6.19	6.19	$[cm]$
55	1.18	1.40	2.08	1.67	4.47	4.87	6.17	5.78	

Table 4.17: *slip sinkage a function of lugs angle*

	slip 10%				slip 25%				
	lugs number				lugs number				
$h[mm]$	10	15	20	25	10	15	20	25	
60	1.77	2.29	2.59	2.84	4.81	5.60	6.53	6.95	
80	1.45	1.97	2.11	1.68	4.56	5.53	6.19	6.19	slip sinkage
100	1.65	2.09	2.09	1.26	5.74	6.14	6.84	5.15	$[cm]$
120	2.17	1.90	1.66	1.66	5.47	6.41	6.45	6.09	

Table 4.18: *slip sinkage as a function of lugs centre length*

	slip 10%				slip 25%				
	lugs number				lugs number				
$l_h[mm]$	10	15	20	25	10	15	20	25	
20	1.79	2.24	2.49	2.24	4.50	5.45	5.84	5.84	
40	1.26	2.41	2.65	2.41	5.95	6.73	6.61	6.09	slip sinkage
60	1.45	1.97	2.11	1.68	4.56	5.53	6.19	6.19	$[cm]$
80	1.41	1.50	1.74	1.06	5.41	5.81	6.29	5.80	

Table 4.19: *slip sinkage as a function of lugs height*

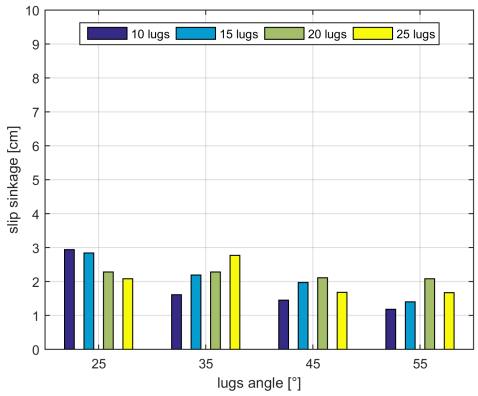

(a) *sinkage as a function of lugs angle at 10% slip*

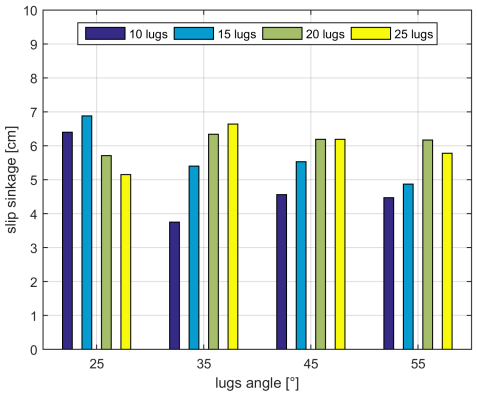

(b) *sinkage as a function of lugs angle at 25% slip*

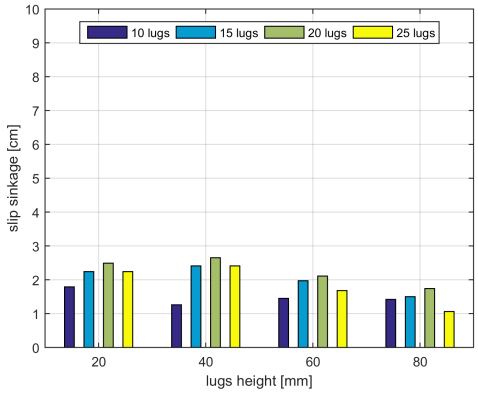

(c) *sinkage as a function of height at 10% slip*

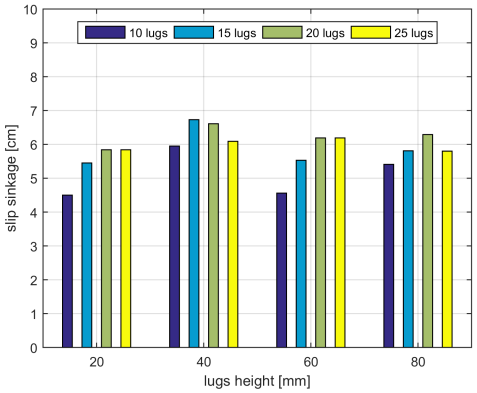

(d) *sinkage as a function of lugs height at 25% slip*

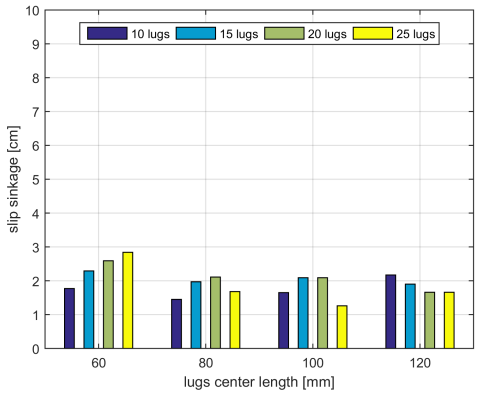

(e) *sinkage as a function of center length at 10% slip*

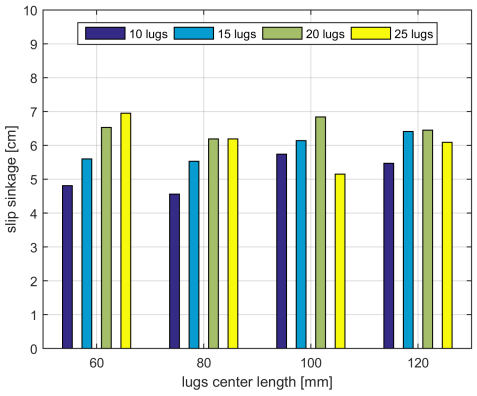

(f) *sinkage as a function of center length at 25% slip*

Figure 4.7: *slip sinkage as a function of lugs angle, height and center length*

Taking into account effects of lugs parameters on wheel slip sinkage, it was observed that slip sinkage decreases with increase of lugs angle and height, taking into account lugs angle, 10 lugs inclined at an angle of $55°$ and $25°$ figure 4.7a gives low and high slip sinkage at slip of 10%, while at 25% slip, 10 and 15 lugs inclined at $35°$ and $25°$ figure 4.7b gives low and high wheel slip sinkage respectively. Considering lugs height on

wheel slip sinkage, 25 and 20 lugs with height of $80mm$ and $40mm$ figure 4.7c gives low and high sinkage at 10% slip, while at high wheel slip 25% figure 4.7d, 10 and 15 lugs with $60mm$ and $40mm$ heights gives low and high slip sinkage respectively. Considering lugs center length on slip sinkage, slip sinkage decreases with increase of center length, also sinkage increases with increase of lugs number although at 10% wheel slip 25 lugs number gives low slip sinkage for $80mm$, $100mm$ and $120mm$ center length. 25 lugs with $100mm$ and $60mm$ center length has low and high slip sinkage at 10% wheel slip, while at 25% wheel slip, 10 and 25 lugs with $80mm$ and $60mm$ center length figure 4.7b gives low and high slip sinkage respectively.

Cohesive particles

Results of traction forces and slip sinkage were tabulated in tables 4.20 to 4.25. Effect of the lugs angle, lugs center length, lugs height, lugs number to traction forces and slip sinkage are shown in figures 4.6 and 4.7 respectively.

Traction Force

	slip 10%				slip 25%				
	lugs number				lugs number				
$\delta[^\circ]$	10	15	20	25	10	15	20	25	
25	2739	2874	2841	2640	3465	3681	3428	3364	
35	2568	2720	2809	2591	3410	3564	3537	3529	traction force
45	2679	2770	2828	2891	3497	3536	3435	3382	$[N]$
55	2909	2909	2775	2775	3323	3379	3298	3323	

Table 4.20: *traction force as a function of lugs angle*

	slip 10%				slip 25%				
	lugs number				lugs number				
$h[mm]$	10	15	20	25	10	15	20	25	
60	2809	2661	2763	2809	3433	3462	3519	3433	
80	2679	2770	2828	2891	3497	3536	3435	3382	traction force
100	2703	2853	3009	2826	3378	3436	3600	3471	$[N]$
120	2844	2727	2807	2804	3468	3406	3533	3551	

Table 4.21: *traction force as a function of lugs centre length*

	slip 10%				slip 25%				
	lugs number				lugs number				
$height[mm]$	10	15	20	25	10	15	20	25	
20	2726	2679	2477	2312	3370	3318	3259	3236	
40	2523	2626	2723	2739	3243	3463	3455	3402	traction force
60	2679	2770	2828	2891	3497	3536	3435	3382	$[N]$
80	2764	2942	2821	2761	3632	3636	3602	3488	

Table 4.22: *traction force as a function of lugs height*

Taking into account effects lugs angle on traction force, it was inferred that traction force decreases with increase of lugs angle at 25% slip figure 4.8b while at 10% slip

figure 4.8a it decreases with increase of angle up to 45° and above that it increases especially for 10 and 15 lugs.

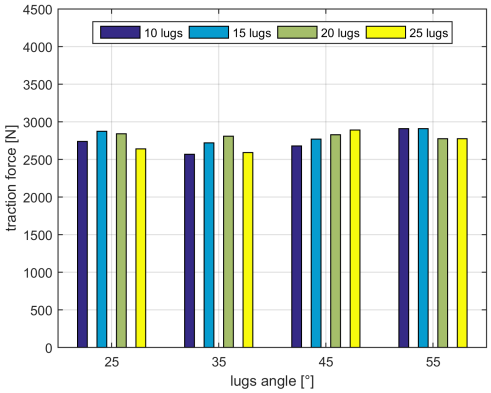

(a) *traction as a function of lugs angle at 10% slip*

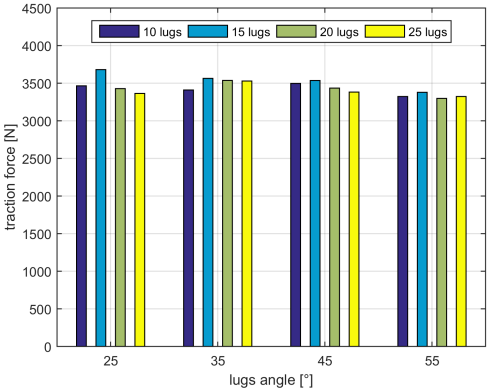

(b) *traction as a function of lugs angle at 25% slip*

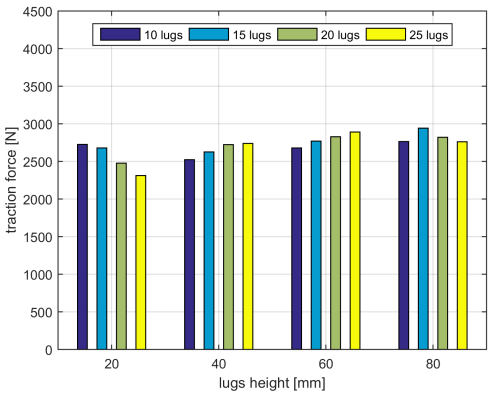

(c) *traction as a function of height at 10% slip*

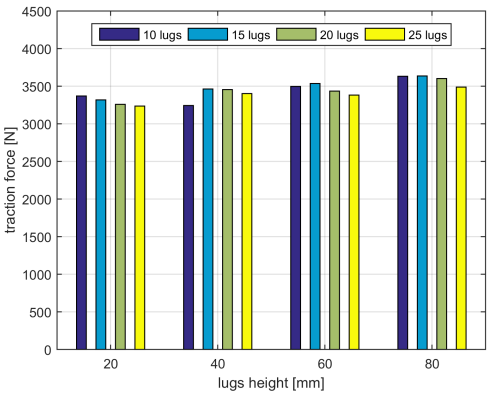

(d) *traction as a function of lugs height at 25% slip*

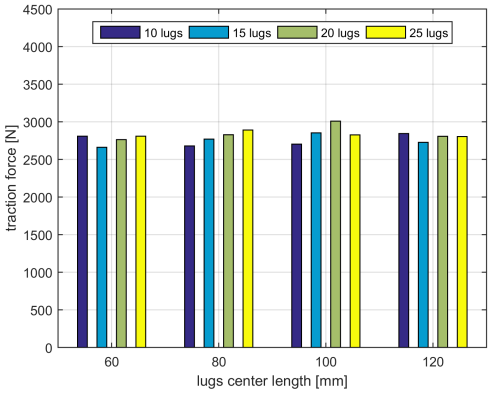

(e) *traction as a function of center length at 10% slip*

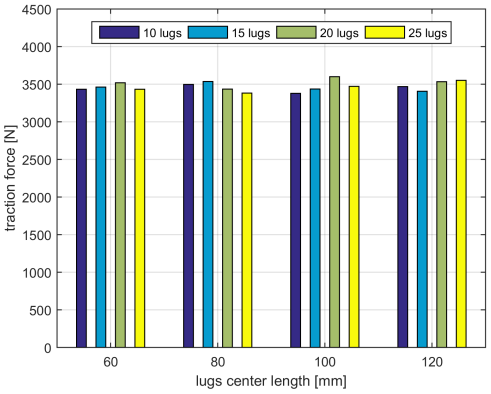

(f) *traction as a function of center length at 25% slip*

Figure 4.8: *traction force as a function of lugs angle, height and center length*

It was also noted that traction force increases with increase of lugs number up to optimal lugs number then decreases with further increase of lugs number for lugs inclined

at $25°$, $35°$ and $45°$, while for lugs iclined at $55°$ traction decreases with increase of lugs number. 10 lugs with an angle of $55°$ and $35°$ figure 4.8a, give high and low traction force 10% wheel slip, while at slip of 25% figure 4.8b, 15 and 20 lugs at an angle of $25°$ and $55°$ gives high and low traction force respectively.

Slip Sinkage

	slip 10%				slip 25%				
	lugs number				lugs number				
$\delta[°]$	10	15	20	25	10	15	20	25	
25	1.94	2.24	2.84	1.66	7.07	6.94	6.94	7.03	
35	1.28	1.36	1.87	1.71	5.73	6.85	7.48	7.28	slip sinkage
45	1.81	2.34	2.31	1.39	6.79	6.69	6.23	6.03	$[cm]$
55	1.95	2.92	2.59	1.95	5.90	6.61	6.15	5.64	

Table 4.23: *slip sinkage a function of lugs angle*

	slip 10%				slip 25%				
	lugs number				lugs number				
$h[mm]$	10	15	20	25	10	15	20	25	
60	2.29	2.13	2.39	2.35	6.49	7.37	7.27	7.17	
80	1.81	2.34	2.31	1.39	6.79	6.69	6.23	6.03	slip sinkage
100	1.86	2.66	2.93	2.89	5.79	7.13	7.42	6.73	$[cm]$
120	1.73	2.13	2.62	2.27	5.44	6.94	7.54	7.90	

Table 4.24: *slip sinkage as a function of lugs centre length*

	slip 10%				slip 25%				
	lugs number				lugs number				
$l_h[mm]$	10	15	20	25	10	15	20	25	
20	1.30	1.33	1.30	1.30	5.37	6.58	6.28	5.79	
40	1.54	2.00	2.34	2.59	6.00	6.60	7.24	6.83	slip sinkage
60	1.81	2.34	2.31	1.39	6.79	6.69	6.23	6.03	$[cm]$
80	1.62	2.21	2.66	2.87	8.01	7.88	7.58	7.17	

Table 4.25: *slip sinkage as a function of lugs height*

Taking into account lugs height figures 4.8c and 4.8d it was noted that traction force increases with increase of lugs height, also for $20mm$ lugs height traction decreases with increase of lugs number while for $40mm$, $60mm$ and $80mm$ lugs heights traction force increases with increase of lugs number. At 10% wheel slip figure 4.8c, 15 and 25 lugs with $80mm$ and $20mm$ height gives high and low traction, while at 25% wheel slip figure 4.8d, 10 lugs with $80mm$ and $40mm$ height gives high and low traction respectively. With regards to lugs center length, traction force increases with increase of center length although the difference in traction is small especially at 25% wheel slip figures 4.8e and 4.8f. It also increases with increase of lugs number at 10% slip, while at 25% slip increases with increase of lugs number for $60mm$, $100mm$ and $120mm$, and for $80mm$ center length it decreases with increase of lugs number.

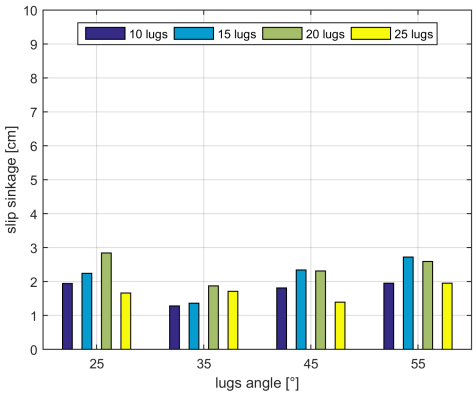

(a) *sinkage as a function of lugs angle at 10% slip*

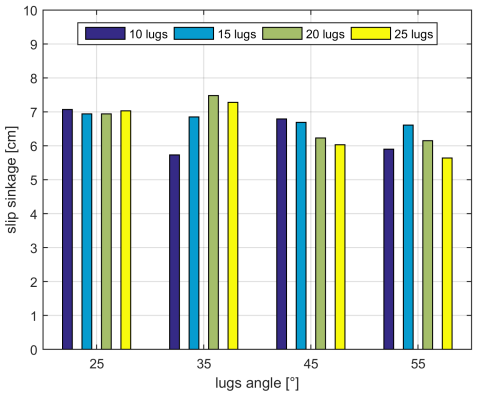

(b) *sinkage as a function of lugs angle at 25% slip*

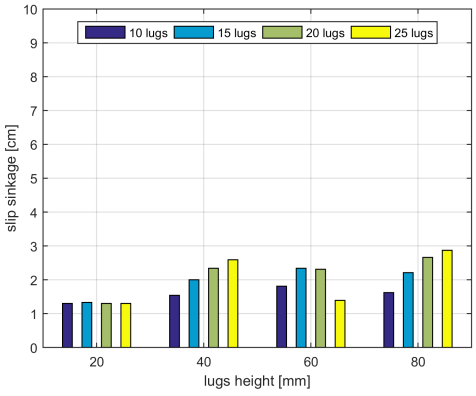

(c) *sinkage as a function of lugs height at 10% slip*

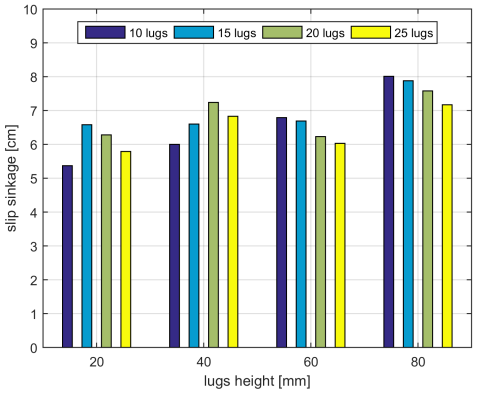

(d) *sinkage as a function of lugs height at 25% slip*

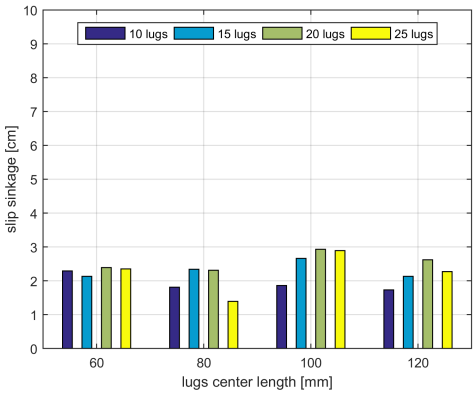

(e) *sinkage as a function of center length at 10% slip*

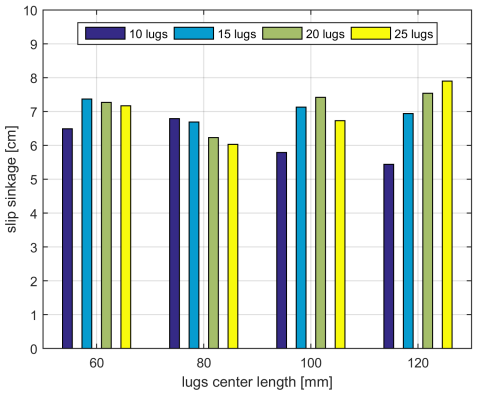

(f) *sinkage as a function of center length at 25% slip*

Figure 4.9: *slip sinkage as a function of lugs angle, height and center length*

20 and 10 lugs with $100mm$ center length gives high and low traction traction both at 10% and 25% wheel slip respectively.

Considering lugs design parameters on slip sinkage of the wheel, and with regards to lugs angle, it was noted that sinkage increases with increase of lugs angle especially at high wheel slip figures 4.9a and 4.9b, also sinkage increases with increase of lugs

number at 10% wheel slip, while at 25% wheel slip for 25° and 45° lugs angle, sinkage decreases with increase of lugs number, for 35° and 55° lugs angles sinkage increases with increase of lugs number. At 10% whgeel slip figure 4.9a, 25 and 20 lugs at an angle of 45° and 25° gives low and high slip sinkage, while at 25% wheel slip figure 4.9b, 25 and 20 lugs with 55° and 35° angle gives low and high sinkage respectively.

Taking into account lugs height figures 4.9c and 4.9d, it was observed that slip sinkage increases with increase of lugs height, also sinkage increases with increase of lugs number at 10% wheel slip, while at 25% wheel slip it increases with increase of lugs number for $40mm$ height and decreases with increase of lugs number for $20mm$, $60mm$ and $80mm$ lugs height. At 10% wheel slip, 25 lugs with $20mm$ and $80mm$ height gives low and high sinkage, while at 25% wheel slip, 10 lugs with $20mm$ and $80mm$ height gives low and high slip sinkage respectively.

With regards to lugs center length figures 4.9e and 4.9f, it was noted sinkage increasese with increase of center length especially at 10% wheel slip, while at 25% slip it decreases for $80mm$ center length and increases for $100mm$ and $120mm$ center length. It also noted that sinkage increases with increase of lugs number both at 10% and 25% wheel slip for $60mm$, $100mm$ and $120mm$ center lengths, and for $80mm$ center length sinkage decreases with increase of lugs number. 25 and 20 lugs with center length of $80mm$ and $100mm$ gives low and high slip sinkage at 10% wheel slip, and 10 and 25 lugs with $120mm$ center length gives low and high sinkage at 25% wheel slip respectively.

4.1.3 Terrain with mixed particles

In this section simulations were carried out by considering terrain with spheres, boxes and convex hulls particles. Size and mass distribution of the particles were same as in section 4.1.1. Mix ratio of particles in terms of numbers in the bin are 80% spheres, 10% squares and 10% convex hulls respectively. Ratio of particles number with respect to shapes are selected in order to limit number of contacts as well the computational time during simulation. Simulation parameters are the same as in the previous sections.

Non Cohesive particles

In this sub-section simulations are carried out by considering terrain with non-cohesive mixed particles to analyse the sensitivity of the lugs parameters on traction force and slip sinkage of the wheel. Simulation results of traction forces and slip sinkage for lugs angle, lugs height and lugs center length were tabulated in tables 4.26 to 4.31 and graphically presented in figures 4.10 and 4.11 respectively.

Traction Force

	slip 10%				slip 25%				
	lugs number				lugs number				
$\delta[^\circ]$	10	15	20	25	10	15	20	25	
25	1512	1592	1620	1380	2368	2428	2463	2228	
35	1503	1740	1709	1597	2305	2453	2405	2453	traction force
45	1358	1479	1577	1649	2192	2285	2414	2358	$[N]$
55	1442	1716	1579	1183	2263	2303	2409	2390	

Table 4.26: *traction force as a function of lugs angle*

	slip 10%				slip 25%				
	lugs number				lugs number				
$h[mm]$	10	15	20	25	10	15	20	25	
60	1223	1339	1496	1563	2128	2215	2273	2304	
80	1358	1479	1577	1649	2192	2285	2414	2358	traction force
100	1532	1603	1651	1600	2278	2303	2284	2228	$[N]$
120	1552	1373	1290	1496	2438	2316	2228	2362	

Table 4.27: *traction force as a function of lugs centre length*

	slip 10%				slip 25%				
	lugs number				lugs number				
$l_h[mm]$	10	15	20	25	10	15	20	25	
20	1148	1248	1298	1405	2125	1913	2115	2225	
40	1206	1275	1513	1497	2152	2193	2314	2245	traction force
60	1358	1479	1577	1649	2337	2285	2428	2358	$[N]$
80	1368	1477	1590	1690	2318	2370	2446	2419	

Table 4.28: *traction force as a function of lugs height*

With regards to lugs angle on traction force, it was noted that traction force decreases with increase of lugs angle especially at 25% wheel slip figure 4.10b, also it increases with increase of lugs number, although at 10% wheel slip figure 4.10a it reaches optimal value and decreases with further increase of lugs number for 25°, 35° and 55° lugs angles, instead for 45° lugs angle it keep increasing with lugs number. 15 lugs inclined at 35° gives high traction at 10% wheel slip and 25 lugs inclined at 55° has low traction, while at 25% wheel slip 20 lugs inclined at 25° gives high traction force and lowest traction force noted with 10 lugs at an angle of 45°.

With regards to lugs height it was noted that traction force increases with increase of lugs height and numbers respectively, At 10% wheel slip figure 4.10c, 25 lugs with $80mm$ height has high traction force, while at 25% wheel slip figure 4.10d, it can be noted that 20 lugs with $80mm$ height gives high traction force.

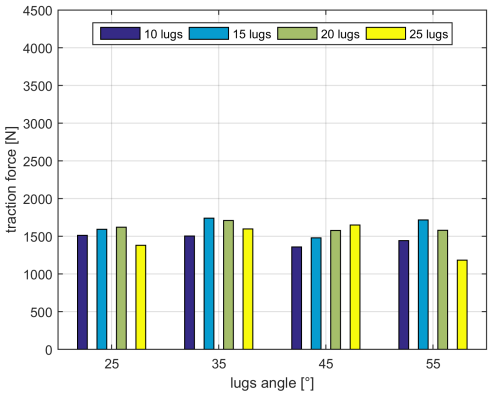

(a) *traction as a function of lugs angle at 10% slip*

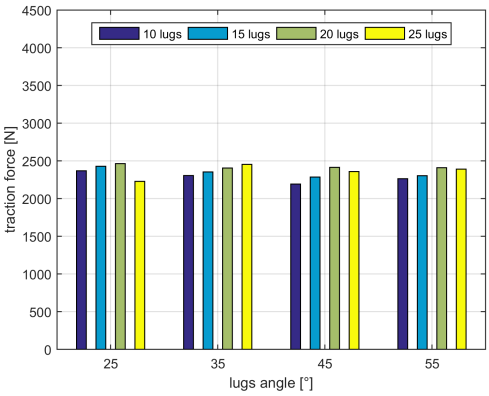

(b) *traction as a function of lugs angle at 25% slip*

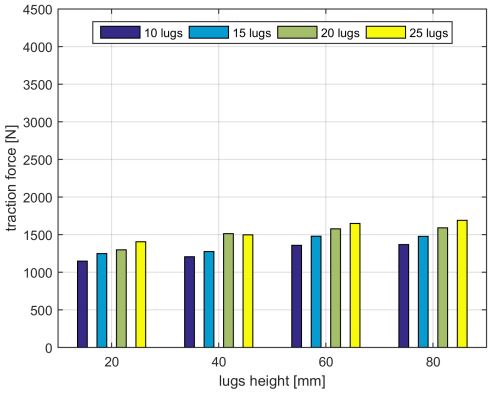

(c) *traction as a function of height at 10% slip*

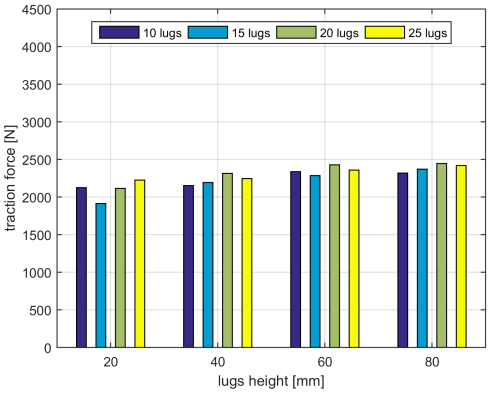

(d) *traction as a function of lugs height at 25% slip*

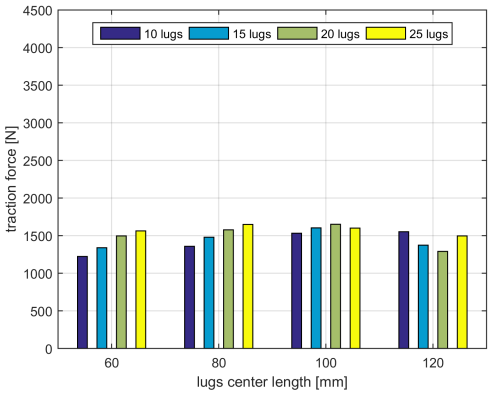

(e) *traction as a function of center length at 10% slip*

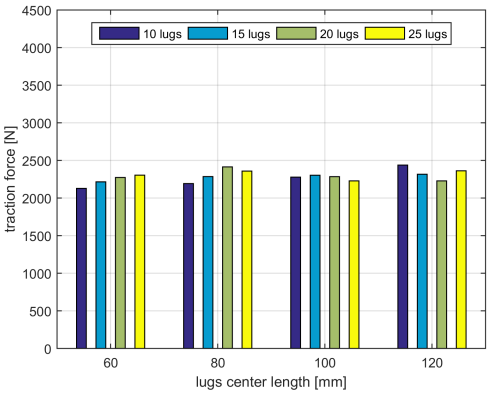

(f) *traction as a function of center length at 25% slip*

Figure 4.10: *traction force as a function of lugs angle, height and center length*

Slip Sinkage

	slip 10%				slip 25%				
	lugs number				lugs number				
$\delta[^\circ]$	10	15	20	25	10	15	20	25	
25	0.89	1.09	1.26	0.90	3.93	4.04	3.73	3.53	
35	1.33	1.60	1.94	1.94	4.66	4.95	5.40	5.40	slip sinkage
45	0.80	1.01	1.28	1.43	4.10	3.90	3.90	4.10	$[cm]$
55	2.26	2.04	1.63	1.23	4.97	4.79	4.60	4.46	

Table 4.29: *slip sinkage a function of lugs angle*

	slip 10%				slip 25%				
	lugs number				lugs number				
$h[mm]$	10	15	20	25	10	15	20	25	
60	0.53	1.20	1.70	1.95	3.46	4.51	5.07	5.30	
80	0.80	1.01	1.28	1.43	4.10	3.90	3.90	4.10	slip sinkage
100	1.34	1.34	1.16	1.01	3.39	3.63	3.73	4.08	$[cm]$
120	0.72	1.25	1.22	1.02	4.34	4.18	4.44	4.68	

Table 4.30: *slip sinkage as a function of lugs centre length*

	slip 10%				slip 25%				
	lugs number				lugs number				
$l_h[mm]$	10	15	20	25	10	15	20	25	
20	1.09	0.99	1.19	1.19	3.52	2.92	3.72	4.02	
40	0.72	1.34	1.57	1.17	3.04	3.50	4.10	4.45	slip sinkage
60	0.80	1.01	1.28	1.43	4.10	3.90	3.90	4.10	$[cm]$
80	0.88	1.51	1.28	0.88	4.09	4.25	4.45	4.15	

Table 4.31: *slip sinkage as a function of lugs height*

Taking into consideration lugs center length figures 4.10e and 4.10f, it was noted that traction force increases with increase of center length up to optimal value then decreases with further increase of center length although few lugs especially 10 lugs keep increasing traction for further increase of center length. Taking into account at 10% wheel slip, 25 lugs with $80mm$ center length gives high traction and 20 lugs with $120mm$ gives lowest traction force, while at high 25% wheel slip, 10 lugs with $120mm$ center length gives high traction force and 10 lugs with $60mm$ center lenght has lowest traction respectively.

Wheel slip sinkage is sensitive to lugs angle as it was noted that slip sinkage increases with increase of lugs angle up to optimal value then decreases with further increase of lugs angle although 45° lugs angle gives low sinkage as compared to 35° and 55° lugs angles both at 10% and 25% wheel slip. It also increases with increase of lugs number but for 55° lugs angle it decreases with increase of lugs number. At 10% wheel slip figure 4.11a 10 lugs inclined at 45° gives low sinkage while 10 lugs at 55° angle gives highest sinkage. At 25% wheel slip figure 4.11b 25 lugs inclined at 25° gives lowest sinkage while 20 lugs inclined at 35° gives highest sinkage respectively.

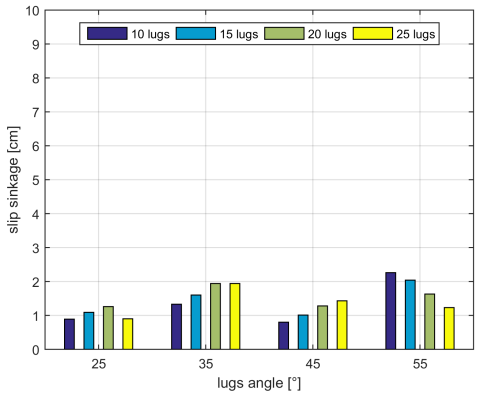

(a) *sinkage as a function of lugs angle at 10% slip*

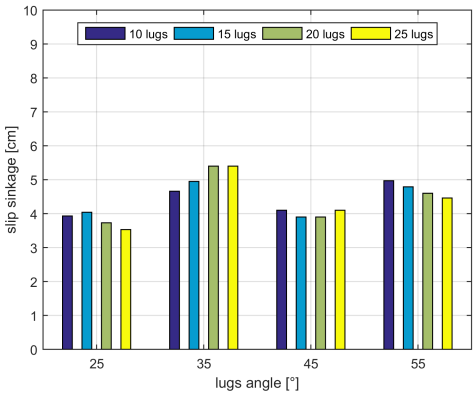

(b) *sinkage as a function of lugs angle at 25% slip*

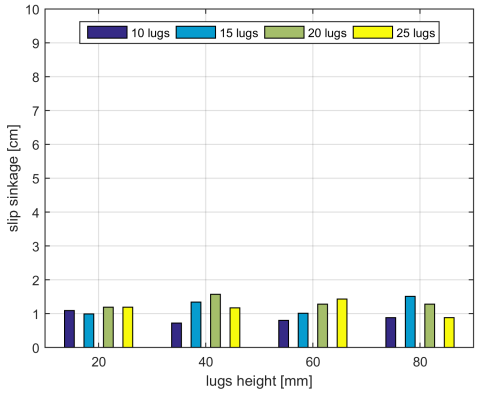

(c) *sinkage as a function of height at 10% slip*

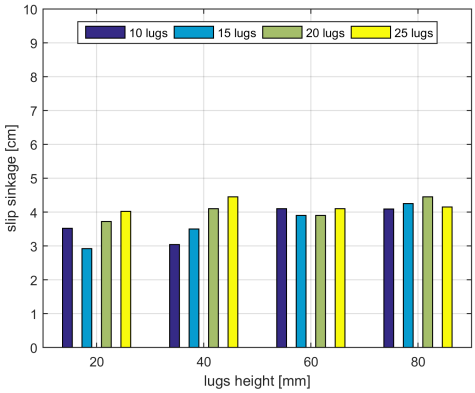

(d) *sinkage as a function of lugs height at 25% slip*

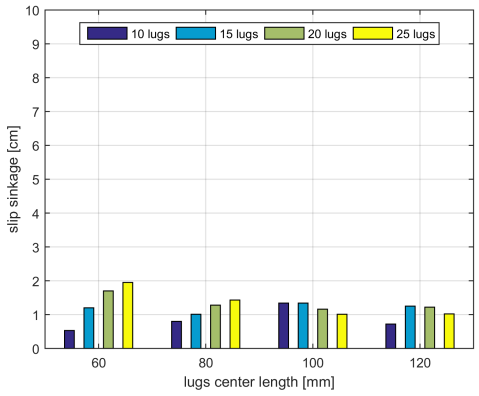

(e) *sinkage as a function of center length at 10% slip*

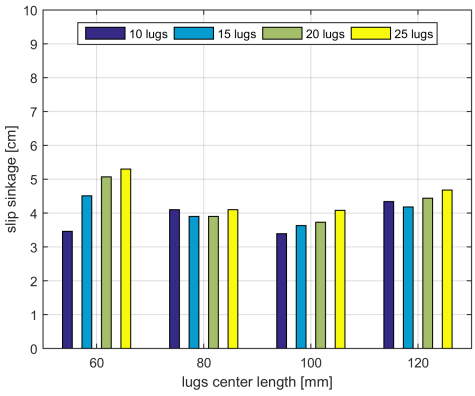

(f) *sinkage as a function of center length at 25% slip*

Figure 4.11: *slip sinkage as a function of lugs angle, height and center length*

Taking consideration of lugs height on slip sinkage of the wheel, it was noted that sinkage increases with increase of lugs height although the difference is small both at 10% and 25% wheel slip figures 4.11c and 4.11d. It also noted that sinkage increase with increase of lugs number. 20 and 10 lugs with $40mm$ height has high and low sinkage at 10% wheel slip, while at 25% wheel slip, it can be noted that 25 and 15 lugs

with $40mm$ and $10mm$ heights gives high and low sinkage respectively.

With regards to center length, it was noted that sinkage decreases with increase of center length up to optimal value then increases with further increase of center legnth figures 4.11e and 4.11f. It also increase with increase of lugs number but decreases with increase of lugs number for $100mm$ center length. At 10% wheel slip 10 and 25 lugs with $60mm$ center length gives lowest and highest sinkage while 25% wheel slip 10 and 25 lugs with $100mm$ and $60mm$ center length gives lowest and highest sinkage respectively.

Cohesive particles

In this sub-section simulations are carried out by considering terrain with cohesive mixed particles to analyse the sensitivity of the lugs parameters on traction force and slip sinkage of the wheel. Simulation results of traction forces and slip sinkage for lugs angle, lugs height and lugs center length were tabulated in tables 4.32 to 4.37 and graphically presented in figures 4.12 and 4.13 respectively.

Traction Force

	slip 10%				slip 25%				
	lugs number				lugs number				
$\delta[^\circ]$	10	15	20	25	10	15	20	25	
25	2633	2750	2925	2633	3239	3311	3352	3221	
35	2787	2928	2884	2610	3162	3323	3424	3289	traction force
45	2691	2889	2816	2650	3332	3253	3202	3203	$[N]$
55	2615	2615	2596	2502	3187	3141	3192	3141	

Table 4.32: *traction force as a function of lugs angle*

	slip 10%				slip 25%				
	lugs number				lugs number				
$h[mm]$	10	15	20	25	10	15	20	25	
60	2229	2617	2670	2643	3109	3236	3274	3373	
80	2691	2889	2816	2650	3332	3253	3202	3103	traction force
100	2758	2742	2698	2643	3332	3259	3282	3235	$[N]$
120	2852	2486	2632	2614	3306	3162	3203	3243	

Table 4.33: *traction force as a function of lugs centre length*

	slip 10%				slip 25%				
	lugs number				lugs number				
$l_h[mm]$	10	15	20	25	10	15	20	25	
20	2462	2562	2626	2377	2927	2979	3095	3027	
40	2711	2636	2530	2481	3133	3072	3170	3133	traction force
60	2691	2889	2816	2650	3332	3253	3202	3103	$[N]$
80	2727	2727	2603	2673	3302	3344	3372	3449	

Table 4.34: *traction force as a function of lugs height*

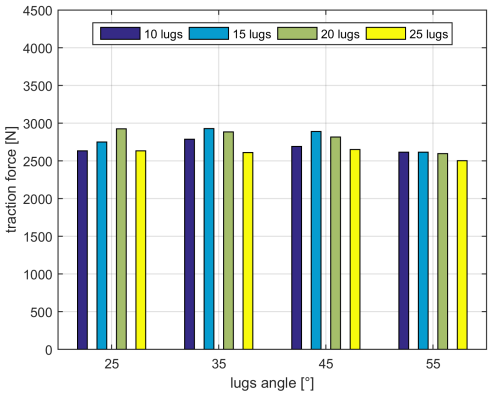

(a) *traction as a function of lugs angle at 10% slip*

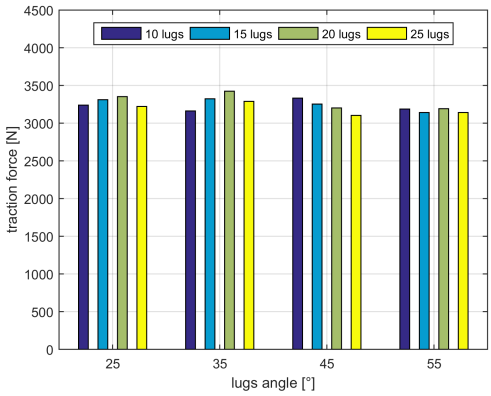

(b) *traction as a function of lugs angle at 25% slip*

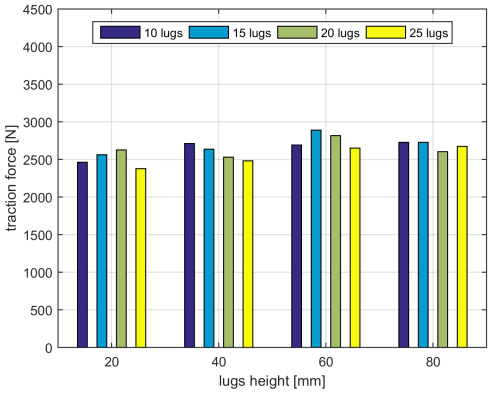

(c) *traction as a function of height at 10% slip*

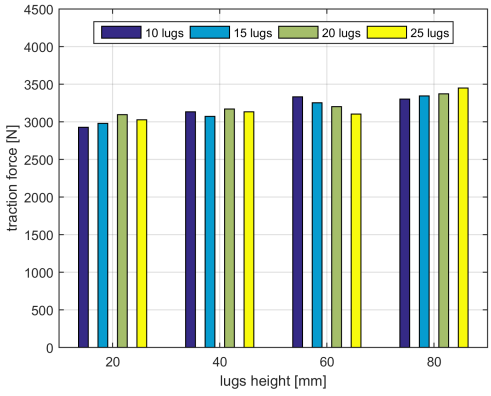

(d) *traction as a function of lugs height at 25% slip*

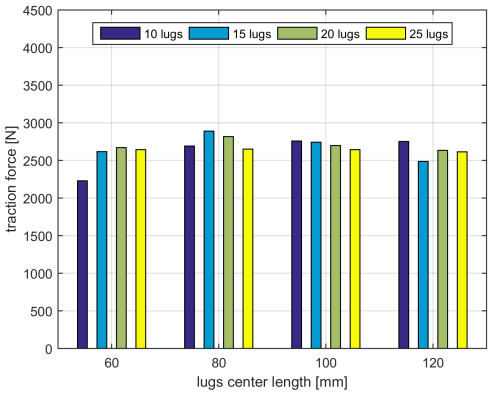

(e) *traction as a function of center length at 10% slip*

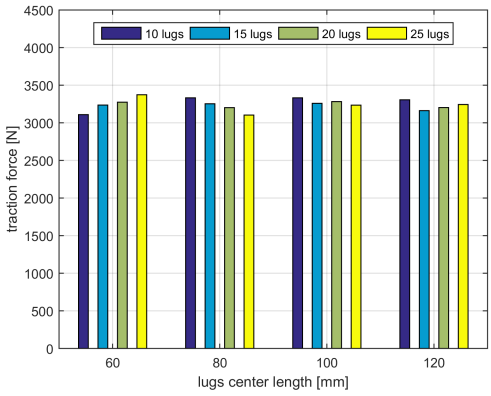

(f) *traction as a function of center length at 25% slip*

Figure 4.12: *traction force as a function of lugs angle, height and center length*

Taking into account results of traction force on regards to lugs angle, it was noted that, traction decreases with increase of lugs angle and lugs number both at 10% wheel slip figure 4.12a and at 25% wheel slip figure 4.12b, but for $55°$ and $45°$ lugs angle decreases with increase of lugs number at respective wheel slip. At 10% wheel slip, 15 lugs with $35°$ lugs angle gives highest traction and 25 lugs with $55°$ lugs angle gives

lowest traction, while at 25% wheel slip, 20 lugs with 35° lugs angle gives highest traction and 25 lugs with 45° lugs angle gives lowest traction respectively.

Considering lugs height on traction force results in figures 4.12c and 4.12d at 10% and 25% wheel slip, it was noted that traction increases with increase of lugs height. At 10% slip traction increases with increase of lugs number and then decreases for further increase of lugs number for $20mm$ abd $60mm$ heights while for $40mm$ and $80mm$ heights it decreases with increase of lugs number, 15 lugs with $60mm$ height gives highest traction force and 25 lugs with $20mm$ height gives lowest traction force. At 25% slip traction increases with increase of lugs number for $20mm$, $40mm$ and $80mm$ heights while for $60mm$ height it decreases with increase of lugs number, 25 lugs with $80mm$ height gives highest traction force and 10 lugs with $20mm$ height gives lowest traction force at respective slip values.

Slip Sinkage

	slip 10%				slip 25%				
	lugs number				lugs number				
$\delta[^\circ]$	10	15	20	25	10	15	20	25	
25	1.22	1.67	2.24	1.46	5.59	6.89	6.67	5.96	
35	1.70	2.27	2.40	1.46	5.90	6.62	6.71	6.82	slip sinkage
45	0.85	1.76	1.76	1.45	5.77	5.84	5.45	4.96	$[cm]$
55	1.49	1.21	0.75	1.29	5.27	5.08	4.99	4.64	

Table 4.35: *slip sinkage a function of lugs angle*

	slip 10%				slip 25%				
	lugs number				lugs number				
$h[mm]$	10	15	20	25	10	15	20	25	
60	1.16	1.89	1.67	1.16	5.46	5.60	5.94	5.65	
80	0.85	1.76	1.76	1.45	5.77	5.84	5.45	4.96	slip sinkage
100	1.89	1.76	1.52	1.17	6.19	6.19	6.19	5.70	$[cm]$
120	1.37	1.46	1.86	1.86	5.24	5.69	5.86	6.13	

Table 4.36: *slip sinkage as a function of lugs centre length*

	slip 10%				slip 25%				
	lugs number				lugs number				
$l_h[mm]$	10	15	20	25	10	15	20	25	
20	1.03	1.60	1.60	1.38	4.61	4.81	5.57	5.68	
40	0.80	0.90	1.24	1.64	5.06	5.46	5.90	5.26	slip sinkage
60	0.85	1.76	1.76	1.45	5.77	5.84	5.45	4.96	$[cm]$
80	1.72	1.52	1.14	1.34	7.29	6.95	6.53	6.36	

Table 4.37: *slip sinkage as a function of lugs height*

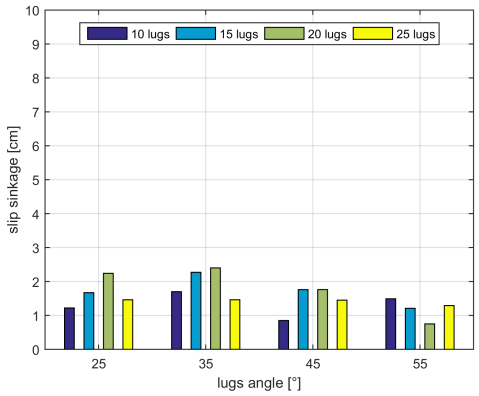

(a) *sinkage as a function of lugs angle at 10% slip*

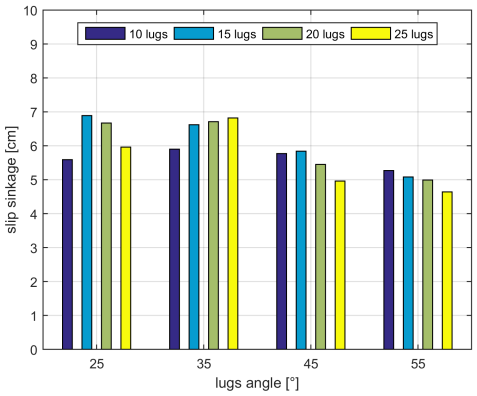

(b) *sinkage as a function of lugs angle at 25% slip*

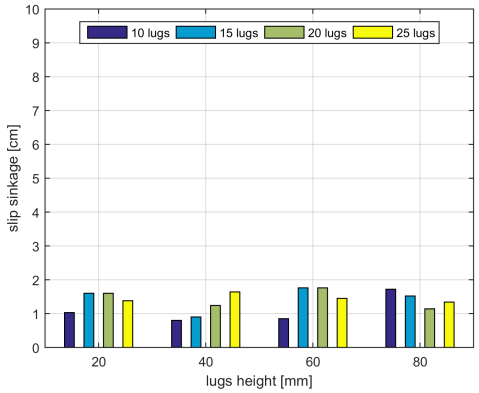

(c) *sinkage as a function of lugs height at 10% slip*

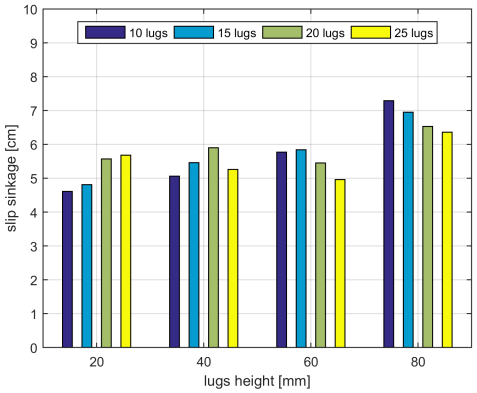

(d) *sinkage as a function of lugs height at 25% slip*

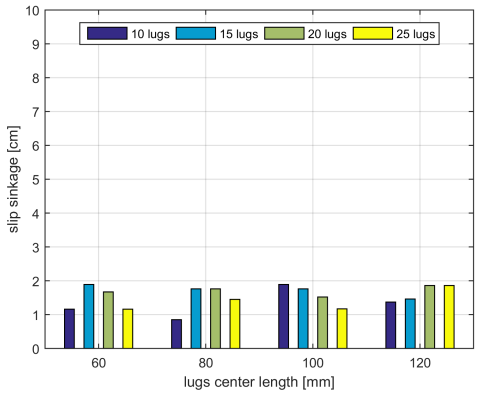

(e) *sinkage as a function of center length at 10% slip*

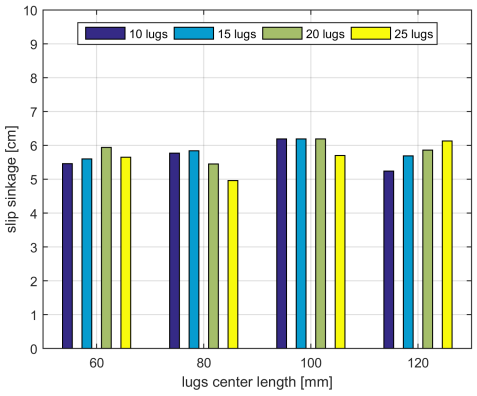

(f) *sinkage as a function of center length at 25% slip*

Figure 4.13: *slip sinkage as a function of lugs angle, height and center length*

Considering lugs center length on traction force results on figures 4.12e and 4.12f at 10% and 25% wheel slip, it was noted that traction force increases with increase of center length up to optimal value and then decreases with further increase of ceneter length especially at 10% wheel slip while at 25% wheel slip increases with increase of lugs center length then decreases for $100mm$ and $120mm$ cnter lengths although the

difference is small. It also increases with increase of lugs number up to optimal value then decreases with further increase of lugs for $60mm$ and $80mm$ center length and for $100mm$ and $120mm$ center length traction decreases with increase of lugs number at 10% slip. At 25% wheel slip, it increases with increase of lugs number for $60mm$ center lenght and for $80mm$, $100mm$ and $120mm$ decreases with increase of lugs number. 15 lugs with $80mm$ center gives highest traction and 10 lugs with $60mm$ center length gives lowest traction at 10% wheel slip while at 25% wheel slip, 25 lugs with $60mm$ center length gives highest traction and 25 lugs with $80mm$ center length gives lowest traction respectively.

Taking into account lugs angle on wheel slip sinkage results in figures 4.13a and 4.13b at 10% and 25% slip, it was observed that sinkage decreases with increase of lugs angle, also at 10% wheel slip sinkage increases with increase of lugs angle up to optimal then decreases with further increase of lugs for 25°, 35° and 45° angles and for 55° angle decreases with increase of lugs while at 25% wheel slip increases with increae of lugs number for 25° and 35° while for 45° and 55° angles decreases with increase of lugs respectively.

Considering lugs height on slip sinkage results in figures 4.13c and 4.13d at 10% and 25% wheel slip, it was inferred that sinkage increases with increase of lugs height. At 10% slip it also increases withincrease of lugs number up to optimal value then decreases with further increase of lugs for $20mm$ and $60mm$ heights, but for $40mm$ height keep increasign with increase of lugs and for $80mm$ height decreases with increase of lugs number. At 25% wheel slip sinkage increases with increase of lugs number up to optimal value and then decreases with further increase of lugs for $40mm$ height, while for $20mm$ height keep increases with increase of lugs and for $60mm$ and $80mm$ heights decreases with increase of lugs number.

Slip sinkage is sensitive to lugs center length, as it was inferred on figures 4.13e and 4.13f at 10% and 25% wheel slip, slip sinkage increases with increase of lugs center length although the difference is small. It also noted that at 10% wheel slip, sinkage increases with increase of lugs number up to optimal value then decreases with large number of lugs for $60mm$ and $80mm$ center length while for $100mm$ center length decreases with increase of lugs, and for $120mm$ center length keep increasing with increase of lugs number. At 25% wheel slip it increases with increase of lugs number for $60mm$ and $120mm$ center length, while for $80mm$ and $100mm$ it decreases with increase of lugs.

4.1.4 Combined lugs parameters

Based on the sensitivity analysis in sections 4.1.1, 4.1.2 and 4.1.3 taking into account wheel traction force, parameters of the lugs were selected according to the results and combined to find the optimal configuration. Parameters selected are 25°, 45° and 45° lugs angle, $80mm$ lugs height, $80mm$ centre length based on highest traction force at respective particle properties. Lugs parameters were then combined to find optimal configuration, and since lugs number also affects traction force all wheel with combined parameters are placed with 10, 15, 20 and 25 lugs respectively.

Simulations were carried out by allowing combined pattern parameter wheels to traverse a cohesive particles terrain. Simulation parameters such as wheel load, wheel speed, particles friction are the same as in section 4.1.1, instead only cohesive particles

are considered in this section. Pattern parameters for combined lugs angle, lugs height and lugs center length are tabulated in table 4.38.

	lugs parameters			
$wheel$	$angle[^\circ]$	$l_h[mm]$	$h[mm]$	
1	25	80	80	
2	35	80	80	wheel number
3	45	80	80	

Table 4.38: *wheel tread pattern parameters*

Terrain with sphere particles

Simulation results of traction force and slip sinkage for all wheels traversing sphere particles terrain were tabulated in tables 4.39 and 4.40 and graphically represented in figures 4.14 and 4.15 respectively.

Traction Force

	slip 10%				slip 25%				
	lugs number				lugs number				
$wheel$	10	15	20	25	10	15	20	25	
1	2831	2589	2729	2831	3473	3484	3524	3451	
2	2887	2658	2694	2733	3440	3490	3430	3376	traction force $[N]$
3	2615	2687	2456	2659	3469	3449	3306	3404	

Table 4.39: *traction force as a function of wheel slip*

Results of traction force shown in figure 4.14a, it was noted that wheel number 2 with 10 lugs has highest traction force at 10% wheel slip, while at high wheel slip figure 4.14b, wheel number 1 with 20 lugs gives highest traction force at 25% wheel slip. Wheel slip sinkage, results in figure 4.15a, it was notes that wheel number 1 with 20 lugs has higher sinkage while wheel number 3 with 20 lugs has lower sinkage at 10% wheel slip. Results shown in figure 4.15b, wheel number 2 with 15 lugs has higher sinkage, while wheel number 3 with 20 lugs has lower sinkage at 25% wheel slip.

Therefore, for terrain with sphere particles, configuration of wheel number 1 table 4.38 with 20 lugs gives high traction force especially at 25% slip, and it has considerable slip sinkage even at high slip although it is slightly higher than wheel number 3 with 25 lugs.

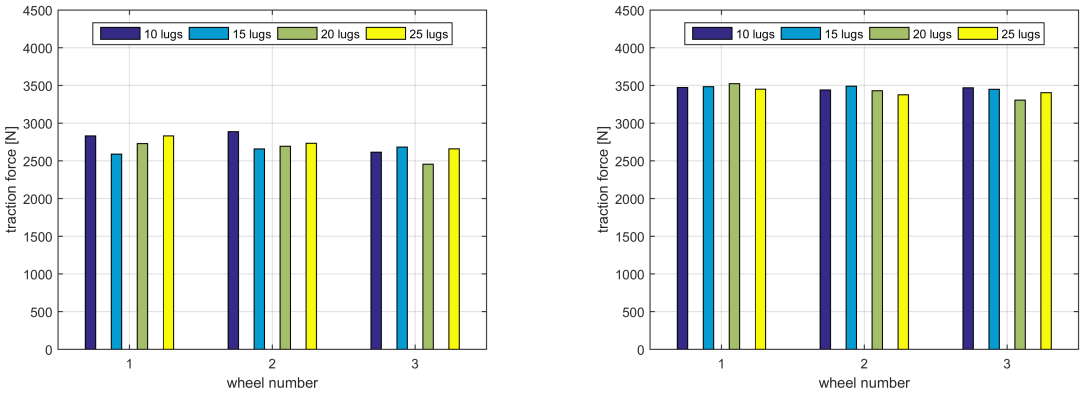

(a) *traction force at 10% slip* **(b)** *traction force at 25% slip*

Figure 4.14: *traction force as a function of wheel slip*

Slip Sinkage

	slip 10%				slip 25%				
	lugs number				lugs number				
$wheel$	10	15	20	25	10	15	20	25	
1	1.62	1.62	1.62	2.52	6.45	6.57	6.87	6.87	
2	1.87	1.53	1.87	2.22	6.45	7.14	6.45	6.45	slip sinkage $[cm]$
3	1.71	1.56	1.33	1.71	6.45	6.45	4.60	5.07	

Table 4.40: *slip sinkage as a function of wheel slip*

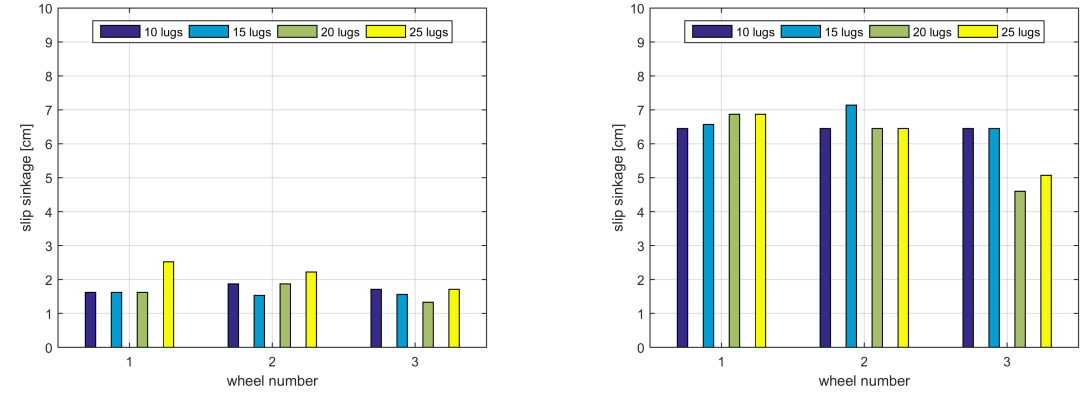

(a) *slip sinkage at 10% slip* **(b)** *slip sinkage at 25% slip*

Figure 4.15: *slip sinkage as a function of wheel slip*

Terrain with square particles

Traction Force

	slip 10%				slip 25%				
	lugs number				lugs number				
wheel	10	15	20	25	10	15	20	25	
1	2759	3013	3058	2759	3566	3680	3680	3600	
2	2802	2915	2700	2802	3508	3608	3544	3627	traction force $[N]$
3	2685	3037	2906	2787	3335	3580	3522	3439	

Table 4.41: *traction force as a function of wheel slip*

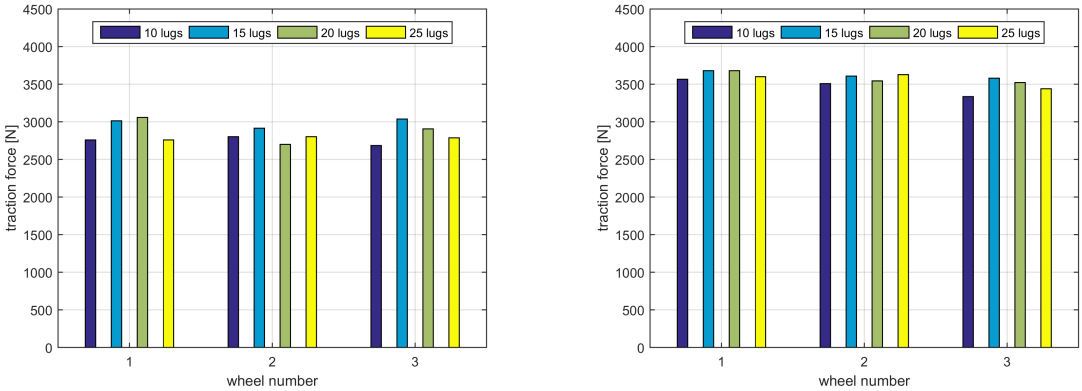

(a) *traction force at 10% slip*

(b) *traction force at 25% slip*

Figure 4.16: *traction force as a function of wheel slip*

Slip Sinkage

	slip 10%				slip 25%				
	lugs number				lugs number				
wheel	10	15	20	25	10	15	20	25	
1	1.34	2.91	3.09	2.20	6.07	7.43	8.13	8.47	
2	2.08	2.26	1.79	2.47	6.76	6.40	5.62	7.67	slip sinkage $[cm]$
3	0.96	2.52	2.52	2.52	4.43	6.90	7.55	4.78	

Table 4.42: *slip sinkage as a function of wheel slip*

Considering results of traction force terrain with square particles, it was noted both at 10% and 25% wheel slip figure 4.16a and 4.16b, wheel number 1 with 20 lugs gives high traction force as compared to wheel 2 and 3 while wheel 3 with 10 lugs gives lowest traction force.

Results of slip sinkage shown in figure 4.17a, it was noted that wheel number 1 with 20 lugs has higher slip sinkage while wheel number 3 with 10 lugs has lower slip sinkage at 10% wheel slip. At 25% slip results in figure 4.17b, wheel number 1 with 25 lugs has higher slip sinkage and wheel number 3 with 10 lugs has lower slip sinkage at 25% wheel slip respectively.

Therefore, for this terrain with square shaped particles, pattern configuration that gives high traction is of wheel number 1 with 20 lugs table 4.38, although it has high sinkage especially at 10% wheel slip.

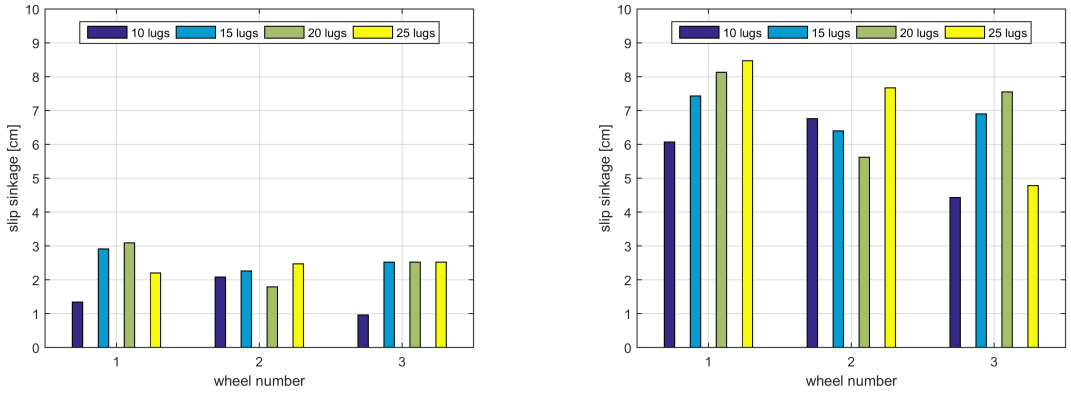

(a) *slip sinkage at 10% slip*

(b) *slip sinkage at 25% slip*

Figure 4.17: *slip sinkage as a function of wheel slip*

Terrain with mixed particles

Traction Force

	slip 10%				slip 25%				
	lugs number				lugs number				
wheel	10	15	20	25	10	15	20	25	
1	2854	2933	3005	2557	3513	3513	3568	3341	
2	2688	2724	3049	2904	3533	3533	3552	3457	traction force $[N]$
3	2599	2847	2753	2687	3397	3383	3369	3273	

Table 4.43: *traction force as a function of wheel slip*

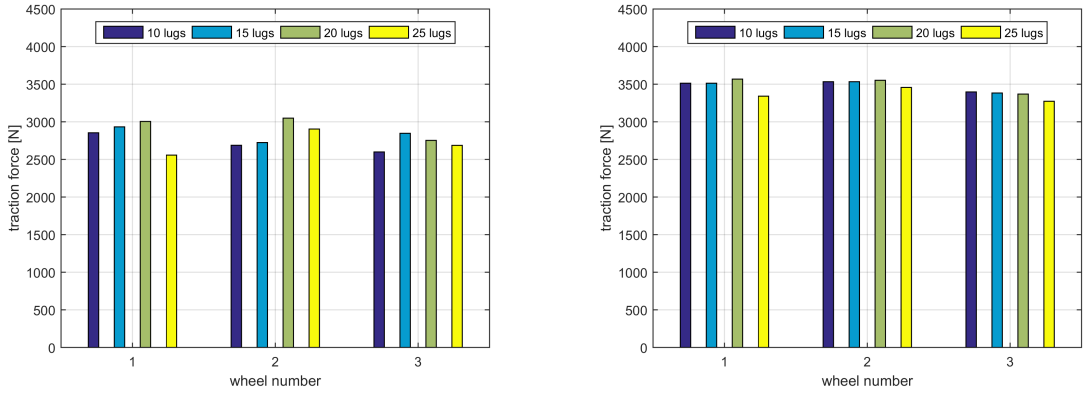

(a) *traction force at 10% slip*

(b) *traction force at 25% slip*

Figure 4.18: *traction force as a function of wheel slip*

Slip Sinkage

	slip 10%				slip 25%				
	lugs number				lugs number				
$wheel$	10	15	20	25	10	15	20	25	
1	1.59	2.03	2.50	1.18	7.70	8.05	7.70	6.87	
2	1.43	1.94	3.64	2.66	5.87	7.18	7.99	7.81	slip sinkage $[cm]$
3	0.60	2.14	1.67	1.67	6.71	6.31	6.31	4.42	

Table 4.44: *slip sinkage as a function of wheel slip*

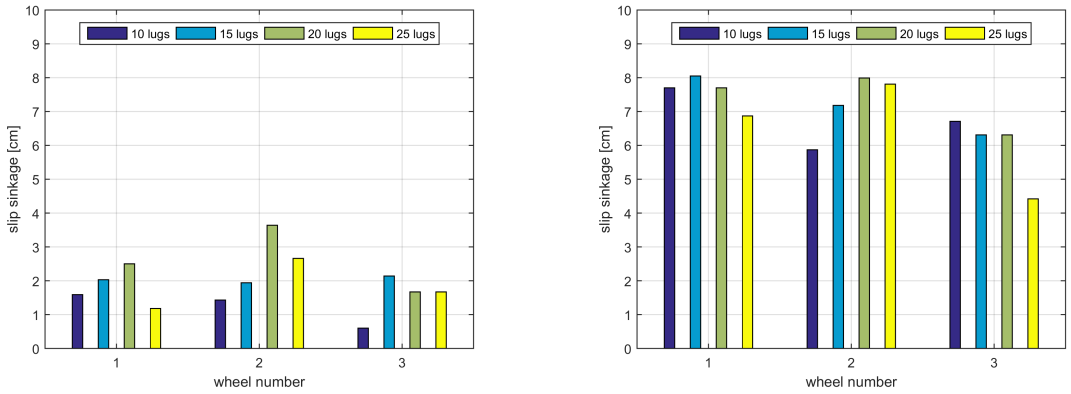

(a) *slip sinkage at 10% slip* **(b)** *slip sinkage at 25% slip*

Figure 4.19: *slip sinkage as a function of wheel slip*

Considering terrain with mixed particles, spheres, boxes and convex hull with mixing ratio given in section 4.1.3, with regards to traction force, it was noted that wheel number 2 with 20 lugs has high traction force both at 10% wheel slip figure 4.18a and at slip of 25% figure 4.18b wheel number 1 with 20 lugs gives high traction force, while wheel number 1 and 3 with 20 lugs at 10% and 25% wheel slip gives lower traction force respectively.

Taking into account wheel slip sinkage, wheel number 3 with 10 lugs has low slip sinkage, while wheel number 2 with 20 lugs has higher sinkage at 10% figure 4.19a. Wheel number 1 with 15 lugs results in figure 4.19b, has higher sinkage as compared to wheel number 3 with 25 lugs which has lower sinkage at 25% wheel slip respectively.

Although wheel number 3 gives low slip sinkage at low and high wheel slip respectively, but it have low traction force as compared to wheel number 1 and 2. Therefore, pattern configuration that gives higher traction force for this type of terrain modelled by assemblage of different shaped particles is that of wheel number 2 table 4.38 both at 10% and 25% wheel slip.

4.2 Soft deformable terrain

Since semi-empirical soil terrain developed can accommodate different wheels with variable pattern parameters, the model was used to perform sensitivity analysis in or-

der to analyse effects of pattern configuration on traction force at various wheel slip. Instead only dry sand terrain was considered in the analysis with wheels in table 4.1.

4.2.1 Variation of lugs angle, height and center length

traction force

	slip 5%				slip 25%				
	lugs number				lugs number				
$\delta[^\circ]$	10	15	20	25	10	15	20	25	
25	5176	5458	5613	5962	7512	7877	8610	8875	
35	5207	5469	5624	5848	7570	8483	8883	9233	traction force
45	4918	5109	5374	5637	7746	8456	9181	9364	$[N]$
55	4394	4810	4902	5050	7307	7810	8510	8856	

Table 4.45: *traction force as a function of lugs angle*

	slip 5%				slip 25%				
	lugs number				lugs number				
$l_h[mm]$	10	15	20	25	10	15	20	25	
20	3891	4062	4128	4312	5258	5454	5489	5534	
40	4845	5044	5238	5499	7009	7232	8143	8636	traction force
60	4918	5109	5374	5637	7746	8456	9181	9364	$[N]$
80	5140	5549	6173	6378	8239	9065	9478	10200	

Table 4.46: *traction force as a function of lugs height*

	slip 5%				slip 25%				
	lugs number				lugs number				
$h[mm]$	10	15	20	25	10	15	20	25	
60	1244	941	750	922	1610	1457	1292	1703	
80	991	1016	1147	1133	1412	1567	1855	1793	traction force
100	1204	1272	948	848	1532	1853	1752	1532	$[N]$
120	1255	923	661	932	1504	1421	1458	1581	

Table 4.47: *traction force as a function of lugs centre length*

From the simulation results in figure 4.20 and with regards to lugs angle figures 4.20a and 4.20b, it was noted that traction force decreases with increase of lugs angle at 5% wheel slip, while at 25% wheel slip traction force increases with increase of lugs angle up to 45° and further increase of angle traction decreases. It was noted that traction force increases with increase of lugs number both at 5% and 25% wheel slip.

With regards to lugs height figures 4.20c and 4.20d, it was noted that traction force increases with increase of lugs height and lugs number both at 5% and 25% wheel slip respectively. Taking into account lugs center length results in figures 4.20e and 4.20f, it was noted that traction force increases with increase of center length up to $80mm$ and further increase of center length traction force decreases both at 5% and 25% wheel slip respectively. Also traction force increases with increase of lugs number.

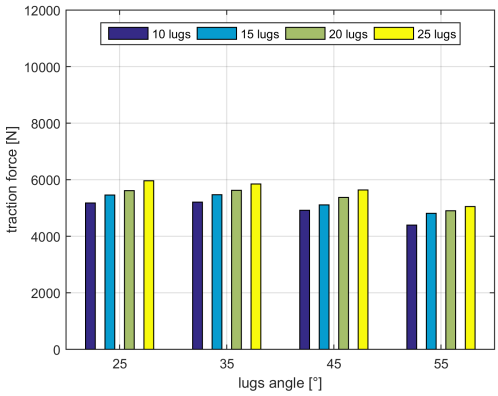

(a) *traction as a function of lugs angle at 5% slip*

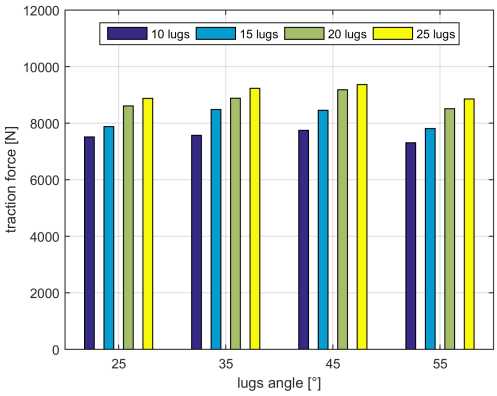

(b) *traction as a function of lugs angle at 25% slip*

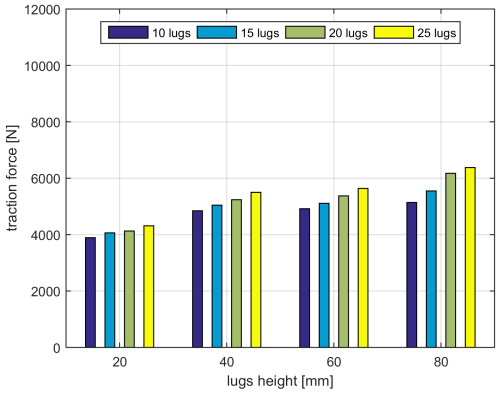

(c) *traction as a function of lugs height at 5% slip*

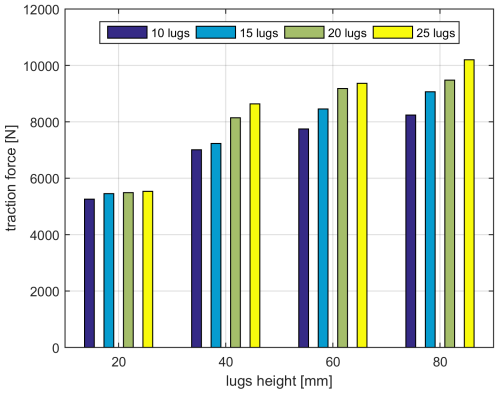

(d) *traction as a function of lugs height at 25% slip*

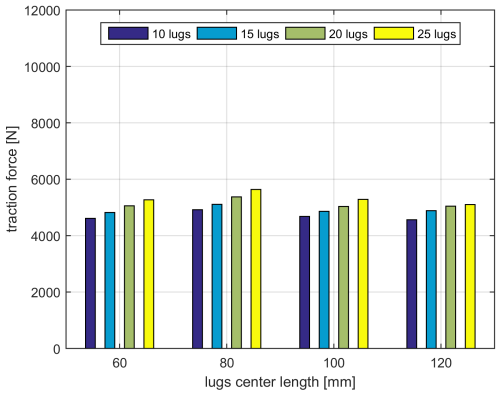

(e) *traction as a function of center length at 5% slip*

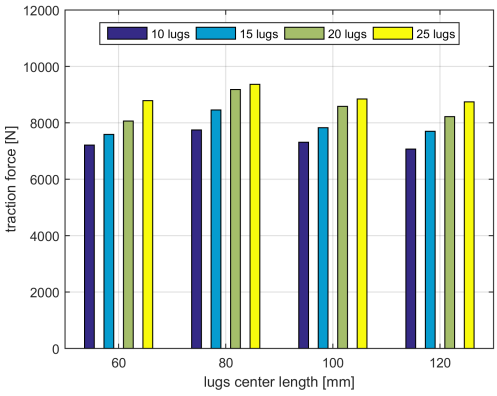

(f) *traction as a function of center length at 25% slip*

Figure 4.20: *traction force as a function of lugs angle, height and center length*

Pattern parameters that gives high traction are $45°$, $80mm$, $80mm$ and 25 lugs angle, height, center length and number respectively. Since 5% wheel slip $25°$ lugs angle and 25 lugs number gives high traction, therefore two wheels; one with $25°$, $80mm$ and $80mm$ lugs angle, lugs height and lugs center length and other with $45°$, $80mm$ and $80mm$ lugs angle, height and center length configurations was used to analyse optimal

pattern configuration.

4.2.2 Combined lugs parameters

wheel	$\delta[^\circ]$	$l_h[mm]$	$h[mm]$	$n_l[]$
1	25	80	80	25
2	45	80	80	25

Table 4.48: *wheel pattern configuration parameter*

traction force

wheel	slip 5%	slip 25%	
1	5603	9435	traction force
2	5597	10320	$[N]$

Table 4.49: *traction force as a function of wheel slip*

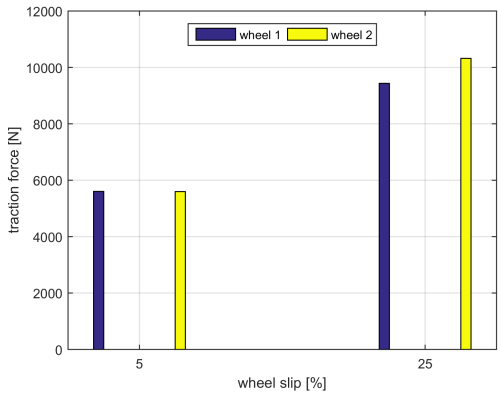

Figure 4.21: *traction force as a function of wheel slip*

From the simulation results of traction force for pattern configuration of wheel 1 and wheel 2, results in figure 4.21, it was noted that wheel 1 gives slightly high traction as compared to wheel 2 at 5% wheel slip, while wheel 2 gives high traction than wheel 1 at 25% wheel slip. Therefore optimal pattern configuration that guarantees high traction for both slip conditions was that of wheel 2 as shown in table 4.48.

4.3 Conclusions

Based on analysis done in sections 4.1 to 4.2 it was noted that, lugs angle, height, center length and number has effect on both traction and slip sinkage. It was also noted that traction force and slip sinkage not only depends on pattern parameters but also on terrain properties, and this results correlates with results of [101, 111].

Particle properties such as shape, size, cohesion, friction coefficient and mixing ratio of particles in the terrain affect pattern configuration performance in terms of traction force and slip sinkage [101] as seen in analysis above. Particles shape influence

number of contact between particles which improve the shearing resistance of the soil, cohesion and friction increase deformation resistance of the soil particles by increasing tangential force which rise from particle friction and contact force, while cohesion force affects elastic and plastic properties of the terrain during interaction. Size of the particles affects terrain stiffness by changing particle packing and void ratio of the terrain. Therefore sensitivity analysis has to be performed considering given terrain properties in order to find the optimal configuration of tread pattern.

Lugs angle affects traction force and slip sinkage as it was noted that changing angle by increasing or reduce it increases and reduces both longitudinal and lateral force of the wheel [18, 18, 71, 102] which in turn increases motion resistance. Lateral force is important to provide holding force to keep vehicle in a straight line of motion or contour for the case of ploughing although lateral force has not been modelled in this model. Slip sinkage also affected by lugs angle because increasing angle increases lugs length which increases contact cylindrical shape and amount of soil particles between lugs which in turn reduce soil disturbance as well as well as slip sinkage.

Lugs center length also affects traction and slip sinkage of the wheel, this is because the center part of the lugs is in 0° angle with respect to central wheel axis, this makes the longitudinal force developed by lugs center part to be utilised only in traction force and no component of its force utilised in lateral holding force. This cause increase of traction force with increase of center length up to optimal length. Although center length increases traction force, but also increases the soil disturbances and leads to increasing slip sinkage of the wheel especially at high wheel slip operation.

Lugs height affects traction force and slip sinkage of the wheel, as was be noted in the sensitivity analysis, increase of lugs height increases traction force, since it increasing the volume of soil between adjacent lugs that interacts with soil at contact point. Also increase of lugs height increases soil disturbances which results to increase of slip sinkage as well as motion resistance especially at high slip, and these results behaviours can be compared to [1, 15, 18, 57, 66, 70].

Number of lugs affects traction and slip sinkage of the wheel because increasing or reducing number of lugs alter lug spacing which in turn change the number of lugs interacting with soil at the contact point and soil volume between successive lugs. This cause change of soil disturbances and shearing area of terrain between the lugs, increasing number of lugs increases lugs that interacts with terrain which in turn increases traction force, these results are comparable to [57, 66, 96, 102] up to optimal spacing. Also increasing number of lugs cause decreases of slip sinkage since it improves shearing of terrain particles between the lugs at contact and cylindrical of the contact that support wheel load.

Combined lugs parameters results analysis of cohesive particles in section 4.1.4 it can be noted that optimal pattern configuration has been identified with respect to soil properties. Combined lugs parameters wheels has been tested on cohesive particles only and the results shows that higher traction and slip sinkage of the wheel with respect to terrain particles shape has been realised in the analysis, although the difference in increase of traction force is slightly small as compared to results before combined lugs parameters in sections 4.1.1, 4.1.2 and 4.1.3.

For soft deformable terrain in sub-section 4.2, it was noted that traction force decreases with increase of lugs angle at 5% wheel slip, while at 25% wheel slip, traction

tends to increase with lugs angle up to 45° and decrease for 55°angle. Also traction force increases with increase of lugs number. Traction force increases with increase of lugs height both at 5% and 25% wheel slip while with center length, traction force increases with increase of center length up to $80mm$ and decreases with further increase of center length.

Since slip sinkage and traction force mostly affect performance of the wheel on deformable terrain [113], the tread parameters has to be taking into consideration when analysing wheel performances on deformable terrain, and consequently an optimal parameters has to be found with respect to given terrain or particle properties. For combined lugs parameters in sub-section 4.2.2, the optimal pattern configuration has been identified which is one with wheel 2 with parameters in table 4.48, although at 5% wheel slip both wheel 1 and 2 has almost same traction force, but at high slip 25% wheel 2 guarantees high traction force as compared to wheel 1.

CHAPTER 5

Optimization Analysis

Chrono::engine model for tyre-soil interaction developed in this work can take into account different tyre size, tread patterns and terrain parameters, hence it were used as a tool to perform optimization analysis of wheel-terrain interaction. Optimisation analysis of wheel-soil interaction with respect to terrain soil characteristics were carried out by considering interaction parameters which mostly affects wheel performance on deformable terrain such as traction force, static sinkage, slip sinkage, slip velocity and forward velocity. To accomplish these a number tyres with different sizes such as diameter, width, pattern parameters are interacted with terrain made by dry sand, loose sand, upland sand and clayey loam sand particles with different properties such as cohesion force, particles type/shape, particles friction, particle density, terrain weight density at selected $1.05rad/s$ wheel angular speed and $13.2kN$ wheel weight respectively.

In order to simplify tread pattern parameters, reference values of 15 and 20 lugs number, 25° and 45° lugs angle, $80mm$ lugs center length, $40mm$ lugs width taken from chapter 4 section 4.1.4 for wheel with higher traction force and slightly less slip sinkage. Although $80mm$ lugs height gives slighlty high traction as compared to $60mm$ lugs height, $60mm$ lugs height for all wheels was chosen since it gives lower slip sinkage of the wheel. Range of spacing that gives high traction is between $200mm$ to $300mm$, $222mm$ lugs spacing were used to calculate number of lugs as in appendix 6 to minimise number of variables which account for many simulations. Diameter and width of the wheels were adopted from BKT agricultural tires technical data book as shown in table 5.1.

Terrain parameters such as cohesion, particle density for upland sand, clayey loam sand were adopted from [106, 107]. Particles friction coefficient adopted in [68] and value of 0.9 friction coefficient were adopted from chapter 3 section 3.6 while mean particles density for dry and loose sand were taken from [64] and the values are tabu-

lated in table 5.2 below. Effects of moisture in terrain is not considered in this model since there was no mechanism for initiating moisture condition in particles, although stated from literature that moisture has an effects to the terrain strength, in which soil strength decreases with increase of moisture content, and this effect can be represented by shear stress-shear displacement relations [52, 86].

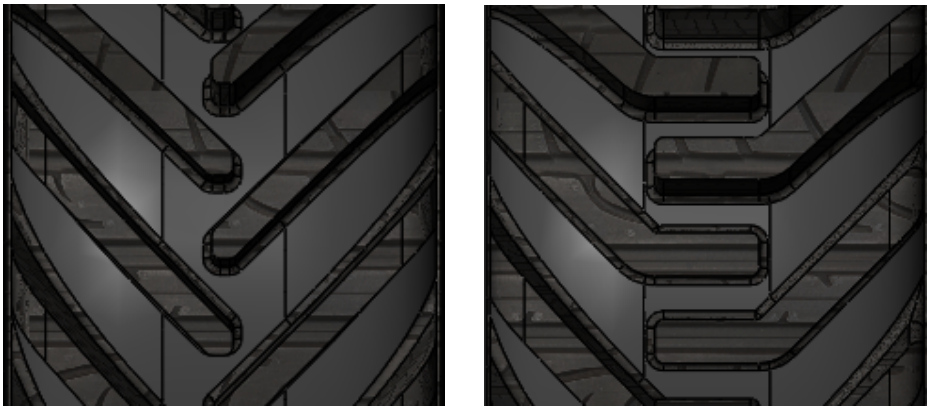

(a) *straight lugs* **(b)** *combined lugs*

Figure 5.1: *lugs type*

wheel	$\delta[^\circ]$	$l_h[mm]$	$h[mm]$	$D_0[mm]$	$w[mm]$	n_l	lugs type
1	25	60	–	1234	479	15	straight
2	25	60	80	1234	479	15	combined
3	25	60	80	1413	530	18	combined
4	25	60	80	1644	611	20	combined
5	45	60	–	1234	479	15	straight
6	45	60	80	1234	479	15	combined
7	45	60	80	1413	530	18	combined
8	45	60	80	1644	611	20	combined

Table 5.1: *wheel design parameters*

5.1 Granular terrain

Simulation results are tabulated in each section tables and represented graphically in the figures as explained in each sections, in which x-axis represents wheel slip in percentage, y-axis represents traction force in $Newton$, slip sinkage in cm, slip velocity in m/s and forward velocity in m/s while different bars represents wheel number as shown in figures legends. Straight and combined lugs type for wheels used in this section are indicated in figure 5.1.

terrain	$k_c[kN/m^{n+1}]$	$k_\phi[kN/m^{n+2}]$	$\rho_p[kg/m^3]$	$p_f[]$	$p_c[kPa]$	$\gamma_b[kg/m^3]$	$n[]$
dry sand	0.99	1528.43	1689	0.7869	1.04	770	1.1
loose sand	65.5	1418	1689	0.9	0	856	0.97
upland sand	74.6	2080	1557	0.7869	3.4	1008	1.1
clayey loam	41.6	2471	1653	0.85	6.1	780	0.73

Table 5.2: *terrain particle properties and parameters [64, 68, 106, 107]*

5.1.1 Dry sand terrain

In this section simulations were carried out by interacting wheel 1 to 8 table 5.1 with terrain made of dry sand particles, with properties shown in table 5.2. Simulations are carried out to analyse variation of wheel traction force, slip sinkage, slip velocity and forward velocity for at least three seconds of traversing time. Simulation results of wheel traction force, slip sinkage, slip velocity and forward velocity are tabulated in tables 5.3 to 5.6 and representaed graphically in figures 5.2 to 5.9.

Traction Force

	slip [%]										
wheel	5	10	15	20	25	30	35	40	45	50	
1	2648	2835	3016	3166	3291	3452	3544	3511	3387	3350	traction
5	2200	2465	2747	2947	3108	3273	3421	3511	3541	3434	force[N]

(a) *traction force wheels with 1234 mm diameter-straight lugs*

	slip [%]										
wheel	5	10	15	20	25	30	35	40	45	50	
2	2778	3029	3208	3331	3493	3622	3668	3661	3596	3526	traction
6	2437	2596	2793	3021	3170	3332	3466	3531	3553	3502	force[N]

(b) *traction force wheels with 1234 mm diameter-combined lugs*

	slip [%]										
wheel	5	10	15	20	25	30	35	40	45	50	
3	2532	2705	2828	2973	3089	3169	3209	3174	3175	3176	traction
7	2208	2501	2690	2889	3034	3126	3142	3125	3126	3127	force[N]

(c) *traction force wheels with 1413 mm diameter-combined lugs*

	slip [%]										
wheel	5	10	15	20	25	30	35	40	45	50	
4	2532	2705	2828	2973	3089	3169	3209	3174	3175	3176	traction
8	2208	2501	2690	2889	3034	3126	3142	3125	3126	3127	force[N]

(d) *traction force wheels with 1644 mm diameter-combined lugs*

Table 5.3: *traction force as a function of wheel slip*

From the simulation results figure 5.2a wheels with straight lugs, it was noted that, wheel 1 has high traction as compared to wheel 5 at slip between 5% to 35%, this is because of increase of lugs angle which increase lateral component of traction force and improves lateral holding force [18]. The difference of traction between the wheels tends to be small above 35% wheel slip. Trend of traction force in figure 5.2b for wheels with combined lugs is similar to those with straight lugs for same wheel diameter. Difference in traction force for wheel with straight and combined lugs figure 5.2a and 5.2b is very small, this shows that effect of lugs type for dry sand terrain is small and it can be neglected.

Increase of wheel diameter decreases traction force, this was noted in figures 5.2c for wheel with $1413mm$ and 5.2d for wheels with $1644mm$ as compared to wheels with diameters $1234mm$ figures 5.2a and 5.2b respectively.

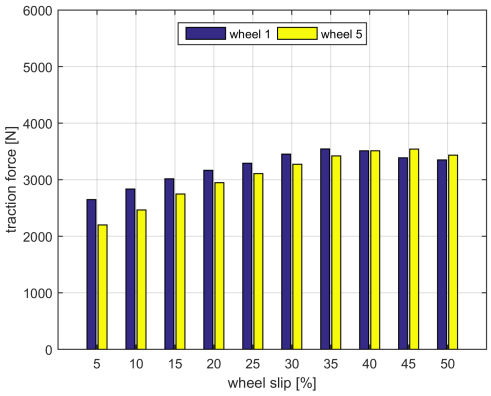

(a) *traction for wheels with 1234 mm diameter-straight lugs*

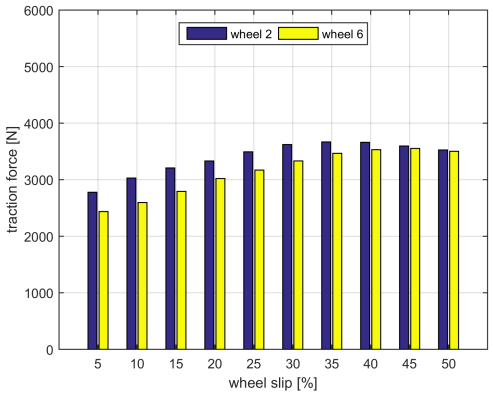

(b) *traction for wheels with 1234 mm diameter-combined lugs*

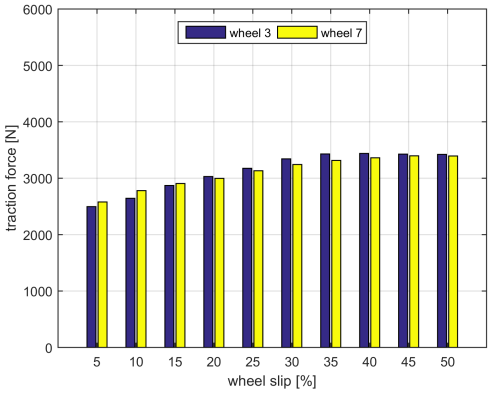

(c) *traction for wheels with 1413 mm diameter-combined lugs*

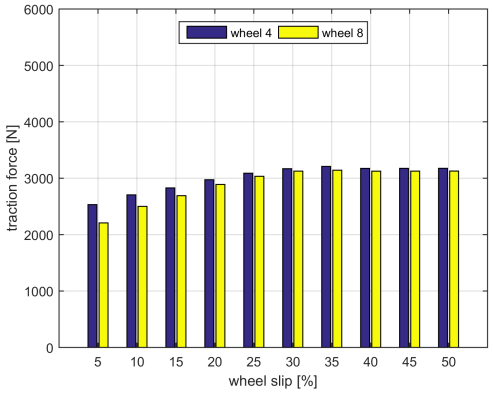

(d) *traction for wheels with 1644 mm diameter-combined lugs*

Figure 5.2: *traction force as a function of wheel slip*

This is because wheel diameter has much effect in motion resistance [106] than width, increase of diameter reduce motion resistance as well as resistive traction of wheel. Trend of traction force for large wheels is similar between $25°$ and $45°$ lugs angle and the difference is small for dry sand terrain especially at high slip above 25% figures 5.2c and 5.2d.

Increase of diameter also has effects on slip sinkage of the wheels, slip sinkage decreases with increase of wheel diameter. This was noted in simulation results figures 5.3a , 5.3b , 5.3c and 5.3d respectively. This shows that increase of wheel diameter improve wheel traverse performance by reducing sinkage for dry sand terrain. Increase of lugs angle also reduces slip sinkage, this is because increase of lugs angle increases lugs length and cause uniform soil disturbance with interacting lugs [18]. This shows that for dry sand terrain, $45°$ lugs angle gives better wheel performance, although it has less traction as compared to $25°$ lugs angle but guarantees less slip sinkage.

Effect of lugs type on slip velocity is very small and it can be neglected in dry sand terrain. This was noted in figures 5.6a and 5.6b for wheels with same diameter. Increase of wheel diameter and lugs angle both has effects on wheel slip velocity in which increase of diameter reduces slip velocity and increase of lugs angle increases slip velocity.

Slip Sinkage

	slip [%]										
wheel	5	10	15	20	25	30	35	40	45	50	
1	0.09	1.11	1.96	2.88	4.10	5.44	7.47	10.49	12.57	13.60	slip
5	0.64	0.90	1.96	2.88	4.10	5.44	6.96	8.82	11.21	14.04	sinkage$[cm]$

(a) *slip sinkage wheels with 1234 mm diameter-straight lugs*

	slip [%]										
wheel	5	10	15	20	25	30	35	40	45	50	
2	0.84	1.56	2.51	3.57	4.89	6.37	7.70	9.93	11.74	14.00	slip
6	0.48	0.98	1.80	2.98	4.48	5.85	7.70	9.56	11.74	14.00	sinkage$[cm]$

(b) *slip sinkage wheels with 1234 mm diameter-combined lugs*

	slip [%]										
wheel	5	10	15	20	25	30	35	40	45	50	
3	0.26	0.83	1.98	2.97	4.36	6.27	8.28	11.06	12.77	12.77	slip
7	0.76	1.40	2.17	2.97	4.03	4.99	6.38	7.89	9.92	11.67	sinkage$[cm]$

(c) *slip sinkage wheels with 1413 mm diameter-combined lugs*

	slip [%]										
wheel	5	10	15	20	25	30	35	40	45	50	
4	0.66	1.28	2.19	3.31	4.40	5.73	7.86	10.69	10.69	10.69	slip
8	0.50	1.38	2.19	3.31	4.40	5.73	7.01	8.57	10.00	10.00	sinkage$[cm]$

(d) *slip sinkage wheels with 1644 mm diameter-combined lugs*

Table 5.4: *slip sinkage as a function of wheel slip*

This is because wheel diameter reduce sinkage as well as entry angle and lugs angle affects wheel slip in which slip velocity is a function of slip and entry angle. This was noted in results figures 5.6a , 5.6b , 5.6c and 5.6d. Lugs angle and diameter affects forward wheel velocity, 45° lugs angle gives increase of forward velocity, this is because of reduced motion resistance with increase of diameter and uniform shearing of soil for interacting lugs as explained before, this noted in figures 5.9.

Taking into account contact patch figures 5.4, 5.10, 5.12, 5.14, 5.8, 5.16, 5.18 and 5.20, it was noted that at 5% wheel slip, lugs traces are amlost clear, but at high slip of 50% lugs traces are not clear. This is because at high slip soil particles are disturbed more and make some lugs traces to interact. Also contact length elongated at high slip due to increase of slip sinkage and lead to increase of motion resistance as well as resistive torque [57].

Contact profile figures 5.5, 5.11, 5.13, 5.15, 5.7, 5.17, 5.19 and 5.21 it was inferred that terrain particles in front of contact profile are compressed more by experiencing high normal force as indicated in color bar. This means that the maximum stress of the terrain at the contact patch occurs between bottom line of the maximum sinkage and entry point of the contact, and this results correlates with stress distribution stated by Wong [106]. Also the contact profile is deep at high slip, this shows also at high slip the wheel experience more sinkage due to slip sinkage, this happen when part of soil in front of the wheel is pushed forward and part of soil at the contact is taken by the lugs when moves as the wheel rotates [15].

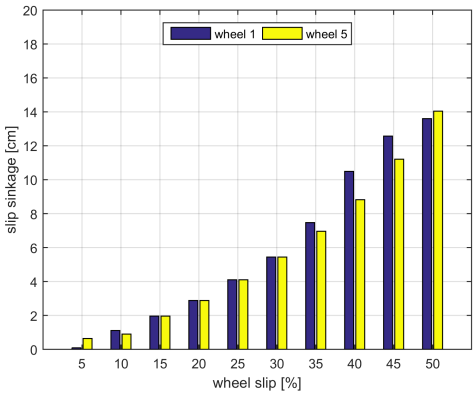

(a) *sinkage for wheels with 1234 mm diameter-straight lugs*

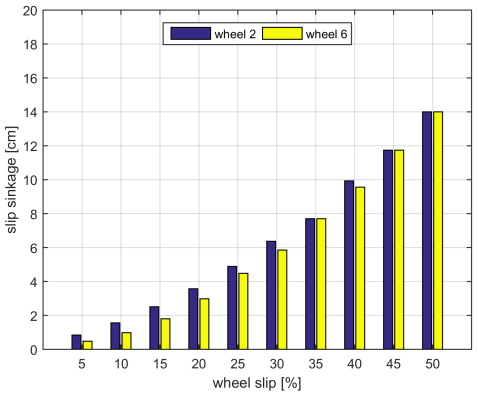

(b) *sinkage for wheels with 1234 mm diameter-combined lugs*

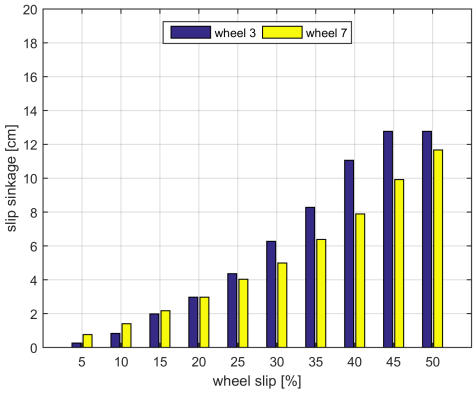

(c) *sinkage for wheels with 1413 mm diameter-combined lugs*

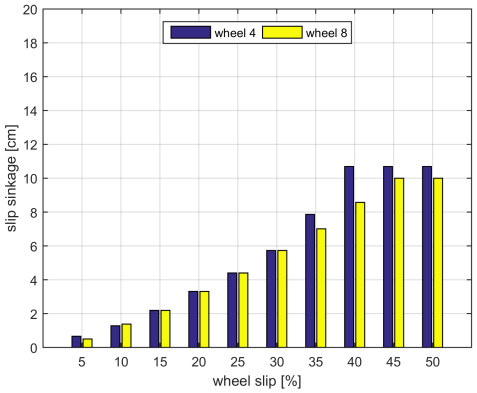

(d) *sinkage for wheels with 1644 mm diameter-combined lugs*

Figure 5.3: *slip sinkage as a function of wheel slip*

Since mobility performance of wheels in deformable terrain has to be with high traction, low slip sinkage and low slip velocity, also wheels on traversing a given terrain has to avoid continuous failure of the supporting soil [15, 17, 19, 106, 110] as well negative impact to ground such as severe compaction which affects productivity of land in agricultural activities, wheels with high traction and cause low sinkage has to be used.

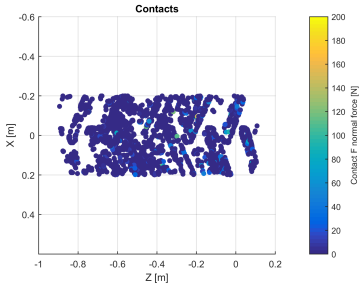

(a) *contact patch at* 5% *wheel slip-wheel* 1

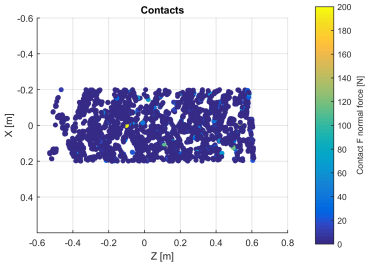

(b) *contact patch at* 50% *wheel slip-wheel* 1

Figure 5.4: *contact patch at* 5% *and* 50% *wheel slip for wheel* 1

Slip Velocity

	slip [%]										
wheel	5	10	15	20	25	30	35	40	45	50	
1	0.017	0.031	0.043	0.052	0.059	0.068	0.074	0.076	0.079	0.083	slip
5	0.020	0.037	0.048	0.058	0.065	0.072	0.079	0.083	0.083	0.084	velocity$[m/s]$

(a) *slip velocity wheels with 1234 mm diameter-straight lugs*

	slip [%]										
wheel	5	10	15	20	25	30	35	40	45	50	
2	0.016	0.028	0.039	0.048	0.056	0.063	0.069	0.072	0.074	0.074	slip
6	0.019	0.035	0.047	0.056	0.063	0.071	0.076	0.078	0.078	0.078	velocity$[m/s]$

(b) *slip velocity wheels with 1234 mm diameter-combined lugs*

	slip [%]										
wheel	5	10	15	20	25	30	35	40	45	50	
3	0.019	0.034	0.044	0.052	0.061	0.063	0.063	0.059	0.057	0.059	slip
7	0.017	0.030	0.042	0.052	0.061	0.070	0.076	0.079	0.076	0.076	velocity$[m/s]$

(c) *slip velocity wheels with 1413 mm diameter-combined lugs*

	slip [%]										
wheel	5	10	15	20	25	30	35	40	45	50	
4	0.017	0.030	0.040	0.050	0.057	0.060	0.058	0.057	0.057	0.057	slip
8	0.022	0.035	0.044	0.052	0.058	0.061	0.062	0.061	0.061	0.061	velocity$[m/s]$

(d) *slip velocity wheels with 1644 mm diameter-combined lugs*

Table 5.5: *slip velocity as a function of wheel slip*

Therefore, wheels 3 , 4 , 7 and 8 with parameters given in table 5.1 performs better in dry sand terrain under wheel load of $13.2kN$ by guarantees high traction and low slip sinkage. Although wheel 3 has a little bit high slip sinkage as compared to wheel 4, 7 and 8, but it maintain a sinkage of below $13cm$ at 45% and 50% wheel slip figure 5.3c.

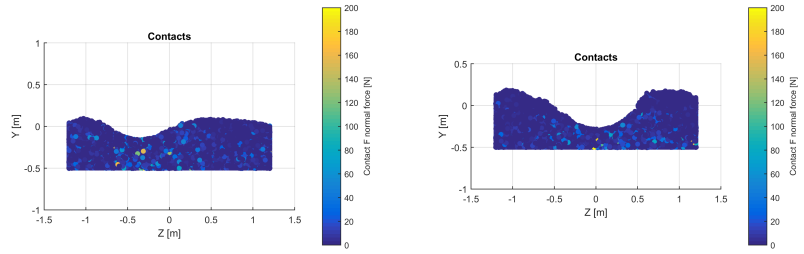

(a) *contact profile at* 5% *wheel slip-wheel* 1 **(b)** *contact profile at* 50% *wheel slip-wheel* 1

Figure 5.5: *contact profile at* 5% *and* 50% *wheel slip for wheel* 1

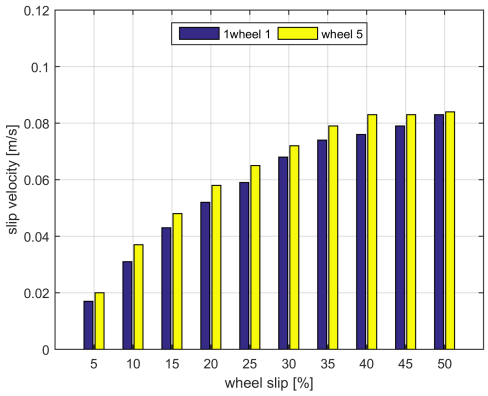

(a) *slip velocity for wheels with 1234 mm diameter-straight lugs*

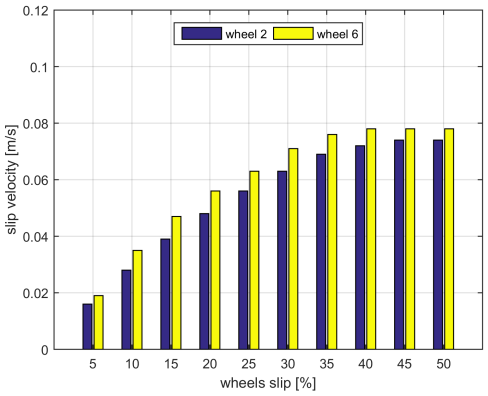

(b) *slip velocity for wheels with 1234 mm diameter-combined lugs*

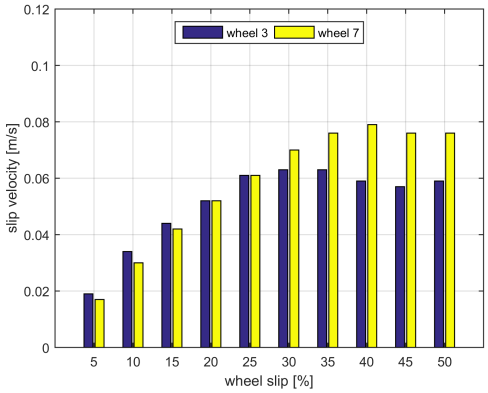

(c) *slip velocity for wheels with 1413 mm diameter-combined lugs*

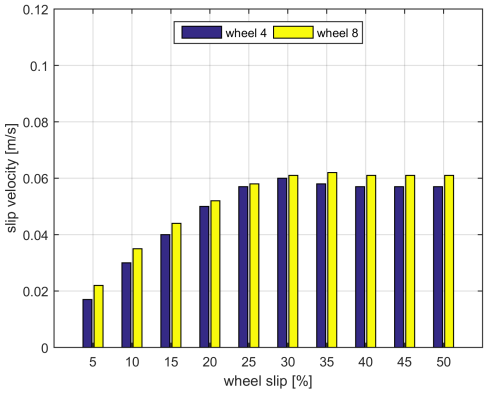

(d) *slip velocity for wheels with 1644 mm diameter-combined lugs*

Figure 5.6: *slip sinkage as a function of wheel slip*

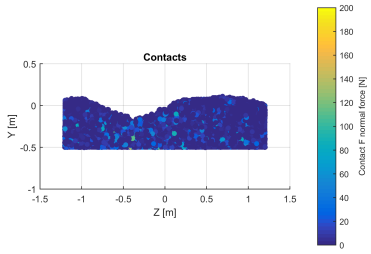

(a) *contact profile at* 5% *wheel slip-wheel* 5

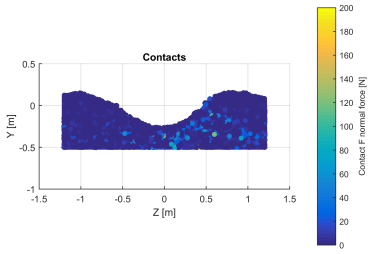

(b) *contact profile at* 50% *wheel slip-wheel* 5

Figure 5.7: *contact profile at* 5% *and* 50% *wheel slip for wheel* 5

Forward Velocity

	slip [%]										
wheel	5	10	15	20	25	30	35	40	45	50	
1	0.34	0.30	0.27	0.23	0.20	0.17	0.14	0.11	0.10	0.08	forward
5	0.38	0.34	0.29	0.25	0.22	0.19	0.15	0.13	0.10	0.08	velocity$[m/s]$

(a) *forward velocity wheels with 1234 mm diameter-straight lugs*

	slip [%]										
wheel	5	10	15	20	25	30	35	40	45	50	
2	0.33	0.28	0.25	0.22	0.19	0.15	0.13	0.11	0.09	0.07	forward
6	0.36	0.33	0.29	0.25	0.21	0.18	0.15	0.12	0.10	0.08	velocity$[m/s]$

(b) *forward velocity wheels with 1234 mm diameter-combined lugs*

	slip [%]										
wheel	5	10	15	20	25	30	35	40	45	50	
3	0.37	0.33	0.28	0.24	0.20	0.15	0.12	0.09	0.07	0.07	forward
7	0.36	0.31	0.28	0.25	0.21	0.18	0.15	0.12	0.10	0.08	velocity$[m/s]$

(c) *forward velocity wheels with 1413 mm diameter-combined lugs*

	slip [%]										
wheel	5	10	15	20	25	30	35	40	45	50	
4	0.36	0.31	0.27	0.22	0.18	0.14	0.11	0.08	0.08	0.08	forward
8	0.42	0.35	0.29	0.23	0.18	0.14	0.12	0.09	0.09	0.09	velocity$[m/s]$

(d) *forward velocity wheels with 1644 mm diameter-combined lugs*

Table 5.6: *forward velocity as a function of wheel slip*

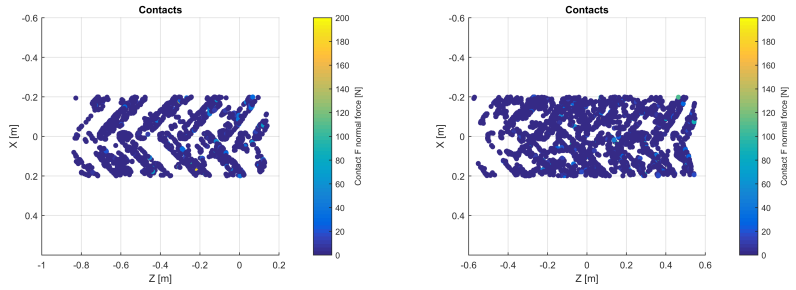

(a) *contact patch at* 5% *wheel slip-wheel* 5 **(b)** *contact patch at* 50% *wheel slip-wheel* 5

Figure 5.8: *contact patch at* 5% *and* 50% *wheel slip for wheel* 5

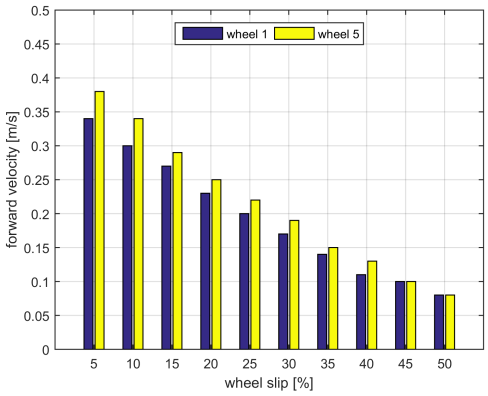

(a) *forward velocity for wheels with 1234 mm diameter-straight lugs*

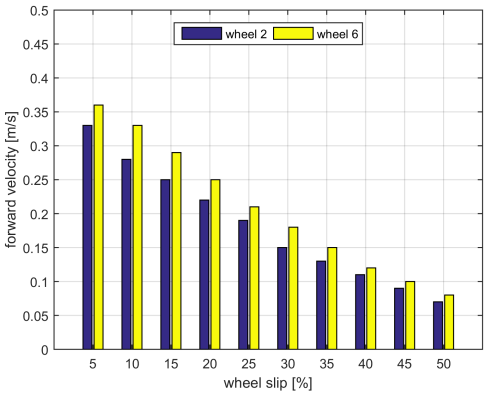

(b) *forward velocity for wheels with 1234 mm diameter-combined lugs*

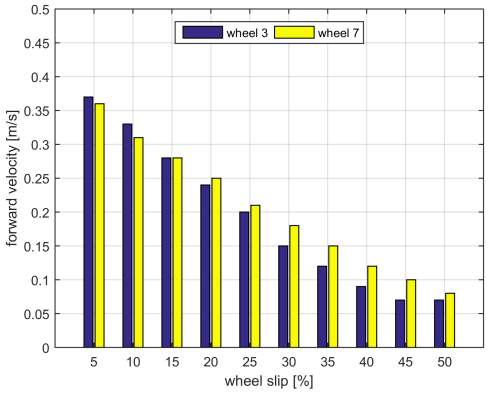

(c) *forward velocity for wheels with 1413 mm diameter-combined lugs*

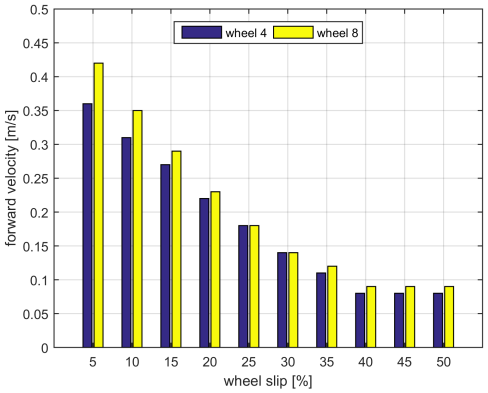

(d) *forward velocity for wheels with 1644 mm diameter-combined lugs*

Figure 5.9: *forward velocity as a function of wheel slip*

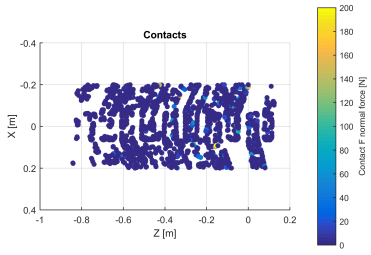

(a) *contact patch at* 5% *wheel slip-wheel* 2

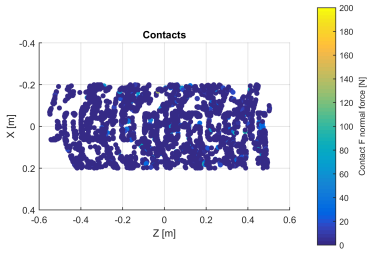

(b) *contact patch at* 50% *wheel slip-wheel* 2

Figure 5.10: *contact patch at* 5% *and* 50% *wheel slip for wheel* 2

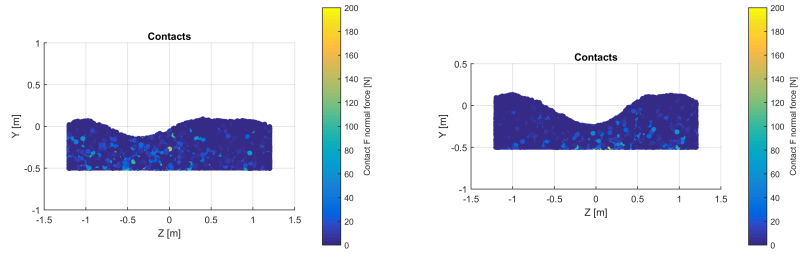

(a) *contact profile at* 5% *wheel slip-wheel* 2 **(b)** *contact profile at* 50% *wheel slip-wheel* 2

Figure 5.11: *contact profile at* 5% *and* 50% *wheel slip for wheel* 2

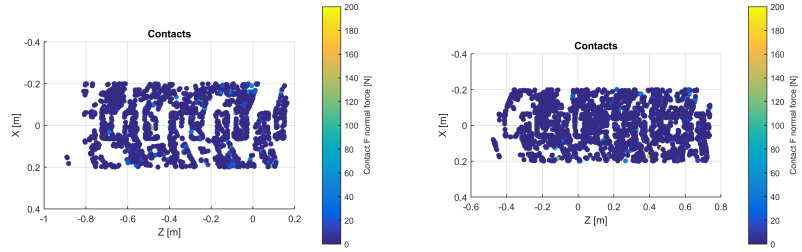

(a) *contact patch at* 5% *wheel slip-wheel* 3 **(b)** *contact patch at* 50% *wheel slip-wheel* 3

Figure 5.12: *contact patch at* 5% *and* 50% *wheel slip for wheel* 3

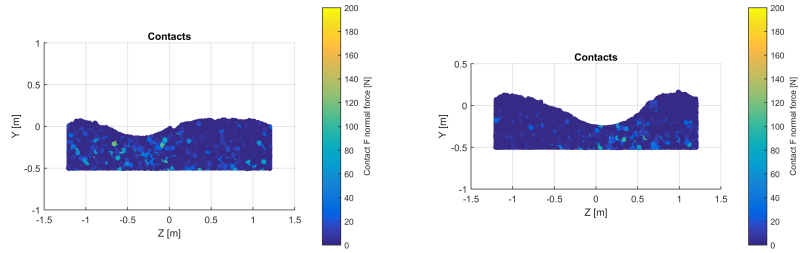

(a) *contact profile at* 5% *wheel slip-wheel* 3 **(b)** *contact profile at* 50% *wheel slip-wheel* 3

Figure 5.13: *contact profile at* 5% *and* 50% *wheel slip for wheel* 3

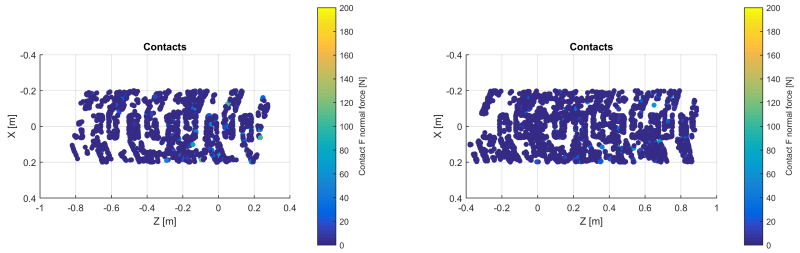

(a) *contact patch at* 5% *wheel slip-wheel* 4 **(b)** *contact patch at* 50% *wheel slip-wheel* 4

Figure 5.14: *contact patch at* 5% *and* 50% *wheel slip for wheel* 4

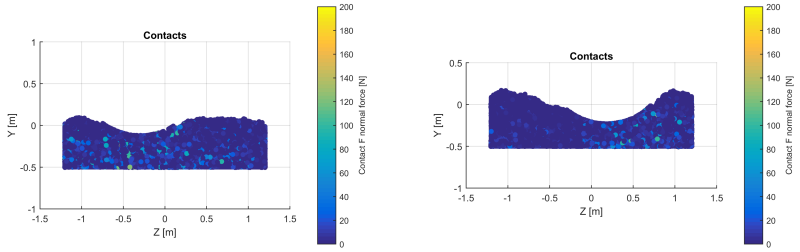

(a) *contact profile at* 5% *wheel slip-wheel* 4 **(b)** *contact profile at* 50% *wheel slip-wheel* 4

Figure 5.15: *contact profile at* 5% *and* 50% *wheel slip for wheel* 4

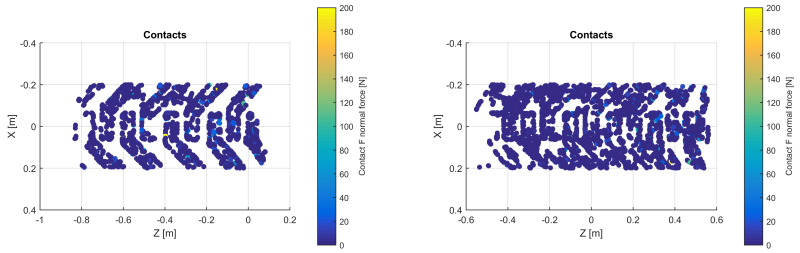

(a) *contact patch at* 5% *wheel slip-wheel* 6 **(b)** *contact patch at* 50% *wheel slip-wheel* 6

Figure 5.16: *contact patch at* 5% *and* 50% *wheel slip for wheel* 6

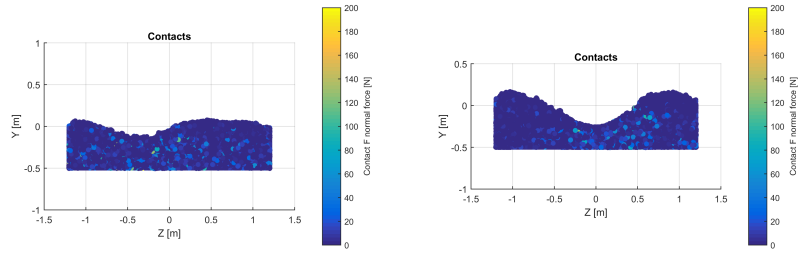

(a) *contact profile at* 5% *wheel slip-wheel* 6 **(b)** *contact profile at* 50% *wheel slip-wheel* 6

Figure 5.17: *contact profile at* 5% *and* 50% *wheel slip for wheel* 6

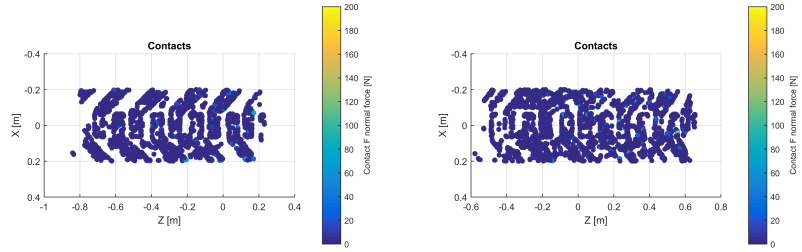

(a) *contact patch at* 5% *wheel slip-wheel* 7 **(b)** *contact patch at* 50% *wheel slip-wheel* 7

Figure 5.18: *contact patch at* 5% *and* 50% *wheel slip for wheel* 7

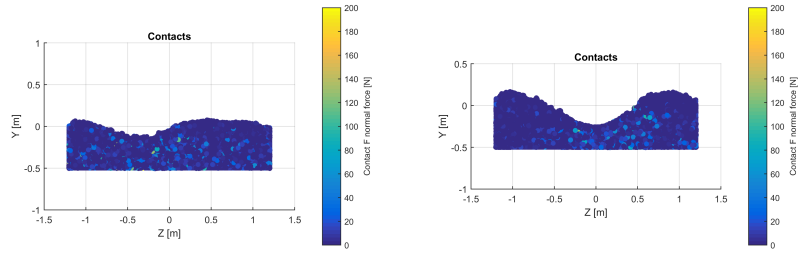

(a) *contact profile at* 5% *wheel slip-wheel* 7 **(b)** *contact profile at* 50% *wheel slip-wheel* 7

Figure 5.19: *contact profile at* 5% *and* 50% *wheel slip for wheel* 7

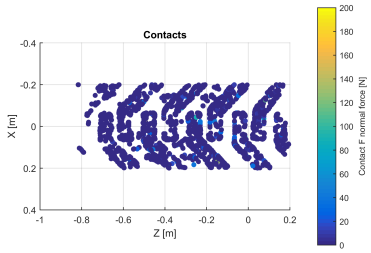

(a) *contact patch at* 5% *wheel slip-wheel* 8

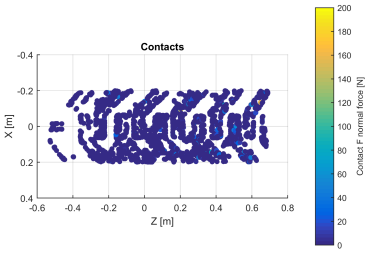

(b) *contact patch at* 50% *wheel slip-wheel* 8

Figure 5.20: *contact patch at* 5% *and* 50% *wheel slip for wheel* 8

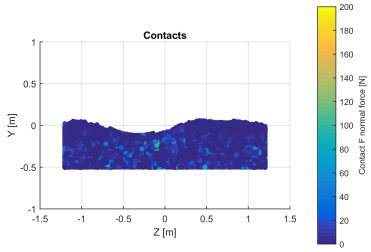

(a) *contact profile at* 5% *wheel slip-wheel* 8

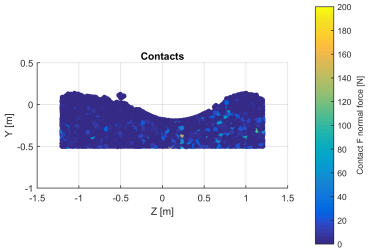

(b) *contact profile at* 50% *wheel slip-wheel* 8

Figure 5.21: *contact profile at* 5% *and* 50% *wheel slip for wheel* 8

5.1.2 Loose sand terrain

In this section simulations were carried out by interacting wheel 1 to 8 table 5.1 with terrain made of loose sand particles, which has mixed particles with properties as shown in table 5.2. Simulation parameters such as angular velocity and number of particles were as in section 5.1.1. Results of traction force, slip sinkage, slip velocity and forward velocity has been tabulated in tables 5.7, 5.8, 5.9 and 5.10 and graphically presented in figures 5.23, 5.27, 5.29 and 5.32 respectively.

Traction Force

	slip [%]										
wheel	5	10	15	20	25	30	35	40	45	50	
1	1800	2097	2389	2609	2876	3110	3318	3450	3409	3305	traction
5	1700	2081	2317	2557	2821	3021	3170	3333	3409	3408	force$[N]$

(a) *traction force wheels with 1234 mm diameter-straight lugs*

	slip [%]										
wheel	5	10	15	20	25	30	35	40	45	50	
2	1800	2115	2390	2655	2927	3224	3430	3543	3541	3403	traction
6	1700	1960	2167	2342	2342	2851	3116	3330	3426	3391	force$[N]$

(b) *traction force wheels with 1234 mm diameter-combined lugs*

	slip [%]										
wheel	5	10	15	20	25	30	35	40	45	50	
3	1857	2093	2431	2685	2952	3168	3265	3275	3266	3266	traction
7	1700	2065	2291	2519	2803	3042	3265	3362	3348	3331	force$[N]$

(c) *traction force wheels with 1413 mm diameter-combined lugs*

	slip [%]										
wheel	5	10	15	20	25	30	35	40	45	50	
4	2042	2334	2525	2706	2913	3075	3182	3228	3238	3238	traction
8	1900	2136	2353	2613	2841	3023	3136	3178	3179	3179	force$[N]$

(d) *traction force wheels with 1644 mm diameter-combined lugs*

Table 5.7: *traction force as a function of wheel slip*

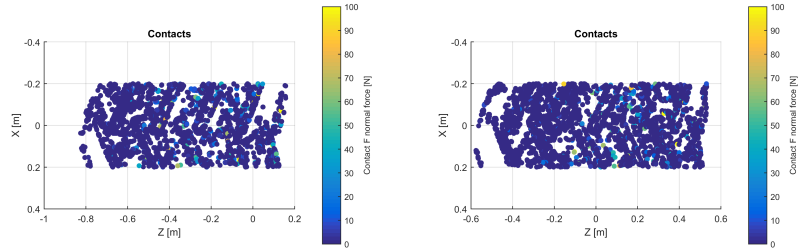

(a) *contact patch at* 5% *wheel slip-wheel* 1 **(b)** *contact patch at* 50% *wheel slip-wheel* 1

Figure 5.22: *contact patch at* 5% *and* 50% *wheel slip for wheel* 1

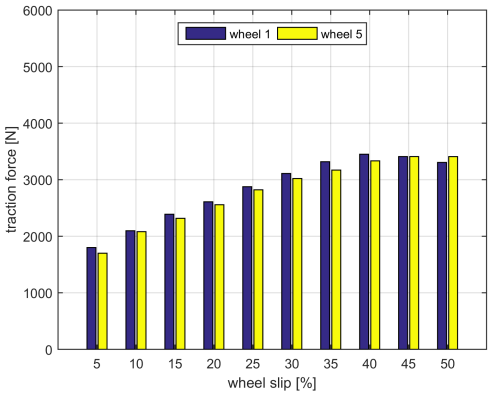

(a) *traction for wheels with 1234 mm diameter-straight lugs*

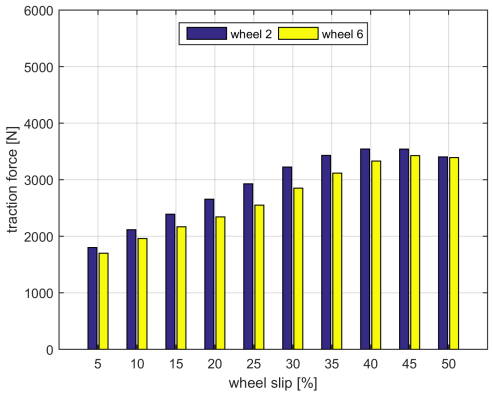

(b) *traction for wheels with 1234 mm diameter-combined lugs*

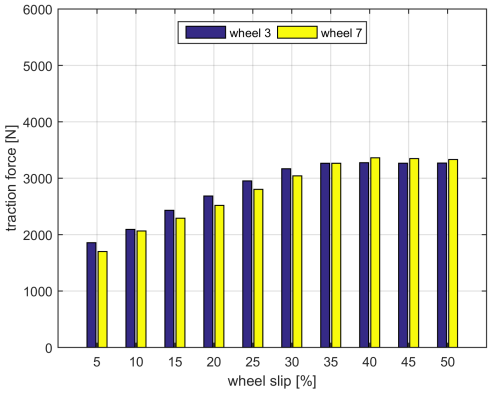

(c) *traction for wheels with 1413 mm diameter-combined lugs*

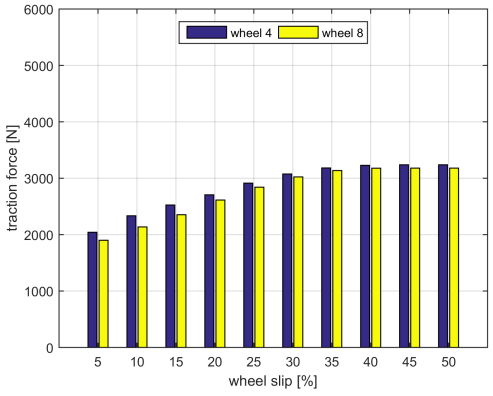

(d) *traction for wheels with 1644 mm diameter-combined lugs*

Figure 5.23: *traction force as a function of wheel slip*

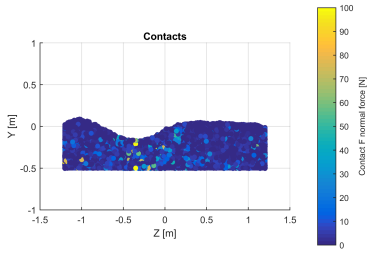

(a) *contact profile at* 5% *wheel slip-wheel* 1

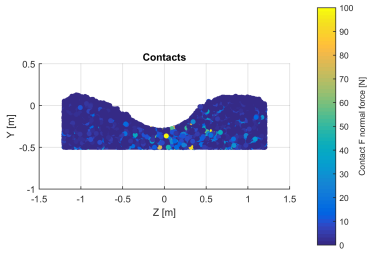

(b) *contact profile at* 50% *wheel slip-wheel* 1

Figure 5.24: *contact profile at* 5% *and* 50% *wheel slip for wheel* 1

Slip Sinkage

	slip [%]										
wheel	5	10	15	20	25	30	35	40	45	50	
1	0.50	1.33	2.12	2.80	4.24	6.22	8.04	11.26	14.41	17.05	slip
5	0.25	0.53	1.30	2.02	3.04	4.94	6.58	8.16	10.77	13.32	sinkage$[cm]$

(a) *slip sinkage wheels with 1234 mm diameter-straight lugs*

	slip [%]										
wheel	5	10	15	20	25	30	35	40	45	50	
2	0.25	1.27	2.03	2.69	4.03	6.51	8.05	10.90	13.30	17.09	slip
6	0.15	0.92	1.63	2.21	3.07	4.88	7.16	9.21	12.14	14.60	sinkage$[cm]$

(b) *slip sinkage wheels with 1234 mm diameter-combined lugs*

	slip [%]										
wheel	5	10	15	20	25	30	35	40	45	50	
3	0.28	1.29	2.08	3.19	5.00	6.49	8.76	10.23	12.39	14.71	slip
7	0.20	1.41	2.08	2.80	4.12	6.14	7.80	10.72	12.81	14.71	sinkage$[cm]$

(c) *slip sinkage wheels with 1413 mm diameter-combined lugs*

	slip [%]										
wheel	5	10	15	20	25	30	35	40	45	50	
4	1.05	2.36	3.10	4.06	5.56	6.99	8.87	10.44	11.50	11.50	slip
8	0.80	1.72	2.54	3.71	5.25	6.65	8.44	9.88	11.27	11.27	sinkage$[cm]$

(d) *slip sinkage wheels with 1644 mm diameter-combined lugs*

Table 5.8: *slip sinkage as a function of wheel slip*

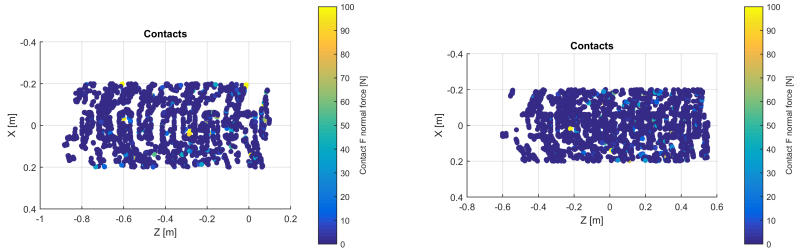

(a) *contact patch at* 5% *wheel slip-wheel* 2 **(b)** *contact patch at* 50% *wheel slip-wheel* 2

Figure 5.25: *contact patch at* 5% *and* 50% *wheel slip for wheel* 2

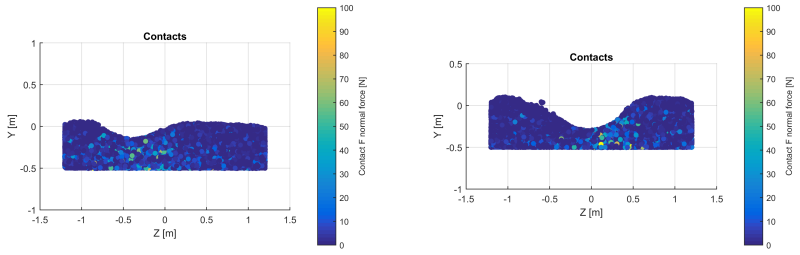

(a) *contact profile at* 5% *wheel slip-wheel* 2 **(b)** *contact profile at* 50% *wheel slip-wheel* 2

Figure 5.26: *contact profile at* 5% *and* 50% *wheel slip for wheel* 2

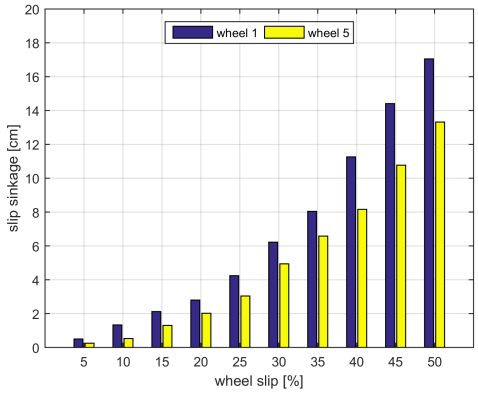

(a) *sinkage for wheels with 1234 mm diameter-straight lugs*

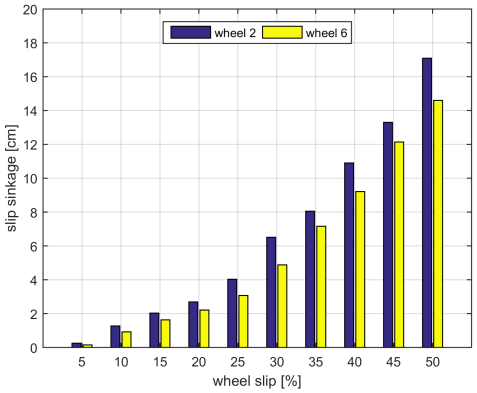

(b) *sinkage for wheels with 1234 mm diameter-combined lugs*

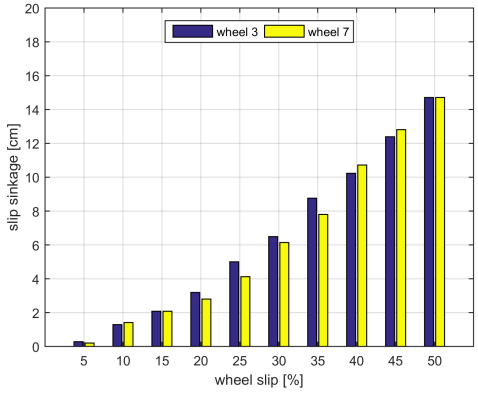

(c) *sinkage for wheels with 1413 mm diameter-combined lugs*

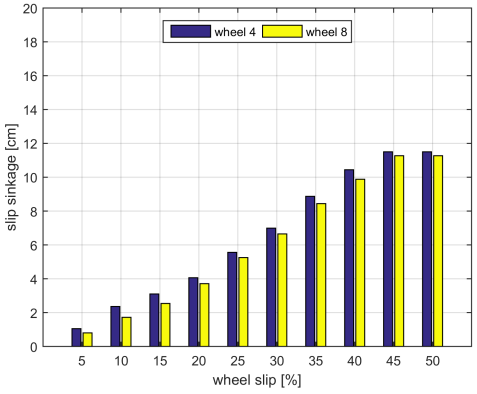

(d) *sinkage for wheels with 1644 mm diameter-combined lugs*

Figure 5.27: *slip sinkage as a function of wheel slip*

Slip Velocity

	slip [%]										
wheel	5	10	15	20	25	30	35	40	45	50	
1	0.025	0.041	0.054	0.066	0.074	0.079	0.085	0.084	0.079	0.077	slip
5	0.025	0.042	0.057	0.069	0.078	0.085	0.090	0.096	0.097	0.095	velocity$[m/s]$

(a) *slip velocity wheels with 1234 mm diameter-straight lugs*

	slip [%]										
wheel	5	10	15	20	25	30	35	40	45	50	
2	0.027	0.039	0.054	0.064	0.073	0.075	0.082	0.080	0.080	0.080	slip
6	0.027	0.041	0.059	0.073	0.084	0.091	0.091	0.096	0.093	0.093	velocity$[m/s]$

(b) *slip velocity wheels with 1234 mm diameter-combined lugs*

	slip [%]										
wheel	5	10	15	20	25	30	35	40	45	50	
3	0.025	0.044	0.055	0.064	0.068	0.074	0.074	0.077	0.074	0.070	slip
7	0.026	0.044	0.059	0.070	0.076	0.078	0.083	0.080	0.079	0.076	velocity$[m/s]$

(c) *slip velocity wheels with 1413 mm diameter*

	slip [%]										
wheel	5	10	15	20	25	30	35	40	45	50	
4	0.023	0.040	0.052	0.060	0.067	0.070	0.066	0.063	0.062	0.062	slip
8	0.025	0.043	0.057	0.064	0.069	0.072	0.070	0.068	0.067	0.066	velocity$[m/s]$

(d) *slip velocity wheels with 1644 mm diameter*

Table 5.9: *slip velocity as a function of wheel slip*

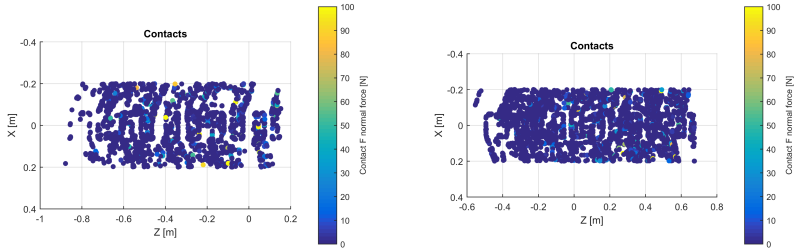

(a) *contact patch at* 5% *wheel slip-wheel* 3 **(b)** *contact patch at* 50% *wheel slip-wheel* 3

Figure 5.28: *contact patch at* 5% *and* 50% *wheel slip for wheel* 3

From the simulation results of traction force figures 5.23a and 5.23b for straight and combined lugs wheels, it was noted that traction force trend is similar for straight and combined lugs, although for combined lugs difference in traction between $25°$ and $45°$ lugs angle is high as compared to straight lugs. $25°$ lugs angle gives high traction force as compared to $45°$ lugs angle. This is because large angle creates more lateral force component than small angle, and this is advantageous for agricultural machines for required lateral holding force to keep the machine on straight contour [71].

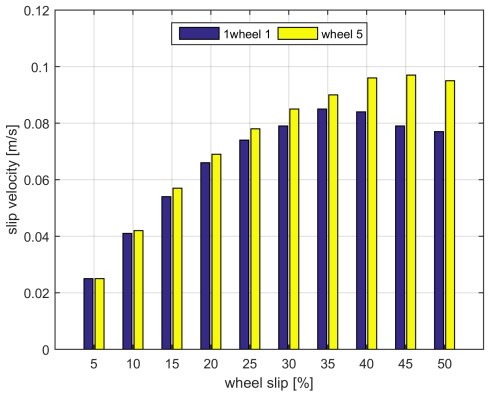

(a) *slip velocity for wheels with 1234 mm diameter-straight lugs*

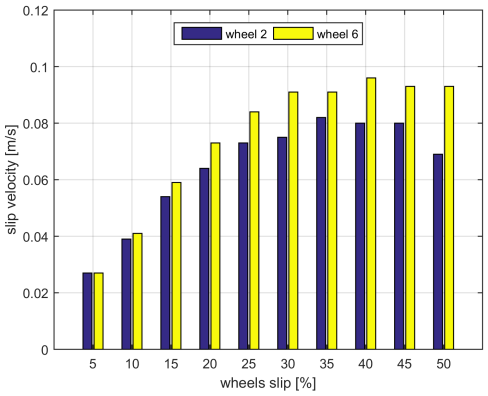

(b) *slip velocity for wheels with 1234 mm diameter-combined lugs*

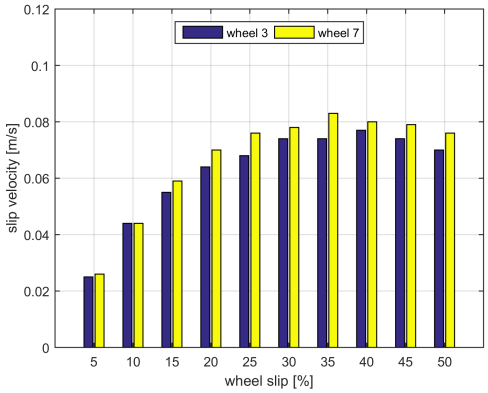

(c) *slip velocity for wheels with 1413 mm diameter-combined lugs*

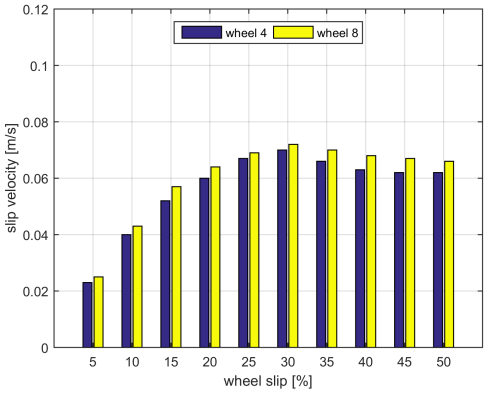

(d) *slip velocity for wheels with 1644 mm diameter-combined lugs*

Figure 5.29: *slip sinkage as a function of wheel slip*

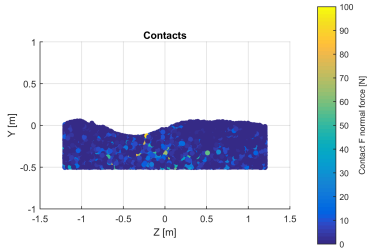

(a) *contact profile at* 5% *wheel slip-wheel* 3

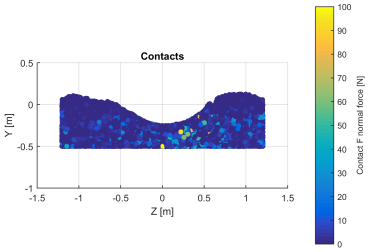

(b) *contact profile at* 50% *wheel slip-wheel* 3

Figure 5.30: *contact profile at* 5% *and* 50% *wheel slip for wheel* 3

Moving to large diameter wheels figures 5.23c and 5.23d trend of traction force within selected slip values is similar and the difference in traction force for $25°$ and $45°$ lugs angle is very small especially above 30% wheel slip. This means that for loose sand terrain lugs angle effects is significant for operation below 30% wheel slip, while above 30% wheel slip effects of lugs angle between $25°$ and $45°$ on traction can be neglected.

Forward Velocity

	slip [%]										
wheel	5	10	15	20	25	30	35	40	45	50	
1	0.43	0.37	0.33	0.29	0.25	0.21	0.16	0.13	0.10	0.08	forward
5	0.43	0.37	0.33	0.29	0.25	0.21	0.18	0.15	0.12	0.10	velocity$[m/s]$

(a) *forward velocity wheels with 1234 mm diameter-straight lugs*

	slip [%]										
wheel	5	10	15	20	25	30	35	40	45	50	
2	0.43	0.37	0.32	0.28	0.24	0.19	0.16	0.12	0.10	0.07	forward
6	0.43	0.39	0.34	0.31	0.28	0.23	0.19	0.15	0.12	0.09	velocity$[m/s]$

(b) *forward velocity wheels with 1234 mm diameter-combined lugs*

	slip [%]										
wheel	5	10	15	20	25	30	35	40	45	50	
3	0.46	0.42	0.34	0.29	0.23	0.18	0.14	0.12	0.09	0.07	forward
7	0.47	0.42	0.35	0.31	0.25	0.21	0.16	0.12	0.10	0.08	velocity$[m/s]$

(c) *forward velocity wheels with 1413 mm diameter-combined lugs*

	slip [%]										
wheel	5	10	15	20	25	30	35	40	45	50	
4	0.45	0.38	0.33	0.27	0.22	0.17	0.13	0.10	0.08	0.07	forward
8	0.47	0.41	0.35	0.29	0.23	0.18	0.13	0.11	0.08	0.08	velocity$[m/s]$

(d) *forward velocity wheels with 1644 mm diameter-combined lugs*

Table 5.10: *forward velocity as a function of wheel slip*

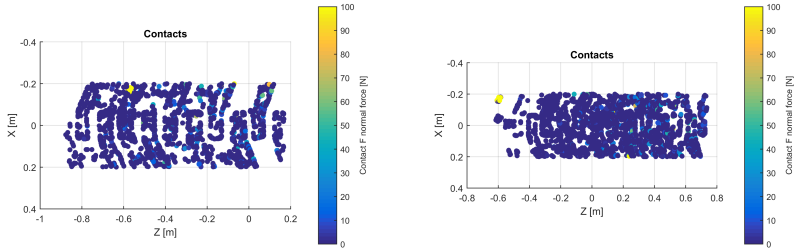

(a) *contact patch at* 5% *wheel slip-wheel* 4 **(b)** *contact patch at* 50% *wheel slip-wheel* 4

Figure 5.31: *contact patch at* 5% *and* 50% *wheel slip for wheel* 4

Taking into account slip sinkage results on figures 5.27a and 5.27b for wheels with small diameters, it was noted that for loose sand these wheels cause a continuous sinkage especially at high slip above 30%, and the effect is high for $25°$ lugs angle. This means that for loose sand terrain under the load of $13.2kN$ using these as driving wheels especially at high slip it may cause wheel to stack in the sand. This situation is one of major problem for traversing and performance of highly deformable terrain such as loose sand [110].

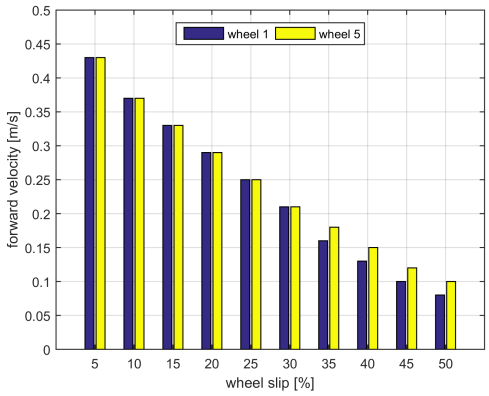

(a) *forward velocity for wheels with 1234 mm diameter-straight lugs*

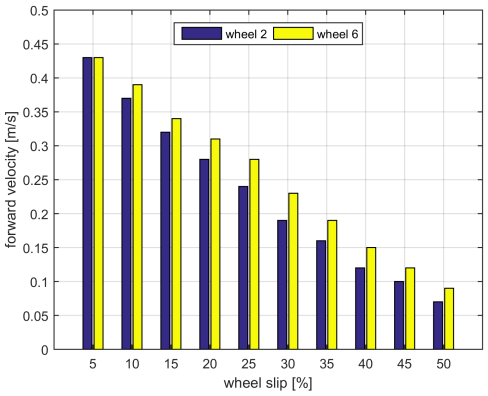

(b) *forward velocity for wheels with 1234 mm diameter-combined lugs*

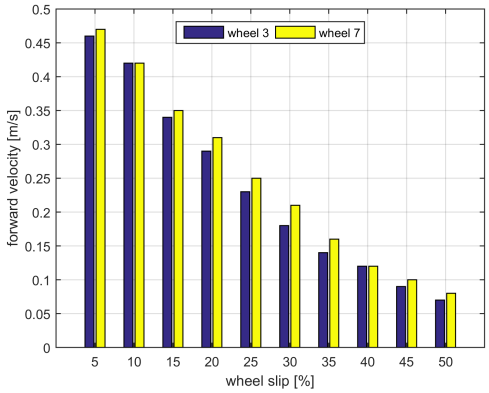

(c) *forward velocity for wheels with 1413 mm diameter-combined lugs*

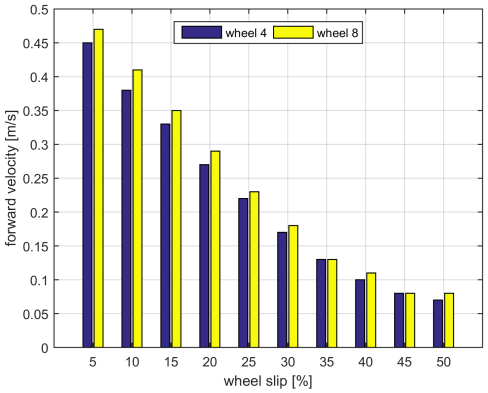

(d) *forward velocity for wheels with 1644 mm diameter-combined lugs*

Figure 5.32: *froward velocity as a function of wheel slip*

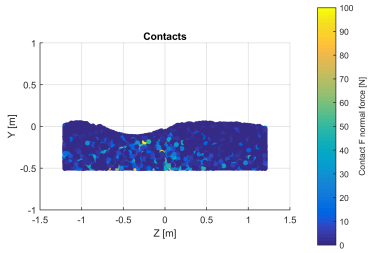

(a) *contact profile at* 5% *wheel slip-wheel* 4

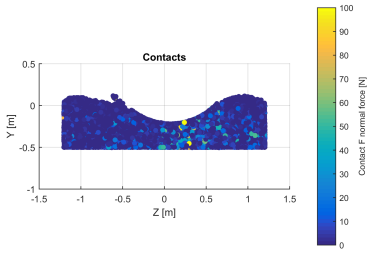

(b) *contact profile at* 50% *wheel slip-wheel* 4

Figure 5.33: *contact profile at* 5% *and* 50% *wheel slip for wheel* 4

Increasing diameter of wheels reduce this effect, and this was noted on results of figure 5.27c and 5.27d, and wheels with $1644mm$ diameter gives better results by limiting sinkage below $12cm$. Effect of lugs angle is small especially at high slip values above 30% wheel slip. This means that for operation such as ploughing which is within 25%

wheel slip wheels 4 , 7 and 8 can be used, but if slip increases above 30% then wheel 4 and 8 is better since it limiting sinkage of below $12cm$ at high wheel slip.

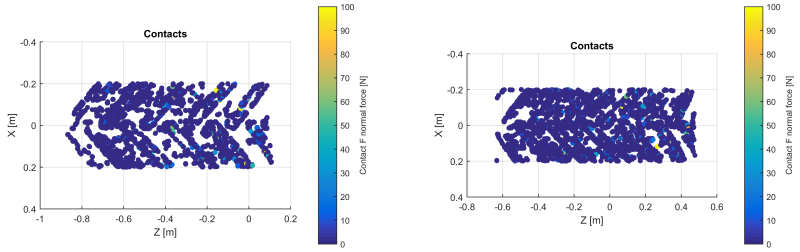

(a) *contact patch at* 5% *wheel slip-wheel* 5 **(b)** *contact patch at* 50% *wheel slip-wheel* 5

Figure 5.34: *contact patch at* 5% *and* 50% *wheel slip for wheel* 5

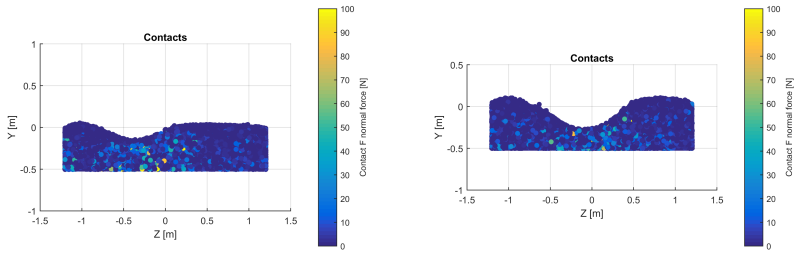

(a) *contact profile at* 5% *wheel slip-wheel* 5 **(b)** *contact profile at* 50% *wheel slip-wheel* 5

Figure 5.35: *contact profile at* 5% *and* 50% *wheel slip for wheel* 5

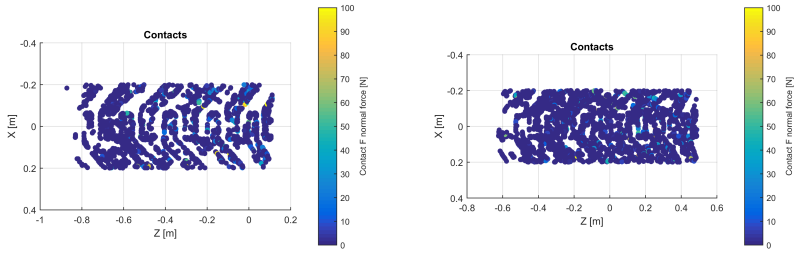

(a) *contact patch at* 5% *wheel slip-wheel* 6 **(b)** *contact patch at* 50% *wheel slip-wheel* 6

Figure 5.36: *contact patch at* 5% *and* 50% *wheel slip for wheel* 6

Taking into account slip velocity results in figure 5.29, it was noted that trend of slip velocity for wheels with straight and combined lugs is similar figures 5.29a and 5.29b. Slip velocity values for wheels with $45°$ lugs angle is almost the same which is approximately $0.1m/s$ at high slip above 30% while for wheel with $25°$ lugs angle is approximately $0.08m/s$ at high slip.

Increasing wheel diameter figures 5.29c and 5.29d, reduces slip velocity. The value is approximately $0.08m/s$ for wheels with $1413mm$ diameter and is even lower below

$0.08m/s$ for wheels with $1644mm$ diameter. This is because slip velocity is a function of slip and entry angle, and these parameters increases with increase of slip sinkage [106], which noted with $1234mm$ and 1413 diameters wheels. This means that large wheels such as $1644mm$ diameter perform better on loose sand terrain under $13.2kN$ wheel load bu guaranteeing low slip velocity.

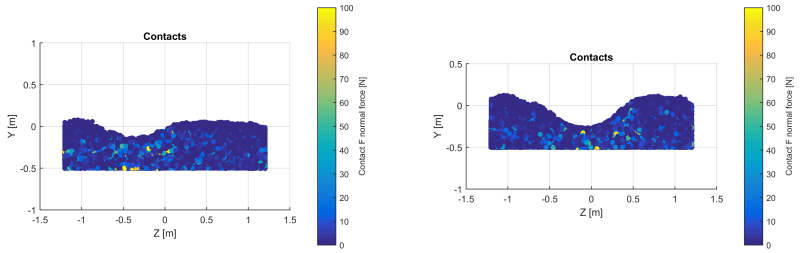

(a) *contact profile at* 5% *wheel slip-wheel* 6 **(b)** *contact profile at* 50% *wheel slip-wheel* 6

Figure 5.37: *contact profile at* 5% *and* 50% *wheel slip for wheel* 6

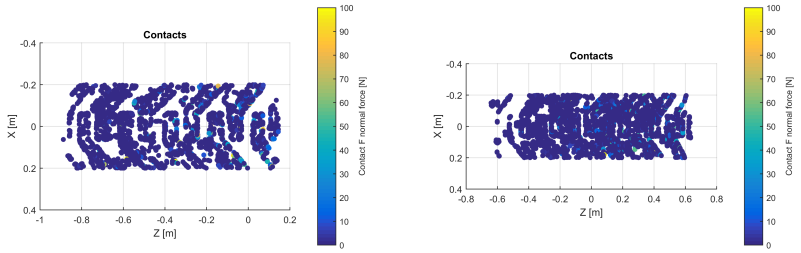

(a) *contact patch at* 5% *wheel slip-wheel* 7 **(b)** *contact patch at* 50% *wheel slip-wheel* 7

Figure 5.38: *contact patch at* 5% *and* 50% *wheel slip for wheel* 7

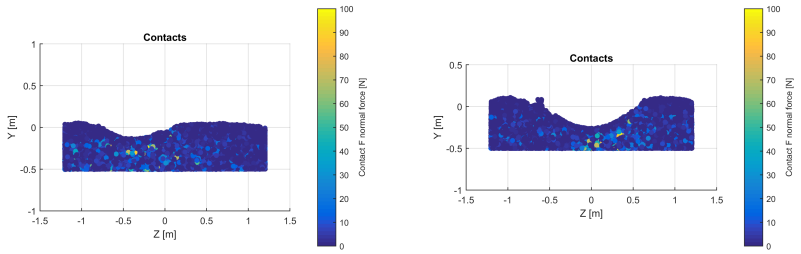

(a) *contact profile at* 5% *wheel slip-wheel* 7 **(b)** *contact profile at* 50% *wheel slip-wheel* 7

Figure 5.39: *contact profile at* 5% *and* 50% *wheel slip for wheel* 7

Also large wheels they have large contact area which supports more load for a given soil bearing capacity and limit maximum normal and shear stresses and avoid continuous failure of the terrain sand [110]. This means that for driving wheels on loose

sand terrain, large diameter wheels for large wheel load gives better traversing even if operated at high wheel slip up to 50%.

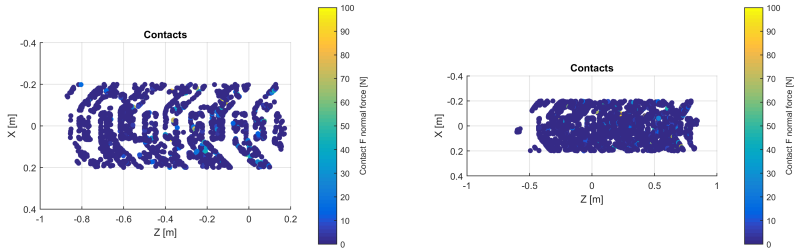

(a) *contact patch at* 5% *wheel slip-wheel* 8 **(b)** *contact patch at* 50% *wheel slip-wheel* 8

Figure 5.40: *contact patch at* 5% *and* 50% *wheel slip for wheel* 8

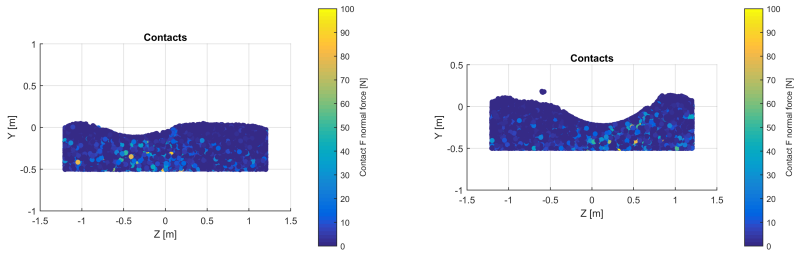

(a) *contact profile at* 5% *wheel slip-wheel* 8 **(b)** *contact profile at* 50% *wheel slip-wheel* 8

Figure 5.41: *contact profile at* 5% *and* 50% *wheel slip for wheel* 8

Taking into account forward velocity of wheels results on figure 5.32, it was noted that trend of velocity is almost similar although there are differences in velocities which increases especially at high slip between $25°$ and $45°$ lugs angle wheels. This is because forward velocity is a residue from the difference of circumferential and slip velocities in which the later increases with increase of sinkage [106], this is noted for wheels with $25°$ than with $45°$ lugs angles.

Taking into account contact patch of the wheel results in figures 5.22, 5.25, 5.28, 5.31, 5.34, 5.36, 5.38 and 5.40 it was noted that contact length become longer at high slip 50% as compared to low slip 5%. This means that at high slip wheel sinkage is high due to increase of slip sinkage of wheel at high slip. Also lugs traces interacts at high slip, which indicates that at high slip soil particles disturbed more and this cause increase of slip sinkage.

Considering contact profile figures 5.24, 5.26, 5.30, 5.33, 5.35, 5.37, 5.39 and 5.41 it was noted that profile is deeper at high slip 50% than at low slip 5%, this shows that at high slip more soil at contact is taken by the lugs when rotates and cause increase of slip sinkage as well as entry angle. Also particles in between bottom line at deepest sinkage and point of entry experience more normal contact force as shown by the color bar. This means that point of maximum stresses is in between these point [106].

From the results analysis made above, it can be concluded that, for loose sand terrain

and high wheel load such as $13.2kN$ wheel 4 and 8 with parameters indicated in table 5.1 perform better by guarantees reasonable traction force, low slip sinkage, low slip velocity which are major interaction parameters to be considered for traversing and performance assessment for highly deformable terrain.

5.1.3 Upland sand terrain

In this section simulations are carried out by interacting wheel 1 to 16 table 5.1 with upland sand terrain, which has mixed particles with properties as shown in table 5.2. Simulation parameters such as angular velocity and number of particles were as in section 5.1.1. Simulation results for traction force, slip sinkage, slip velocity and forward velocity are tabulated in tables 5.11, 5.12, 5.13 and 5.14 and presented graphically in figures 5.43, 5.47, 5.49 and 5.52 respectively.

Traction Force

	slip [%]										
wheel	5	10	15	20	25	30	35	40	45	50	
1	2508	2812	2968	3178	3347	3471	3560	3508	3351	3351	traction
5	2477	2643	2812	2959	3121	3251	3358	3436	3440	3379	force[N]

(a) *traction force wheels with 1234 mm diameter-straight lugs*

	slip [%]										
wheel	5	10	15	20	25	30	35	40	45	50	
2	2675	2905	3093	3235	3391	3473	3501	3408	3240	3217	traction
6	2597	2905	3093	3235	3363	3473	3536	3521	3435	3351	force[N]

(b) *traction force wheels with 1234 mm diameter-combined lugs*

	slip [%]										
wheel	5	10	15	20	25	30	35	40	45	50	
3	2303	2503	2755	2979	3164	3243	3274	3268	3239	3207	traction
7	2189	476	2476	2839	2985	3117	3212	3368	3264	3243	force[N]

(c) *traction force wheels with 1420 mm diameter*

	slip [%]										
wheel	5	10	15	20	25	30	35	40	45	50	
4	2459	2632	2801	2947	3055	3111	3148	3156	3140	3116	traction
8	2433	2669	2801	2947	3055	3111	3148	3156	3151	3144	force[N]

(d) *traction force wheels with 1644 mm diameter-combined lugs*

Table 5.11: *traction force as a function of wheel slip*

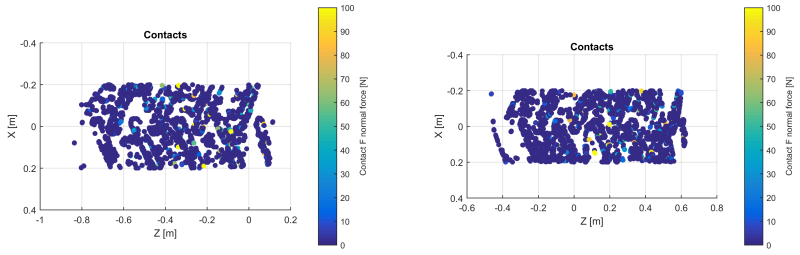

(a) *contact patch at* 5% *wheel slip-wheel* 1 **(b)** *contact patch at* 50% *wheel slip-wheel* 1

Figure 5.42: *contact patch at* 5% *and* 50% *wheel slip for wheel* 1

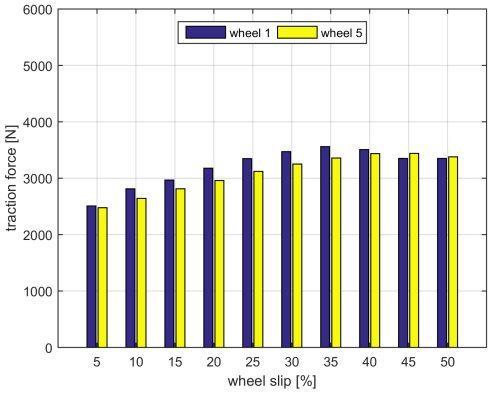

(a) *traction for wheels with 1234 mm diameter-straight lugs*

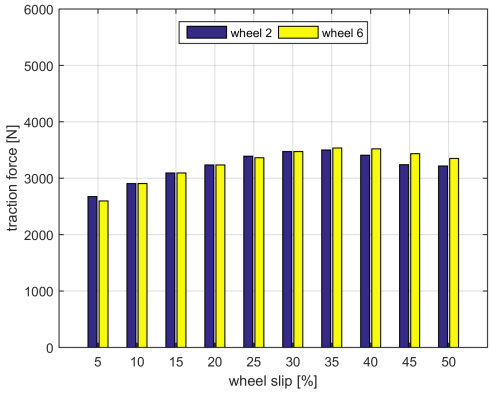

(b) *traction for wheels with 1234 mm diameter-combined lugs*

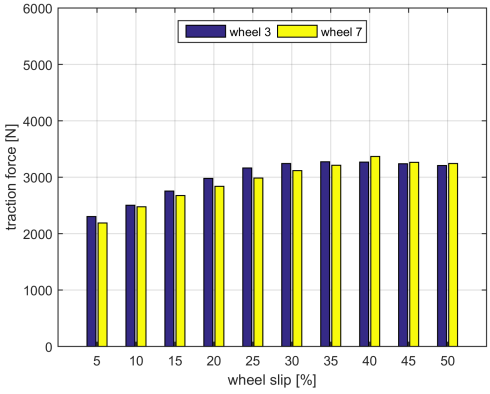

(c) *traction for wheels with 1413 mm diameter-combined lugs*

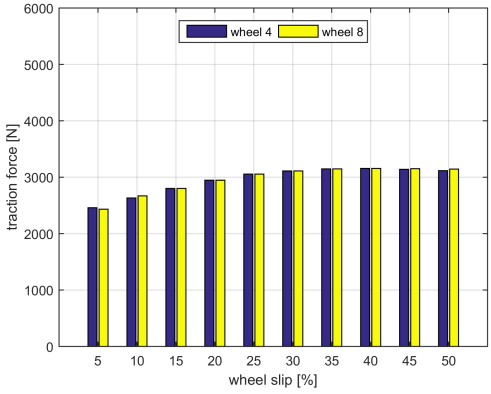

(d) *traction for wheels with 1644 mm diameter-combined lugs*

Figure 5.43: *traction force as a function of wheel slip*

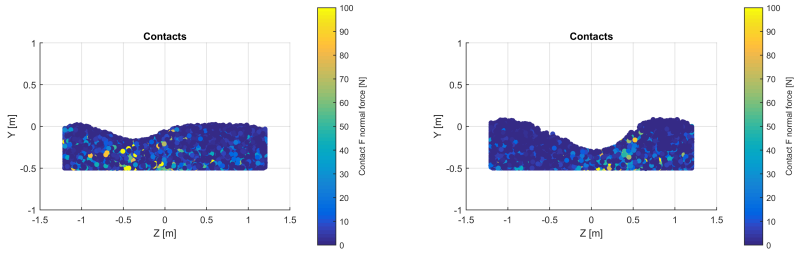

(a) *contact profile at* 5% *wheel slip-wheel* 1 **(b)** *contact profile at* 50% *wheel slip-wheel* 1

Figure 5.44: *contact profile at* 5% *and* 50% *wheel slip for wheel* 1

From the results of traction force figure 5.43 it was noted that trend of traction force is almost similar for all wheels. For wheel 1 and wheel 5 figure 5.43a, traction force is high for wheel 1 in the range of 5% and 40% slip, above that slip the difference in traction force is small. This is because of different lugs angles between wheel 1 and 5. Increase of lugs angle reduces longitudinal effects of the lugs on traction force, but also increase lateral force by creating lateral component of traction force.

Slip Sinkage

	slip $[\%]$										
wheel	5	10	15	20	25	30	35	40	45	50	
1	0.32	0.82	1.56	3.25	4.58	6.15	8.54	10.81	14.49	14.49	slip
5	0.32	0.68	1.32	2.23	3.60	4.98	6.31	8.22	10.29	12.12	sinkage$[cm]$

(a) *slip sinkage wheels with 1234 mm diameter-straight lugs*

	slip $[\%]$										
wheel	5	10	15	20	25	30	35	40	45	50	
2	0.61	1.36	2.32	3.55	4.97	6.65	8.54	11.22	13.81	13.81	slip
6	0.61	1.36	2.32	3.35	4.45	5.58	7.60	9.48	11.98	13.60	sinkage$[cm]$

(b) *slip sinkage wheels with 1234 mm diameter-combined lugs*

	slip $[\%]$										
wheel	5	10	15	20	25	30	35	40	45	50	
3	0.74	1.45	2.76	4.41	6.06	7.72	9.35	10.72	12.59	13.24	slip
7	0.40	1.23	1.94	3.12	4.44	5.68	7.34	9.00	10.78	12.03	sinkage$[cm]$

(c) *slip sinkage wheels with 1413 mm diameter-combined lugs*

	slip $[\%]$										
wheel	5	10	15	20	25	30	35	40	45	50	
4	1.09	1.90	2.90	3.78	4.86	6.09	7.01	8.22	9.25	10.59	slip
8	0.38	1.57	2.50	3.55	4.86	6.09	7.45	8.75	9.53	10.25	sinkage$[cm]$

(d) *slip sinkage wheels with 1644 mm diameter-combined lugs*

Table 5.12: *slip sinkage as a function of wheel slip*

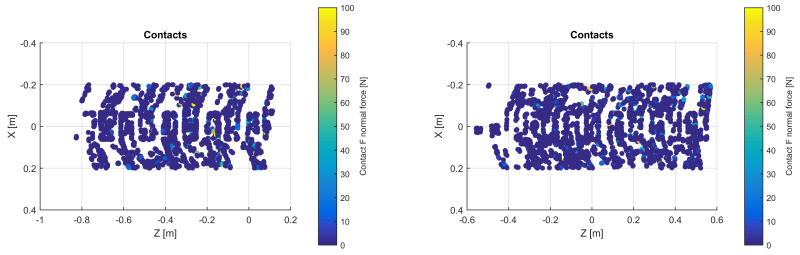

(a) *contact patch at* 5% *wheel slip-wheel* 2 **(b)** *contact patch at* 50% *wheel slip-wheel* 2

Figure 5.45: *contact patch at* 5% *and* 50% *wheel slip for wheel* 2

For combined lugs results of figure 5.43b it was noted that difference in traction force between wheel 2 and 6 is very small for slip below 30%, and the trend is similar for both wheels. This means that the effect of lugs angle for this terrain is small for combined lugs, and this results is similar also for wheels 3, 7, 4 and 8 figures 5.43c and 5.43d. Traction force is high for wheels 1-5, 2-6, 3-7 as compared to wheels 4-8, this is because of low slip sinkage for wheels 4-8 especially at high slip.

Taking into account slip sinkage results in figure 5.47, it was inferred that wheel 1 has high sinkage as compared to wheel 5 figure 5.47a. This is because of small lugs angle for wheel 1 as compared to wheel 5 as shown in table 5.1.

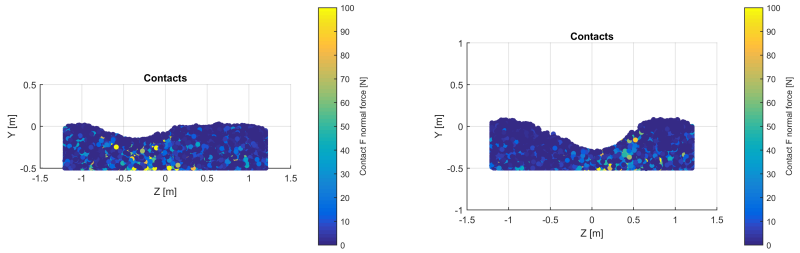

(a) *contact profile at* 5% *wheel slip-wheel* 2 **(b)** *contact profile at* 50% *wheel slip-wheel* 2

Figure 5.46: *contact profile at* 5% *and* 50% *wheel slip for wheel* 2

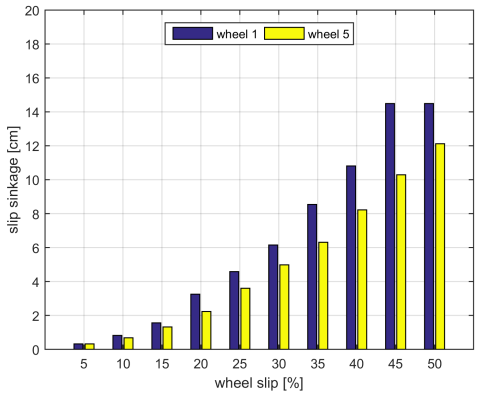

(a) *sinkage for wheels with 1234 mm diameter-straight lugs*

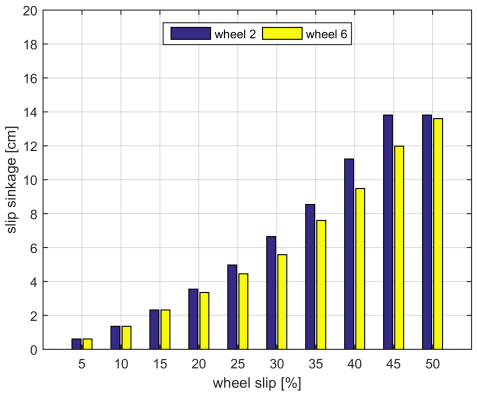

(b) *sinkage for wheels with 1234 mm diameter-combined lugs*

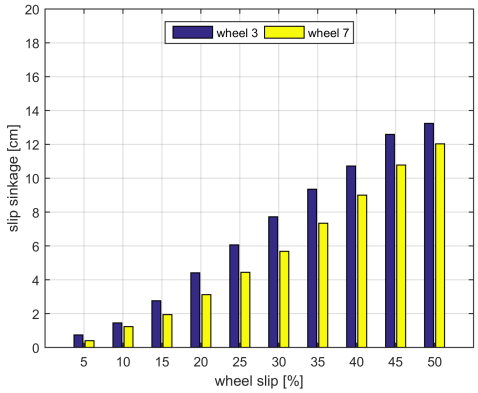

(c) *sinkage for wheels with 1413 mm diameter-combined*

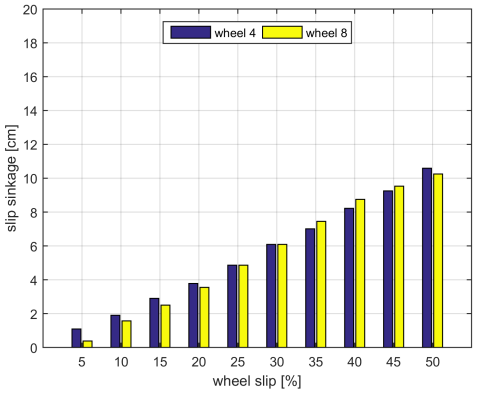

(d) *sinkage for wheels with 1644 mm diameter-combined lugs*

Figure 5.47: *slip sinkage as a function of wheel slip*

Results of slip sinkage between straight and combined lugs figures 5.47a and 5.47b shows that straight lugs has high sinkage that combined lugs especially at high slip, and this might be caused advantage of combination of staright $0°$ and straight $25°$ or $45°$ which reduce slidding of soil particles at contact when rotate with wheel during interaction.

Slip Velocity

	slip [%]										
wheel	5	10	15	20	25	30	35	40	45	50	
1	0.018	0.032	0.045	0.053	0.061	0.067	0.067	0.068	0.062	0.062	slip
5	0.018	0.035	0.048	0.060	0.067	0.075	0.083	0.085	0.088	0.091	velocity$[m/s]$

(a) *slip velocity wheels with 1234 mm diameter-straight lugs*

	slip [%]										
wheel	5	10	15	20	25	30	35	40	45	50	
2	0.017	0.030	0.042	0.051	0.059	0.066	0.069	0.070	0.071	0.075	slip
6	0.018	0.031	0.042	0.051	0.059	0.068	0.073	0.077	0.077	0.079	velocity$[m/s]$

(b) *slip velocity wheels with 1234 mm diameter-combined lugs*

	slip [%]										
wheel	5	10	15	20	25	30	35	40	45	50	
3	0.020	0.036	0.046	0.054	0.059	0.062	0.063	0.065	0.062	0.064	slip
7	0.021	0.037	0.049	0.059	0.067	0.076	0.078	0.080	0.080	0.080	velocity$[m/s]$

(c) *slip velocity wheels with 1413 mm diameter-combined lugs*

	slip [%]										
wheel	5	10	15	20	25	30	35	40	45	50	
4	0.018	0.032	0.042	0.051	0.056	0.060	0.062	0.063	0.063	0.061	slip
8	0.020	0.032	0.042	0.052	0.059	0.064	0.065	0.065	0.067	0.068	velocity$[m/s]$

(d) *slip velocity wheels with 1644 mm diameter-combined lugs*

Table 5.13: *slip velocity as a function of wheel slip*

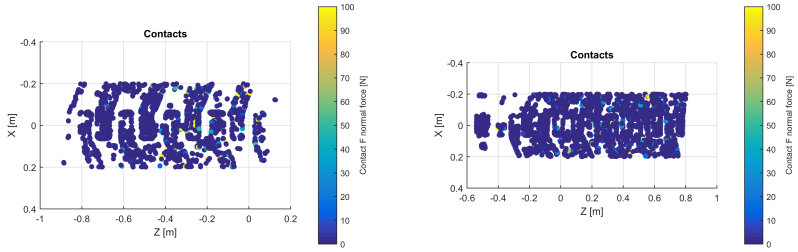

(a) *contact patch at* 5% *wheel slip-wheel* 3 **(b)** *contact patch at* 50% *wheel slip-wheel* 3

Figure 5.48: *contact patch at* 5% *and* 50% *wheel slip for wheel* 3

Increase of wheel diameter reduces slip sinkage results in figure 5.47c and 5.47d and difference in sinkage between $25°$ and $45°$ lugs angle is very small for large wheels. This is because of increase of contact length with increase of wheel diameter which reduce deformation rate of the soil and support more load at contact.

Trend of slip velocity for all wheel is ismilar although large lugs angle $45°$ has high slip velocity as compared to small lugs angle$25°$. This is due to effects of lugs angle on lateral flow of terrain particles during interaction. Slip velocity decrease with increase of wheel diameter, this was noted in figure 5.49, this is because slip velocity is a

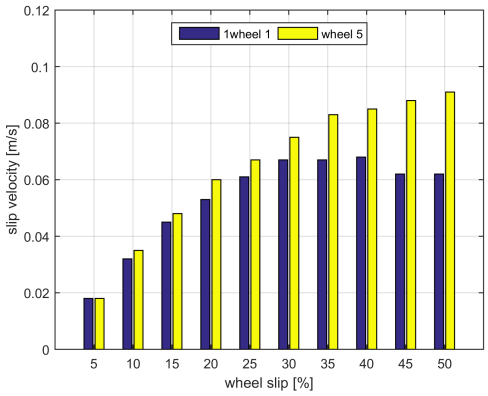

(a) *slip velocity for wheels with 1234 mm diameter-straight lugs*

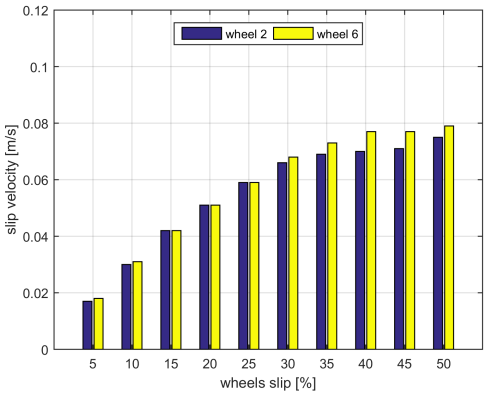

(b) *slip velocity for wheels with 1234 mm diameter-combined lugs*

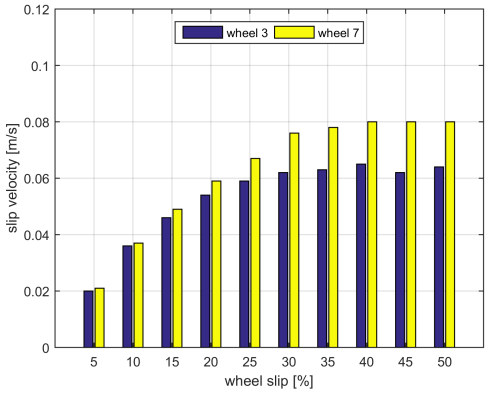

(c) *slip velocity for wheels with 1413 mm diameter-combined lugs*

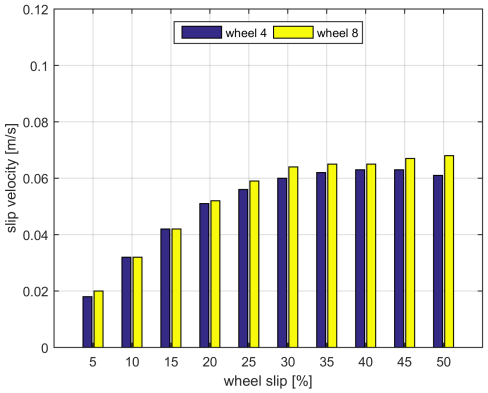

(d) *slip velocity for wheels with 1644 mm diameter-combined lugs*

Figure 5.49: *slip velocity as a function of wheel slip*

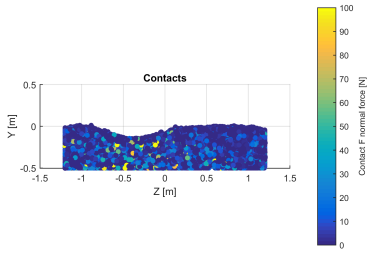

(a) *contact profile at* 5% *wheel slip-wheel* 3

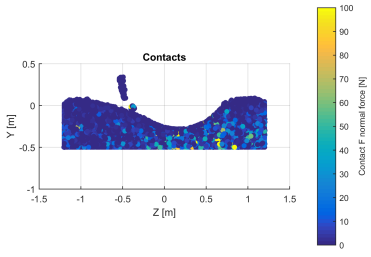

(b) *contact profile at* 50% *wheel slip-wheel* 3

Figure 5.50: *contact profile at* 5% *and* 50% *wheel slip for wheel* 3

function of slip and entry angle and entry angle increases with increase of diameter for the same sinkage and this increases contact length.

Forward velocity of wheels results in figure 5.52, it was noted that trend is similar for all wheels although there some difference in velocity between wheels with $25°$ and $45°$ lugs angles, but this difference is small. This is because of forward velocity depends

on sinkage and slip velocity, and which is difference between for wheels with large and small lugs angle.

Taking into account contact patch of the wheels results in figures 5.42, 5.45, 5.48, 5.51, 5.54, 5.56, 5.58 and 5.60, it was noted that contact patch is clear and short at 5% and unclear and long at 50%, this shows that soil particles are disturbed more at high slip, and this makes lugs traces to interact when the lugs tends to develop high traction force.

Forward Velocity

	slip [%]										
wheel	5	10	15	20	25	30	35	40	45	50	
1	0.36	0.30	0.27	0.23	0.19	0.16	0.13	0.10	0.07	0.07	forward
5	0.36	0.32	0.29	0.25	0.22	0.19	0.16	0.13	0.11	0.09	velocity$[m/s]$

(a) *forward velocity wheels with 1234 mm diameter-straight lugs*

	slip [%]										
wheel	5	10	15	20	25	30	35	40	45	50	
2	0.34	0.29	0.26	0.23	0.19	0.16	0.13	0.11	0.09	0.09	forward
6	0.35	0.29	0.26	0.23	0.20	0.17	0.14	0.12	0.10	.09	velocity$[m/s]$

(b) *forward velocity wheels with 1234 mm diameter-combined lugs*

	slip [%]										
wheel	5	10	15	20	25	30	35	40	45	50	
3	0.39	0.35	0.29	0.23	0.18	0.15	0.12	0.10	0.08	0.07	forward
7	0.41	0.35	0.31	0.26	0.22	0.18	0.15	0.12	0.10	0.09	velocity$[m/s]$

(c) *forward velocity wheels with 1413 mm diameter-combined lugs*

	slip [%]										
wheel	5	10	15	20	25	30	35	40	45	50	
4	0.38	0.32	0.27	0.22	0.18	0.15	0.12	0.10	0.08	0.06	forward
8	0.38	0.32	0.27	0.23	0.18	0.15	0.12	0.10	0.08	0.07	velocity$[m/s]$

(d) *forward velocity wheels with 1613 mm diameter-combined lugs*

Table 5.14: *forward velocity as a function of wheel slip*

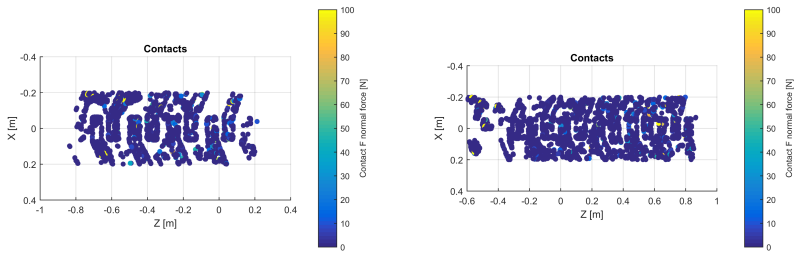

(a) *contact patch at* 5% *wheel slip-wheel* 4 **(b)** *contact patch at* 50% *wheel slip-wheel* 4

Figure 5.51: *contact patch at* 5% *and* 50% *wheel slip for wheel* 3

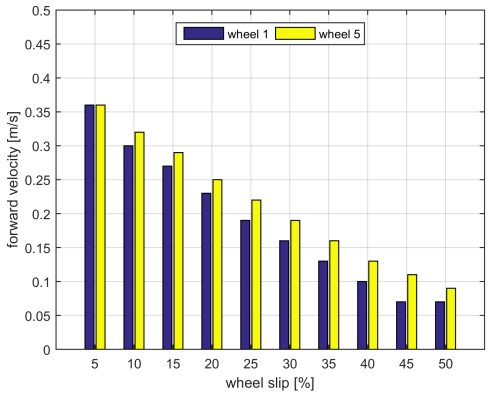

(a) *forward velocity for wheels with 1234 mm diameter-straight lugs*

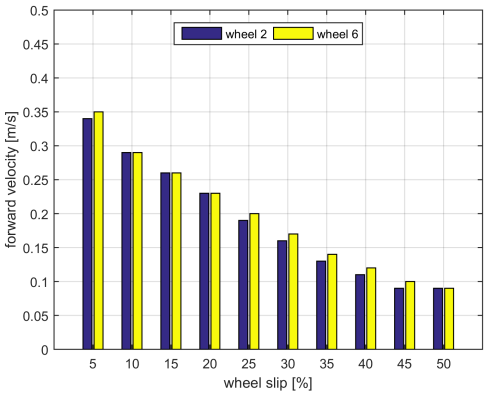

(b) *forward velocity for wheels with 1234 mm diameter-combined lugs*

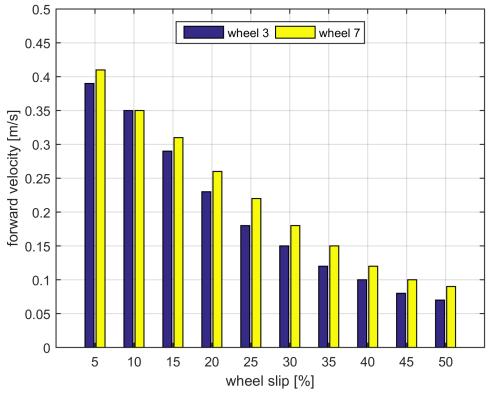

(c) *forward velocity for wheels with 1413 mm diameter-combined lugs*

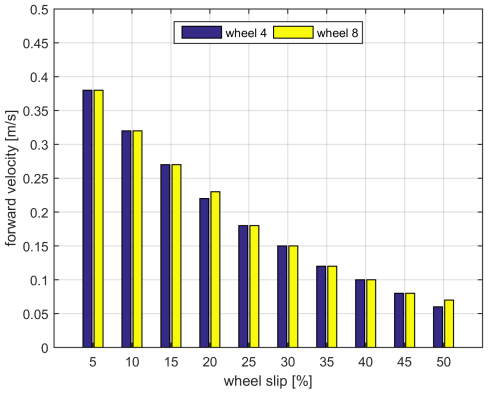

(d) *forward velocity for wheels with 1644 mm diameter-combined lugs*

Figure 5.52: *forward velocity as a function of wheel slip*

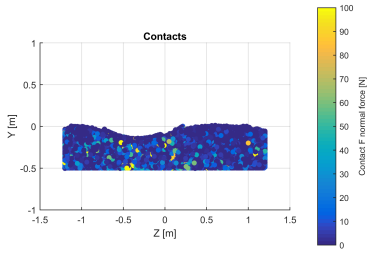

(a) *contact profile at* 5% *wheel slip-wheel* 4

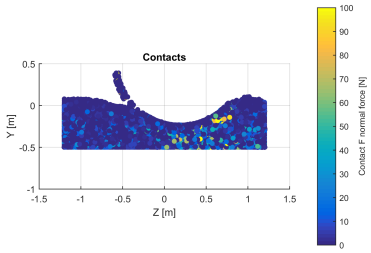

(b) *contact profile at* 50% *wheel slip-wheel* 4

Figure 5.53: *contact profile at* 5% *and* 50% *wheel slip for wheel* 4

Considering contact profile figures 5.44, 5.46, 5.50, 5.53, 5.55, 5.57, 5.59 and 5.61, it was noted that contact profile is deeper for small wheels $1234mm$ diameter as compared to large wheels $1644mm$ diameter at high slip, this is because of high slip sinkage. It can be noted that wheels tends to take some particles from the contact figure

5.50 and 5.53 when rotate and this shows clearly the effect of clean-up. Also particles build up in front of the wheel especially at high slip, which shows build-up effect in interaction for deformable terrain.

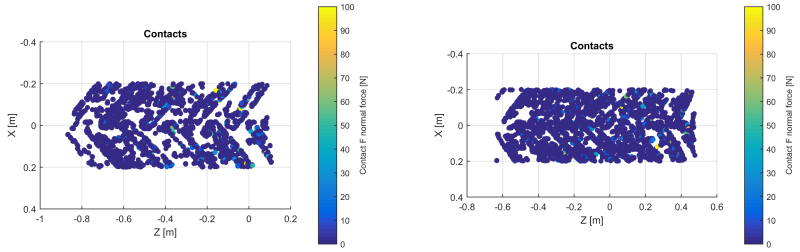

(a) *contact patch at* 5% *wheel slip-wheel* 5 **(b)** *contact patch at* 50% *wheel slip-wheel* 5

Figure 5.54: *contact patch at* 5% *and* 50% *wheel slip for wheel* 5

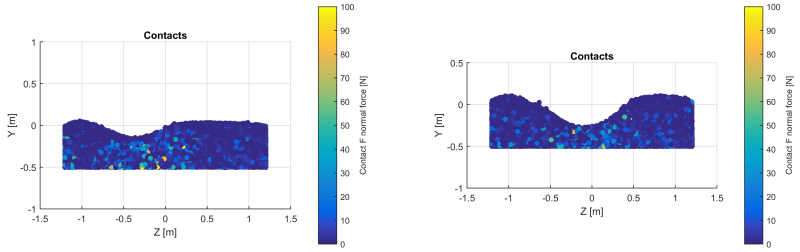

(a) *contact profile at* 5% *wheel slip-wheel* 5 **(b)** *contact profile at* 50% *wheel slip-wheel* 5

Figure 5.55: *contact profile at* 5% *and* 50% *wheel slip for wheel* 5

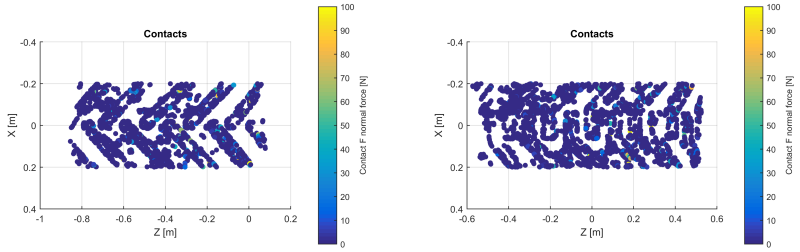

(a) *contact patch at* 5% *wheel slip-wheel* 6 **(b)** *contact patch at* 50% *wheel slip-wheel* 6

Figure 5.56: *contact patch at* 5% *and* 50% *wheel slip for wheel* 6

From the results analysis above it was conclude that wheels 3 , 4 , 5 , 6 , 7 and 8 have good performance in a given terrain, since they have high traction, low slip sinkage and slip velocity, although wheels with $25°$ has increase of slip sinkage especially at high slip of 50% but it reaches a constant value below $14cm$.

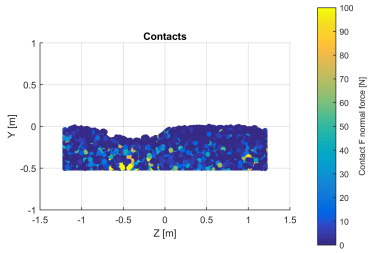

(a) *contact profile at* 5% *wheel slip-wheel* 6

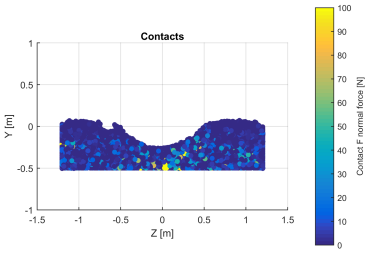

(b) *contact profile at* 50% *wheel slip-wheel* 6

Figure 5.57: *contact profile at* 5% *and* 50% *wheel slip for wheel* 6

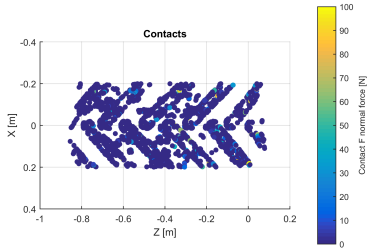

(a) *contact patch at* 5% *wheel slip-wheel* 7

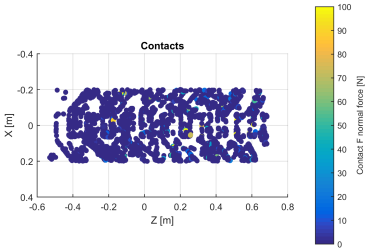

(b) *contact patch at* 50% *wheel slip-wheel* 7

Figure 5.58: *contact patch at* 5% *and* 50% *wheel slip for wheel* 7

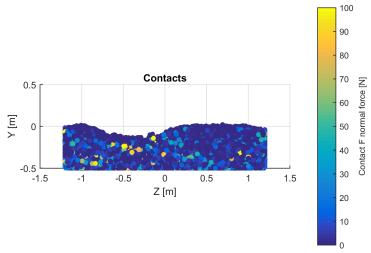

(a) *contact profile at* 5% *wheel slip-wheel* 7

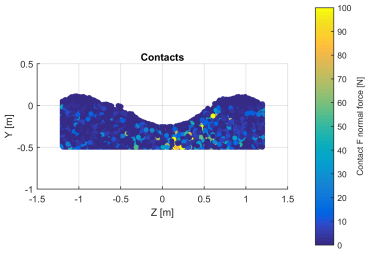

(b) *contact profile at* 50% *wheel slip-wheel* 7

Figure 5.59: *contact profile at* 5% *and* 50% *wheel slip for wheel* 7

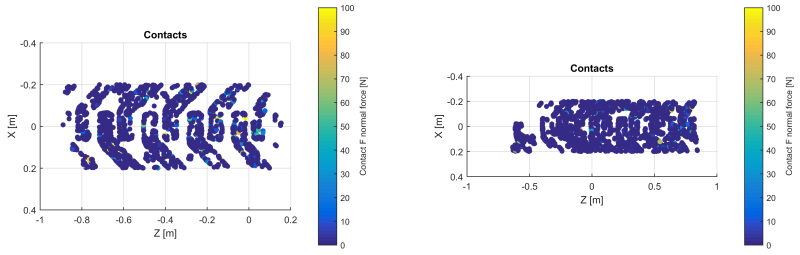

(a) *contact patch at* 5% *wheel slip-wheel* 8 **(b)** *contact patch at* 50% *wheel slip-wheel* 8

Figure 5.60: *contact patch at* 5% *and* 50% *wheel slip for wheel* 8

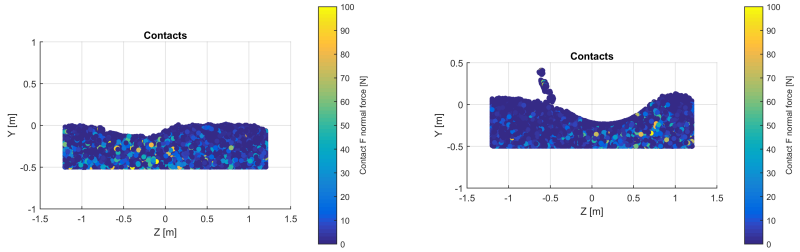

(a) *contact profile at* 5% *wheel slip-wheel* 8 **(b)** *contact profile at* 50% *wheel slip-wheel* 8

Figure 5.61: *contact profile at* 5% *and* 50% *wheel slip for wheel* 8

5.1.4 Clayey loam sand terrain

In this section simulations were carried out by interacting wheel 1 to 8 table 5.1 with clayey loam terrain, which has sphere, boxes and convex hulls particles with properties as shown in table 5.2. Simulation parameters such as angular velocity and number of particles were as in section 5.1.1. Simulation results for traction force, slip sinkage, slip velocity and forward velocity of the wheels were tabulated in tables 5.15 to 5.18 while figures 5.64 to 5.72 represents there results graphically.

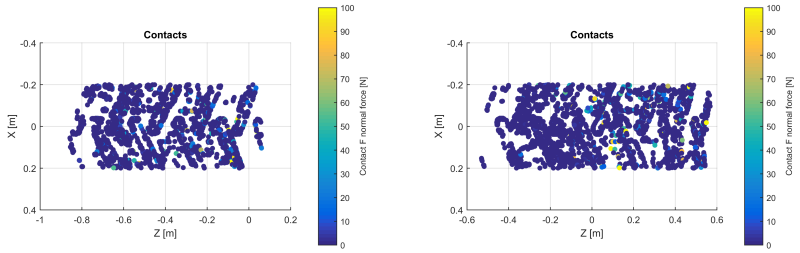

(a) *contact patch at* 5% *wheel slip-wheel* 1 **(b)** *contact patch at* 50% *wheel slip-wheel* 1

Figure 5.62: *contact patch at* 5% *and* 50% *wheel slip for wheel* 1

Traction Force

	slip [%]										
wheel	5	10	15	20	25	30	35	40	45	50	
1	2552	2780	2962	3177	3368	3513	3546	3511	3430	3298	traction
5	2453	2725	2943	3064	3173	3303	3422	3474	3478	3352	force$[N]$

(a) *traction force wheels with 1234 mm diameter-straight lugs*

	slip [%]										
wheel	5	10	15	20	25	30	35	40	45	50	
2	2459	2697	2939	3139	3347	3537	3577	3494	3452	3406	traction
6	2417	2697	2908	3089	3215	3377	3458	3456	3354	3216	force$[N]$

(b) *traction force wheels with 1234 mm diameter-combined lugs*

	slip [%]										
wheel	5	10	15	20	25	30	35	40	45	50	
3	2629	2855	3035	3210	3343	3401	3410	3376	3299	3299	traction
7	2464	2660	2827	3007	3171	3296	3346	3305	3277	3277	force$[N]$

(c) *traction force wheels with 1420 mm diameter*

	slip [%]										
wheel	5	10	15	20	25	30	35	40	45	50	
4	2324	2549	2767	2946	3063	3147	3147	3140	3116	3116	traction
8	2402	2598	2741	2907	3028	3106	3147	3160	3131	3131	force$[N]$

(d) *traction force wheels with 1644 mm diameter-combined lugs*

Table 5.15: *traction force as a function of wheel slip*

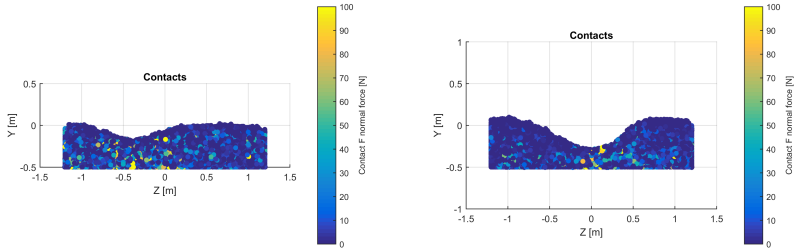

(a) *contact profile at* 5% *wheel slip-wheel* 1 **(b)** *contact profile at* 50% *wheel slip-wheel* 1

Figure 5.63: *contact profile at* 5% *and* 50% *wheel slip for wheel* 1

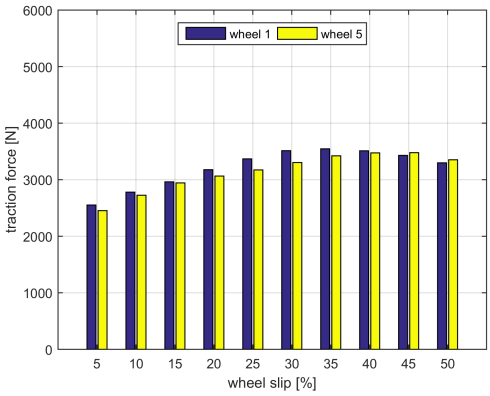

(a) *traction for wheels with 1234 mm diameter-straight lugs*

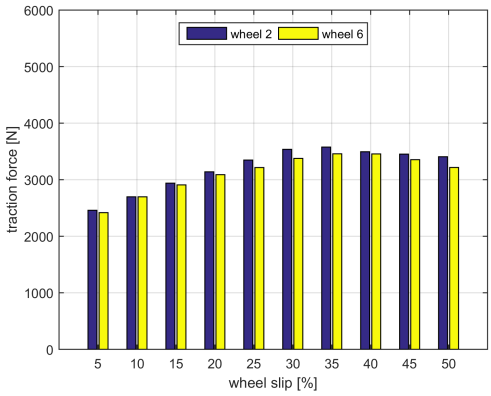

(b) *traction for wheels with 1234 mm diameter-combined lugs*

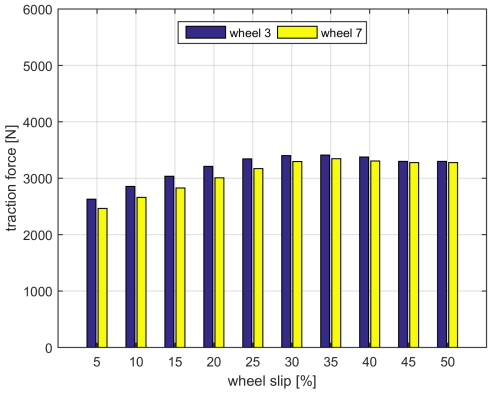

(c) *traction for wheels with 1413 mm diameter-combined lugs*

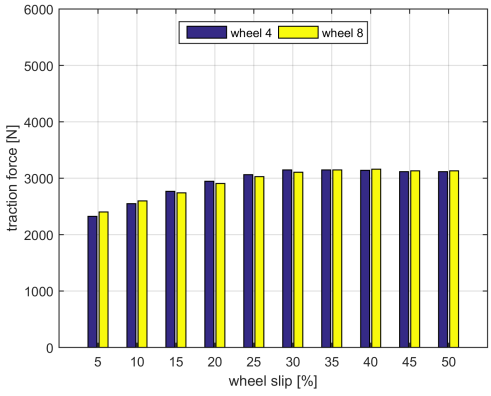

(d) *traction for wheels with 1644 mm diameter-combined lugs*

Figure 5.64: *traction force as a function of wheel slip*

From the simulation results of traction force figure 5.64, it was noted that trend of traction force for all wheel is similar, and the difference in traction force between wheels with $25°$ and $45°$ lugs angle is very small, this results is different from dry sand, loose sand terrain in previous sections. This means that as the cohesiveness of terrain increases effects of lugs angle on traction force decreases. Traction force is high for wheels with $1234mm$ diameter than wheels with $1644mm$ diameter, this difference is caused by slip sinkage which is high for wheels with $1234mm$ diameter. The difference in traction force between wheels with $1234mm$ and $1413mm$ diameters is small, this means that for clayey loam terrain due to high cohesion, small difference in wheel diameter has small difference in traction force, and the effect can be neglected. Also difference of traction force is very small for wheel with straight and combined lugs figure 5.64a and 5.64b, for same diameter and it can be neglected.

Slip Sinkage

	slip [%]										
wheel	5	10	15	20	25	30	35	40	45	50	
1	0.26	0.85	1.50	2.64	4.37	6.03	8.10	9.73	11.53	14.11	slip
5	0.26	0.85	1.50	2.28	3.43	4.71	6.03	8.06	10.59	14.11	sinkage$[cm]$

(a) *slip sinkage wheels with 1234 mm diameter-straight lugs*

	slip [%]										
wheel	5	10	15	20	25	30	35	40	45	50	
2	0.25	0.42	1.28	2.60	3.95	5.98	8.82	11.29	12.93	12.93	slip
6	0.52	1.32	2.05	3.10	4.35	5.73	7.46	9.53	12.16	13.01	sinkage$[cm]$

(b) *slip sinkage wheels with 1234 mm diameter-combined lugs*

	slip [%]										
wheel	5	10	15	20	25	30	35	40	45	50	
3	0.76	1.67	2.93	4.18	5.75	7.02	8.43	10.10	12.03	12.03	slip
7	0.76	1.67	2.62	3.97	5.24	7.02	8.78	11.02	12.04	12.03	sinkage$[cm]$

(c) *slip sinkage wheels with 1413 mm diameter-combined lugs*

	slip [%]										
wheel	5	10	15	20	25	30	35	40	45	50	
4	1.03	2.27	3.75	4.93	6.05	7.25	8.04	8.95	9.28	9.28	slip
8	1.03	1.77	2.55	3.57	4.58	5.48	6.83	8.00	9.13	9.13	sinkage$[cm]$

(d) *slip sinkage wheels with 1644 mm diameter-combined lugs*

Table 5.16: *slip sinkage as a function of wheel slip*

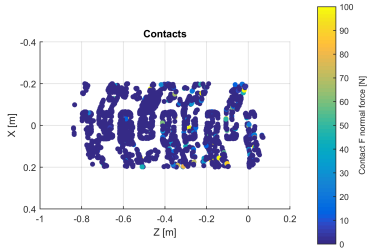

(a) *contact patch at* 5% *wheel slip-wheel* 2

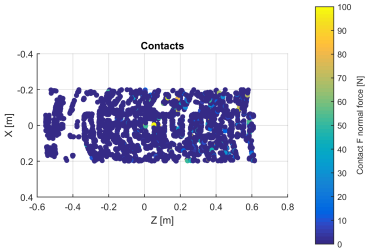

(b) *contact patch at* 50% *wheel slip-wheel* 2

Figure 5.65: *contact patch at* 5% *and* 50% *wheel slip for wheel* 2

wheel slip sinkage in this terrain results in figure 5.66, it was noted that difference in slip sinkage for wheels with straight and combined lugs figures 5.66a and 5.66b is small and trend is similar although large lugs angle $45°$ has low slip sinkage especially below 45% wheel slip. Increasing wheel diameter reduces slip sinkage, this results is similar in dry sand, loose sand and upland sand terrain in previous section, although in loose and dry sand slip sinkage for small wheels $1234mm$ diameter is high especially at high slip. This is caused by high cohesiveness of clayey loam sand terrain.

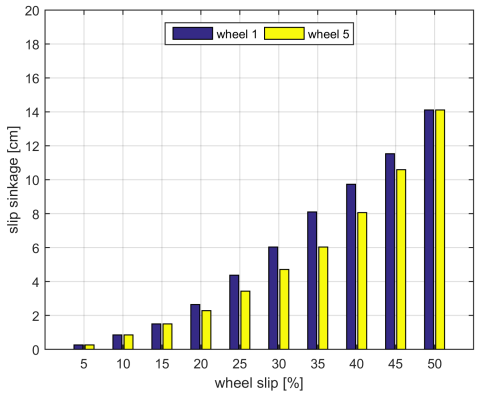

(a) *sinkage for wheels with 1234 mm diameter-straight lugs*

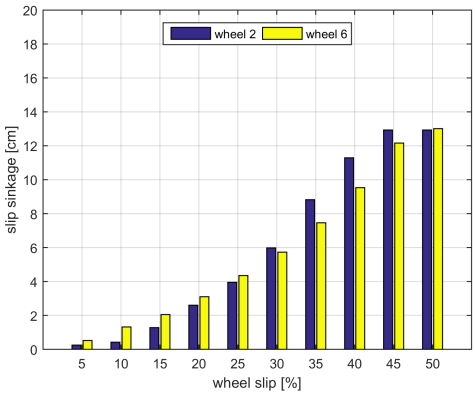

(b) *sinkage for wheels with 1234 mm diameter-combined lugs*

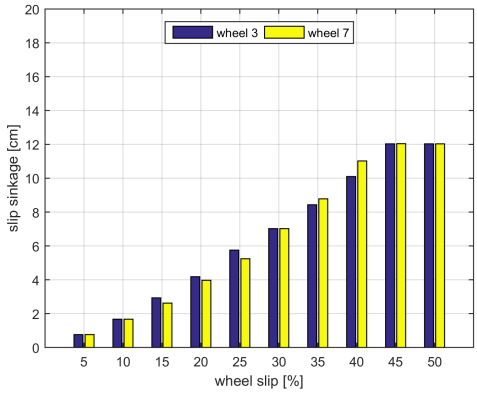

(c) *sinkage for wheels with 1413 mm diameter-combined*

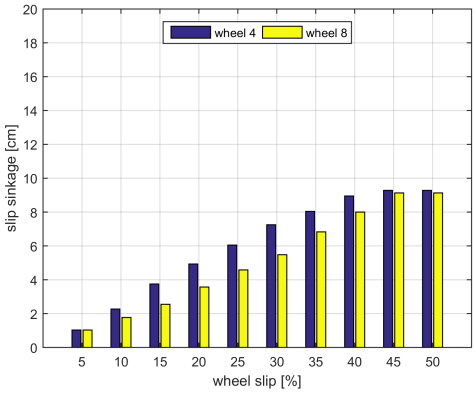

(d) *sinkage for wheels with 1644 mm diameter-combined lugs*

Figure 5.66: *slip sinkage as a function of wheel slip*

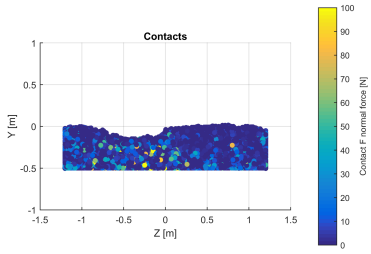

(a) *contact profile at* 5% *wheel slip-wheel* 2

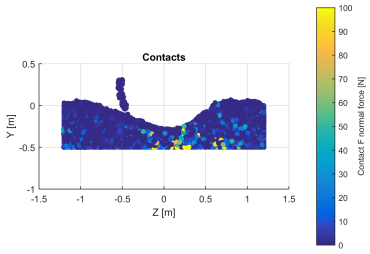

(b) *contact profile at* 50% *wheel slip-wheel* 2

Figure 5.67: *contact profile at* 5% *and* 50% *wheel slip for wheel* 2

Slip Velocity

	slip [%]										
wheel	5	10	15	20	25	30	35	40	45	50	
1	0.019	0.032	0.045	0.053	0.060	0.066	0.068	0.072	0.074	0.070	slip
5	0.019	0.033	0.045	0.055	0.064	0.073	0.080	0.084	0.083	0.080	velocity$[m/s]$

(a) *slip velocity wheels with 1234 mm diameter-straight lugs*

	slip [%]										
wheel	5	10	15	20	25	30	35	40	45	50	
2	0.019	0.033	0.044	0.051	0.059	0.063	0.063	0.062	0.062	0.062	slip
6	0.019	0.033	0.045	0.054	0.062	0.070	0.075	0.077	0.076	0.075	velocity$[m/s]$

(b) *slip velocity wheels with 1234 mm diameter-combined lugs*

	slip [%]										
wheel	5	10	15	20	25	30	35	40	45	50	
3	0.018	0.030	0.039	0.048	0.052	0.056	0.060	0.061	0.058	0.059	slip
7	0.018	0.032	0.042	0.050	0.059	0.064	0.065	0.066	0.063	0.063	velocity$[m/s]$

(c) *slip velocity wheels with 1413 mm diameter-combined lugs*

	slip [%]										
wheel	5	10	15	20	25	30	35	40	45	50	
4	0.020	0.032	0.041	0.048	0.053	0.054	0.057	0.060	0.064	.064	slip
8	0.020	0.032	0.041	0.050	0.058	0.062	0.063	0.064	0.064	0.064	velocity$[m/s]$

(d) *slip velocity wheels with 1644 mm diameter-combined lugs*

Table 5.17: *slip velocity as a function of wheel slip*

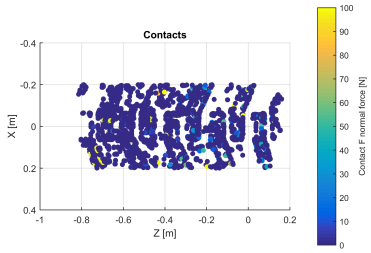

(a) *contact patch at* 5% *wheel slip-wheel* 3

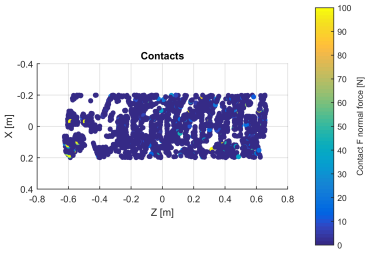

(b) *contact patch at* 50% *wheel slip-wheel* 3

Figure 5.68: *contact patch at* 5% *and* 50% *wheel slip for wheel* 3

Taking into account wheel slip velocity results in figure 5.69, it was inferred that slip velocity decreases with increase of wheel diameter. It increases and reach a constant value at 30% slip for wheels with $1413mm$ and $1644mm$ diameter figures 5.69c and 5.69d. For wheels with $1234mm$ diameter it increases and reach a constant value above 35% slip figures 5.69a and 5.69b, but for combined lugs inclined at $25°$ wheel 2 figure 5.69b, it reaches constant value above 25% slip. These difference in slip velocity is caused by difference in slip and slip sinkage of wheels as slip sinkage results.

Difference in slip velocity for wheels with straight and combined lugs figure 5.69a and 5.69b is small for large lugs angle $45°$, although for straight lugs slip velocity is

little bit high than combined lugs at high slip above 25% wheel slip. Also trend of slip velocity is similar for all wheels although $25°$ lugs angle has low slip velocity as compared to $45°$ lugs angle, this difference is caused by difference in slip sinkage.

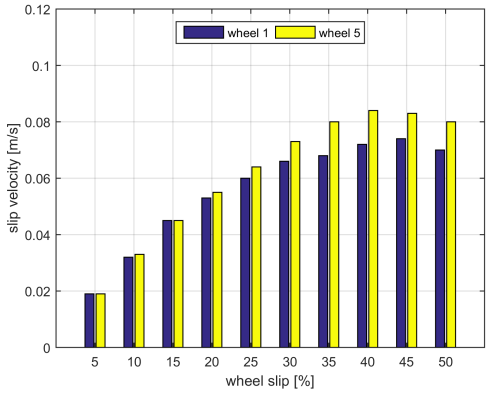

(a) *slip velocity for wheels with 1234 mm diameter-straight lugs*

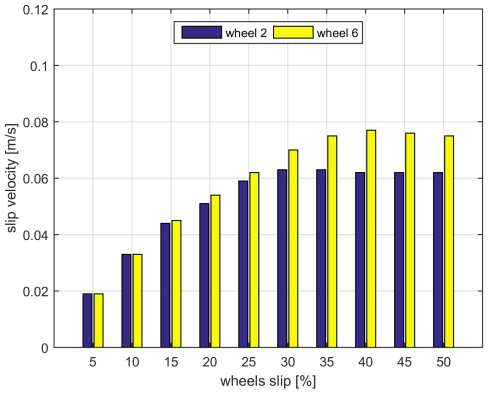

(b) *slip velocity for wheels with 1234 mm diameter-combined lugs*

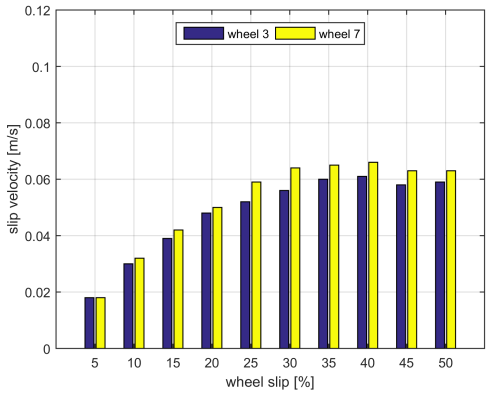

(c) *slip velocity for wheels with 1413 mm diameter-combined lugs*

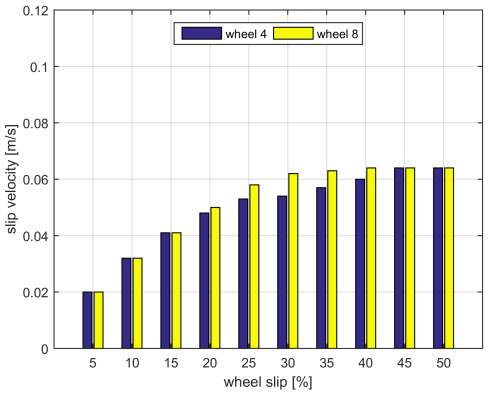

(d) *slip velocity for wheels with 1644 mm diameter-combined lugs*

Figure 5.69: *slip sinkage as a function of wheel slip*

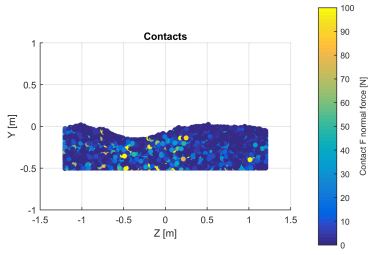

(a) *contact profile at* 5% *wheel slip-wheel* 3

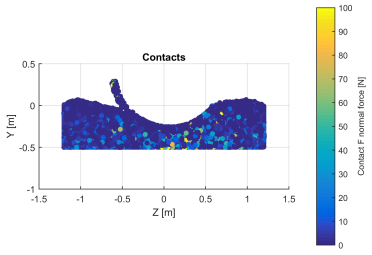

(b) *contact profile at* 50% *wheel slip-wheel* 3

Figure 5.70: *contact profile at* 5% *and* 50% *wheel slip for wheel* 3

Forward Velocity

	slip [%]										
wheel	5	10	15	20	25	30	35	40	45	50	
1	0.35	0.31	0.27	0.23	0.19	0.16	0.13	0.11	0.09	0.07	forward
5	0.36	0.31	0.27	0.24	0.22	0.18	0.15	0.13	0.10	0.08	velocity$[m/s]$

(a) *forward velocity wheels with 1234 mm diameter-straight lugs*

	slip [%]										
wheel	5	10	15	20	25	30	35	40	45	50	
2	0.36	0.31	0.27	0.24	0.19	0.15	0.12	0.09	0.07	0.07	forward
6	0.36	0.31	0.27	0.24	0.21	0.17	0.14	0.12	0.09	0.09	velocity$[m/s]$

(b) *forward velocity wheels with 1234 mm diameter-combined lugs*

	slip [%]										
wheel	5	10	15	20	25	30	35	40	45	50	
3	0.35	0.30	0.25	0.21	0.16	0.14	0.11	0.09	0.08	0.08	forward
7	0.37	0.32	0.28	0.24	0.19	0.15	0.12	0.10	0.09	0.09	velocity$[m/s]$

(c) *forward velocity wheels with 1413 mm diameter-combined lugs*

	slip [%]										
wheel	5	10	15	20	25	30	35	40	45	50	
4	0.40	0.33	0.27	0.21	0.17	0.13	0.11	0.09	0.08	0.08	forward
8	0.38	0.33	0.28	0.23	0.18	0.15	0.12	0.10	0.08	0.08	velocity$[m/s]$

(d) *forward velocity wheels with 1613 mm diameter-combined lugs*

Table 5.18: *forward velocity as a function of wheel slip*

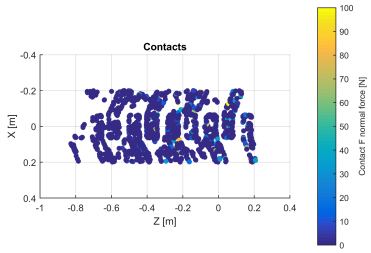

(a) *contact patch at* 5% *wheel slip-wheel* 4

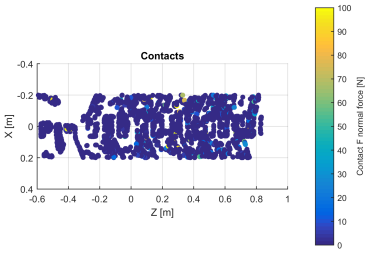

(b) *contact patch at* 50% *wheel slip-wheel* 4

Figure 5.71: *contact patch at* 5% *and* 50% *wheel slip for wheel* 4

Trend of forward velocity of the wheels results in figure 5.72, is similar although there some difference between wheels with $25°$ and $45°$ lugs angle, and this difference is caused by difference in slip sinkage and slip velocity of wheels. Effect of lugs type results in figures 5.72a and 5.72b, in forward velocity is very small for this terrain, this is because of small differnce in slip sinkage and slip velocity for the wheels.

Taking into account contact patch of wheels results in figures 5.62, 5.65, 5.68, 5.71, 5.74, 5.76, 5.78 and 5.80, it was inferred that lugs tresses are clear at 5% wheel slip, and interfered at 50% wheel slip, this means that soil disturbance by lugs increases with increase of slip. Also contact patch is long at 50% wheel slip as compared at 5% wheel

slip, this is because of high sinkage of wheel at high slip which cause large entry and exit angles.

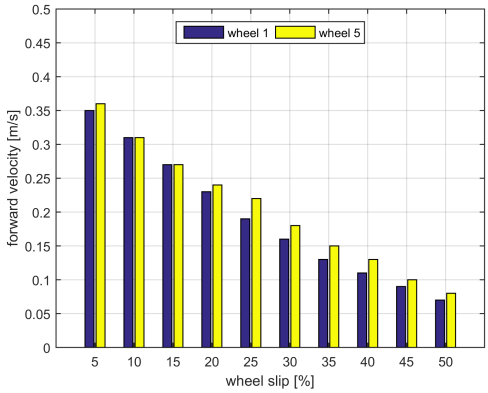

(a) *forward velocity for wheels with 1234 mm diameter-straight lugs*

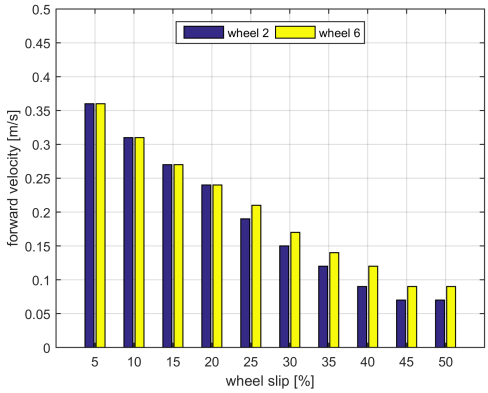

(b) *forward velocity for wheels with 1234 mm diameter-combined lugs*

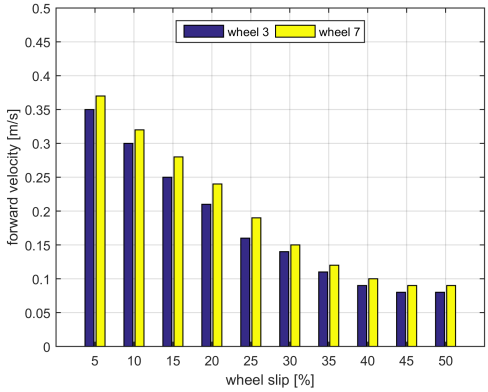

(c) *forward velocity for wheels with 1413 mm diameter-combined lugs*

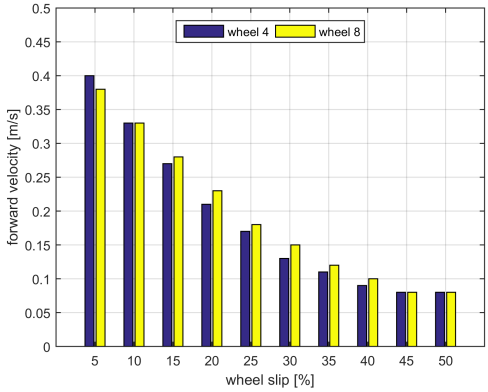

(d) *forward velocity for wheels with 1644 mm diameter-combined lugs*

Figure 5.72: *forward velocity as a function of wheel slip*

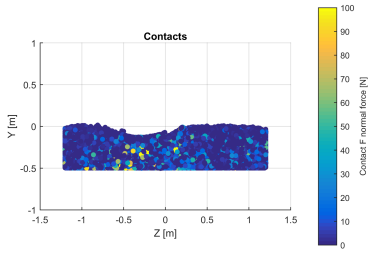

(a) *contact profile at* 5% *wheel slip-wheel* 4

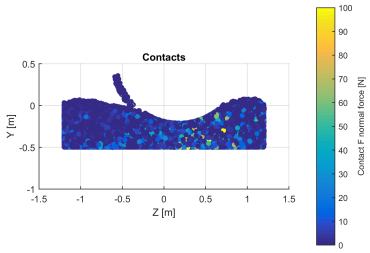

(b) *contact profile at* 50% *wheel slip-wheel* 4

Figure 5.73: *contact profile at* 5% *and* 50% *wheel slip for wheel* 4

Contact profiles results in figures 5.63, 5.67, 5.70, 5.73, 5.75, 5.77, 5.79 and 5.81, it

can be observed that contact profile is deeper at 50% wheel slip than at 5% wheel slip, this is because of high slip sinkage at high slip. Also change of color for contact normal force shows that particles in front of dead bottom center experiences more contact force, and this means that stresses are more at that point as compared to ather point at the contact patch, this agrees with Wong stresses distribution [106].

At high 50% wheel slip figures 5.67, 5.70 and 5.73, it can be observed that some of the soil particles fills lugs space and rotates with the lugs, this is by the contact plot between particle and wheel above contact patch.

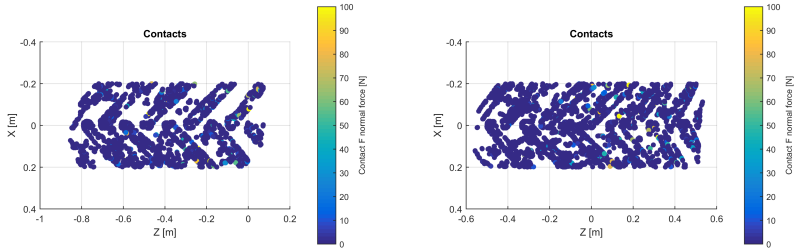

(a) *contact patch at* 5% *wheel slip-wheel* 5 **(b)** *contact patch at* 50% *wheel slip-wheel* 5

Figure 5.74: *contact patch at* 5% *and* 50% *wheel slip for wheel* 5

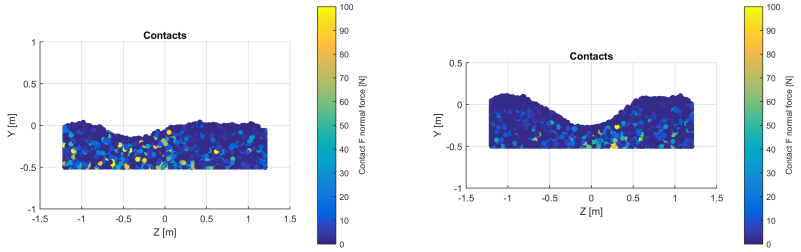

(a) *contact profile at* 5% *wheel slip-wheel* 5 **(b)** *contact profile at* 50% *wheel slip-wheel* 5

Figure 5.75: *contact profile at* 5% *and* 50% *wheel slip for wheel* 5

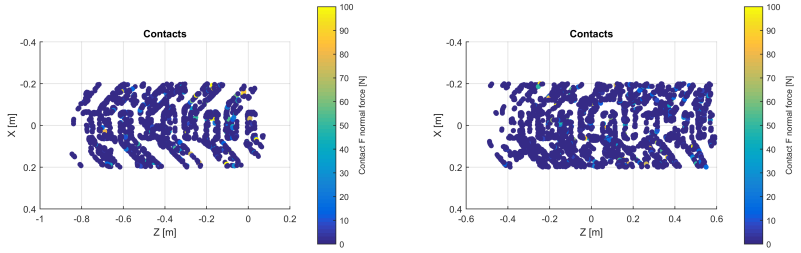

(a) *contact patch at* 5% *wheel slip-wheel* 6 **(b)** *contact patch at* 50% *wheel slip-wheel* 6

Figure 5.76: *contact patch at* 5% *and* 50% *wheel slip for wheel* 6

This means that for high cohesive terrain posibility of wheel lugs spacing to be filled by soil and reduce effects of lugs is high especially at high slip, or if the wheel will experience spinning/skidding. This effect of lugs spaces to be filled with soil particles and rotates with the wheel will reduce traction force and draw bar pull force since effects of lugs on traction will be reduces.

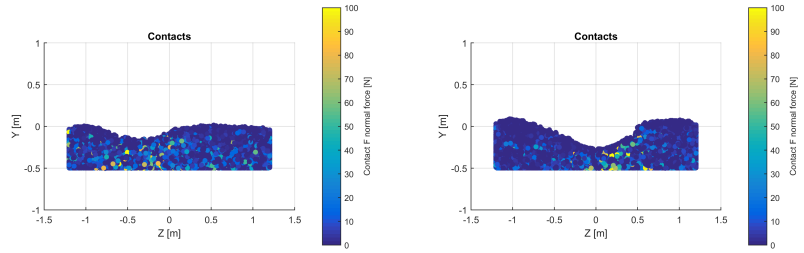

(a) *contact profile at* 5% *wheel slip-wheel* 6 **(b)** *contact profile at* 50% *wheel slip-wheel* 6

Figure 5.77: *contact profile at* 5% *and* 50% *wheel slip for wheel* 6

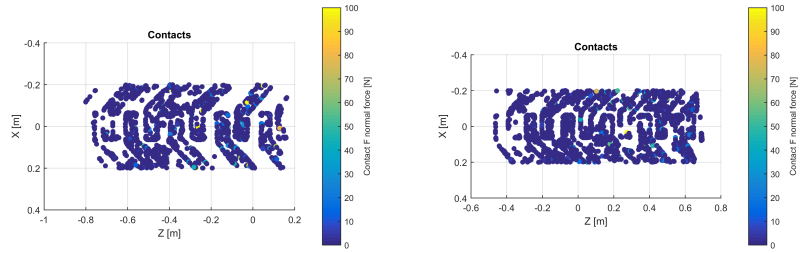

(a) *contact patch at* 5% *wheel slip-wheel* 7 **(b)** *contact patch at* 50% *wheel slip-wheel* 7

Figure 5.78: *contact patch at* 5% *and* 50% *wheel slip for wheel* 7

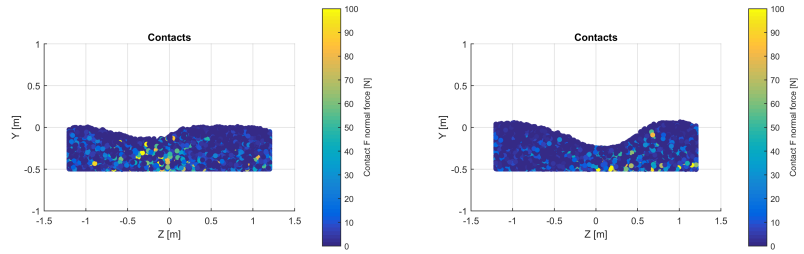

(a) *contact profile at* 5% *wheel slip-wheel* 7 **(b)** *contact profile at* 50% *wheel slip-wheel* 7

Figure 5.79: *contact profile at* 5% *and* 50% *wheel slip for wheel* 7

From analysis of the results for clayey loam sand terrain, it was concluded that, all wheels 1 to 8 has good performance on this terrain. Although $1234mm$ diameter wheels has high traction force than large wheels $1413mm$ and $1644mm$ diameters, but large

wheels performs better because it has low slip sinkage and slip velocity as compared to small wheels. Also effects of $25°$ and $45°$ lugs angle on wheel performance can be neglected since it is very small. For operations such as ploughing which needs lateral holding force to keep agricultural machine in a straight contour, then $45°$ lugs angle wheels has to be used instead of small angle [71].

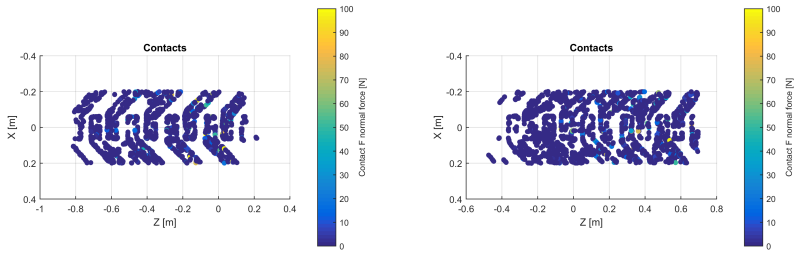

(a) *contact patch at* 5% *wheel slip-wheel* 8 **(b)** *contact patch at* 50% *wheel slip-wheel* 8

Figure 5.80: *contact patch at* 5% *and* 50% *wheel slip for wheel* 8

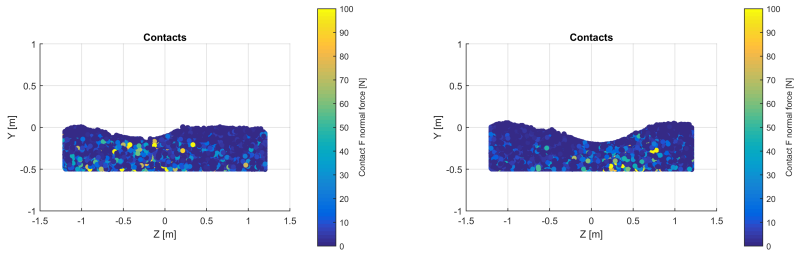

(a) *contact profile at* 5% *wheel slip-wheel* 8 **(b)** *contact profile at* 50% *wheel slip-wheel* 8

Figure 5.81: *contact profile at* 5% *and* 50% *wheel slip for wheel* 8

5.1.5 Drawbar pull and tractive efficiency

In this sub-section analysis were carried out torealise effects of wheel parameters on drawbar pull and tractive efficiency. Two terrains, upland and clayey loam sandy table 5.2 are considered.

From the simulation results analysis figure 5.82, it was able to be noted that drawbar pull is a function of terrain properties. This is because motion resistance, slip sinkage are functions of terrain properties. For upland sand terrain wheels has low drawbar pull and for wheel 1 and 2 figure 5.82a starts developing drawbar pull at above 15% wheel slip, while below that slip value the wheel has negative drawbar pull.

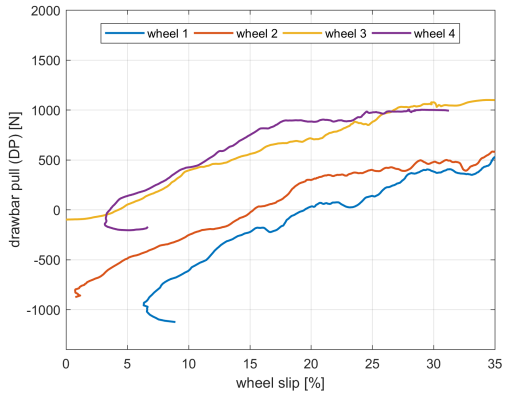

(a) *drawbar pull as a function of wheel slip-upland terrain*

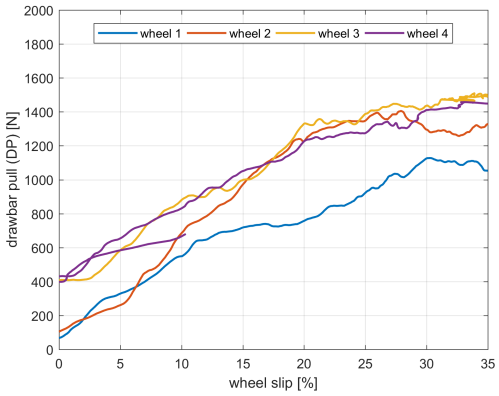

(b) *drawbar pull as a function of wheel slip-clayey terrain*

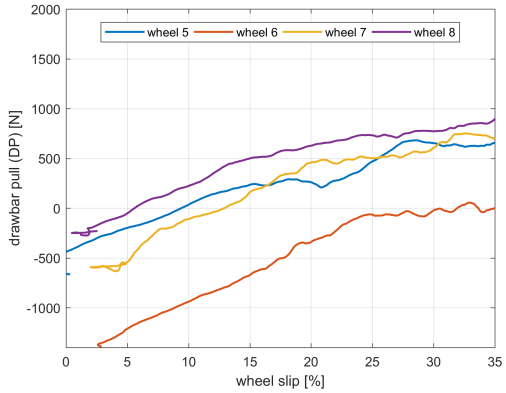

(c) *drawbar pull as a function of wheel slip-upland terrain*

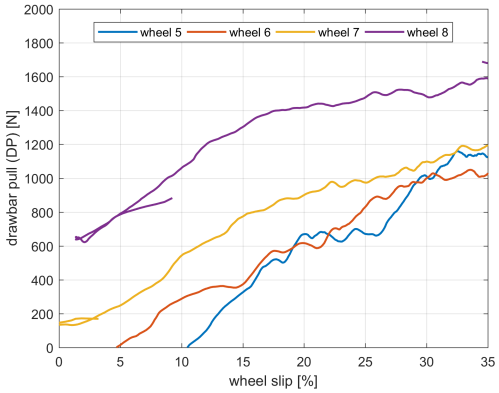

(d) *drawbar pull as a function of wheel slip-clayey terrain*

Figure 5.82: *drawbar pull for upland and clayey sand terrain*

This means that the wheel is been pushed by its weight due to high slip sinkage at that wheel load below 15% wheel slip. For wheel 5 and 6 figure 5.82c, wheel 5 develops drawbar pull above 10% wheel slip and below that slip it has negative drawbar pull, wheel 6 instead does not develop drawbar pull even at high slip.

For clayey sand terrain figure 5.82b, all wheels 1 to 4 develop drawbar pull, although wheel 1 has lower drawbar pull as compared to other wheels, this is because wheel 1 has straight lugs which develop low traction as compared to wheels 2, 3 and 4 which has combined lugs. For wheels 5 to 8 figure 5.82d, wheel 5 starts developing drawbar pull above 10% wheel slip, and wheel 6 develop drawbar pull above 5% wheel slip, wheels 7 and 8 guarantees non negative drawbar pull even at low slip value, an wheel 8 has higher drawbar pull as compared to other wheels. This is because wheel 7 and 8 has large diameter and width which cause low slip sinkage as compared to slip sinkage of wheels 4 and 5 which has small diameter and width.

Since negative drawbar pull will also give negative tractive efficiency and is not desired for performance of wheels on deformable terrain, for wheels 1, 2, 5 and 6 and for this terrain parameters, wheel load has to be reduced in order to reduce slip sinkage. In order to estimate allowable wheel load for the given terrain, using equation 3.48, and average sinkage of large wheels which was $0.052593m$, then calculated wheel load was

$6730N$. Simulations was carried using this load to analyse drawbar pull and tractive efficiency for performance improvement on a given terrain.

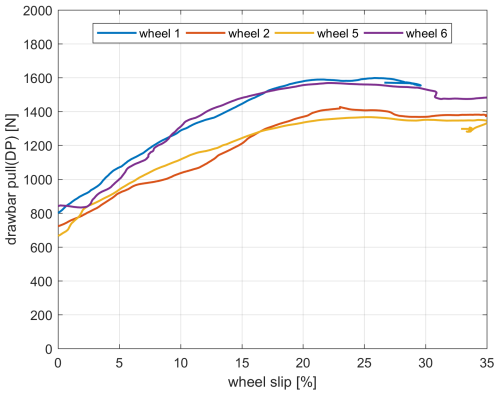

(a) *drawbar pull as a function of wheel slip-upland terrain*

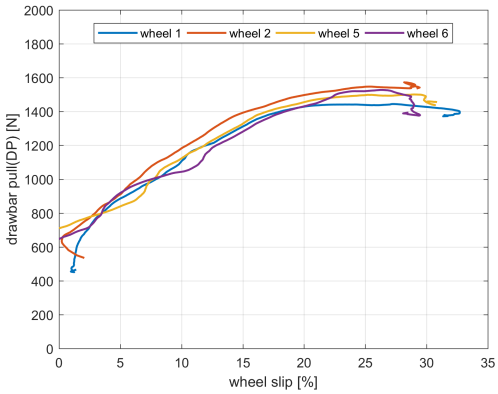

(b) *drawbar pull as a function of wheel slip-clayey terrain*

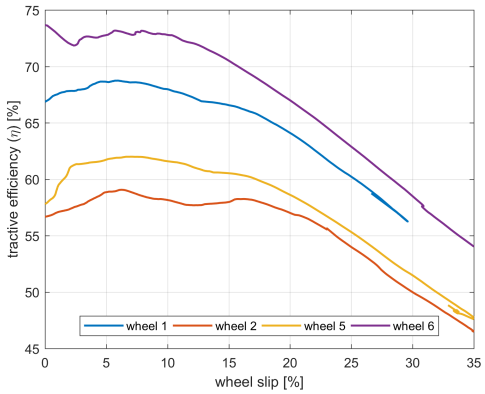

(c) *tractive efficiency as a function of wheel slip-upland terrain*

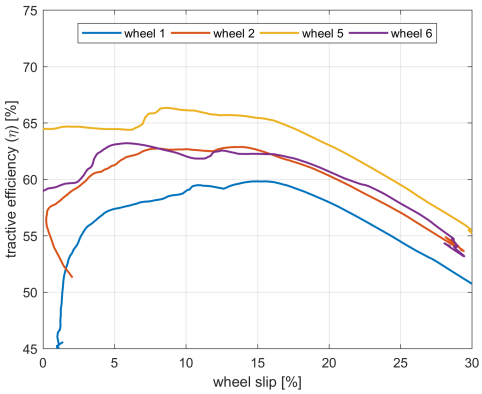

(d) *tractive efficiency as a function of wheel slip-clayey terrain*

Figure 5.83: *drawbar pull and tractive efficiency for upland and clayey sand terrain*

From the results analysis in figure 5.83, it was noted that drawbar pull improved for both terrain, and all wheels guarantees a maximum drawbar pull not less than $1.2kN$. Also it was noted that wheel 1 and 6 figure 5.83a has almost same drawbar pull which is higher than wheel 2 and 5 for upland terrain. For clayey terrain figure 5.83b, all wheels has almost same drawbar pull at all wheel slip.

Since it was a little bit difficult to decide which wheel performs better only by using drwabar pull which is of very small difference between alls wheels, tractive efficiency which is another index for performance analysis was evaluated. From the results analysis figure 5.83c it was noted that, wheel 6 has higher tractive efficiency as compared to other wheels for upland sand, while for clayey terrain figure 5.83d, wheel 5 has higher tractive efficiency than other wheels.

Although all wheels has almost same drawbar pull, but they has significant difference in tractive efficiency. this leads to the conclusion that wheel 6 and 5 performs better by guarantees high drawbar pull and tractive efficiency in upland and clayey terrain respectively.

5.2 Soft deformable soil

In this section simulations were carried out by interacting soft deformable soil with wheels in table 5.1. Simulations are carried out considering dry sand terrain table 5.2 and results of wheel traction force are tabulated in tables 5.19a to 5.19d and represented graphically in figures 5.84a to 5.84d. Slip sinkage and contact pressure are shown in figures with respective colour bar which shows colour range with respect to sinkage and contact pressure.

Traction Force

	slip [%]					
wheel	10	15	20	25	30	
1	5165	5828	6430	6881	7101	traction
5	5232	5995	6601	7258	7426	force[N]

(a) *traction force wheels with 1234 mm diameter-straight lugs*

	slip [%]					
wheel	10	15	20	25	30	
2	5659	6043	6627	6871	7247	traction
6	5591	6247	7183	7330	7679	force[N]

(b) *traction force wheels with 1234 mm diameter-combined lugs*

	slip [%]					
wheel	10	15	20	25	30	
3	5511	6226	6921	7245	7402	traction
7	5517	6384	6857	7768	7729	force[N]

(c) *traction force wheels with 1413 mm diameter-combined lugs*

	slip [%]					
wheel	10	15	20	25	30	
4	5757	6848	7477	7747	8186	traction
8	5996	6958	7490	8072	8722	force[N]

(d) *traction force wheels with 1644 mm diameter-combined lugs*

Table 5.19: *traction force as a function of wheel slip*

From the simulation results of traction force in figure 5.84, it was noted that increase of slip increases traction force. Wheel diameter has an effects on traction force in which increase of wheel diameter increases traction force. It was also noted that large lugs angle supplies high traction force especially at high slip while at low slip the difference is not significant.

Taking into account slip sinkage of the wheel figures 5.85, 5.89, 5.93, 5.97, 5.87, 5.91, 5.95 and 5.99, it was noted that colour intensity from blue to red increases with increase of slip, this means that slip sinkage increases with increase of wheel slip. Also slip sinkage decreases with increase of wheel diameter and decrease with increase of lugs angle.

With regards to contact pressure results in figures 5.86, 5.90, 5.94, 5.98, 5.88, 5.92, 5.96 and 5.100, it was noted that colour intensity increases from blue to red with increase of wheel slip, this means that contact pressure increases with increase of wheel

slip and decreases with increase of wheel diameter. Also contact pressure decreases with increase of lugs angle

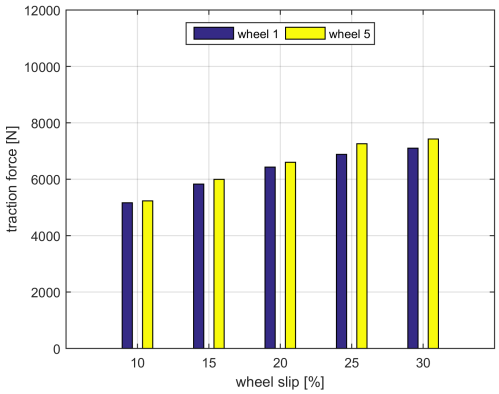

(a) *traction for wheels with 1234 mm diameter-straight lugs*

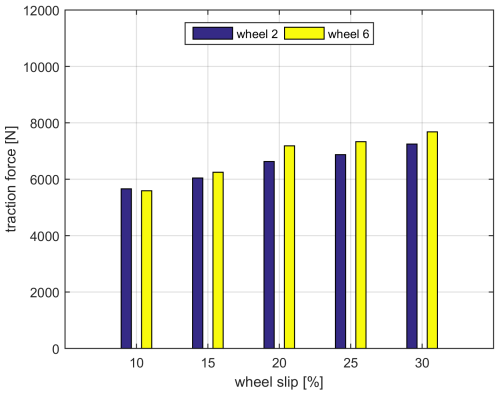

(b) *traction for wheels with 1234 mm diameter-combined lugs*

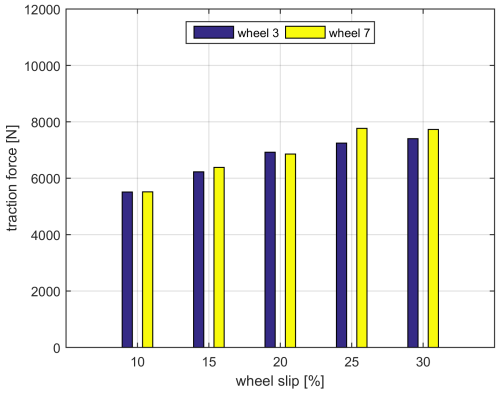

(c) *traction for wheels with 1413 mm diameter-combined lugs*

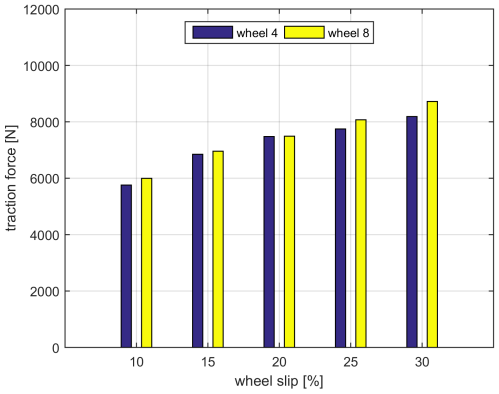

(d) *traction for wheels with 1644 mm diameter-combined lugs*

Figure 5.84: *traction force as a function of wheel slip*

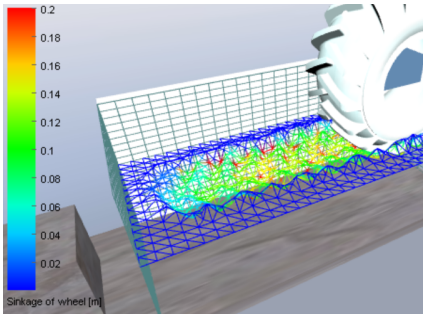

(a) *slip sinkage at* 10% *wheel slip-wheel* 1

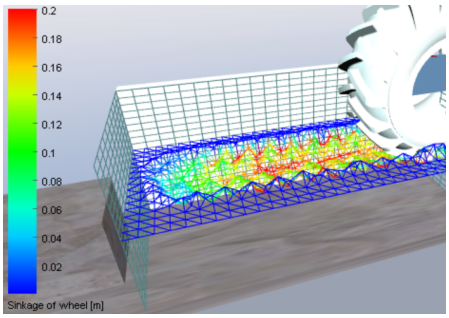

(b) *slip sinkage at* 30% *wheel slip-wheel* 1

Figure 5.85: *slip sinkage at* 10% *and* 30% *wheel slip for wheel* 1

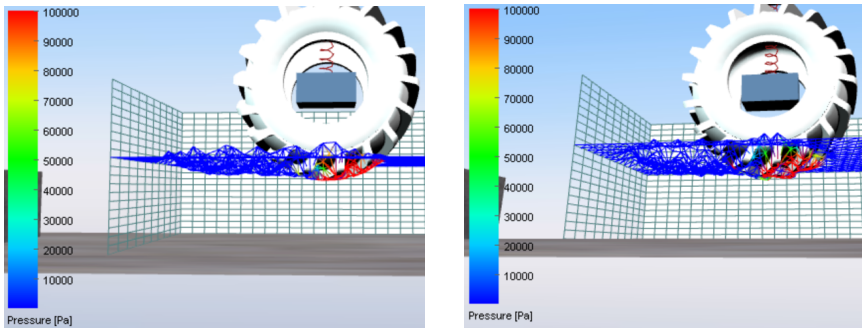

(a) *contact pressure at* 10% *wheel slip-wheel* 1 **(b)** *contact pressure at* 30% *wheel slip-wheel* 1

Figure 5.86: *contact pressure at* 10% *and* 30% *wheel slip for wheel* 1

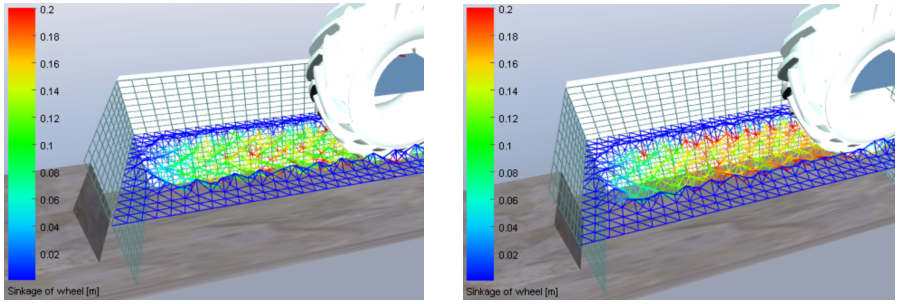

(a) *slip sinkage at* 10% *wheel slip-wheel* 5 **(b)** *slip sinkage at* 30% *wheel slip-wheel* 5

Figure 5.87: *slip sinkage at* 10% *and* 30% *wheel slip for wheel* 5

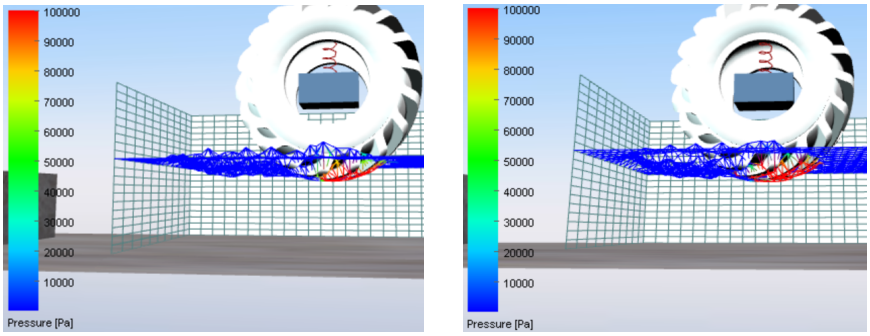

(a) *contact pressure at* 10% *wheel slip-wheel* 5 **(b)** *contact pressure at* 30% *wheel slip-wheel* 5

Figure 5.88: *contact pressure at* 10% *and* 30% *wheel slip for wheel* 5

From the simulation results analysis above, it was able to conclude that large wheels performs better by supplying high traction force, at the same time reduces slip sinkage, contact pressure. Large lugs angle also ensures high traction force even at high wheel slip and also can reduce soil failure because it reduces contact pressure. For the case of lugs type combined lugs gives slightly high traction force as compared to straight lugs and the difference in traction force is significant especially at high wheel slip.

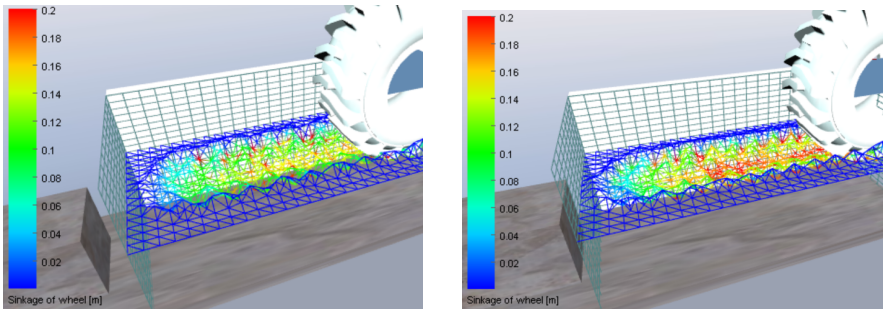

(a) *slip sinkage at* 10% *wheel slip-wheel* 2 **(b)** *slip sinkage at* 30% *wheel slip-wheel* 2

Figure 5.89: *slip sinkage at* 10% *and* 30% *wheel slip for wheel* 2

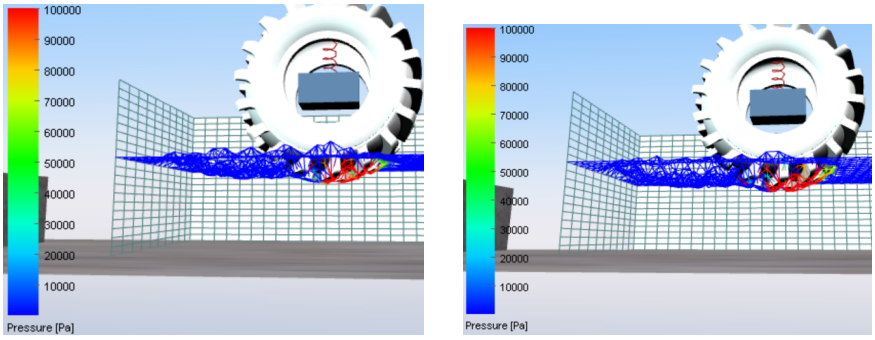

(a) *contact pressure at* 10% *wheel slip-wheel* 2 **(b)** *contact pressure at* 30% *wheel slip-wheel* 2

Figure 5.90: *contact pressure at* 10% *and* 30% *wheel slip for wheel* 2

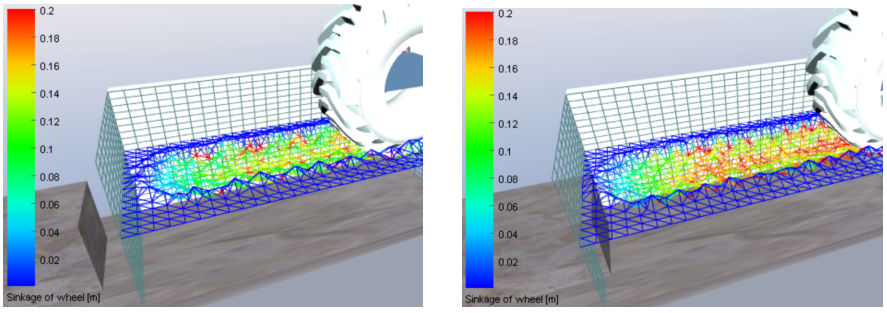

(a) *slip sinkage at* 10% *wheel slip-wheel* 6 **(b)** *slip sinkage at* 30% *wheel slip-wheel* 6

Figure 5.91: *slip sinkage at* 10% *and* 30% *wheel slip for wheel* 6

Although combined lugs has slightly increase of slip sinkage and contact pressure especially at high slip but it supplies high traction force at respective slip, therefore they performs better than wheels with straight lugs for soils with properties like dry sand considered in this analysis.

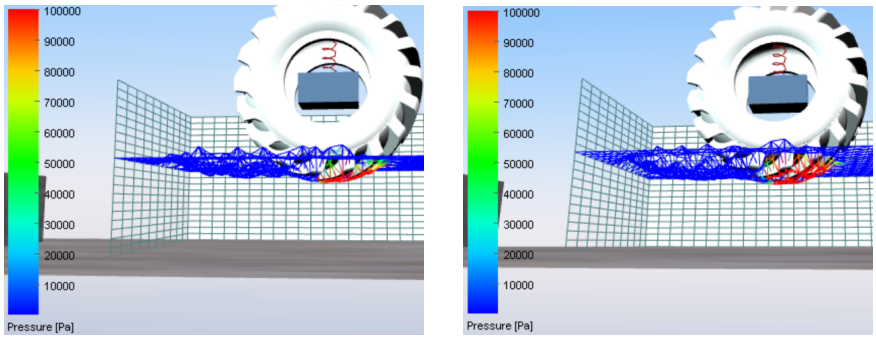

(a) *contact pressure at* 10% *wheel slip-wheel* 6 **(b)** *contact pressure at* 30% *wheel slip-wheel* 6

Figure 5.92: *contact pressure at* 10% *and* 30% *wheel slip for wheel* 6

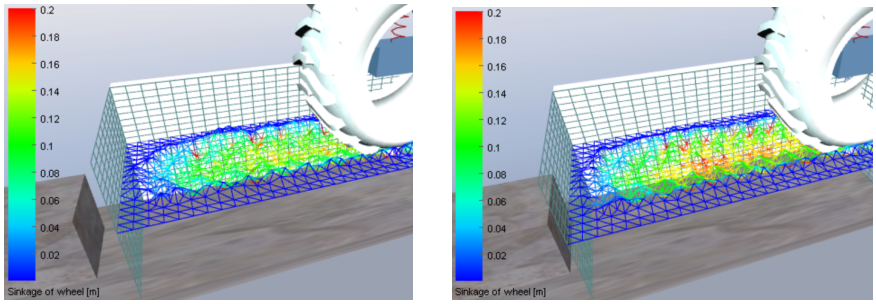

(a) *slip sinkage at* 10% *wheel slip-wheel* 3 **(b)** *slip sinkage at* 30% *wheel slip-wheel* 3

Figure 5.93: *slip sinkage at* 10% *and* 30% *wheel slip for wheel* 3

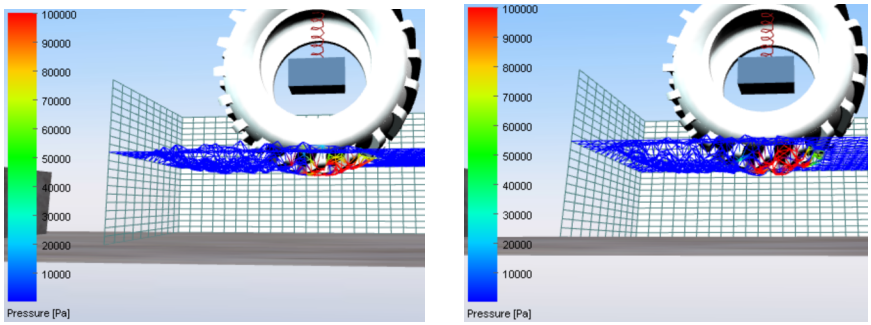

(a) *contact pressure at* 10% *wheel slip-wheel* 3 **(b)** *contact pressure at* 30% *wheel slip-wheel* 3

Figure 5.94: *contact pressure at* 10% *and* 30% *wheel slip for wheel* 3

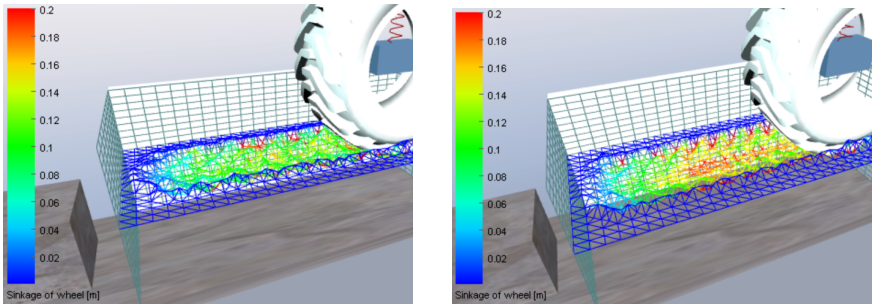

(a) *slip sinkage at* 10% *wheel slip-wheel* 7 **(b)** *slip sinkage at* 30% *wheel slip-wheel* 7

Figure 5.95: *slip sinkage at* 10% *and* 30% *wheel slip for wheel* 7

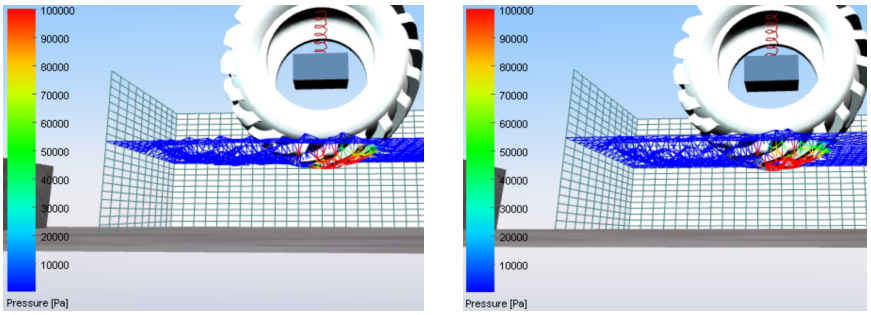

(a) *contact pressure at* 10% *wheel slip-wheel* 7 **(b)** *contact pressure at* 30% *wheel slip-wheel* 7

Figure 5.96: *contact pressure at* 10% *and* 30% *wheel slip for wheel* 7

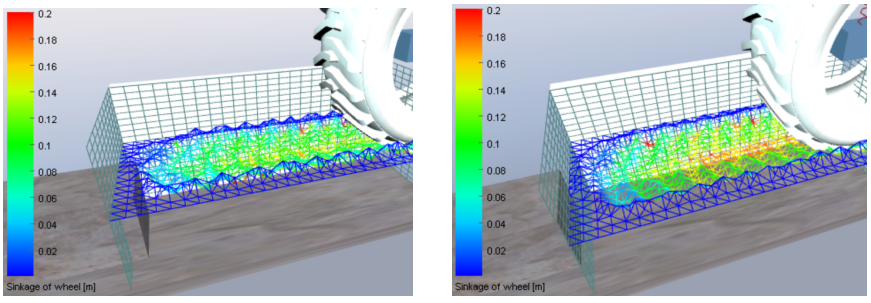

(a) *slip sinkage at* 10% *wheel slip-wheel* 4 **(b)** *slip sinkage at* 30% *wheel slip-wheel* 4

Figure 5.97: *slip sinkage at* 10% *and* 30% *wheel slip for wheel* 4

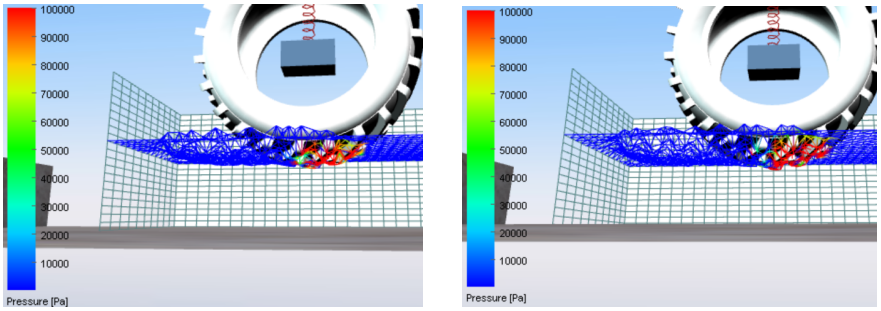

(a) *contact pressure at* 10% *wheel slip-wheel* 4 **(b)** *contact pressure at* 30% *wheel slip-wheel* 4

Figure 5.98: *contact pressure at* 10% *and* 30% *wheel slip for wheel* 4

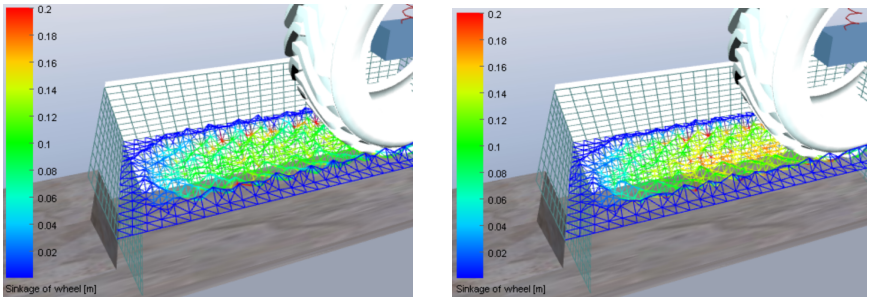

(a) *slip sinkage at* 10% *wheel slip-wheel* 8 **(b)** *slip sinkage at* 30% *wheel slip-wheel* 8

Figure 5.99: *slip sinkage at* 10% *and* 30% *wheel slip for wheel* 8

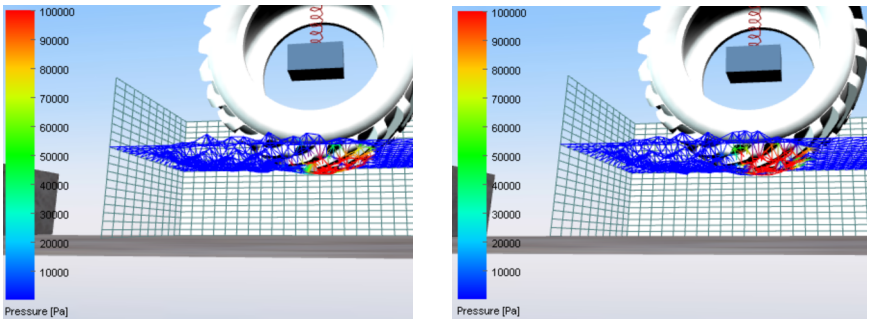

(a) *contact pressure at* 10% *wheel slip-wheel* 8 **(b)** *contact pressure at* 30% *wheel slip-wheel* 8

Figure 5.100: *contact pressure at* 10% *and* 30% *wheel slip for wheel* 8

5.3 Conclusions

From the optimisation analysis made in these sections 5.1.1, 5.1.2, 5.1.3, 5.1.4 and 5.2 by considering four different terrains; dry sand, loose sand, upland sand and clayey loam sand which stipulated by Wong [106], shows capability of the model developed to perform optimisation analysis. Different properties of the terrain such as cohesion, particle friction coefficient, particle density, terrain bulky density has been taken into account to analyse its effects on performance indices such as traction force, slip sink-

age, slip velocity and forward velocity for wheels with different diameters, width, lugs number, lugs angle and lugs type.

From the results it was observed that, cohesion, friction coefficient, particle density and terrain bulky density affects wheel performances. Also wheel parameters affects its performance when interacting with deformable terrain. Increase of wheel diameter decreases slip sinkage, slip velocity as well as motion resistance and this lead to better performance. Although small diameter wheels gives high traction force as compared to large wheels, but it has high slip sinkage especially at high wheel slip, this may lead to high motion resistance and wheel may stuck in the soil. This effects of high slip sinkage is reduced by increasing cohesion of theterrain as observed in clayey loam terrain. Increase in cohesion of terrain leads to increase of deformation resistance due to interaction and this reduces slip sinkage as well as motion resistance [106].

From the results it was inferred that lugs angle affects performance of wheels, decrease of lugs angle increases traction force and slip velocity especially below 30% wheel slip, this effects in traction force decreases as cohesion of terrain increases. This is because with small angle lugs lateral soil flow is small as compared to large angle and this leads to lugs to act like bulldozer cutting blade which increases soil deformation resistance force and develop more traction force [106]. Although small lugs angle gives high traction as compared to large lugs angle, but also increases slip sinkage especially at high slip and this affects performance of the wheel. Also this effects of lugs angle on traction force and slip sinkage reduces with increase of terrain cohesion. 45° lugs angle is recommended for agricultural operation such as ploughing in order to develop sufficient lateral holding force to keep machine in contour [71].

Results analysis shows that lugs tresses are clear at 5% wheel slip, but tends to interact with one another at 50% slip as observed on contact patch plot of wheels, this indicates that more soil disturbances due to lugs lugs-interactions occurs at high slip which leads to high slip sinkage at high slip. Also contact patch large at 50% slip as compared to one at 5% slip, this indicates that at high slip entry and exit angles are larger than at low slip. From the contact profile of the terrain it has been observed that more contact force experienced by particles during interaction occurs in front of the maximum sinkage point or bottom dead center of wheel, this indicates that maximum stresses at the contact patch does not occurs at point of maximum sinkage [106].

It was also observed from the results, for more cohesive terrain, particles stick between lugs space and rotate with the wheel. This was noted from the contact plot which protrude at contact patch profile at 50% wheel slip. This means that for more cohesive terrain such as clay soil terrain, when wheels operates at high slip or more draw bar pull is needed this may lead to wheel lugs space to be filled by soil and wheel looses tractive ability and leads to wheel spinning or poor performances [106].

Improvement of the wheel performance on a given terrain can be achieved by evaluating allowable wheel load with a given wheel and soil parameters.This was clearly shown in analysis in sub-section 5.1.5. Also it was noted that for better decision of the wheel performance, analysing other performance indexes such as drawbar pull and tractive efficiency ensures reliable decisions.

From analysis in section 5.2, it was inferred that, interaction parameters and contact pressure are function of wheel parameters. Large wheel diameters has less contact pressure than small diameter wheels, for large wheels it ensures less probability of soil

failure under high contact pressure. Also it was noted that contact pressure is a function of wheel slip.

Finally, from the analysis in this chapter it was able to concludes that, for analysis of wheel performance in deformable terrain, it is recommended to evaluate more performance indexes such as traction force, slip sinkage, slip velocity, drawbar pull and tractive efficiency as well as contact pressure for better analysis and proper decisions for performance and improvements recommendations.

CHAPTER 6

Conclusions

The aim of this thesis were to give a tool for studying and analysing interaction between tire and deformable terrain by considering discreteness deformation which gives rise to common effects such as bulldozing effects, cleaning up with respect to soil rheology. The model was able to represent terrain as assemblage of particles as well plane soft deformable which account for these effects during interaction.

The model uses rigid wheels which modelled in CAD software and exported to it and analyses influence of wheel design parameters on tractive performance with respect to terrain parameters. In the simulation results model realistically represents deformability of terrain during interaction by giving out wheel resistive torque, slip ratio, slip sinkage, slip velocity and forward velocity at different soil characteristics.

The performance of rigid wheel on deformable terrain gives out promising results in which effects of discontinuous deformation by considering longitudinal and lateral deformation with respect to particle properties such as shape, size, cohesion, friction, density, mass distribution and mixing ratio has been achieved with the model. Also a pre-compactor was added to the model to analyse the effect of terrain pre-compaction to interaction parameters, in which it was inferred that pre-compaction of terrain increases deformation resistance. This reduce sinkage of wheel due to slip which in turn decrease longitudinal motion resistance as well resistive torque. Interaction parameters are function of soil compaction resistance, effects of pre-compaction weight has to be taken into consideration for wheel performance analysis in case of positive impact to ground as the case of construction.

Since the model simulation results shows sensitivity of tire design parameters and soil characteristics on interaction parameters and the model is flexible for accommodating different tires, it was used to perform sensitivity and optimisation analysis of tread pattern with respect to soil characteristics. From the analysis it was shown the not

only pattern parameters has influence on tractive performance but also soil characteristics and its effects has to be taken into consideration for sensitivity and optimisation analysis. This model was able to accommodate different particle shape which influence multi contact of particles and this improves interlocking as well shear strength, which reduce wheel sinkage. Also, form the simulation results analysis it was inferred that contact pressure not only a function of wheel parameters but also a function of wheel slip, and it increases with increase of wheel slip.

Finally the model was validated with experimental and numerical results available in the literature, model results of traction force at respective wheel slip shows a good correlation in which it guarantees an error less than 7% .

Appendix A

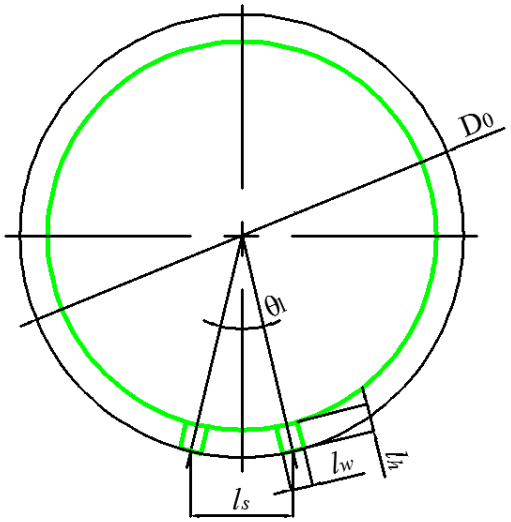

Figure 6.1: *wheel design parameters*

From the geometry of figure 6.1, lugs spacing can be calculated from

$$l_s = D_0 sin(\frac{\theta_l}{2})$$

.

Angle between lugs can be calculated from number of lugs and circular angle as

$$\theta_l = \frac{360^\circ}{n_l}$$

and ratio of lugs height to width is given as

$$Ratio_{h/w} = \frac{lugscenterlength(h)}{wheelwidth(w)}$$

.

Therefore, from reference lugs number of 15 and 20, angle between them can be calculated as

$$\theta_l = \frac{360^\circ}{15} = 24^\circ$$

and

$$\theta_l = \frac{360^\circ}{20} = 18^\circ$$

Taking reference outside diameter of the wheel $1.42m$, lugs spacing can be calculated using equation above as

$$l_s = 1.42 * sin(\frac{24^\circ}{2}) = 0.295m$$

and

$$l_s = 1.42 * sin(\frac{18^\circ}{2}) = 0.222m$$

and mean value of $0.259m$ lugs spacing is taken for calculating lugs circular position angle and lugs number.

Number of lugs for wheel diameters, $1234mm$, $1413mm$ and $1644mm$ can be calculated using equation above, where by angle between lugs can be calculated, and using lug spacing of $259mm$.

$$\theta_l = 2 * arcsin(\frac{259}{1234}) = 24^\circ$$

,

$$\theta_l = 2 * arcsin(\frac{259}{1413}) = 21^\circ$$

and

$$\theta_l = 2 * arcsin(\frac{259}{1644}) = 18^\circ$$

Therefore, lugs number will be

$$\frac{360^\circ}{24^\circ} = 15$$

,

$$\frac{360^\circ}{21^\circ} = 18$$

and

$$\frac{360^\circ}{18^\circ} = 20$$

, while lugs center length of $120mm$ was taken from chapter 4 for value that gives high traction force.

Bibliography

[1] Ozoemena Anthony Ani, He Xu, Yi-ping Shen, Shao-gang Liu, and Kai Xue. Modeling and multiobjective optimization of traction performance for autonomous wheeled mobile robot in rough terrain. *Journal of Zhejiang University SCIENCE C*, 14(1):11–29, 2013.

[2] Mihai Anitescu and Florian A Potra. Formulating dynamic multi-rigid-body contact problems with friction as solvable linear complementarity problems. *Nonlinear Dynamics*, 14(3):231–247, 1997.

[3] Mihai Anitescu and Alessandro Tasora. An iterative approach for cone complementarity problems for nonsmooth dynamics. *Computational Optimization and Applications*, 47(2):207–235, 2010.

[4] Johan Arvidsson and Sasa Ristic. Soil stress and compaction effects for four tractor tyres. *Journal of Terramechanics*, 33(5):223–232, 1996.

[5] A Battiato and E Diserens. Tractor traction performance simulation on differently textured soils and validation: A basic study to make traction and energy requirements accessible to the practice. *Soil and Tillage Research*, 166:18–32, 2017.

[6] Robert Bauer, Winnie Leung, and Tim Barfoot. Experimental and simulation results of wheel-soil interaction for planetary rovers. In *Intelligent Robots and Systems, 2005.(IROS 2005). 2005 IEEE/RSJ International Conference on*, pages 586–591. IEEE, 2005.

[7] GF Botta, D Rivero, M Tourn, F Bellora Melcon, O Pozzolo, G Nardon, R Balbuena, A Tolon Becerra, H Rosatto, and S Stadler. Soil compaction produced by tractor with radial and cross-ply tyres in two tillage regimes. *Soil and Tillage Research*, 101(1):44–51, 2008.

[8] GF Botta, A Tolon-Becerra, M Tourn, X Lastra-Bravo, and D Rivero. Agricultural traffic: Motion resistance and soil compaction in relation to tractor design and different soil conditions. *Soil and tillage research*, 120:92–98, 2012.

[9] MV Braunack. A tyre option for sugarcane haulout trucks to minimise soil compaction. *Journal of terramechanics*, 41(4):243–253, 2004.

[10] Bernard Brogliato and Vincent Acary. Numerical methods for nonsmooth dynamical systems. *Lecture Notes in Applied and Computational Mechanics*, 35, 2008.

[11] Christopher A Brooks, Karl D Iagnemma, and Steven Dubowsky. Visual wheel sinkage measurement for planetary rover mobility characterization. *Autonomous Robots*, 21(1):55–64, 2006.

[12] Brendan J Chan and Corina Sandu. A novel wheel-soil interaction model for off-road vehicle dynamics simulation. In *ASME 2007 International Design Engineering Technical Conferences and Computers and Information in Engineering Conference*, pages 1049–1059. American Society of Mechanical Engineers, 2007.

[13] Brendan Juin-Yih Chan. *Development of an off-road capable tire model for vehicle dynamics simulations*. PhD thesis, Virginia Polytechnic Institute and State University, 2008.

[14] Luc Clijmans, Herman Ramon, J Langenakens, and Josse De Baerdemaeker. The influence of tyres on the dynamic behaviour of a lawn mower. *Journal of terramechanics*, 33(4):195–208, 1996.

[15] Liang Ding, Zongquan Deng, Haibo Gao, Jianguo Tao, Karl D Iagnemma, and Guangjun Liu. Interaction mechanics model for rigid driving wheels of planetary rovers moving on sandy terrain with consideration of multiple physical effects. *Journal of Field Robotics*, 32(6):827–859, 2015.

[16] Liang Ding et al. Improved explicit-form equations for estimating dynamic wheel sinkage and compaction resistance on deformable terrain. *Mechanism and Machine Theory*, 86:235–264, 2015.

[17] Liang Ding, Hai-bo Gao, Zong-quan Deng, and Jian-guo Tao. Wheel slip-sinkage and its prediction model of lunar rover. *Journal of Central South University of Technology*, 17(1):129–135, 2010.

[18] Liang Ding, Haibo Gao, Zongquan Deng, Keiji Nagatani, and Kazuya Yoshida. Experimental study and analysis on driving wheels' performance for planetary exploration rovers moving in deformable soil. *Journal of Terramechanics*, 48(1):27–45, 2011.

[19] Liang Ding, Haibo Gao, Zongquan Deng, Kazuya Yoshida, and Keiji Nagatani. Slip ratio for lugged wheel of planetary rover in deformable soil: definition and estimation. In *Intelligent Robots and Systems, 2009. IROS 2009. IEEE/RSJ International Conference on*, pages 3343–3348. IEEE, 2009.

[20] KA Abd El-Gawwad, DA Crolla, AMA Soliman, and FM El-Sayed. Off-road tyre modelling iii: effect of angled lugs on tyre performance. *Journal of Terramechanics*, 36(2):63–75, 1999.

[21] CW Fervers. Improved fem simulation model for tire–soil interaction. *Journal of Terramechanics*, 41(2):87–100, 2004.

[22] Jonathan Fleischmann. Dem-pm contact model with multi-step tangential contact displacement history. *Simulation-Based Engineering Laboratory, University of Wisconsin-Madison, Technical Report No. TR-2015-06*, 2015.

[23] Jonathan Fleischmann, Radu Serban, Dan Negrut, and Paramsothy Jayakumar. On the importance of displacement history in soft-body contact models. *Journal of Computational and Nonlinear Dynamics*, 11(4):044502, 2016.

[24] Alberto Gallina, Andreas Gibbesch, Rainer Krenn, Tadeusz Uhl, and Bernd Schäfer. Multibody simulation of planetary rover mobility in condition of uncertain soft terrain. *Procedia IUTAM*, 13:118–126, 2015.

[25] Alberto Gallina, Rainer Krenn, and Bernd Schäfer. On the treatment of soft soil parameter uncertainties in planetary rover mobility simulations. *Journal of Terramechanics*, 63:33–47, 2016.

[26] Andreas Gibbesch, Rainer Krenn, Florian Herrmann, Bernd Schäfer, Bernhard Rebele, Elie Allouis, and Thomas Diedrich. Multi-body system and contact simulation within the design development of planetary surface exploration systems. *iSairas. Sapporo, Japan*, 2010.

[27] G Gilardi and I Sharf. Literature survey of contact dynamics modelling. *Mechanism and machine theory*, 37(10):1213–1239, 2002.

[28] Christoph Glocker and Friedrich Pfeiffer. An lcp-approach for multibody systems with planar friction. *Proceedings of the CMIS*, 92:13–30, 1992.

[29] Carsten Harnisch, Bjoern Lach, Roland Jakobs, Markos Troulis, and Oliver Nehls. A new tyre–soil interaction model for vehicle simulation on deformable ground. *Vehicle System Dynamics*, 43(sup1):384–394, 2005.

[30] Alan C Hindmarsh, Peter N Brown, Keith E Grant, Steven L Lee, Radu Serban, Dan E Shumaker, and Carol S Woodward. Sundials: Suite of nonlinear and differential/algebraic equation solvers. *ACM Transactions on Mathematical Software (TOMS)*, 31(3):363–396, 2005.

[31] Gerhard Hippmann. An algorithm for compliant contact between complexly shaped surfaces in multibody dynamics. *Multibody Dynamics, Jorge AC Ambrosio (Ed.), IDMEC/IST, Lisbon, Portugal, July*, 14, 2003.

[32] Suksun Hutangkabodee, Yahya Hashem Zweiri, Lakmal Dasarath Seneviratne, and Kaspar Althoefer. Soil parameter identification for wheel-terrain interaction dynamics and traversability prediction. *International Journal of Automation and Computing*, 3(3):244–251, 2006.

[33] Karl Iagnemma, Shinwoo Kang, Christopher Brooks, and Steven Dubowsky. Multi-sensor terrain estimation for planetary rovers. In *Proceedings of the 8th international symposium on artificial intelligence, robotics, and automation in space. IEEE Press, New York*, 2003.

[34] Karl Iagnemma, Shinwoo Kang, Hassan Shibly, and Steven Dubowsky. Online terrain parameter estimation for wheeled mobile robots with application to planetary rovers. *IEEE Transactions on Robotics*, 20(5):921–927, 2004.

[35] Karl Iagnemma, Carmine Senatore, Brian Trease, Raymond Arvidson, Keith Bennett, Amy Shaw, Feng Zhou, Lauren Van Dyke, and Randel Lindemann. Terramechanics modeling of mars surface exploration rovers for simulation and parameter estimation. In *ASME 2011 International Design Engineering Technical Conferences and Computers and Information in Engineering Conference*, pages 805–812. American Society of Mechanical Engineers, 2011.

[36] RA Irani, RJ Bauer, and A Warkentin. A dynamic terramechanic model for small lightweight vehicles with rigid wheels and grousers operating in sandy soil. *Journal of Terramechanics*, 48(4):307–318, 2011.

[37] Genya Ishigami, Masatsugu Otsuki, Takashi Kubota, and Karl Iagnemma. Modeling of flexible and rigid wheels for exploration rover on rough terrain. In *the 28th International Symposium on Space Technology and Science, Okinawa, Japan, 5-12 JUne, 2011*, 2011.

[38] Zoltan Janosi and Ben Hanamoto. An analysis of the drawbar pull vs slip relationship for track laying vehicles. Technical report, DTIC Document, 1961.

[39] Danny M Kaufman and Dinesh K Pai. Geometric numerical integration of inequality constrained, nonsmooth hamiltonian systems. *SIAM Journal on Scientific Computing*, 34(5):A2670–A2703, 2012.

[40] Yoshiyuki Kawase, Hiroshi Nakashima, and Akira Oida. An indoor traction measurement system for agricultural tires. *Journal of Terramechanics*, 43(3):317–327, 2006.

[41] Thomas Keller. A model for the prediction of the contact area and the distribution of vertical stress below agricultural tyres from readily available tyre parameters. *Biosystems engineering*, 92(1):85–96, 2005.

[42] Thomas Keller, Pauline Défossez, Peter Weisskopf, Johan Arvidsson, and Guy Richard. Soilflex: A model for prediction of soil stresses and soil compaction due to agricultural field traffic including a synthesis of analytical approaches. *Soil and Tillage Research*, 93(2):391–411, 2007.

[43] Thomas Keller and Mathieu Lamandé. Challenges in the development of analytical soil compaction models. *Soil and Tillage Research*, 111(1):54–64, 2010.

[44] Rainer Krenn, Andreas Gibbesch, and Gerd Hirzinger. Contact dynamics simulation of rover locomotion. 2008.

[45] Rainer Krenn and Gerd Hirzinger. Simulation of rover locomotion on sandy terrain–modeling verification and validation. 2008.

[46] Rainer Krenn and Gerd Hirzinger. Scm–a soil contact model for multi-body system simulations. 2009.

[47] H Kruggel-Emden, E Simsek, S Rickelt, S Wirtz, and V Scherer. Review and extension of normal force models for the discrete element method. *Powder Technology*, 171(3):157–173, 2007.

[48] H Kruggel-Emden, S Wirtz, and V Scherer. A study on tangential force laws applicable to the discrete element method (dem) for materials with viscoelastic or plastic behavior. *Chemical Engineering Science*, 63(6):1523–1541, 2008.

[49] Rattan Lal and Manoj K Shukla. *Principles of soil physics*. CRC Press, 2004.

[50] Jonah H Lee. Statistical modeling and comparison with experimental data of tire–soil interaction for combined longitudinal and lateral slip. *Journal of Terramechanics*, 58:11–25, 2015.

[51] K Legnemma, Christopher Brooks, and Steven Dubowsky. Visual, tactile, and vibration-based terrain analysis for planetary rovers. In *Aerospace Conference, 2004. Proceedings. 2004 IEEE*, volume 2, pages 841–848. IEEE, 2004.

[52] Lin Li and Corina Sandu. On the impact of cargo weight, vehicle parameters, and terrain characteristics on the prediction of traction for off-road vehicles. *Journal of Terramechanics*, 44(3):221–238, 2007.

[53] Zhongchao Liang, Haibo Gao, Liang Ding, Zongquan Deng, and Jianjun Qu. Analysis of driving efficiency for lrv wheels using forced-slip method. *Advances in Space Research*, 54(10):2122–2130, 2014.

[54] Roy Lichtenheldt and Bernd Schäfer. Locomotion on soft granular soils: a discrete element based approach for simulations in planetary exploration. 2013.

[55] CH Liu and JY Wong. Numerical simulations of tire-soil interaction based on critical state soil mechanics. *Journal of Terramechanics*, 33(5):209–221, 1996.

[56] CH Liu, JY Wong, and HA Mang. Large strain finite element analysis of sand: model, algorithm and application to numerical simulation of tire–sand interaction. *Computers & Structures*, 74(3):253–265, 2000.

[57] Jicheng Liu, Haibo Gao, Zongquan Deng, and Jianguo Tao. Effect of slip on tractive performance of small rigid wheel on loose sand. *Intelligent Robotics and Applications*, pages 1109–1116, 2008.

[58] Modest Lyasko. Slip sinkage effect in soil–vehicle mechanics. *Journal of Terramechanics*, 47(1):21–31, 2010.

[59] Margarida Machado, Pedro Moreira, Paulo Flores, and Hamid M Lankarani. Compliant contact force models in multibody dynamics: Evolution of the hertz contact theory. *Mechanism and Machine Theory*, 53:99–121, 2012.

[60] J Matthews and JDC Talamo. Ride comfort for tractor operators: Iii. investigation of tractor dynamics by analogue computer simulation. *Journal of Agricultural Engineering Research*, 10(2):93–108, 1965.

[61] Hammad Mazhar, Toby Heyn, Dan Negrut, and Alessandro Tasora. Using nesterov's method to accelerate multibody dynamics with friction and contact. *ACM Transactions on Graphics (TOG)*, 34(3):32, 2015.

[62] Hammad Mazhar, Toby Heyn, Arman Pazouki, Daniel Melanz, Andrew Seidl, Aaron Bartholomew, Alessandro Tasora, and Dan Negrut. Chrono: a parallel multi-physics library for rigid-body, flexible-body, and fluid dynamics. *Mechanical Sciences*, 4(1):49–64, 2013.

[63] Virginia T McLemore, Kelly M Donahue, Erin Phillips, Nelia Dunbar, Patrick Walsh, Luiza AF Gutierrez, Samuel Tachie-Menson, Heather R Shannon, Virgil W Lueth, Andrew R Campbell, et al. Characterization of goathill north mine rock pile, questa molybdenum mine, questa, new mexico. In *International Conference of Acid Rock Drainage (ICARD). ASMR, St. Louis*, 2006.

[64] Gareth Meirion-Griffith and Matthew Spenko. A pressure-sinkage model for small-diameter wheels on compactive, deformable terrain. *Journal of Terramechanics*, 50(1):37–44, 2013.

[65] Namjoo Moslem and Golbakhshi Hossein. Numerical simulation of tire/soil interaction using a verified 3d finite element model. *Journal of Central South University*, 21(2):817–821, 2014.

[66] H Nakashima, H Fujii, A Oida, M Momozu, Y Kawase, H Kanamori, S Aoki, and T Yokoyama. Parametric analysis of lugged wheel performance for a lunar microrover by means of dem. *Journal of Terramechanics*, 44(2):153–162, 2007.

[67] H Nakashima and A Oida. Algorithm and implementation of soil–tire contact analysis code based on dynamic fe–de method. *Journal of Terramechanics*, 41(2):127–137, 2004.

[68] Hiroshi Nakashima and Taizo Kobayashi. Effects of gravity on rigid rover wheel sinkage and motion resistance assessed using two-dimensional discrete element method. *Journal of terramechanics*, 53:37–45, 2014.

[69] Hiroshi Nakashima and Yuzuru Takatsu. Analysis of tire tractive performance on deformable terrain by finite element-discrete element method. *Journal of computational science and technology*, 2(4):423–434, 2008.

[70] Hiroshi Nakashima, Yuzuru Takatsu, Hisanori Shinone, Hisao Matsukawa, and Takahiro Kasetani. Fe-dem analysis of the effect of tread pattern on the tractive performance of tires operating on sand. *Journal of Mechanical Systems for Transportation and Logistics*, 2(1):55–65, 2009.

[71] Silvia Negrini. *On the modelling of deformable tyre on deformable soil for tread pattern design optimization*. PhD thesis, Italy, 2013.

[72] Dan Negrut, Rajiv Rampalli, Gisli Ottarsson, and Anthony Sajdak. On an implementation of the hilber-hughes-taylor method in the context of index 3 differential-algebraic equations of multibody dynamics (detc2005-85096). *Journal of computational and nonlinear dynamics*, 2(1):73–85, 2007.

[73] VN Nguyen and S Inaba. Effects of tire inflation pressure and tractor velocity on dynamic wheel load and rear axle vibrations. *Journal of Terramechanics*, 48(1):3–16, 2011.

[74] VN Nguyen, T Matsuo, S Inaba, and T Koumoto. Experimental analysis of vertical soil reaction and soil stress distribution under off-road tires. *Journal of Terramechanics*, 45(1):25–44, 2008.

[75] Lauro Ojeda, Johann Borenstein, and Gary Witus. Terrain trafficability characterization with a mobile robot. In *Defense and Security*, pages 235–243. International Society for Optics and Photonics, 2005.

[76] Catherine O'Sullivan and Jonathan D Bray. Selecting a suitable time step for discrete element simulations that use the central difference time integration scheme. *Engineering Computations*, 21(2/3/4):278–303, 2004.

[77] Hans Pacejka. *Tire and vehicle dynamics*. Elsevier, 2005.

[78] Jong-Shi Pang and David E Stewart. A unified approach to discrete frictional contact problems. *International Journal of Engineering Science*, 37(13):1747–1768, 1999.

[79] Laura E Ray. Autonomous terrain parameter estimation for wheeled vehicles. In *SPIE Defense and Security Symposium*, pages 69621H–69621H. International Society for Optics and Photonics, 2008.

[80] Giulio Reina. *Methods for wheel slip and sinkage estimation in mobile robots*. INTECH Open Access Publisher, 2010.

[81] Giulio Reina, Genya Ishigami, Keiji Nagatani, and Kazuya Yoshida. Vision-based estimation of slip angle for mobile robots and planetary rovers. In *Robotics and Automation, 2008. ICRA 2008. IEEE International Conference on*, pages 486–491. IEEE, 2008.

[82] Giulio Reina, Lauro Ojeda, Annalisa Milella, and Johann Borenstein. Wheel slippage and sinkage detection for planetary rovers. *IEEE/Asme Transactions on Mechatronics*, 11(2):185–195, 2006.

[83] Bernd Schäfer, Andreas Gibbesch, Rainer Krenn, and Bernhard Rebele. Planetary rover mobility simulation on soft and uneven terrain. *Vehicle System Dynamics*, 48(1):149–169, 2010.

[84] P Schenker, T Huntsberger, P Pirjanian, S Dubowsky, K Iagnemma, and V Sujan. Rovers for intelligent, agile traverse of challenging terrain. 2003.

[85] Per Schjønning, Mathieu Lamandé, Frede A Tøgersen, Johan Arvidsson, and Thomas Keller. Modelling effects of tyre inflation pressure on the stress distribution near the soil–tyre interface. *Biosystems Engineering*, 99(1):119–133, 2008.

[86] Ingobert C Schmid. Interaction of vehicle and terrain results from 10 years research at ikk. *Journal of terramechanics*, 32(1):3–26, 1995.

[87] C Senatore and C Sandu. Off-road tire modeling and the multi-pass effect for vehicle dynamics simulation. *Journal of Terramechanics*, 48(4):265–276, 2011.

[88] C Senatore and C Sandu. Torque distribution influence on tractive efficiency and mobility of off-road wheeled vehicles. *Journal of Terramechanics*, 48(5):372–383, 2011.

[89] P Servadio, A Marsili, and NP Belfiore. Analysis of driving seat vibrations in high forward speed tractors. *Biosystems engineering*, 97(2):171–180, 2007.

[90] H Shibly, Karl Iagnemma, and S Dubowsky. An equivalent soil mechanics formulation for rigid wheels in deformable terrain, with application to planetary exploration rovers. *Journal of terramechanics*, 42(1):1–13, 2005.

[91] I Shmulevich, U Mussel, and D Wolf. The effect of velocity on rigid wheel performance. *Journal of terramechanics*, 35(3):189–207, 1998.

[92] Leonardo E Silbert, Deniz Ertaş, Gary S Grest, Thomas C Halsey, Dov Levine, and Steven J Plimpton. Granular flow down an inclined plane: Bagnold scaling and rheology. *Physical Review E*, 64(5):051302, 2001.

[93] T Šmerda and J Čupera. Tire inflation and its influence on drawbar characteristics and performance–energetic indicators of a tractor set. *Journal of Terramechanics*, 47(6):395–400, 2010.

[94] David Stewart and Jeffrey C Trinkle. An implicit time-stepping scheme for rigid body dynamics with coulomb friction. In *Robotics and Automation, 2000. Proceedings. ICRA'00. IEEE International Conference on*, volume 1, pages 162–169. IEEE, 2000.

[95] David E Stewart. Rigid-body dynamics with friction and impact. *SIAM review*, 42(1):3–39, 2000.

[96] Jianguo Tao, Liang Ding, Qiquan Quan, and Haibo Gao. Development and experiments of a test-bed for wheel-soil interaction of lunar rover. In *12th European Conference on Spacecraft Structures, Materials and Environmental Testing*, volume 691, page 202, 2012.

[97] A Tasora, M Anitescu, S Negrini, and D Negrut. A compliant visco-plastic particle contact model based on differential variational inequalities. *International Journal of Non-Linear Mechanics*, 53:2–12, 2013.

[98] Alessandro Tasora, Radu Serban, Hammad Mazhar, Arman Pazouki, Daniel Melanz, Jonathan Fleischmann, Michael Taylor, Hiroyuki Sugiyama, and Dan Negrut. Chrono: An open source multi-physics dynamics engine. In *International Conference on High Performance Computing in Science and Engineering*, pages 19–49. Springer, 2015.

[99] Alessandro Tasora, Marco Silvestri, and Paolo Righettini. Architecture of the chrono:: engine physics simulation middleware. In *Proceedings of Multibody Dynamics 2007, ECCOMAS thematic conference*. Citeseer, 2007.

[100] K. Terzaghi, R.B. Peck, and G. Mesri. *Soil Mechanics in Engineering Practice*. Wiley-Interscience publication. Wiley, 1996.

[101] Futoshi Wakui and Yoshiaki Terumichi. Numerical simulation of tire-ground system considering soft ground characteristics. *Journal of System Design and Dynamics*, 5(8):1650–1661, 2011.

[102] C Watyotha, D Gee-Clough, and VM Salokhe. Effect of circumferential angle, lug spacing and slip on lug wheel forces. *Journal of terramechanics*, 38(1):1–14, 2001.

[103] Thomas R Way, Donald C Erbach, Alvin C Bailey, Eddie C Burt, and Clarence E Johnson. Soil displacement beneath an agricultural tractor drive tire. *Journal of terramechanics*, 42(1):35–46, 2005.

[104] Thomas R Way and Tadashi Kishimoto. Interface pressures of a tractor drive tyre on structured and loose soils. *Biosystems Engineering*, 87(3):375–386, 2004.

[105] Thomas R Way, Tadashi Kishimoto, H Allen Torbert, Eddie C Burt, and Alvin C Bailey. Tractor tire aspect ratio effects on soil bulk density and cone index. *Journal of terramechanics*, 46(1):27–34, 2009.

[106] Jo Yung Wong. *Theory of ground vehicles*. John Wiley & Sons, 2008.

[107] Jo Yung Wong. *Terramechanics and off-road vehicle engineering: terrain behaviour, off-road vehicle performance and design*. Butterworth-heinemann, 2009.

[108] Kaiming Xia. Finite element modeling of tire/terrain interaction: Application to predicting soil compaction and tire mobility. *Journal of Terramechanics*, 48(2):113–123, 2011.

[109] Kaiming Xia and Yunming Yang. Three-dimensional finite element modeling of tire/ground interaction. *International journal for numerical and analytical methods in geomechanics*, 36(4):498–516, 2012.

[110] Runhuai Yang, Min Xu, Xu Liang, Shiwu Zhang, Yong Cheng, Hongcheng Xu, and Jie Yang. Experimental study and dem analysis on rigid driving wheel's performance for off-road vehicles moving on loose soil. In *Mechatronics and Automation (ICMA), 2011 International Conference on*, pages 142–147. IEEE, 2011.

[111] Mengyan Zang and Chunlai Zhao. Numerical simulation of rigid wheel running behavior on sand terrain. *APCOM & ISCM*, 2013.

[112] HP Zhang and HA Makse. Jamming transition in emulsions and granular materials. *Physical Review E*, 72(1):011301, 2005.

[113] Chunlai Zhao and Mengyan Zang. Analysis of rigid tire traction performance on a sandy soil by 3d finite element–discrete element method. *Journal of Terramechanics*, 55:29–37, 2014.